Metabolic alterations in non-alcoholic fatty liver disease (NAFLD): Consequences of AGXT downregulation on glyoxylate detoxification

Dissertation

zur Erlangung des akademischen Grades des Doktors
der Naturwissenschaften (Dr. rer. nat.) an der Fakultät für Chemie und
Chemische Biologie der Technischen Universität Dortmund

vorgelegt von

Kathrin Gianmoena
Staatl. gepr. Lebensmittelchemikerin

Dortmund 2017

1. Gutachter: Prof. Dr. Jan G. Hengstler
2. Gutachter: PD Dr. Leif Dehmelt

Tag der Disputation: 22.08.2017

Für Papa

Table of contents

Table of contents

Abstract

Non-alcoholic fatty liver disease (NAFLD) encompasses a wide range of liver diseases, where excessive hepatic lipid accumulation is a common factor. It is highly prevalent worldwide, and is associated with an elevated risk of developing more severe liver diseases, as well as cardiovascular and renal diseases, such as the formation of kidney stones. The aim of this study was to identify and investigate lipid-associated metabolic and functional alterations in steatotic livers and hepatocytes. For this purpose, a mouse model of NAFLD, the leptin deficient *ob/ob* mouse, was implemented and its steatotic phenotype investigated. *In vitro* induction of steatosis was established in HepG2 cells and in primary mouse hepatocytes to more directly study the consequences of lipid accumulation. Macrovesicular steatosis was confirmed in the hepatocytes of *ob/ob* mice as well as in the *in vitro* steatosis model, and was manifested by the displacement of nuclei towards the periphery and by a perturbed autophagy flux, thus recapitulating features of human NAFLD.

To estimate the impact of hepatic lipid accumulation on global gene expression across species, hepatic genome-wide expression data of human NAFLD, of the leptin deficient *ob/ob* mouse model, and of lipid-loaded HepG2 cells were compared. Here, 22 deregulated genes in mouse and human NAFLD, as well as in the *in vitro* model of lipid accumulation were identified. Among the 22 genes, the liver specific *AGXT* gene, encoding the alanine-glyoxylate aminotransferase (AGXT), was found to be downregulated. The enzyme AGXT is essential for the detoxification of glyoxylate to glycine in order to prevent the formation of oxalate, a factor that increases the predisposition to developing kidney stones. For this reason, further steps focused on exploring the downregulation of AGXT upon fatty liver as the molecular mechanism underlying the increased risk of kidney stones in patients with NAFLD.

The steatosis-associated repression of AGXT was validated in a small, independent collection of primary human hepatocytes, in a Western diet-induced mouse model of NAFLD, and in the *in vitro* steatosis model of primary mouse hepatocytes, as well as in an additional hepatic cell line. In the leptin deficient *ob/ob* mouse model, the repression of Agxt was accompanied by a reduced hepatic glycine concentration and by a slightly increased urinary oxalate excretion. These observations implied physiological consequences of the decreased expression of Agxt due to the reduced glyoxylate detoxification capacity in this mouse model of NAFLD. Moreover, cultivated *ob/ob* hepatocytes produced more oxalate upon treatment with the

Abstract

glyoxylate precursor hydroxyproline compared to the *ob/+* hepatocytes, and thus suggested an increased susceptibility towards hydroxyproline levels in steatosis.

The downregulation of AGXT in fatty liver was associated with hypermethylation of its promotor in steatotic primary human and murine hepatocytes. This indicated a possible methylation-dependent regulation of AGXT expression *in vivo*. The *in vitro* model of steatosis was not able to recapitulate this feature, suggesting alternative mechanisms of transcriptional downregulation of AGXT.

Altogether, the present study describes the hepatic steatosis-dependent deregulation of the glyoxylate detoxification pathway *via* AGXT repression. It could demonstrate that the lipid-dependent downregulation of AGXT in hepatocytes can result in increased generation of oxalate, and thus susceptibility for renal calcium oxalate deposits. It is the first known report, identifying the downregulation of AGXT as a missing molecular link between fatty liver and the increased risk of kidney stones in patients with NAFLD.

Zusammenfassung

Die nichtalkoholische Fettlebererkrankung (*non-alcoholic fatty liver disease*, NAFLD) umfasst eine Bandbreite von Lebererkrankungen, die eine exzessive hepatische Lipidakkumulierung gemeinsam haben. Weltweit ist die Prävalenz von NAFLD hoch und sie ist nicht nur mit der Entstehung ernsterer Lebererkrankungen assoziiert, sondern auch mit kardiovaskulären und renalen Erkrankungen, wie Nierensteinen. Das Ziel dieser Studie war es, lipid-assoziierte metabolische und funktionelle Veränderungen in steatotischen Lebern und Hepatozyten zu identifizieren und zu untersuchen. Zu diesem Zweck wurde das Leptin-defiziente *ob/ob*-Mausmodell für NAFLD herangezogen und sein steatotischer Phänotyp wurde analysiert. Des Weiteren wurde ein *in vitro*–Steatosemodell in HepG2-Zellen und primären Maushepatozyten etabliert, um die direkten Konsequenzen von Lipidakkumulation zu untersuchen. Makrosteatose wurde sowohl in Hepatozyten von *ob/ob*-Mäusen, also auch in solchen des *in vitro*-Steatosemodells bestätigt und durch die Deplatzierung des Zellkerns in die Peripherie sowie den gestörten Autophagiefluss, beides Merkmale der humanen NAFLD, verdeutlicht.

Um den Einfluss hepatischer Lipidakkumulation auf die globale Genexpression speziesübergreifend abzuschätzen, wurden genomweite Expressionsdaten von humaner NAFLD, von dem Leptin-defizienten *ob/ob*-Mausmodell und von steatotischen HepG2-Zellen miteinander verglichen. Dabei wurden 22 Gene identifiziert, die sowohl in muriner und humaner NAFLD als auch durch Lipidakkumulation im *in vitro*-Modell dereguliert wurden. Unter diesen Genen wurde die Herabregulierung des leberspezifischen *AGXT*-Gens, das die Alanin-Glyxoylat-Aminotransferase (AGXT) codiert, beobachtet. Das Enzym AGXT ist essentiell für die Detoxifizierung von Glyoxylat zu Glycin, um die Bildung von Oxalat vorzubeugen. Oxalat ist ein Faktor, der die Anfälligkeit für die Entstehung von Nierensteinen erhöht. Aus diesem Grund wurde der weitere Fokus dieser Dissertation auf die steatose-bedingte Herabregulierung von AGXT, als möglicher Mechanismus für das erhöhte Risiko von Nierensteinen in NAFLD-Patienten, gelegt.

Die steatose-assoziierte Repression von AGXT wurde sowohl in einer kleinen, unabhängigen Sammlung primärer humaner Hepatozyten und in einem *Western diet*-Mausmodell von NAFLD, als auch in den *in vitro*-Steatosemodellen von primären Maushepatozyten und einer weiteren Leberzelllinie bestätigt. Die Agxt-Herabregulierung in dem *ob/ob*-Mausmodell ging mit einer reduzierten hepatischen Konzentration von Glycin und einer leichten Erhöhung der

Zusammenfassung

täglichen renalen Oxalatausscheidung einher. Diese Beobachtungen deuteten auf physiologische Konsequenzen der verminderten Agxt-Expression, durch eine reduzierte Glyoxylatdetoxifizierungskapazität, in dem *ob/ob*-Mausmodell hin. Darüber hinaus produzierten kultivierte Hepatozyten der *ob/ob*-Maus, nach Behandlung mit dem Glyoxylatvorläufer Hydroxyprolin, mehr Oxalat als die Kontrollhepatozyten der *ob/+*-Maus. Dies deutete eine erhöhte Empfindlichkeit gegenüber Hydroxyprolin bei Lebersteatose an.

Die reduzierte Expression von AGXT in der Fettleber ging mit der Hypermethylierung seines Promotors in steatotischen primären humanen und murinen Hepatozyten einher. Das wies auf eine mögliche methylierungsabhängige Regulation der AGXT-Expression *in vivo* hin. Das *in vitro*-Steatosemodell war nicht in der Lage dieses Merkmal zu rekapitulieren und deutet somit an, dass es alternative Mechanismen für die transkriptionelle Herabregulierung von AGXT gibt.

Zusammengefasst beschreibt die vorliegende Studie die lebersteatose-bedingte Deregulierung der Glyoxylatdetoxifizierung durch AGXT-Repression. Sie konnte zeigen, dass die lipidabhängige Herabregulierung von AGXT in Hepatozyten zu einer vermehrten Bildung von Oxalat führen kann und dadurch die Suszeptibilität für renale Calciumoxalatablagerungen erhöht. Es ist die erste bekannte Untersuchung, die die verminderte Expression von AGXT als fehlende molekulare Verbindung zwischen der Fettleber und dem erhöhten Risiko von Nierensteinen in Patienten mit NAFLD identifiziert.

1. Introduction

1.1 Epidemiology of non-alcoholic fatty liver disease

Non-alcoholic fatty liver disease (NAFLD) encompasses a spectrum of fatty liver diseases ranging from simple steatosis to steatohepatitis, fibrosis and cirrhosis that can ultimately lead to hepatocellular carcinoma (Bugianesi et al. 2002; Powell et al. 1990; Schaffner and Thaler 1986). The main feature of NALFD is the excessive accumulation of fat in the liver, which is defined by steatosis in more than 5% of the hepatocytes (European Association for the Study of the Liver 2016). In order to diagnose NAFLD, secondary causes of hepatic lipid accumulation, such as heavy alcohol consumption, steatogenic medication, virus infection and hereditary disorders need to be excluded (Chalasani et al. 2012). The European Association for the Study of the Liver (EASL) defined heavy alcohol consumption with respect to NAFLD as the daily intake of more than 30 g of pure ethanol for men and 20 g pure ethanol for women (Ratziu et al. 2010). Furthermore, the American as well as the European Association for the study of the Liver have placed NAFLD into the two distinct categories: non-alcoholic fatty liver (NAFL) and non-alcoholic steatohepatitis (NASH). NAFL represents simple hepatic steatosis with no signs of inflammation or hepatocellular injury; whereas, NASH covers the spectrum of more severe liver diseases, including inflammation with or without fibrosis the in presence of hepatic steatosis (Chalasani et al. 2012; European Association for the Study of the Liver 2016). Worldwide, NALFD is a major underlying feature of liver diseases and the most common cause for elevated liver enzymes (Vernon et al. 2011; Younossi et al. 2016). Importantly, NAFLD, in particular NASH, is associated with increased overall mortality compared to the general population (Adams et al. 2005; Ong et al. 2008). Furthermore, patients suffering from NASH exhibit elevated liver-related mortality (Ekstedt et al. 2006; Matteoni et al. 1999; Stepanova et al. 2013).

1.1.1 Prevalence of NAFLD

Assessing the prevalence of NAFLD in the general population is difficult, because it is highly variable, and depends on the method applied for diagnosis and on the studied population. The current gold standard to diagnose NAFLD is a biopsy of the liver; an invasive procedure that is not feasible for screening entire populations. Nevertheless, in studies investigating the potential of living individuals to donate liver they found a NAFLD prevalence of 10% in Korea

and of 20% in the USA when the degree of steatosis was set above 30%, diagnosed by liver biopsy (Lee et al. 2007; Marcos et al. 2000). Ultrasound is one of the most widely-used, non-invasive diagnosis method to diagnose NAFLD, which revealed a prevalence between 17% in India and 46% in the USA (Vernon et al. 2011). Younossi and co-workers reported that the global NAFLD prevalence is 25% based on imaging techniques to diagnose NAFLD. Although NAFLD is quite common, only a small subgroup suffers from NASH. It is estimated that 7-30% of all NAFLD patients have NASH, which indicates an overall prevalence between 1.5% and 6.5% (Younossi et al. 2016).

Interstingly, ethnicity also has an enormous impact on NAFLD's frequency. Hispanics are reported to have the highest prevalence, followed by white and African Americans (Browning et al. 2004). The genetic variation I148M of the *PNPLA3* gene, encoding the patatin-like phospholipase-3/adiponutrin, is strongly associated with increased hepatic fat content. This particular mutation is most common in Hispanics and is a potential explanation for the ethnicity differences with regard to NAFLD (Romeo et al. 2008).

1.1.2 NAFLD is associated with the metabolic syndrome

NAFLD is more prevalent in patients with existing metabolic disorders compared to those in general population (Vernon et al. 2011). Usually, several metabolic disorders occur simultaneously and are defined as the metabolic syndrome, which includes abdominal obesity, dyslipidemia, raised blood pressure and insulin resistance (Expert Panel on Detection Evaluation and Treatment of High Blood Cholesterol 2001). Obese patients undergoing bariatric surgery have increased prevalence of NAFLD, ranging from 63% (Boza et al. 2005) up to over 90% (Machado et al. 2006; Ong et al. 2005). Furthermore, elevated body mass index (BMI) and waist circumference are associated with the presence of NAFLD (Bedogni et al. 2005).

Insulin resistance is related to NAFLD (Marchesini et al. 1999) and accumulation of hepatic liver fat is closely associated to hepatic, muscle and adipose tissue insulin resistance in obese persons (Korenblat et al. 2008). In addition, patients with type II diabetes have a higher prevalence of NAFLD, which was associated with obesity, hypertriglyceridemia and high to normal alanine aminotransferase levels (Leite et al. 2009).

In brief, obesity and insulin resistance, as well as type II diabetes are closely related to NAFLD. For that reason, NAFLD is sometimes considered as a hepatic manifestation of the metabolic

syndrome (Fotbolcu and Zorlu 2016; Marchesini et al. 2001). This assumption is however controversially discussed. Smits and colleague performed a confirmatory factor analysis of cross-sectional data, derived from the Third National Health and Nutrition Examination Survey, NHANES III (National Center for Health Statistic 1994), and found no evidence that NAFLD is an independent component of the metabolic syndrome. They consider NAFLD rather as a separate condition, which is strongly associated with the metabolic syndrome (Smits et al. 2013).

1.2 Progression of NAFLD

Simple steatosis and NASH can develop into more severe types of liver diseases. Simple steatosis, if it progresses, is reported to progress very slowly (Pais et al. 2011; Teli et al. 1995; Wong et al. 2010). For instance, a new study, investigating the progression of/to fibrosis from NAFL and NASH, reported that simple steatosis increases the fibrosis stage every 14 years, whereas NASH has a progression rate that correspond to one fibrosis stage every seven years (Singh et al. 2015).

Fat accumulation in the liver is a main feature of NAFLD as described in Chapter 1.1. There are several mechanisms underlying this lipid accumulation, such as the oversupply of fatty acids and their assembly into triglyceride (Postic and Girard 2008). Fatty acids arise from several sources, including their release upon the lipolysis of adipose tissue, diet, and hepatic *de novo* synthesis of fatty acids, which are then esterified to glycerol (Donnelly et al. 2005). In addition to the increased production of lipids/triglycerides, decreased degradation of fatty acids as well as reduced excretion of hepatic very low density lipoprotein (VLDL) containing triglycerides can also contribute to the accumulation of lipids (Postic and Girard 2008).

It is currently controversial whether lipid accumulation, i.e. simple steatosis, always occurs before NASH and thus symbolizes the initiation of the development of NASH. Day and colleague proposed the so called "two hit" hypothesis in 1998, by suggesting that the development of fatty liver is the so-called "first hit", which increases the susceptibility of the liver to "second hits". These two hits result in hepatocyte injury, and consequently in inflammation of the liver (Day and James 1998). Examples of second hits are lipid peroxidation, reactive oxygen species, free fatty acids, and the release of Tumour necrosis factor α (TNFα) (Day 2002; Day and James 1998). However, this theory fails to explain why simple steatosis, in contrast to NASH, rarely progresses to more severe liver disease. Therefore, multiple hit

Introduction

hypotheses have been proposed that try to explain the complexity of NAFLD progression (Figure 1.1), accompanied with the suggestion to consider simple fatty liver and NASH as two separate diseases (Buzzetti et al. 2016; Tilg and Moschen 2010).
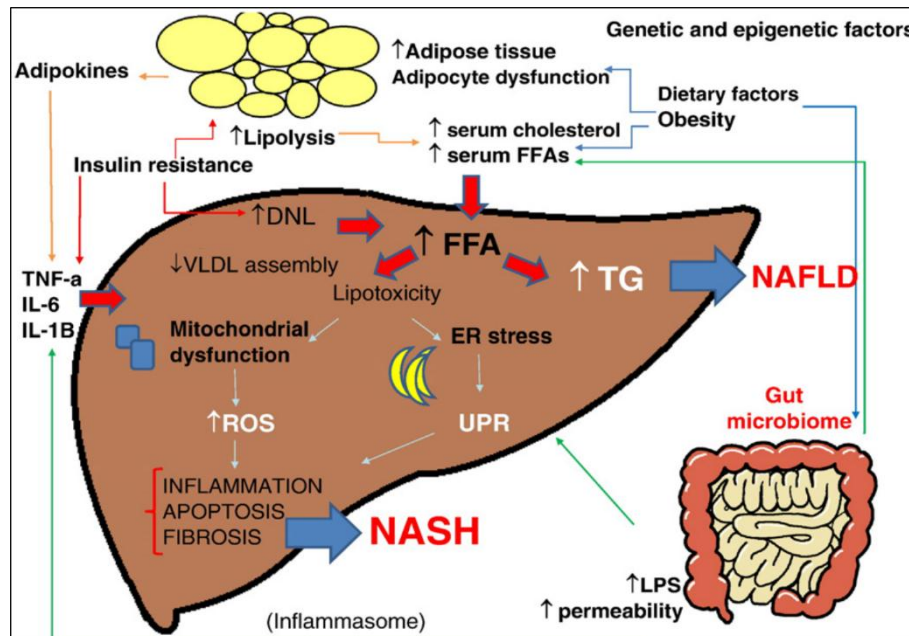
Figure 1.1: Multiple hit hypothesis for the development of NAFLD (modified from Buzzetti et al. 2016).

1.2.1 Hepatic lipid accumulation and insulin resistance

The accumulation of triglycerides may not always indicate a hepatotoxic event, but can represent a hepatoprotective process by which cells deal with excessive free fatty acids (Dowman et al. 2010). Mouse models with increased capacity to form triglycerides are more protected from systemic inflammation (Koliwad et al. 2010); whereas, mice with impaired triglyceride synthesis show more liver damage and inflammation (Yamaguchi et al. 2007).

As mentioned above, NAFLD and NASH are closely linked to peripheral insulin resistance (Sanyal et al. 2001), which is characterized by increased insulin release due to decreased insulin sensitivity. Elevated insulin levels influence lipid metabolism, for example, insulin stimulates hepatic *de novo* lipogenesis by the activation/overexpression of the transcription factor sterol regulatory element-binding protein-1c (SREBP-1c), which in turn regulates the transcription of lipogenic genes (Horton et al. 2002; Shimano et al. 1999). In addition, insulin does not suppress lipolysis in adipose tissue as under normal conditions and the efflux of free fatty acids to the liver increases (Lewis et al. 2002). Elevated levels of free fatty acids are

strongly associated with increased expression of the pro-inflammatory cytokine TNFα, which may explain the fatty acid-mediated hepatic lipotoxicity (Feldstein et al. 2004).

1.2.2 Gut microbiota-dependent release of endotoxins

The gut microbiota is another widely discussed parameter in NAFLD and its progression (Buzzetti et al. 2016). The blood supply of the liver comes mainly from the portal vein (70% - 75%), and thus represents an important link between the intestine and the liver. Thus, the liver is exposed to various intestinal metabolites and nutrients (Abdel-Misih and Bloomston 2010). The composition of the gut microbiota is strongly dependent on the diet of the host (Wu et al. 2011). NASH patients have a higher prevalence of small intestinal bacterial overgrowth accompanied by elevated serum values of TNFα (Wigg et al. 2001). Additionally, NASH patients seem to have an increased susceptibility for gut leakage (Farhadi et al. 2008). Both observations were confirmed in NAFLD patients in a study conducted by Miele and colleagues, who explained that the higher permeability may be due to a disruption of intercellular tight junctions in the intestine (Miele et al. 2009). Bacterial overgrowth in combination with the elevated permeability of the gut may together increase the exposure of the liver to gut-derived endotoxins, consisting of lipopolysaccharides (LPS). Recent studies support this by showing increased serum levels of endotoxins in terms of NAFLD than in controls (Harte et al. 2010; Wong et al. 2015).

Mouse models of NAFLD, namely mice on high fat diet and genetically obese leptin deficient mice exhibit increased plasma levels of endotoxins, which were reduced upon antibiotic treatment also accompanied with change of gut microbiota (Cani et al. 2008). LPS are thought to play an important role in the progression of NASH, mediated by an increase in the expression of Toll like receptor 4 (TLR4) as well as CD14. TRL4 is predominantly expressed in cells of the immune system, especially in macrophages and dendritic cells (Medzhitov et al. 1997), and recognizes LPS most likely after LPS binds to its co-receptor CD14 (da Silva Correia et al. 2001). Stimulation of TLR4 activates the production of pro-inflammatory cytokines, such as TNFα, Interleukin-1 (alpha and beta) and interleukin-6 (Il-6) (Luster et al. 1994; Medzhitov 2001). Rivera and colleagues demonstrated that Kupffer cells - liver resident macrophages - and TLR4 have an immense impact on NAFLD progression. The authors showed that Kupffer cell depletion, as well as the absence of TLR4 attenuate hepatic inflammation and injury in a diet-induced model of NASH (Rivera et al. 2007).

1.2.3 Pro- and anti-inflammatory signalling in NAFLD

LPS is not the only TLR4 trigger. Free fatty acids are also able to stimulate TLR4 in adipose tissue, which results in increased levels of TNFα and Interleukin 6 (Il-6) (Shi et al. 2006). Both hepatic and serum levels of TNFα, as well as the expression of the TNFα receptor are elevated in patients suffering from NASH with severe fibrosis (Crespo et al. 2001). Moreover, increased expression as well as plasma concentrations of Il-6 are found in NASH patients, but not in patients with simple steatosis (Wieckowska et al. 2008). These findings suggest an important role of pro-inflammatory cytokines in the pathogenesis of NAFLD.

In addition to pro-inflammatory cytokines, adipose tissue also releases anti-inflammatory adipokines, such as adiponectin (Tilg and Moschen 2006). Adiponectin's main anti-inflammatory functions include the suppression of the synthesis of TNFα (Yokota et al. 2000) and interferon-γ (IFNγ), as well as the induction of the production of anti-inflammatory cytokines, such as interleukin-10 (Il-10) in leukocytes (Wolf et al. 2004). Furthermore, adiponectin stimulates β-oxidation of fatty acids in rat hepatocytes and the downregulation of the above-mentioned transcription factor SREBP-1c, altogether leading to the reduction in *de novo* lipogenesis (Tilg and Moschen 2006). Serum levels of adiponectin are markedly decreased in obese patients (Arita et al. 1999). Interestingly, the concentration of adiponectin increases upon weight loss, with a concomitant decrease in Il-6 levels, suggesting a cytokine-dependent regulation of adiponectin (Bruun et al. 2003). Also, an earlier study reported that patients with type II diabetes presented with a marked decrease of adiponectin levels which were restored upon weight loss (Hotta et al. 2000). Moreover, the hepatic expression of adiponectin and its receptors were found to be reduced in NASH patients but not in patients with simple steatosis (Kaser et al. 2005). Another study reported a negative correlation between the plasma concentration of adiponectin and the hepatic triglyceride content as well as insulin resistance (Bugianesi et al. 2005). However, no correlation was observed with the severity of NAFLD, indicating that the severity of NAFLD was not associated with reduced levels of adiponectin (Bugianesi et al. 2005). In contrast, Musso and colleagues found a strong association between the degree of hypoadiponectinemia and the severity of NASH, suggesting lower levels of adiponectin in advanced fibrosis (Musso et al. 2005). In agreement, treatment with pioglitazone, a peroxisome proliferator–activated receptor γ (PPARγ) agonist, increased the plasma levels of adiponectin in NASH patients and led to a histological improvement of

NASH (Belfort et al. 2006). Altogether, these findings indicate that a decreased expression of adiponectin is associated with NAFLD and may play a role in the progression of NAFLD.

1.2.4 Mitochondrial abnormalities and dysfunction

Prior work has shown that NAFLD patients have increased β-oxidation and hepatic oxidative stress, which is only observed in NASH mitochondria with defective structures as well as megamitochondria (Caldwell et al. 1999; Sanyal et al. 2001). Moreover, the activity of the mitochondrial respiratory chain enzyme complex is decreased in livers of NASH patients (Pérez-Carreras et al. 2003). Augmented β-oxidation leads to increased delivery of electrons to the mitochondrial respiratory chain, caused by decreased activity of the chain, which impairs proper transfer of electrons. This altogether contributes to an increased formation of reactive oxygen species (ROS), and in particular the formation of superoxide anion radicals (Pessayre and Fromenty 2005; St-Pierre et al. 2002). ROS can directly damage the mitochondrial DNA, and disturb the mitochondrial respiratory chain by damaging its polypeptides. Furthermore, it increases the degree of lipid peroxidation that contributes to the oxygen imbalance and ROS, which in turn stimulates the hepatic production of TNFα that can lead to hepatocyte cell death (Pessayre et al. 2001). Accumulation of free cholesterol within hepatic mitochondria has been shown to result in the depletion of mitochondrial glutathione, and consequently to the increased susceptibility of hepatocytes to TNF signalling in steatohepatitis (Mari et al. 2006). Mitochondria dysfunction/abnormality is strongly associated with NAFLD, but it is still not clear whether this is a consequence of or a contributing factor towards the progression of NAFLD.

1.2.5 Activation of the unfolded protein response

The unfolded protein response (UPR) is another mechanism, which has been discussed to play a role in the progression of NAFLD (Tilg and Moschen 2010). UPR is triggered by the disruption of endoplasmic reticulum (ER) homeostasis, namely ER stress, which results from the accumulation of misfolded proteins, elevated secretory protein production, or imbalanced redox status (Kaufman 2002). Additionally, ER stress might be responsible for insulin resistance/hyperinsulinemia in obesity since its alleviation by drug treatment improved insulin sensitivity and glucose homeostasis in obese and diabetic mice (Ozcan et al. 2006). Several studies reported an activation of the UPR during NAFLD. For example, Puri and co-workers reported in 2008 an increase in phosphorylation of Eif2α in NAFLD patients, which leads to an

arrest in the translational protein synthesis, as part of the UPR. However, the authors were not able to show the recovering mechanism of UPR in these patients, perhaps due to continued ER stress. In addition, NASH was found to be associated with c-Jun N-terminal kinase (JNK) activation (Puri et al. 2008a), with comparable results obtained in a mouse study from Rinella and colleagues. Here, NASH was induced in diabetic mice by a methionine-choline-deficient diet and the persistent activation of Eif2α in form of its phosphorylation, indicative of UPR, as well as activation of JNK were reported (Rinella et al. 2011).

1.2.6 Genetic and epigenetic factors

Genetic predisposition seems to have influence on the severity of NAFLD (Vernon et al. 2011). Carriers of the aforementioned polymorphism in the *PNPLA3* gene encoding the protein variant l148M have a higher risk for developing NAFLD accompanied with necroinflammation and fibrosis (Valenti et al. 2010). In agreement, the polymorphism of *TM6SF2* is not only associated with increased hepatic lipid content (Kozlitina et al. 2014), but also with advanced fibrosis/cirrhosis (Liu et al. 2014).

Epigenetics is a further discussed mechanism involved in the progression of NAFLD (reviewed by Lee et al. 2017). There are several ways in which epigenetic alterations may influence the liver with regard to lipid accumulation and the pathogenesis of NAFLD. Briefly, epigenetic is a phenomenon that has enormous impact on the expression of genes without changing the sequence of DNA bases. One of the most studied epigenetic modification is the methylation of DNA; these methylations occur at the C5 position of cytosine residues next to guanine, so called CpG sites, catalysed by DNA methyltransferases (DNMTs) (Tollefsbol 2011). DNA methylation in the regulatory region of a gene is usually accompanied by the downregulation or silencing of that gene (Cedar 1988). Murphy and colleagues proposed that a different methylation pattern might distinguish mild from advanced NAFLD, where in general less CpG sites are methylated in advanced NAFLD compared to mild NAFLD (Murphy et al. 2013). DNA methylation is influenced by diet (Tollefsbol 2011). Diets that are deficient in methyl donors like folate reduce the DNA methylation in the liver leading to hepatic lipid (da Silva et al. 2014). Interestingly, liver biopsy samples from NALFD patients before and after weight loss due to bariatric surgery show that NAFLD-related DNA methylation are partially reversible (Ahrens et al. 2013).

In addition to DNA methylation, histone modifications as well as microRNAs are also proposed to be relevant in the pathogenesis of NAFLD (Lee et al. 2017). Histone modifications are important for the regulation of chromatin structure and function, which affects DNA related processes, e.g. gene transcription (Herceg and Murr 2011). Deviant histone modifications are associated and involved in the development of insulin resistance that leads to steatosis (Lee et al. 2014; Ling and Groop 2009). An imbalance between histone acetylation and histone deacetylation may be an underlying cause for the progression of NAFLD to hepatocellular carcinoma (Tian et al. 2013).

MicroRNAs are short endogenous RNA sequences, which regulate gene expression by degradation or repression of targeted mRNAs (Ambros 2004). In NAFLD, aberrant profiles of microRNAs are found and specific microRNAs are involved in the progression from steatosis to more sever forms of NALFD (Ferreira et al. 2014).

1.3 Autophagy and NAFLD

Autophagy is a conserved mechanism by which misfolded proteins as well as damaged organelles are degraded, and was recently identified as a regulator of lipid metabolism (Singh et al. 2009). Recent studies have also implicated autophagy in NAFLD (Gonzalez-Rodriguez et al. 2014; Kwanten et al. 2014). Degradation in autophagy is a dynamic process comprising the engulfment of cargo and the formation of double-membraned autophagosomes, and their subsequent fusion with the lysosome (Xie and Klionsky 2007). The actual degradation of the cargo occurs in a fusion product called the autolysosome. Autophagy is important in the maintenance of cellular homeostasis in order to avoid accumulation of damaged organelles, long lived proteins, and lipid droplets (Singh et al. 2009; Xie and Klionsky 2007).

The relationship between autophagy and NAFLD is two-sided. On the one hand, inhibition of autophagy causes accumulation of triglycerides and lipid droplets indicating a lipolytic function of autophagy; on the other hand, abnormally high levels of intracellular lipids impair autophagy-related clearance of lipids (Singh et al. 2009). Potential reasons for the impaired clearance include an altered lipid composition of the membrane, which reduces the fusion capacity of the autophagosomes with the lysosomes upon long lipid stimulation (Koga et al. 2010), or inhibited acidification of autophagosomes that prevents degradation (Inami et al. 2011).

Introduction

Upon lipid stimulation in a rat model, a biphasic behaviour of autophagy was reported by Papackova and co-workers in 2012. A short term challenge with increased lipid supply stimulated the autophagic flux; whereas, long term treatment with a high fat diet led to a blockage of the autophagic flux (Papackova et al. 2012). Moreover, hepatic autophagy was impaired in both genetic and diet induced mouse models of NAFLD (Inami et al. 2011; Singh et al. 2009; Yang et al. 2010), as well in patients with NAFLD (Gonzalez-Rodriguez et al. 2014). In patients, the autophagic flux was shown to be decreased during steatosis (Kashima et al. 2014); a dysfunction that correlated with hepatic inflammation (Fukuo et al. 2014).

Interestingly, previous studies have reported a connection between the compromised autophagy and elevated levels of ER stress in human and murine NAFLD (Gonzalez-Rodriguez et al. 2014; Yang et al. 2010). Autophagy and ER stress are tightly linked because ER stress induces autophagy for cell survival (Ogata et al. 2006).

Hyperinsulinemia has also been reported together with elevated ER stress during suppressed autophagy (Liu et al. 2009; Yang et al. 2010). It has been proposed that elevated levels of insulin disturb autophagy by supressing important autophagy genes mediated by the transcription factor FoxO1, but this is investigated only *in vitro* so far (Liu et al. 2009). In contrast, FOXO1 was described to be upregulated in a small group of NASH patients (Valenti et al. 2008). Nevertheless, restoring autophagy during steatosis by overexpressing the autophagy related gene *Atg7* in a NAFLD mouse model reversed ER stress and decreased insulin levels (Yang et al. 2010).

There is evidence that lipid and hyperinsulinemia dependent impairment of autophagy stimulate further lipid accumulation and insulin resistance by decreasing lipolysis and increasing ER stress (Figure 1.2, Amir and Czaja 2011), which may lead to apoptosis (Gonzalez-Rodriguez et al. 2014).
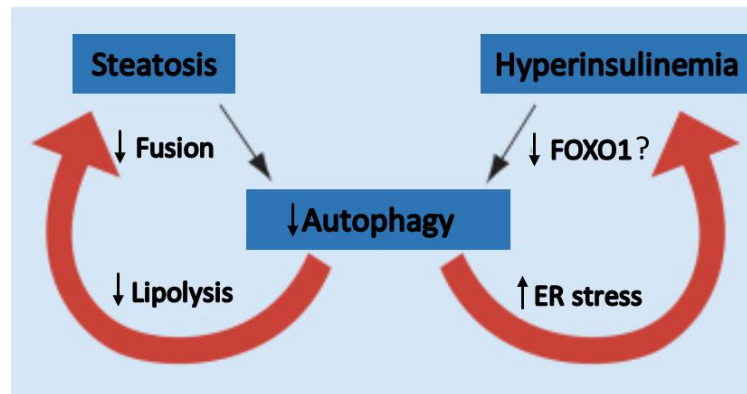
Figure 1.2: Reduced macroautophagy – intercellular interplay in NAFLD. In NAFLD, steatosis and hyperinsulinemia may reduce autophagy. Lipid accumulation may disturb autophagic flux by preventing the fusion of autophagosomes and lysosomes or inhibit autolysosymal degradation by missing acidification. The inhibitory effect of hyperinsulinemia on autophagy may be due to reduced FoxO1 expression and activity. The reduced autophagy may then contribute to further lipid accumulation by impairing lipolytic breakdown of lipids. Additionally, the impaired autophagy may promote insulin resistance upon increased ER stress (modified from Amir and Czaja 2011).

1.4 Mouse models to study NAFLD

As seen above, the pathogenesis of NAFLD, and in particular NASH is complex and not fully understood. Therefore, animal models representing histological and pathophysiological stages of NAFLD are necessary to elucidate the complexity of NAFLD's pathogenesis. Since human NALFD is strongly associated with obesity, insulin resistance and type II diabetes (Chapter 1.1.2), these features need to be mirrored by the animal model. So far, there are animal models available, which are able to recapitulate single hallmarks of NAFLD, but unfortunately not the complete histopathology and physiological properties of human NALFD from steatosis to HCC (Lau et al. 2017). In Table 1.1, a short overview of several mouse models of NAFLD, inclusive of their ability to reflect the features of human NAFLD, is given. More information on selected mouse models is provided in more detail in sections 1.4.1 to 1.4.3.

Table 1.1 Overview of mouse models of NAFLD (based on Anstee and Goldin 2006; Lau et al. 2017; Schattenberg and Galle 2010)

Model	Obesity	IR	Steatosis	NASH	Fibrosis
Genetic					
ob/ob	✓	✓	✓	no	no
db/db	✓	✓	✓	no	no
KK-A^y	✓	✓	✓	no	no
Diet induced					
High fat diet	✓	✓	✓	✓	?
MCD diet	no	no	✓	✓	✓
High fat and high cholesterol diet	✓	?	✓	✓	✓
Combination					
db/db + MCD diet	✓	✓	✓	✓	✓
ob/ob + LPS	✓	✓	✓	✓	no

In the current work, both genetic and diet induced models were used, and therefore a more detailed description is provided for these specific models.

1.4.1 The leptin deficient *ob/ob* mouse model

The *ob/ob* mouse possesses a spontaneous mutation that leads to obesity, and was first described in 1949 (Ingalls et al. 1950). The mutation occurs in the leptin gene (Friedman et al. 1991; Zhang et al. 1994) and results in obese, hyperphagic, hyperinsulinemic and hyperglycaemic mice (Coleman 1978; Mayer et al. 1953). Administration of leptin decreases their food intake and reduces body weight and body fat, indicating that leptin regulates appetite (Halaas et al. 1995; Pelleymounter et al. 1995). *Ob/ob* mice develop steatosis, but they do not develop NASH under normal conditions. However, LPS treatment of *ob/ob* mice triggers the progression of steatosis to steatohepatitis (Faggioni et al. 1999; Yang et al. 1997). Importantly, *ob/ob* mice are resistant to fibrosis, which characterizes leptin as a potential contributor to hepatic fibrogenesis (Leclercq et al. 2002). Thus, the *ob/ob* mouse model reflects the metabolic syndrome and simple steatosis that is observed in humans. Even though it cannot be used to study the complete progression from simple steatosis to fibrosis/cirrhosis, the *ob/ob* mouse model is useful when investigating the effect of lipid accumulation on hepatocytes functionality as well as the progression from steatosis to steatohepatitis.

1.4.2 The leptin resistant *db/db* mouse model

In contrast to the *ob/ob* mouse model, *db/db* mice produce leptin, but due to a mutation of their leptin receptor gene they are resistant to leptin (Chen et al. 1996). This autosomal recessive mutation that leads to diabetes, hyperinsulinemia as well as obesity was first observed in 1966 (Hummel et al. 1966). Similar to the *ob/ob* mice, *db/db* mice develop simple steatosis without progression to NASH when fed a standard diet. A methionine-choline deficient diet (MCD) induces hepatic inflammation and fibrosis in *db/db* mice (Sahai et al. 2004). This genetic mouse model, like the *ob/ob* mouse model, exhibits features of the human metabolic syndrome, and similar to the *ob/ob* mouse model, is a good tool to study simple steatosis. Upon the administration of an appropriate trigger, it is possible to study the progression to NASH including fibrosis.

1.4.3 High fat diet induced NAFLD

High fat diet (HFD) models reflect the human situation of obesity due to increased dietary supply of fat and carbohydrates that stimulate hepatic fatty acid uptake or *de novo* synthesis (Anstee and Goldin 2006). The composition of the diets varies, but most of the calories come from fat (usually 45 - 75%), which is sufficient to increase obesity, insulin resistance and hepatic steatosis (Schattenberg and Galle 2010). In addition, the strain, sex and age of the mouse all have an impact on the success of the HFD-induced obesity (Nishikawa et al. 2007; West et al. 1992). Male C57Bl6 mice on a HFD show hepatocytes ballooning, decreased adiponectin levels and hyperglycaemia after 16 weeks on the diet (Eccleston et al. 2011). Fifty weeks on the HFD result in steatohepatitis as well as slight fibrosis and hyperinsulinemia in male C57Bl6 mice (Ito et al. 2007). In conclusion, although HFD models require more time to obtain the required phenotype, they more accurately represent the human NAFLD.

1.5 Association between the metabolic syndrome and kidney stones

NAFLD is strongly associated with obesity (Bedogni et al. 2005), insulin resistance (Marchesini et al. 1999) and in general with the metabolic syndrome (Marchesini et al. 2001). Apart from liver-related diseases, NAFLD patients have an increased risk for other diseases. For example, the prevalence as well as incidence of cardiovascular diseases are higher in patients suffering from NAFLD (Targher et al. 2010), and there is a strong association between the severity of NAFLD and an increased risk of chronic kidney disease (Musso et al. 2014).

Introduction

Previous studies have suggested that the development of kidney stones is related to both the metabolic syndrome and traits of the metabolic syndrome in humans. Obesity, in particular visceral obesity, is strongly associated with an elevated risk of kidney stone formation (Akarken et al. 2015; Taylor et al. 2005). Moreover, an increased body mass index in the presence of hypertension is related to an increased risk of calcium oxalate stones (Polat et al. 2015). Conversely, Torricelli and colleagues reported a link between dyslipidaemia and a risk of kidney stones that is independent of obesity and other components of the metabolic syndrome (Torricelli et al. 2014). Interestingly, increasing BMI have a marked impact on the urinary composition; in particular, the kidney stone promotors oxalate and uric acid are increased (Negri et al. 2008; Shavit et al. 2015; Taylor and Curhan 2006). Both overweight and obese men and women are strongly associated with an increased risk of calcium oxalate stones, but overweight and obese men are more prone to stone formation than overweight women (Siener et al. 2004). Overall, the metabolic syndrome as a whole is accompanied by an increased risk of developing kidney stone disease (Jeong et al. 2011; Sakhaee et al. 2012), and the more traits of the syndrome that are present, the greater the risk (Kohjimoto et al. 2013; West et al. 2008).

The renal stone composition of patients with metabolic syndrome was found to be mainly calcium oxalate; not surprising since most kidney stones usually consist of calcium oxalate (Kadlec et al. 2012). Recently, a direct association between NAFLD and urolithiasis was reported (Einollahi et al. 2013; Nam et al. 2016). The frequency of kidney stones in NAFLD patients was 19% higher than in those patients without NAFLD supporting NALFD as risk factor for renal stone formation (Nam et al. 2016).

One study suggests that the severity of type II diabetes is an important risk factor for the development of kidney stones/of kidney stone disease (Weinberg et al. 2014). However, there is currently no known molecular link that could be responsible for the increased prevalence of kidney stone disease with regard to the metabolic syndrome and NAFLD.

1.6 Glyoxylate metabolism in mammals

Recently, glyoxylate was identified as a plasma marker for type II diabetes, even before a diabetes diagnosis (Nikiforova et al. 2014). Glyoxylate is a highly reactive aldehyde of the intermediary metabolism that is generated mainly from glycolate, hydroxyproline and glycine in humans; oxidation of glyoxylate results in oxalate - a metabolic end product in mammals that is excreted *via* the kidneys (Salido et al. 2012). Endogenous oxalate synthesis mainly occurs in the liver (Holmes and Assimos 1998), but also erythrocytes were identified as small source of oxalate (Knight et al. 2016). The oxidization of glyoxylate is mainly catalysed by lactate dehydrogenase (LDH, Figure 1.3), which is abundant in the cytosol (Salido et al. 2012).
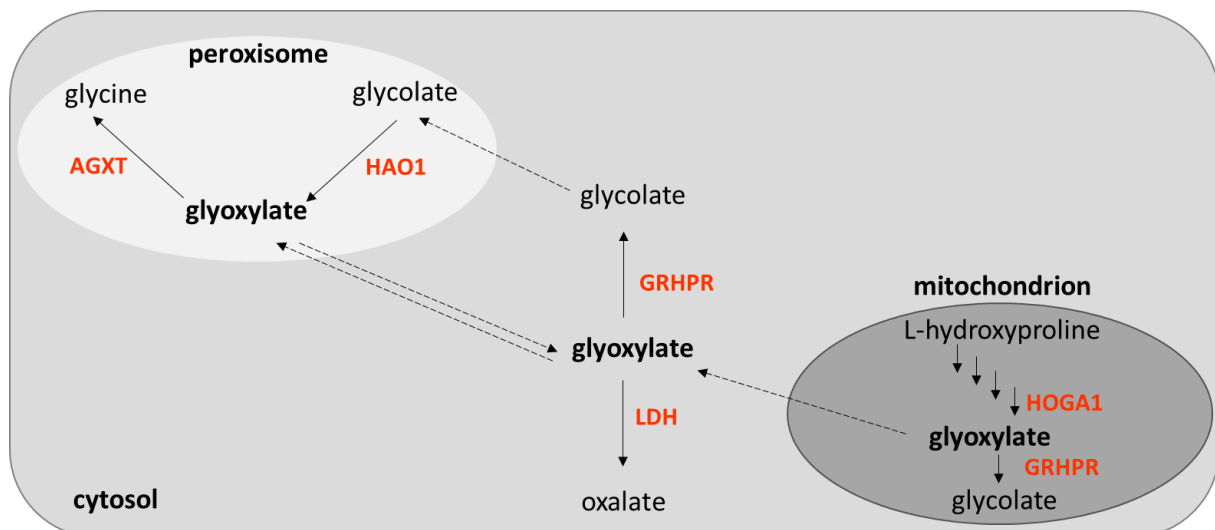
Figure 1.3: Simplified illustration of the production and metabolism of glyoxylate in hepatocytes. Figure does not cover the entire glyoxylate metabolism.

To limit oxalate production, the endogenous glyoxylate synthesis proceeds within peroxisomes and mitochondria. Within peroxisomes, glyoxylate can be produced from glycine, a reaction catalysed by D-amino acid oxidase, or from glycolate *via* hydroxyacid oxidase 1 (HAO1) (Salido et al. 2012). However, the peroxisome can also import glyoxylate from the cytosol and mitochondria since its membrane is permeable to small mono- and divalent anions, such as glycolate and glyoxylate, especially due to the channel-forming protein PXMP2 (Rokka et al. 2009).

The peroxisomal detoxification of glyoxylate is catalysed by the alanine-glyoxylate aminotransferase (AGXT). This enzyme is abundant in hepatic peroxisomes and tolerates high glyoxylate concentrations without reduced or inhibited forward reaction (Cellini et al. 2007).

Introduction

In mitochondria, the precursor of glyoxylate is hydroxyproline, which is metabolized *via* four enzymatic reactions to glyoxylate and pyruvate (Adams and Frank 1980). The endogenous source of hydroxyproline arises from collagen turnover, since hydroxyproline is not reused for collagen synthesis, but newly produced by the posttranslational modification of proline during its biosynthesis (Salido et al. 2012). The daily release of hydroxyproline upon collagen turnover is estimated at 240 – 420 mg, and leads to a daily formation of 140 – 240 mg glyoxylate (Knight et al. 2006). Dietary collagen represents an exogenous source of hydroxyproline (Phang et al. 2001). Apart from the peroxisomal AGXT, the cytosolic and mitochondrial glyoxylate reductase/hydroxypyruvate reductase (GRHPR) is able to detoxify glyoxylate to glycolate in order to limit the oxalate production (Figure 1.3, Salido et al. 2012).The detoxification of glyoxylate and the limitation of oxalate formation are important since dysfunction of these processes can have severe outcomes such as primary hyperoxalurias as summarized below.

Primary hyperoxalurias (PH) are rare inborn disorders of glyoxylate metabolism that lead to an excessive production of oxalate, which cause recurrent urolithiasis and nephrocalcinosis that injure the kidneys and can result in end stage kidney disease (ESKD) (Hoppe et al. 2009). The prevalence of PH is estimated to be 1 to 3 persons per million with an incidence rate of 1 per 100,000 live birth each year in Europe (Cochat et al. 1995; Kopp and Leumann 1995; Woerden van et al. 2003). However, the estimated number of cases might be higher due to under diagnosis. There are three different types of PH. The most prevalent is PH1, which represents around 80% of all primary hyperoxaluria cases; the remaining 20% are diagnosed with either primary hyperoxaluria type 2 (PH2) or type 3 (PH3) (Salido et al. 2012). PH1 results from the inefficient and/or defective detoxification of glyoxylate by AGXT due to mutations in the *AGXT* gene (see section 1.7). PH2, like PH1, is an autosomal recessive disorder caused by mutations in the *GRHPR* gene, encoding the enzyme GRHPR (Cramer et al. 1999). More than 50 mutations are known that lead to the loss of protein expression or loss of protein activity of GRHPR [1]. A result of the defective or inefficient GRHPR function is the accumulation of glyoxylate and hydroxypyruvate in the cytosol, which are converted to oxalate and glyceric acid by LDH (Hoppe et al. 2009). The increased oxalate levels cause recurrent nephrolithiasis and less frequently nephrocalcinosis. Overall, the outcome of PH2 is not as severe as for PH1 and the disease rarely progresses to ESKD (Hoppe et al. 2009; Milliner et al. 2001; Salido et al. 2012). PH3 was more recently identified and develops due to mutations in the *HOGA1* gene (Belostotsky et al. 2010). *HOGA* encodes the mitochondrial enzyme 4-hydroxy-2-oxoglutarate

aldolase (HOGA1), which catalyses the last step of the hydroxyproline breakdown by cleaving 4-hydroxy-2-oxoglutarate into glyoxylate and pyruvate (Adams and Frank 1980). To date, more than 40 mutations in *HOGA1* gene are reported [1]. It was suggested that in the absence of functional HOGA1, cytosolic aldolases transform 4-hydroxy-2-oxoglutarate into glyoxylate (Monico et al. 2011). Hitherto, there are no reports of ESKD arising from PH3, but there is evidence that PH3 becomes more frequent than PH2 (Salido et al. 2012). In addition to PH, secondary hyperoxaluria has also been reported, which is not due to genetic disorders. Instead, the high oxalate concentration observed in secondary hyperoxaluria can be the result of i) increased intake of oxalate rich diet or the abuse of oxalate precursors like vitamin C or ethylene glycol, ii) intestinal malabsorption due to chronic diseases, such as chronic inflammatory bowel disease or cystic fibrosis, iii) increased gut bacteria production, and iv) unknown reasons (Hoppe et al. 2003; Lorenzo et al. 2014).

1.7 Alanine-glyoxylate aminotransferase

The alanine-glyoxylate aminotransferase (AGXT; EC 2.6.1.44) catalyses the transamination of glyoxylate to glycine using alanine as amino group-donor (see Figure 1.4). During this project, a lipid-dependent transcriptional downregulation of AGXT was found, which prompted the further investigation of the enzyme.
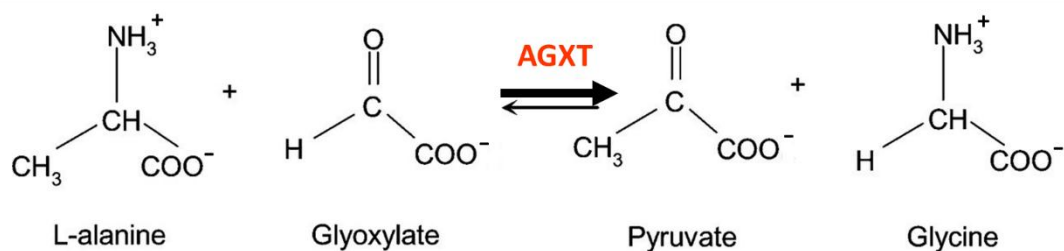
Figure 1.4: Enzymatic reaction catalysed by AGXT. Glyoxylate receives an amino group from alanine and pyruvate and glycine are produced. AGXT catalysed reaction is shifted to the products (Cellini et al. 2007).

There are two isoenzymes known, namely AGXT1 and AGXT2, which were identified in rat liver approximately 40 years ago, and are localized in different cellular compartments (Noguchi et al. 1978). AGXT2 is found primarily in mitochondria; whereas, the cellular localization of AGXT1 is dependent on the species (Takada and Noguchi 1982). Even though AGXT1 and AGXT2 share the above-mentioned transamination reaction, AGXT1 is mainly responsible for glyoxylate detoxification (Rodionov et al. 2014). The intracellular distribution of AGXT1 is evolutionary dependent on the species' diet and the major site of glyoxylate production

(Birdsey et al. 2004). Herbivores' dietary precursor of glyoxylate is glycolate, which is oxidized in the peroxisome to glyoxylate. Therefore, AGXT1 is peroxisomal in herbivores. In contrast, the major source of glyoxylate in carnivores is hydroxyproline that is metabolized to glyoxylate within the mitochondria. Thus, in carnivores, AGXT1 is localized to the mitochondria. In omnivores (e.g. rodents), AGXT1 is located within the peroxisomes as well as in the mitochondria. In most humans, AGXT1 is located primarily in the peroxisomes if not mistargeted to the mitochondria by mutations (Birdsey et al. 2004; Danpure 1997). Since AGXT1 plays the major role in glyoxylate metabolism, it is hereafter referred to as AGXT.

AGXT is a homodimeric enzyme composed of two units with 392 amino acid residues, and each monomer binds its cofactor pyridoxyl-5'-phosphate (PLP) *via* a Schiff base (Zhang et al. 2003). In humans, the C-terminal of this protein contains a KKL type 1 peroxisomal targeting sequence type 1 (PTS1) that ensures the import of AGXT in peroxisomes *via* PTS1 receptor Pex5p (Motley et al. 1995). AGXT is encoded by the *AGXT* gene in humans and its coding sequence consists of eleven exons spread over 10 kB on chromosome 2q36-37 (Purdue et al. 1991). Mutations of the gene resulting in a non-functional or mistargeted AGXT lead to the disease primary hyperoxaluria type 1 (PH1), first described in 1986 (Danpure and Jennings 1986). So far, more than 200 mutations of *AGXT* are known that cause PH1 [1].

1.8 Calcium oxalate deposits in kidneys

Mutations in the *AGXT* gene as well as traits of the metabolic syndrome increase the risk for calcium oxalate kidney stone formation, as described above in sections 1.5 and 1.6. The prevalence of kidney stones in the USA is approximately 8.8%, with men more prone to developing kidney stones than women (10.6% vs 7.1%), and obese individuals having a higher incidence of kidney stones compared to normal weight persons (11.2% vs 6.1%) (Scales et al. 2012). Compared to 1994, the prevalence of kidney stones increased in both genders (men: 6.3%, women: 4.1% (Stamatelou et al. 2003). Approximately 80% of the kidney stone consist of calcium oxalate and calcium phosphate (Coe et al. 2005).

There are several mechanisms that potentially play a role in the development of calcium kidney stones, but urinary concentrations of calcium and/or oxalate are important factors (Evan 2010). The average daily excretion amount of oxalate ranges from 30 to 44 mg/d, with men excreting slightly higher amounts; urinary oxalate values equal or above 45 mg/d, corresponding to 500 μmol/d, are considered to be hyperoxaluric (Curhan et al. 2001). With

respect to body surface area, normal oxalate excretion is below 450 µmol/1.73 m² per day and hyperoxaluria is defined when more than 500 µmol/1.73 m² oxalate per day is excreted (Salido et al. 2012). The stone formation relies on the supersaturation of salts. This occurs when salt concentration of a solution is that high that it changes to the solid phase and precipitates. This situation in turn can be due to low urine volume or excessive excretion of oxalate, calcium or both ions (Evan 2010). Within the nephron, the functional subunit of the kidney, the concentrations of calcium and oxalate varies due to the reabsorption of water. As suggested by Robertson, the concentration of calcium and oxalate are highest in the descending limb of the loop of Henle within the nephron, and leading to the formation of calcium oxalate crystals. In addition, supersaturation of calcium and oxalate can also occur in the collection duct of the kidney due to final adjustment of water in the urine (Robertson 2004). A schema of a nephron is depicted below (Figure 1.5).
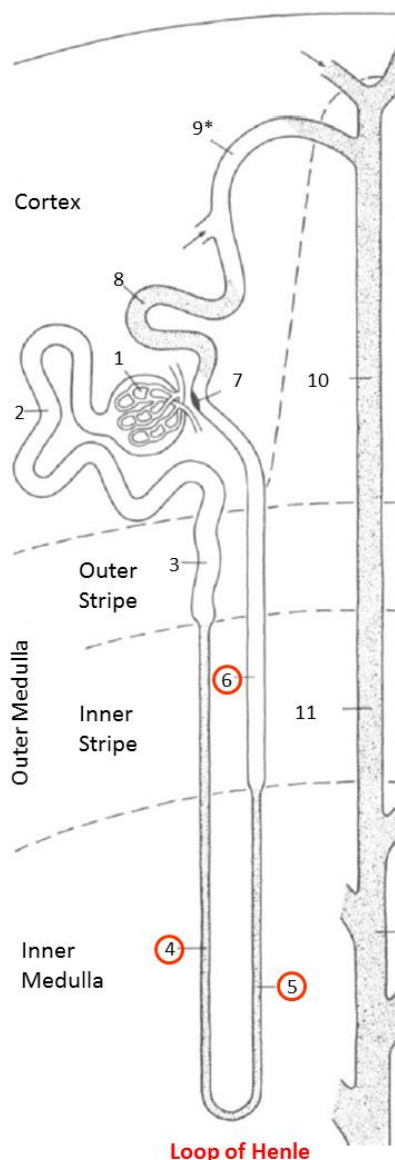
Altogether, this shows that metabolites excreted by the liver, e.g. oxalate, can affect the physiology of other organs, e.g. the kidney

Figure 1.5 Schema of a nephron. This scheme depicts a long-looped nephron together with the collecting system. 1 = Renal corpuscle including Bowman's capsule and the glomerulus; 2 = Proximal convoluted tubule; 3 = Proximal straight tubule; 4 = Descending thin limb; 5 = Ascending thin limb; 6= Distal straight tubule (thick ascending limb); 7 = Macula densa located within the final portion of the thick ascending limb; 8 = Distal convoluted tubule; 9* = Connecting tubule of the juxtamedullary nephron that forms an arcade; 10 = Cortical collecting duct; 11 = Outer medullary collecting duct; 12 = Inner medullary collecting duct (Kriz and Bankir 1988)**.**

1.9 Aim of the work

NAFLD is a common liver disorder worldwide that is strongly associated with the metabolic syndrome, comprising obesity, insulin resistance, hypertension and dyslipidaemia. The pathogenesis of NAFLD is still incompletely understood, and in addition to an elevated risk of disease progression, NAFLD has systemic consequences, such as cardiovascular disease and chronic kidney disease. Fat accumulation in the liver may compromise hepatic metabolic functions, which in turn may not only affect the liver itself but also impact other organs.

The major aim of the current project was to understand metabolic alterations upon lipid accumulation in the liver. For this purpose, the leptin deficient *ob/ob* mouse model was investigated and an *in vitro* model of steatosis was established to study the direct impact of lipid accumulation on the normal function of hepatocytes. Moreover, genome-wide gene expression alterations were explored to allow the identification of deregulated genes both in mouse and in human NAFLD. Affymetrix gene array analysis was performed from the *ob/ob* mouse and gene expression data from human NAFLD patients were obtained from publically available datasets. These datasets were the main components of a pipeline to identify steatosis-associated genes across species. Additionally, Affymetrix gene array analysis of the *in vitro* steatosis model was performed and integrated into the aforementioned pipeline.

Based on this genomic approach, potentially interesting genes among the identified deregulated genes were selected for further studies. After validation of the observed gene expression alterations in additional and independent models, consequences of gene deregulation for liver metabolism were explored.

Among the selected genes, the alanine-glyoxylate aminotransferase (*AGXT*) was found to be downregulated in mouse and human NAFLD and upon lipid accumulation *in vitro*. This liver-specific enzyme plays a crucial role in glyoxylate detoxification, catalysing its conversion to glycine and avoiding excessive generation of oxalate. Downregulation of AGXT in the steatotic liver has not been described so far and may represent a risk factor for oxalate kidney stone formation in NAFLD. Therefore, the second part of this work focused on exploring the hypothesis that the downregulation of AGXT upon hepatic lipid accumulation represents the molecular link between NAFLD and calcium oxalate deposits in kidneys (Figure 1.6).
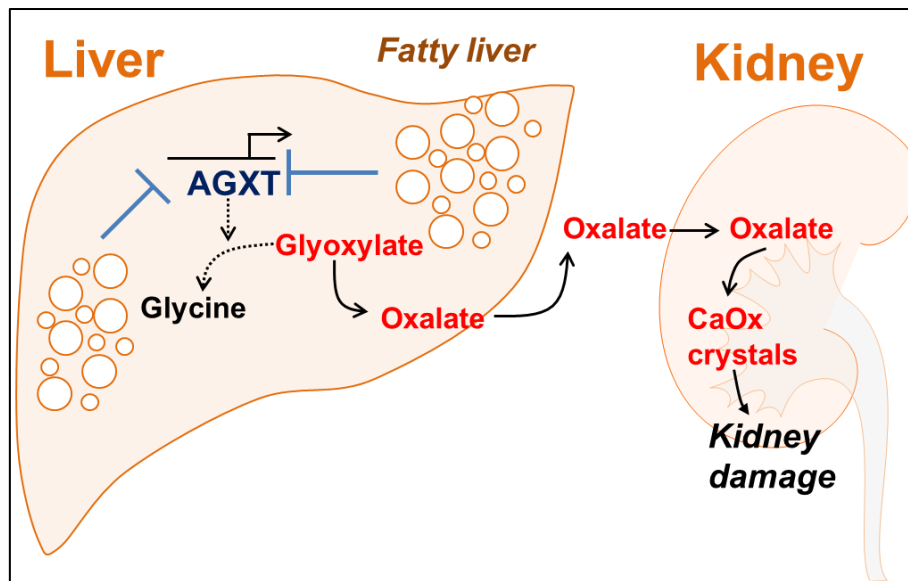
Figure 1.6: Illustration of working hypothesis. Hepatic steatosis leads to downregulation of AGXT, which in turn impairs glyoxylate detoxification and ultimately might result in high urinary oxalate levels, increasing the risk for kidney stones.

2. Materials and Methods

2.1 Material

2.1.1 Technical equipment

Table 2.1: Equipment

Equipment	Company
Autosampler MPS-2	Gerstel
Balance	EW, Kern
Bunsen Burner	IBS Fireboy Plus, Integra Biosciences
Blot imager Vilber Fusion Fx7	Vilber Lourmat
Casy cell Counter	Roche
Centrifuge with cooling function	Biofuge Fresco, Heraeus
Centrifuge with cooling function 5424R	Eppendorf
Centrifuge MiniSpin plus	Eppendorf
Concentrator Plus	Eppendorf
Confocal microscope (LSM)	FV1000 Olympus
CO_2 incubator	Binder
Electrophoresis unit Mini-PROTEAN®	BioRad
Electrophoresis unit SE260	Höfer
EVOQ™ Elite Triple Quadrupole	Bruker
Fume hood	Waldner
GC column DB-5MS, 25 m x 0.25 mm x 0.25µm	Agilent
GC-MS system GC 6890, MS 5973N	Agilent
LC system 1100er series	Agilent
LC Column: Hi-Plex-H (300 × 6.5 mm, 8 µm)	Agilent
Magnetic stirrer IKAMAG RCT	Ikamag
Microscope BX41	Olympus
Microscope eclipse TS 100	Nikon
Microscope Primo Vert	Zeiss, Software ZEN from Zeiss
Microwave oven	Bosch
MiSeq	Illumina
Modular tissue embedding center	Thermo Fisher Scientific
NanoDrop ND-1000	Thermo Fisher Scientific
NMR-Spektrometer Avance III (600 MHz)	Bruker
pH meter	Schott
Pipets (10 µL, 2 µL, 100 µL, 200 µL, 1 ml, 5 ml)	Eppendorf
Pipet boy	Integra
Plate reader infinite M200 Pro	Tecan
Power pack HC	BioRad
Power pack P25T	Biometra
Precision balance EW150-3M	Kern
Precision balance ME235P	Sartorius
qPCR system ABI 7500	Applied Biosystems

Rocking Platform	VWR
Shaker KS 260 basic	IKA
Slide drying oven TDO Sahara	Medite
Sliding Microtome HM 450	Microm
Sonicator sonoplus mini	Bandelin
Spin Tissue Processor STP 120	Thermo Fisher Scientific
Sterile hood	Hereaus
Thermo cycler Tgradient	Biometra
Thermomixer	Eppendorf
Thermo shaker PHMT Grant-bio	Keison
Thermo shaker	peqlab
Transfer chamber fast blot B44	Biometra
Transfer chamber Trans-Blot SD	BioRad
Vacuum pump	Vacuubrand
Vortex-Genie2	Bender & Hobein
Water purification system Maxima Ultrapure Water	ELG
Water bath	Labortechnik

2.1.2 Consumables

Table 2.2: Consumables

Consumables	Company
Cell scraper (25 mm)	Sarstedt
Cover slips	VWR
Embedding cassettes	Carl Roth
Freezing container (Mr. Frosty)	Thermo Fisher Scientific
GeneChip® Human Genome U133 Plus 2.0 array	Affymetrix
GeneChip® Mouse Genome 430 2.0 Array	Affymetrix
Glass inserts, 200µL	VWR
Glass vials (1.5 ml -4 ml)	VWR
Metabolic cage for single mouse	Tecniplast
MicroAmp® Optical Adhesive Film	Thermo Fisher Scientific
MicroAmp® Optical 96-Well Reaction Plate	Thermo Fisher Scientific
Microscope slide SuperFrost Plus	Thermo Fisher Scientific
Minisart® syringe filters (0.45 µM)	Sartorius
Needle 26G	BD bioscience
NuPAGE®4 – 12% Bis-Tris	Thermo Fisher Scientific
Pestle and Microtube	VWR
Pipets	Eppendorf
Pipet tips (filtered/not filtered)	Sarstedt
PVDF Membrane	Perkin Elmer
RNase-free Microfuge Tubes 1.5 ml	Thermo Fisher Scientific
Reaction tubes (0.5 - 50 ml)	Sarstedt
Screw cap with septum	VWR

Materials and Methods

Serological pipets (5 ml, 10 ml, 25 ml)	Sarstedt
Syringe 1 ml	BD bioscience
Tissue culture flasks (75 cm², 175 cm²)	Sarstedt
Tissue culture plates (6-, 12-, 24, 96-well format)	Sarstedt
96-Well plates black	GreinerBio
96-Well plates transparent	Sarstedt
Whatman-Paper 3mm	VWR

2.1.3 Chemicals and dyes

Table 2.3: Chemicals and dyes

Chemicals/dyes	Company
Acetic acid	Carl Roth
Ammonium persulfate	Sigma-Aldrich
Bafilomycin A	Sigma-Aldrich
Bodipy (493/503)	Thermo Fisher Scientific
Bovine serum albumin (BSA)	Carl Roth
Bovine serum albumin (BSA), fatty acid free	Sigma-Aldrich
Bromphenol blue	Carl Roth
Calcium chloride	Carl Roth
Chloroform	Carl Roth
Citric acid monohydrate	Carl Roth
Collagenase from Clostridium hystolyticum	Sigma-Aldrich
p-Coumaric acid	Sigma-Aldrich
Creatinine hydrochlorid	Sigma-Aldrich
4',6-diamidino-2-phenylindole (DAPI)	Thermo Fisher Scientific
Dimethyl sulfoxide (DMSO)	Sigma-Aldrich
Dithiothreitol (DTT)	Sigma-Aldrich
Triethylene glycol diamine tetraacetic acid (EGTA)	Carl Roth
Entellan®	Merck
Eosin Y disodium salt	Sigma-Aldrich
Ethanol, absolute	Carl Roth
Ethylenediaminetetraacetic acid (EDTA)	Carl Roth
Fetal Calf serum (FCS) Sera Plus	Pan-Biotech
FluorPreserve reagent	Calbiochem
Glucose	Carl Roth
L-Glutamine	Sigma-Aldrich
Glycerol	Carl Roth
Glycine	Carl Roth
Helium 5.0	Air Products
HEPES	Carl Roth
Hydrochloric acid 32%	Carl Roth
Hydrogen peroxide 30%	Merck
L-Hydroxyproline	ApplChem

Luminol	Sigma-Aldrich
Magnesium chloride	Carl Roth
Magnesium sulphate	Sigma-Aldrich
Methanol, HPLC grade	Carl Roth
Methyl-*tert*-butyl ether (MTBE)	Merck
Nonidet P-40 substitute (NP-40)	Roche
N-tert-Butyldimethylsilyl-N-methyltrifluoroacetamide (MTBSTFA)	Sigma-Aldrich
Oil Red O	Sigma-Aldrich
Oleic acid	Sigma-Aldrich
Oxalic acid (1,2-13C2, 99%)	Cambridge Isotope Laboratories, Inc.
Paraffin Histowax Surgipath paraplast	Leica
Paraformaldehyde 4% (PFA)	Carl Roth
Picric acid	Sigma-Aldrich
Potassium chloride	Carl Roth
Potassium dihydrogen phosphate	Carl Roth
2-Propanol	Carl Roth
Rhodamine Phalloidin conjugate	Thermo Fisher Scientific
Rotihistol®	Carl Roth
SDS pellets	Carl Roth
Sodium chloride	Carl Roth
Sodium deoxycholate	Carl Roth
Sodium glycolate	Thermo Fisher Scientific
Sodium glyoxylate monohydrate	Sigma-Aldrich
Sodium hydrogen phosphate	Carl Roth
Sodium hydroxide pellets	Carl Roth
Tetramethylethylenediamine (TEMED)	Carl Roth
Toluene	VWR
Trioctylphosphine oxide (TOPO)	Sigma-Aldrich
Tris	Carl Roth
Tris-HCl	Carl Roth
TritonX-100	Sigma-Aldrich
Tween20	Sigma-Aldrich
Tween80	Sigma-Aldrich
Vinblastine sulphate	Sigma-Aldrich
Xylol	VWR

2.1.4. Commercial buffers and reagents

Table 2.4: Commercial buffers and reagents

Buffer/reagent	Company
Acrylamide (30% (v/v))	Carl Roth
Amino acid solution	PAN-Biotech
Anode-/Cathode-buffer concentrate A & K	Carl Roth

Materials and Methods

Diethylpyrocarbonate treated (DEPC) water	Thermo Fisher Scientific
Duotrol® urine liquid level1 & 2	Biomed Labordiagnostik GmbH
Ketamine 100 mg/ml	Ratiopharm
Mayer's haemalaun solution	Merck
NuPAGE® MES SDS Running Buffer (20X)	Thermo Fisher Scientific
Phosphatase-Inhibitor-Cocktail II&III	Sigma-Aldrich
Precision Plus Protein Dual Colour standards	BioRad
Protease-Inhibitor-Cocktail	Sigma-Aldrich
QIAzol Lysis-Reagent	Qiagen
Rompun 2%	Bayer Health Care
Taqman Universal PCR Master Mix	Thermo Fisher Scientific

2.1.5 Prepared buffers and reagents

Table 2.5: Prepared buffers and reagents for gel electrophoresis and Western blotting

Buffer	Compounds	Concentration
Anode buffer	Buffer concentrate A	10%
	Methanol	20%
	in ultrapure water	
APS solution	Ammonium persulfate	10% (w/v)
	in ultrapure water	
Blocking solution	BSA	5% (w/v)
	in TBS-T	
Cathode buffer	Buffer concentrate K	10%
	Methanol	20%
	in ultrapure water	
Chemiluminescent solution	Luminol	2.5 mM
	p-Coumaric acid	0.2 mM
	in 0.1 M Tris	
Loading buffer (5x)	Bromophenol blue	0.05% (w/v)
	DTT	0.25 M
	Glycerol	50% (v/v)
	SDS	5% (w/v)
	Tris-HCl	0.225 M
PBS (10x)	KCl	27 mM
	KH_2PO_4	18 mM
	Na_2HPO_4	100 mM
	NaCl	1.37 M
	in ultrapure water,	
RIPA buffer	Tris-HCl	50mM (pH 7.5)
	NaCl	150 mM
	NP-40	1%
	Sodium deoxycholate	0.5%
	SDS	0.5%

Running buffer (10x)	Glycine	1.92 M
	SDS	1% (w/v)
	Tris	0.25 M g
	in ultrapure water, pH 8.3	
SDS solution	SDS	10% (w/v)
	in ultrapure water	
Separation buffer	Tris	3 M
	in ultrapure water,	
	pH adjusted to 8.8	
Stacking buffer	Tris	0.47 M
	in ultrapure water,	
	pH adjusted to 6.8	
Stripping buffer	Glycine	0.2 M
	SDS	0.1% (w/v)
	Tween 20	1% (v/v)
	in ultrapure water,	
	pH adjusted to 2.2	
TBS (10x)	NaCl	1.5 M
	Tris	0.5 M
	in ultrapure water, pH adjusted to 7.4	
TBS-T	10x TBS	10% (v/v)
	Tween20	0.1% (v/v)

Table 2.6: Prepared buffers for IHC

Buffer	Compounds	Concentration
Citrate buffer	Citrate 1xH$_2$O	0.01 M
	In ultrapure water, pH adjusted to 6	
Haematoxylin	Mayer's haemalaun	20% (v/v)
	In ultrapure water	

Table 2.7: Prepared buffers for perfusion

Buffer	Compounds	Amount
Collagenase buffer	Amino acid solution	30 ml
	CaCl$_2$ solution (19 g/l CaCl$_2$* 2 H$_2$O)	10 ml
	Collagenase Type 1	100 mg
	Glucose solution (9 g/l)	155 ml
	Glutamine (7 g/ml)	2.5 ml
	HEPES (60 g/l) (pH 8.5)	25 ml
	KH buffer	25 ml
EGTA buffer	Amino acid solution	60 ml
	EGTA solution (47.5 g/l)	1.6 ml
	Glucose solution (9 g/l)	248 ml
	Glutamine (7 g/l)	4 ml

Materials and Methods

	HEPES (60 g/l) (pH 8.5)	30 ml
	KH buffer	30 ml
KH buffer	KCl	1.75 g
	KH_2PO_4	1.6 g
	NaCl	60 g
	Filled to 1 l with ultrapure water	
	Adjust pH to 7.4	
Suspension buffer	Albumin Fraction V	400 mg
	Amino acid solution	30 ml
	$CaCl_2$ solution (19 g/l $CaCl_2$* 2 H_2O)	1.6ml
	Glucose solution (9 g/l)	124 ml
	Glutamine (7 g/ml)	2 ml
	HEPES (60 g/l) (pH 7.6)	20 ml
	KH buffer	20 ml
	$MgSO_4$ solution (24.6 g/l $MgSO_4$ * 7 H_2O)	0.8 ml

Table 2.8: Commercial assays and kits

Kits	Company
BCA Protein assay	Thermo Fisher Scientific
CellTiter-Blue® assay	Promega
DAB Peroxidase substrate kit	Vector Laboratories
High-Capacity cDNA Reverse Transcription Kit	Thermo Fisher Scientific
Triglyceride quantification assay	Abcam
VECTASTAIN Elite ABC Kit (rabbit)	Vector Laboratories
Von Kossa Kit	Abcam

2.1.6 Cell lines

HepG2 cells

This adherent cell line was derived from liver tissue of a 15–year-old male Caucasian who suffered from a well-differentiated hepatocellular carcinoma in 1983. It was purchased from ATCC (product: ATCC®HB-8065™).

Huh7 cells

The Huh7 cell line was generated from a well differentiated hepatocellular carcinoma of a 57-year-old Japanese male in 1982 (Nakabayashi et al. 1982). This cell line was a gift from an internal collaboration partner.

For cell line authentication, a frozen aliquot of each cell line was sent to the Leibniz institute DSMZ-German Collection of Microorganisms and Cell Cultures. The identity was confirmed for both cell lines.

2.1.7 Cell culture reagents

Table 2.9: Medium and additives

Cells/cell lines	Medium	Company
Primary mouse hepatocytes	William's E medium	PAN -Biotech
	+ Dexamethasone (100 nM)	Sigma-Aldrich
	+ Gentamycin (10 µg/ml)	PAN-Biotech
	+ Insulin (ITS) 100x (2 ng/ml)	Sigma-Aldrich
	+ Penicillin/Streptomycin(100 U/ml)	PAN-Biotech
	+ Stable L- Glutamine (2 mM)	PAN-Biotech
	(+ Sera plus 10% for attaching)	PAN-Biotech
HepG2	Dulbecco's Modified Eagle Medium (DMEM), 4.5 g/l Glucose	PAN-Biotech
	+ Sera Plus (10%)	PAN-Biotech
	+ Penicillin/Streptomycin (100 U/ml; only for cultivation, not during experiments)	PAN-Biotech
Huh7	Dulbecco's Modified Eagle Medium (DMEM), 4.5 g/l Glucose	PAN-Biotech
	+ Sera Plus (10%)	PAN-Biotech
	+ Penicillin/Streptomycin (100 U/ml; only for cultivation, not during experiments)	PAN-Biotech

Table 2.10: Additional cell culture supplies

Reagents	Company
Acetic acid glacial	Carl Roth
Casyton	Roche
Collagen rat tail lyophilised	Roche
DMEM10x, 1 g/l glucose	PAN-Biotech
DMSO	Sigma-Aldrich
Collagen rat tail lyophilised	Roche
Lipofectamine RNAiMAX	Life technologies
OptiMEM	Life technologies
10xPBS	See Table 2.5
Trypan blue	Sigma-Aldrich
Trypsin 0.05% EDTA	Pan-Biotech

2.1.8 Laboratory mice

Table 2.11: Mice

Mouse	Gender	Age at arrival	Company
Lep^{ob}/Lep^{ob} & Lep^{ob}/+ Lepr^{db}/Lepr^{db} & Lepr^{db}/+, C57BL/6N	male	8 weeks	Janvier labs

Table 2.12: Mouse feed

Reagents	Company
Pellet standard diet R/M-H 10-mm	Ssniff
Powder standard diet R/M-H	Ssniff
Western diet (containing 45% kcal fat, 20% kcal fructose and 2% cholesterol)	Research Diets Inc., Catalogue-number D09100301

2.1.9 Antibodies

2.1.9.1 Primary antibodies

Table 2.13: Primary antibodies for Western blotting and immunohistochemistry

Antibody	Host	Cat#/Company
anti Agxt	Rabbit	HPA035370, Sigma-Aldrich
anti LC3	Rabbit	#2775, Cell signalling
anti p62	Mouse	ab56416, Abcam
anti glutamine-synthetase	Rabbit	G2781, Sigma-Aldrich
anti α-Tubulin	Mouse	sc-8035, Santa Cruz

Table 2.14: Primary antibodies for immunofluorescence

Antibody	Host	Cat#/Company
anti DPPIV	Goat	AF954, R&D systems
anti α-Tubulin	Mouse	T9026, Sigma-Aldrich

2.1.9.2 Secondary antibodies

Table 2.15: Secondary antibodies for Western blotting

Antibody	Host	Cat#/Company
anti mouse HPR linked	Horse	#7076, Cell Signaling
anti rabbit HPR linked	Goat	#7074, Cell Signaling

Table 2.16 Secondary antibodies for immunofluorescence

Antibody	Host	Cat#/Company
anti goat Alexa fluor® 647	Donkey	#705606147, Jackson Immuno Research
anti mouse Alexa fluor® 647	Donkey	#715606151, Jackson Immuno Research

2.1.10 Taqman gene expression assays

Table 2.17: Taqman gene expression assays (Thermo Fisher Scientific)

Target gene	Mouse	Human
Agxt	Mm00507980_m1	Hs00163584_m1
Eif2a	Mm01289723	
Gapdh	4352932E	4352934E
Grhpr	Mm00519119_m1	Hs00201903_m1
Hao1	Mm00439249_m1	Hs00213909_m1
UBC		Hs00824723_m1

2.1.11 Small interfering RNA (siRNA)

Table 2.18: Small interfering RNA

Target	Assay ID	Company
AGXT	s1189	
AGXT	s223463	Thermo Fisher Scientific
AGXT	s223464	
Non sense (control)	AM4635	

2.2 Methods

2.2.1 Cultivation of cell lines

HepG2 cells and Huh7 cells were incubated under sterile conditions at 37 °C and 5% CO_2. The atmosphere was saturated with aqueous vapour. Both cell lines were cultured in Dulbecco's modified eagle media (DMEM) with 4.5 g/l Glucose and 10% sera Plus (full media). Twice to three times per week, the cell lines were sub-cultured to guarantee constant growth. Therefore, only sterile material and solutions were used and all working steps were performed in a laminar flow cabinet. First, the medium was removed from the tissue flask and the cell monolayer was carefully washed with 1xPBS. Next, trypsin-EDTA was added and the flask was placed for 5-7 min in the warm incubator to accelerate the detachment of the cells. Afterwards, Huh7 cells were resuspended in fresh full medium and plated in a new culture flask in a 1/3 to 1/6 dilution. HepG2 cells were resuspended in fresh full media, transferred to a 50 ml tube and centrifuged for 5 min at 64xg. The medium supernatant was aspirated and the HepG2 cell pellet was carefully but thoroughly resuspended in 1 ml fresh medium to separate individual cells. Nine ml full media was added and the cells were re-seeded with a 1/3 to 1/6 dilution in a new tissue flask. This additional centrifugation was necessary since HepG2 cells tend to grow in cell "islands" and it was difficult to obtain a single cell suspension. These cells did not form a real monolayer in contrast to Huh7 cells.

Before cells were seeded for experiments in plates, they were counted either with the Casy counter or with the Neubauer counting chamber. For the latter method, trypan blue staining was used to determine the viability.

2.2.1.1 Freezing and thawing of cell lines

Cell lines can be permanently stored in liquid nitrogen without aging (Lindl and Gstraunthaler 2008). Therefore, adherent cells were detached as mentioned above. After resuspension in fresh full media, the cell suspension was transferred to a tube and centrifuged for 5 min at 64xg. Next, the medium was removed and the cell pellet was resuspended in an appropriate volume of sera plus containing 10% DMSO to avoid ice crystal formation. 1 ml aliquots were filled into cryo vials, placed in a freezing container and stored at -80 °C for several days. The freezing container was filled with 2-propanol and provided a consistent cooling rate of

1 °C/min, which was required for a successful cryo preservation. Afterwards, the pre-frozen cells were transferred into the liquid nitrogen tank for long-term storage.

For thawing, the cryo vial was placed in a water bath of 37 °C to quickly defrost the cell suspension. When only a small frozen core was left, the cells were transferred into a 15 ml tube containing 8 ml pre-warmed fresh full media. The cryo vial was rinsed with 1 ml full media which was then added to the 15 ml tube. The cells were centrifuged for 5 min at 64xg and the DMSO containing media was aspirated. The pellet was resuspended in 12 ml full media and the cells were seeded in a T75 flask.

2.2.1.2 Transient inhibition of gene expression *via* RNA interference

RNA interference is a cellular mechanism to inhibit the expression of a specific gene *via* degradation of *messenger*RNA by double-stranded RNA (Fire et al. 1998). In this thesis, small interfering double stranded RNA (siRNA) was used to reduce the expression of AGXT in HepG2 cells. Therefore, three different short oligonucleotide sequences binding specifically to different exons of the *AGXT* gene were used in combination with lipofectamine RNAiMAX. Scrambled siRNA, which did not bind specifically was used as a negative control.

All siRNA experiments were performed in a 6-well plate and the reverse transfection method was applied. For the reverse transfection, the complex of lipofectamine RNAiMAX and siRNA is firstly allowed to form in a well before cells are added. Therefore, 500 µL OptiMEM were pipetted to each well and 10 nmol siRNA was added. After gentle shaking, 5 µL lipofectamine RNAiMAX was added and left for 20 to 30 min to form liposomal siRNA complexes. In the meantime, cells were trypsinised, centrifuged and counted. Depending on the length of the experiment, appropriate cell densities between $1x10^5$ and $2.5x10^5$ were added to each well. The transfection medium was replaced by full media after 24 h. The quality of AGXT knockdown was checked every time at the RNA or protein level.

2.2.2 Housing conditions of mice

Mice were bought at an age of eight weeks from Janvier Labs, and allowed to acclimatise for one week. They had access to water and feed ad libitum and were kept under a 12 h light – 12 h dark cycle. The performed experiments were approved by the animal welfare authority. Mice were handled according to the Principles of Laboratory Care and considering the

recommendations of the Society of Laboratory Animal Science (Gesellschaft für Versuchstierkunde, GV-SOLAS, Germany).

2.2.3 Isolation and cultivation of primary hepatocytes

2.2.3.1 Hepatocytes isolation

2.2.3.1.1 Mouse hepatocytes

The method for the isolation of primary hepatocytes from a mouse liver was based on a two-step perfusion (Seglen 1976). With this technique, the whole liver is converted to a suspension of viable hepatocytes. The liver perfusion proceeded under physiological conditions of the mouse and usually yielded hepatocytes with a viability above 90%. To obtain cells, the mouse was narcotised with an intraperitoneal injection of Rompun® (25-40 mg/kg) and ketamine (50-80 mg/kg). The anaesthesia was controlled by testing the pain sensitivity *via* the pedal reflex. Next, the mouse was fixed in a dorsal position on a grid table and the abdominal cavity was opened longitudinally. The vena cava was incised and a blunted needle was inserted, which was connected to a flexible tube that passed through a pump and ended in the appropriate buffer. First, the liver was perfused with pre-warmed EGTA buffer at a flow rate of 9 ml/min for 10 to 15 min to remove the blood and Ca^{2+} dependent adhesion factors. If the needle was placed correctly, the liver would lose its red-brown colour instantly. Next, EGTA buffer was exchanged for collagenase buffer (37 °C) to digest the extracellular matrix and to reduce the cell-cell contacts. Again, a flow rate of 9 ml/min was applied for 10 to 15 min depending on the collagenase activity. This perfusion step was deemed successful and thus stopped when the liver became soft and lustrous. The liver was excised carefully and taken out with forceps at the thoracal blood vessels. It was placed in a petri dish filled with suspension buffer and transferred into a laminar flow cabinet. Under sterile conditions, the liver capsule was opened and the liver cells were released into the suspension buffer supported by shaking the capsule gently within the buffer. This cell suspension was filtered through a 100 μm cell strainer and transferred to a 50 ml tube. Next, the cell suspension was centrifuged for 5 min at 4 °C and at 50xg to roughly remove non-parenchymal cells (NPC) from hepatocytes. NPC containing supernatant was removed and the hepatocyte pellet was resuspended in 10 ml suspension buffer by gently inverting the tube several times. The hepatocytes were placed on ice and an aliquot was diluted with the suspension buffer before being diluted with trypan blue solution (1:2). The stained cell suspension was pipetted into each chamber of the Neubauer counting

chamber. The amount of viable and dead blue stained cells were counted and the viability calculated.

2.2.3.1.2 Human hepatocytes

Primary human hepatocytes were isolated from patients undergoing liver surgery in the cooperation clinics: Charité Berlin and the university hospitals in Munich and in Regensburg. Hepatocytes of the latter mentioned hospitals were bought from the company Hepacult. Before the liver resection was performed, informed consent of each patient was obtained. The hepatocytes were isolated with the two-step isolation procedure as described above. Isolated hepatocytes were transported as a suspension on ice overnight from the clinics to our laboratory. Upon arrival, the hepatocytes were carefully resuspended in William's E medium and the cells were counted with the Neubauer counting chamber using trypan blue to determine the viability.

2.2.3.2 Cultivation of primary mouse hepatocytes

Primary mouse hepatocytes were cultured under sterile conditions at 37 °C and 5% CO_2 within aqueous saturated vapour. In this thesis, the primary mouse hepatocytes were cultured in a collagen coated well with a thicker layer of collagen on top. 10 mg rat tail collagen was dissolved in 40 ml 0.2% acetic acid for the coating or in 9 ml for the thick layer at 4 °C overnight to generate a 250 µg/ml and 1.1 mg/ml collagen solution, respectively. Next, the required cell culture dish was rinsed with 250 µg/ml collagen solution and left to dry for several hours or overnight inside the laminar flow. Before cells were added, the monolayer was washed three times with William's E medium without additives to increase the pH of the collagen layer. After that, William's E medium containing all additives (full media) and 10% sera plus was pipetted into the wells and the appropriate number of freshly isolated hepatocytes was added (Table 2.19). The cells were evenly distributed by gently shaking the plate, which was then placed in the incubator for 3 h for attachment. The second collagen layer was prepared on ice by mixing 1 part of 10x DMEM and 9 parts of 1.1 mg/ml collagen solution for a concentration of 1 mg/ml collagen. This mixture was neutralised with 1 M NaOH which was indicated by the colour change of the solution from yellow to pink. Afterwards, the attached hepatocytes were carefully washed with pre-warmed William's E medium to remove dead and non-attached cells before being covered with the thick collagen layer. The appropriate volume for the second layer was added (Table 2.19) and the plate was kept in the incubator to polymerise for

45 min. After successful polymerisation, William's E medium with additives (full media) was added.

Table 2.19: Conditions for primary hepatocytes cultivation

Plate	Cell number	1 mg/ml collagen	William's E medium &additives
6-well plate	850000 cells/well	350 µl	2 ml
12-well plate	400000 cells/well	200 µl	1 ml
24-well plate	200000 cells/well	100 µl	0.5 ml

2.2.4 Collection of liver tissue and kidneys from mice

Liver tissue from mice was collected to conduct RNA and protein analysis, as well as triglyceride quantification and histological stainings in order to find differences between the lipid-loaded liver and the normal liver. Mice were anaesthetised with an intraperitoneal injection of Rompun® (25-40 mg/kg) and ketamine (50-80 mg/kg), with the obese mice requiring a higher dose than the lean controls. After the mice were fully narcotised (see above), they were fixed in a dorsal position on a surgical table and the abdominal cavity was opened longitudinally. The liver was excised and weighed before washing in 1xPBS in a petri dish. One liver lobe was placed in a tissue cassette in 4% paraformaldehyde (PFA) for staining analysis. The remaining liver lobes were dissected in small sections and snap-frozen in liquid nitrogen. Those liver pieces were stored at -80 °C until RNA isolation or protein and triglyceride extraction were performed. If required, both kidneys were carefully excised after liver collection and placed within tissue cassettes in 4% PFA for Pizzolato staining (see 2.2.18.4).

2.2.5 24 h urine collection

To analyse the daily excreted amount of oxalate of mice, 24 h urine collections with metabolic cages for a single mouse were conducted on at least two consecutive days. One mouse was placed in one metabolic cage and had free access to water and feed powder. The excreted urine was collected in a small tube filled with 35 µL 6 M HCl to acidify the urine directly. The acidification was necessary to avoid the conversion of ascorbic acid to oxalic acid and to prevent bacterial growth. The daily uptake of water and food was recorded and the mice were weighed before and after the time in the metabolic cage. Usually, a weight loss of not more than 10% was consistently observed. Daily excreted urine was transferred to a tube and centrifuged for 10 min at 179xg and room temperature to remove feed powder. The urinary

supernatant was aliquoted and stored at -80 °C for further analysis. The daily urine samples of each mouse were analysed separately before an average of the excreted compounds in the urine per mouse was calculated.

2.2.6 Gene expression analysis

2.2.6.1 RNA isolation

RNA from cells and liver tissue was isolated using QIAzol reagent (QIAgen) for phenol-chloroform extraction. QIAzol consists of guanidinium thiocyanate and phenol, which lyses cell membranes and inhibits RNases (Chomczynski and Sacchi 1987). Snap frozen liver sections were homogenised in 1 ml QIAzol by a pestle and sonicated (50% power, 30 s, 5 s pulse, 2 s break) while kept on ice. Cells, cultivated in 6 well plate, were placed on ice, the medium supernatant was aspirated and the cells were lysed in 1 ml QIAzol. After scraping, the cell lysates were transferred to 2 ml-reaction tubes and sonicated on ice as mentioned above. Moreover, 1-5 million of freshly isolated mouse or human hepatocytes were resuspended in 1 ml QIAzol and sonicated in the same way as described before.

Subsequently, 200 µL chloroform were added to each reaction tube and the samples were shaken thoroughly for 20 s. To improve the phase separation, the samples were incubated for several minutes at room temperature before centrifuged at 4 °C, 12000xg for 15 min. The upper aqueous RNA containing phase was transferred to a reaction tube containing 500 µL 2-propanol to precipitate the RNA. The samples were incubated at room temperature for 10 min followed by a 15 min centrifugation step at 12000xg and 4 °C. The RNA pellet was washed twice: first, with 850 µL 100% ethanol and after a 5 min centrifugation at 4 °C and 10000xg and second, with 850 µL 75% ethanol. The supernatant was completely removed and the RNA pellet was air-dried for several minutes. The RNA was dissolved in 15-100 µL DEPC-treated water, depending on the size of the pellet, and its concentration was determined photometrically with the Nanodrop2000 (Thermo Fisher Scientific). RNA samples were stored at – 80 °C until further analysis.

2.2.6.2 cDNA synthesis

RNA was converted to cDNA prior to use in real-time polymerase chain reaction (PCR) for gene expression analysis. The high capacity cDNA reverse transcription kit (Applied Biosystems) was used to reversely transcribe the RNA into single stranded cDNA. 500 ng – 2 µg RNA were mixed

with appropriate volumes of 10x RT-Buffer, 10x random primers, 25x dNTP mix and reverse transcriptase. The total volume of this reaction mix was adjusted to 20 µL with DEPC water. The chosen conditions of the thermo cycler (Tgradient, Biometra) are listed in Table 2.20.

Table 2.20: Thermo cycler programme to transcribe RNA into cDNA

Step	Temperature	Time
Incubation	25 °C	10 min
Reverse transcription	37 °C	120 min
Inactivation	85 °C	5 min
	4 °C	∞

All cDNA samples were diluted with DEPC-water to a final concentration of 10 ng/µL and stored at -20 °C.

2.2.6.3 Quantitative real-time Polymerase Chain Reaction (qPCR)

Quantitative real-time PCR is a sensitive method to detect and quantify differences in gene expression of a target gene. This technique is based on conventional PCR which is characterised by the annealing and elongation of a primer bound to a specific target sequence of a single stranded DNA until the complementary strand is completed. To quantify the produced DNA with real-time PCR, a fluorescent signal is measured continuously whose intensity correlates with the amount of amplified PCR product (Higuchi 1993). In this work, TaqMan probes were applied that hybridised to the DNA template strand between the primers, and carry a fluorescent reporter on the 5'-end and a quencher on the 3'- end. Due to this close proximity there is a fluorescence resonance energy transfer (FRET) between the quencher and the reporter which suppresses the fluorescent signal. The used DNA polymerase has a 5'-3' exonuclease activity that results in a separation of the TaqMan probes from the template strand which are cleaved into single nucleotides (Holland et al. 1991). Hereby, the fluorescent reporter and quencher are spatially separated and a fluorescent signal occurs. The intensity of the fluorescent signal is proportional to the amplified DNA concentration. The fluorescence is illustrated as a function of time and so-called Ct values are set. Ct values describe the number of cycles necessary until the fluorescent signal crosses a threshold and enters the exponential phase.

All gene expression measurements were performed with a 7500 Real-Time PCR System (Applied Biosystems). 25 ng cDNA was mixed with 2x universal mastermix and 20x specific

TaqMan probe. The total volume per reaction was adjusted to 20 µL with DEPC water. All samples were measured in technical duplicates and for each probe water instead of cDNA was used as a negative control. The standard conditions for the amplification are listed in Table 2.21.

Table 2.21: Parameters for standard amplification

Step	Temperature	Time	Cycles/Repetitions
	50 °C	2 min	1
Activation of DNA polymerase	95 °C	10 min	1
DNA denaturation	95 °C	15 s	40
Annealing and Elongation	60 °C	1 min	

The gene expression levels were calculated with the $2^{-\Delta\Delta Ct}$ method (Livak and Schmittgen 2001). This is a relative quantification method that compares the expression levels of the gene of interest (GOI) and of a housekeeping gene (HKG) of the test sample in relation to a control situation (= calibrator). So-called housekeeping genes are endogenous control genes whose expressions do not alter under stressed or changed conditions. In this work, Gapdh, Eif2a or UBC were applied as endogenous controls and their expression levels were used to normalise the expression of the gene of interest ($\Delta Ct = Ct_{GOI} - Ct_{HKG}$). This ΔCt first needs to be calculated for a test (e.g. steatotic) sample ($\Delta Ct1$) and separately for a control (e.g. non-steatotic) sample ($\Delta Ct2$). Afterwards, the ΔCt values of the test samples and the control samples were compared ($\Delta\Delta Ct = \Delta Ct1 - \Delta Ct2$) to find differences due to test conditions. In order to see the differences between test and control samples easily, the calculation $2^{-\Delta\Delta Ct}$ was applied. The $2^{-\Delta\Delta Ct}$ value of control samples were 1; if the $2^{-\Delta\Delta Ct}$ value of the test sample is greater than 1, this is an indication of an upregulation of the gene of interest compared to the control sample and vice versa for $2^{-\Delta\Delta Ct}$ values below 1.

2.2.6.4 Affymetrix gene array analysis

For global gene expression analysis, RNA samples of *ob/ob* and *ob/+* mouse livers as well as of HepG2 cells incubated with 0.5 mM OA/BSA for 24 h, 72 h or 5 days and corresponding full media controls were analysed by Affymetrix gene array. Therefore, extracted RNA (100 ng/µl) were sent to the Gene Expression Affymetrix Facility at the Center for Molecular Medicine in Cologne. Briefly, the RNA sample was prepared as follows: RNA was converted to cDNA by reverse transcription and subsequently transcribed reversely *in vitro* to biotinylated cRNA using the GeneChip® IVT labeling kit. Afterwards, the biotinylated cRNA was purified and

fragmented using Affymetrix's protocol. Next, cRNA was hybridised to the corresponding array chip: GeneChip® Mouse Genome 430 2.0 array for mouse RNA and GeneChip® Human Genome U133 Plus 2.0 array for human RNA. After hybridisation, the samples were washed and stained with streptavidin-phycoerytherin. With scanning, the fluorescent signal of phycoerytherin was measured.

Biostatistical analysis of the gene array data was performed by our collaborators at the faculty of statistics at the Technical University of Dortmund, Germany. Briefly, the gene expression array data were normalised using the Robust Multi-array Average algorithm (Irizarry et al. 2003). The calculation of the differential gene expression was conducted with the statistical software R package limma (Smyth et al. 2005); data from non-steatotic *ob/+* mouse livers and full media treated HepG2 cells, respectively, were used as reference. The p-values were adjusted for multiple testing with the method of Benjamini and Hochberg (Benjamini and Hochberg 1995).

2.2.7 Protein analysis

2.2.7.1 Protein extraction

Proteins were extracted from liver tissue, as well as from primary hepatocytes and cell lines. Tissue and cells were lysed with RIPA lysis buffer containing 1:100 protease inhibitor and phosphatase cocktail II and III. Depending on the source material, slightly different procedures were applied:

a) **Snap frozen liver tissue**: 1 ml RIPA buffer was added to a piece of tissue on ice. This was homogenised with a pestle and sonicated. After 20 min incubation on ice, the homogenates were centrifuged for 10 min at 4 °C and 13000 rpm. The supernatants were collected in new tubes.

b) **Primary cell culture:** 6 well plates were placed on ice and medium was aspirated. The cells were carefully rinsed with 1xPBS before 0.3 - 0.5 ml RIPA buffer was added to each well. Cells were scraped and collected in a 1.5 ml tube. After sonification, lysates were incubated for 20 min on ice before they were centrifuged for 10 min at 13000 rpm and 4°C. The supernatants were transferred to new tubes.

c) **Cell culture:** 6 well plates were placed on ice and medium was aspirated. The cells were carefully rinsed with 1xPBS. Depending on the confluency of the monolayer, 75-200 µL RIPA buffer was added to the cells on ice. After some minutes on ice, the cells were scraped and transferred to a 1.5 ml tube followed by the sonification step.

All protein lysates were stored at -20 °C or -80 °C.

2.2.7.2 Protein quantification

The bicinchoninic acid (BCA) protein assay (Thermo Fisher Scientific) was used to quantify the protein content of the lysates. This assay combines the well-known Biuret reaction, which describes the reduction of Cu^{2+} to Cu^+ by peptide bonds under alkaline conditions, and the sensitive colorimetric detection of Cu^+ with BCA. Two BCA molecules and one Cu^+ molecule form a purple chelate complex with an absorbance at 562 nm that is proportional to the protein concentration (Smith et al. 1985).

Depending on the expected protein concentration, the protein lysates were diluted with 1xPBS before measurement. 5 µL of the (diluted) sample were mixed with 195 µL BCA working reagent, consisting of 49 parts of solution A and 1 part of solution B in a well of a 96 well plate. A standard curve of bovine serum albumin (BSA), ranging from 0 µg/ml to 2000 µg/ml, was prepared the same way. Both the samples and each BSA standard were set up in duplicates. The plate was incubated for 30 min at 37 °C before the absorbance at 562 nm was measured in a plate reader (Infinite M200 Pro, Tecan). Based on the standard curve, the protein concentrations of the samples were calculated.

2.2.7.3 Western blot

2.2.7.3.1 SDS-Polyacrylamide gel electrophoresis (SDS-PAGE)

SDS-Polyacrylamide gel electrophoresis is a widely-used technique for the analysis of proteins. Protein mixtures are separated in a gel in an electric field according to their electrophoretic mobility which is dependent on weight and charge. The anionic detergent sodium dodecyl sulphate (SDS) linearises proteins and covers their charge negatively (Shapiro et al. 1967). Hereby, the electrophoretic mobility is only dependent on the weight, not the charge of the proteins since the charge/weight ratio remains constant.

Materials and Methods

Gel preparation

The gels used for SDS-PAGE were either freshly prepared or bought (Thermo Fisher Scientific). Gels were cast using the Mini-PROTEAN Tetra electrophoresis system (BioRad) following the manufacturer's instructions. Two 1.5 mm thick 10% separation gels consisted of 6.4 ml ultrapure water, 5.28 ml acrylamide solution (30% v/v), 4 ml separation buffer, 160 µL 10% (w/v) SDS solution, 6.4 µL TEMED and 160 µL 10% (w/v) APS solution. These compounds were mixed thoroughly and cast between two glass plates within a vertical frame. To avoid oxidation and evaporation, each gel was overlaid with 1 ml of 2-propanol. After the gels were completely polymerised, the 2-propanol was removed and the stacking gels were cast on top. Two stacking gels were prepared using 4.8 ml ultrapure water, 1 ml acrylamide solution (30% v/v), 0.8 ml stacking buffer, 65 µL 10% (w/v) SDS solution, 5 µL TEMED and 100 µL 10% (w/v) APS solution. Directly after casting the stacking gels, combs were added to form loading wells. These gels were stored in a humid bag at 4 °C for a maximum of 1 week. Small-size proteins, like LC3, were analysed with gradient polyacrylamide gels (4 – 12% BisTris) from NUPAGE (Thermo Fisher Scientific).

Gel electrophoresis

Equal amounts of each sample's protein were mixed with 5 x loading buffer and denatured at 95 °C for 5 min. The loading buffer comprised dithiothreitol (DTT) to reduce disulphide bonds of the proteins for a better protein separation during electrophoresis. In the meantime, the gels were fit in their chambers and filled with 1 x running buffer. Denatured protein samples and 4 µL of Precision Plus Protein Dual Colour standard (BioRad) were added to the wells of the gels. The initially applied current for the electrophoresis was 20 mA/gel and was increased up to 40 mA/gel as soon as the samples passed the stacking gel. The electrophoresis was stopped right before the samples reached the end of the gel.

2.2.7.3.2 Transfer

In the next step, proteins were blotted from the gel to a PVDF membrane to immobilise them as well as to make them accessible to antibody detection on the other hand. The transfers were performed electrophoretically with the semidry blot system from Biometra or BioRad. The transfer chamber consisted of two horizontal plates, which were either the anode (lower plate) or the cathode (upper plate). The membrane was activated in methanol and left in anode buffer for several minutes to equilibrate. On the anode plate, twelve Whatman papers

soaked with anode puffer were placed. The activated membrane was laid onto them and covered with the gel. Since bubbles between the membrane and the gel would disturb the transfer, those were carefully removed with a roller. Four Whatman papers, which were pre-equilibrated in cathode buffer, were arranged on top of the gel. The chamber was closed with the cathode plate and connected to the power supply. The transfer was usually performed at 234 mA or 315 mA, depending on the size of the gel (5 mA/cm²), for 40 min. After the transfer, the membrane was washed in ultrapure water and incubated for one hour in 5% BSA in TBS-T to block unspecific binding between the membrane and the antibody.

2.2.7.3.3 Antibody incubation and protein detection

After blocking, the membranes were incubated with specific primary antibodies, appropriately diluted in 5% BSA TBS-T over night at 4 °C and constantly shaken. The next day, the membranes were washed three times at 10 min with TBS-T before incubated with the secondary horseradish peroxidase (HRP) linked antibody for one hour at room temperature. The secondary antibodies were diluted appropriately in 5% BSA TBS-T. Information about the antibodies and their dilutions are listed in Table 2.22. This incubation was followed by three 10 min TBS-T washing steps. The protein detection was performed *via* chemiluminescence, where the membranes were incubated with 5 ml chemiluminescent solution and 3 µL hydrogen peroxide. The conjugated HRP of the secondary antibody catalysed the oxidation of luminol which was accompanied by light emission at 428 nm. The emission of light was captured by the Blot-Imager Vilber Fusion Fx7 (Vilber Lourmat), which illustrated a specific signal for the protein of interest. After imaging, the membranes were incubated with stripping buffer for 30 min to remove the antibodies and, after the above-mentioned blocking step, the membranes could be used for further protein analysis. If required, the bands of proteins were quantified densitometrically with the software ImageJ.

Table 2.22: Parameters for antibody incubation (Western blotting)

Primary antibody	Secondary antibody	Dilution	Incubation
anti α-tubulin	anti mouse	1:1000/1:5000 in BSA	O/N 4 °C/ 1 h RT
anti β-actin	anti mouse	1:5000/1:10000 in BSA	30 min RT/20 min RT
anti Agxt	anti rabbit	1:1000/1:5000 in BSA	O/N 4 °C/ 1 h RT
anti LC3	anti rabbit	1:1000/1:5000 in BSA	O/N 4 °C/ 1 h RT
anti p62	anti rabbit	1:1000/1:5000 in BSA	O/N 4 °C/ 1 h RT

2.2.8 Preparation of oleic acid – BSA complex solution

Lipid droplet formation in cell lines and primary mouse hepatocytes was induced by incubation with oleic acid (OA) bound to BSA. BSA was used because free fatty acids are usually bound to serum albumin when transported within plasma (Gordon and Cherkes 1956). The concept for the preparation of the complex was similar to the protocol from Cousin and colleagues (Cousin et al. 2001), but modified with regard to the temperature and concentrations.

First, a 60 mM OA stock solution in 0.01 M NaOH was prepared. Therefore, 0.01 M NaOH was heated up to 70°C and an appropriate volume of OA (liquid at room temperature) was added. After stirring for 30 min at 70 °C in the dark, this solution was cooled and mixed with usually three droplets of 1 M NaOH to dissolve the OA completely. In the meantime, fatty acid free BSA was rehydrated in ultrapure water to prepare a 2.5 mM BSA solution. Next, one part of the 60 mM OA solution was mixed with four parts of the 2.5 mM BSA stock solution (molecular ratio OA to BSA was 6:1) and this OA/BSA-solution was stirred for maximum 1 hour at room temperature to form OA/BSA complexes. For a control solution, four parts of the 2.5 mM BSA stock solution were diluted with one part of 0.01 M NaOH. After sterile filtration (0.45 µm filter), the complex and control solutions were stored at -20°C and used within 3-4 weeks.

2.2.9 Induction of lipid droplet formation in cell lines and cultivated mouse hepatocytes

Lipid droplets were formed *in vitro* after cells were incubated with OA/BSA solution. Therefore, the cell lines or mouse hepatocytes were cultivated in an appropriate system and they were incubated with different concentrations of OA/BSA complexes in media one day after seeding. For HepG2 cells, two conditions were tested: OA/BSA was diluted in serum-free DMEM or in normal DMEM with 10% sera plus; both conditions led to lipid accumulation, indicating that HepG2 cells do not need to be forced to form lipid droplets by serum withdrawal. Therefore, normal, sera plus containing cultivation media (Table 2.9) was used to dilute OA/BSA. For each experiment, a full media control and a BSA control with matching concentration compared to OA/BSA condition was used. The applied OA concentrations ranged from 0.167 mM to maximum 4.5 mM to find non-toxic concentrations. The time of incubation varied from 24 h up to five days to mimic both an acute and more chronic-like situation. Medium was changed every two to three days.

2.2.10 Cell viability assay

To estimate the viability of HepG2 cells after oleic acid treatment, the CellTiter-Blue® viability assay (Promega) was applied. This assay uses the blue dye resazurin which will be reduced to the highly fluorescent dye resorufin by viable cells. Reduced resorufin production is an indicator of non-viable cells.

HepG2 cells were seeded at an appropriate density into wells of a 96-well microtiter plate with black walls and a flat, transparent bottoms. After one day of attachment, HepG2 cells were incubated with several OA/BSA and BSA concentrations or full media. For each condition, 8 wells, meaning 8 technical replicates, were prepared. After 24 h, 72 h and 5 d the medium was replaced by 120 µL of a CellTiter-Blue® containing medium, which contained a sixth CellTiter-Blue®reagent (Promega). After 4 h incubation at 37 °C, the fluorescent signal was measured at $579_{Ex}/584_{Em}$ nm in a plate reader (Infinite M200 Pro, Tecan).

2.2.11 Extraction and enzymatic quantification of triglycerides (TG)

The amount of triglycerides in liver tissue and cells was quantified enzymatically with a triglyceride quantification kit (Abcam). This assay is based on the cleavage of fatty acids from the glycerol backbone by a lipase. Glycerol is oxidised and then reacts with a probe to generate a fluorescent signal (535_{Ex} /587_{Em} nm).

2.2.11.1 Extraction of triglycerides

Triglycerides (TG) were extracted with 5% aqueous NP-40 solution in combination with a heating and cooling procedure. Depending on the source material, slightly different approaches were performed:

a) **Snap frozen liver tissue**: The tissue was weighed and 5% NP-40 solution was added (1 ml for 100 mg tissue). The tissue was homogenised with a pestle first and sonicated afterwards to completely release the TG from the tissue.

b) **Primary human hepatocytes**: 2.5 – 5 million freshly isolated human hepatocytes were centrifuged for 1 min at 4 °C and 400xg, the supernatants were removed and the cells were carefully washed in PBS. The centrifugation was repeated and after the supernatant was aspirated, the pellet was resuspended in 1 ml 5% NP-40 solution.

c) **Cell lines**: Cell lines were plated in a 6-well dish and incubated with or without OA/BSA complex for several days. On the day of harvest, the media was aspirated and the monolayer was rinsed with 1xPBS once. The PBS was removed and 100 µL 5% NP-40 was added per well. The cells were lysed with a scraper and collected in a tube.

To segregate the plasma membrane and to solubilise the triglycerides, the extracts were heated up to 90 °C for 3 min and then allowed to cool down to room temperature. The heating step was repeated, followed by a centrifugation for 2 min at top speed to remove any insoluble material. The supernatant was collected and an aliquot was diluted appropriately.

2.2.11.2 Enzymatic quantification of triglycerides

This assay was performed in a black 96 well plate with a flat, clear bottom to measure a fluorescence signal. One to 5 µl of the diluted sample was added to a well and the volume was adjusted to 50 µl with assay buffer. Each sample was usually measured in duplicates and a background control that was not incubated with lipase was applied. Two µL lipase was added to samples but not to the background samples. After 20 min incubation at room temperature, 50 µL reaction mix (see Table 2.23) was added to each well followed by an incubation of 1 hour at room temperature. Afterwards, the fluorescence signals were measured with 535 nm excitation and 587 nm emission in the plate reader (Infinite M200 Pro, Tecan). Simultaneously, the protein concentrations of the diluted extracts were determined using the BCA assay to normalise the relative fluorescence unit (RFU). The data analysis proceeded as follows: First, the blanks (buffer with/without lipase) were subtracted from each reading. Then, the samples were background-corrected to consider only the glycerol arising from tri-, di- and monoglycerides but not the free glycerol. The applied amount of proteins within the extract was calculated and the RFU were divided by the corresponding protein amount to normalise the signal.

Table 2.23: TG reaction mix

Compound	1 sample
Assay buffer	47.6 µL
Probe	0.4 µL
Enzyme mix	2 µL

2.2.12 Stimulation of oxalate formation *in vivo* and *in vitro*

To investigate the role of reduced Agxt expression, oxalate precursor compounds were applied *in vivo* as well as *in vitro*. The amounts of excreted oxalate in urine and cell culture supernatant were analysed.

2.2.12.1 Glyoxylate diet of *ob/ob* and *ob/+* mice

Ten *ob/ob* and ten *ob/+* mice were both divided into two groups à 5 mice. One group had drinking water enriched with 0.5% sodium glyoxylate monohydrate for eight days. The second group received plain drinking water. Each mouse had its own cage and free access to water and food. The body weight and water intake were measured daily. On day six of the diet, mice were transferred to a single mouse metabolic cage (Tecniplast) and 24 h urine was collected for two consecutive days. Then, the mice were once more transferred to a normal cage and the diet was stopped. After a recovery time of 3 weeks, the urinary oxalate levels normal again. The same experimental set up was conducted, this time receiving 0.1% sodium glyoxylate monohydrate that was dissolved in tap water. The mice that were previously given the glyoxylate enriched drinking water received the glyoxylate diet once more; whereas, the mice that were part of the control group in the first round, were selected once more as control mice and received untreated drinking water.

2.2.12.2 Glyoxylate treatment of AGXT knockdown HepG2 cells

HepG2 cells were transfected with siRNA which targeted AGXT mRNA to knockdown AGXT. Non-transfected HepG2 cells and those transfected with scrambled siRNA served as control situations: After 6 days of knockdown; HepG2 cells were incubated with 1 ml full media containing 0 mM, 0.2 mM or 1 mM glyoxylate for 24 h. Next, the supernatants were collected in 2 ml tubes on ice and frozen at -80 °C. The HepG2 cells were rinsed with 1xPBS and their proteins were collected as described in section 2.2.7.1c.

2.2.12.3 Oxalate precursor treatment of primary hepatocytes from *ob/ob* and *ob/+* mice

Primary mouse hepatocytes of *ob/ob* and *ob/+* mice were isolated and cultivated in 6-well plates for 24 h as described in Chapter 2.2.3.2. Then, they were incubated with 1 ml William's E medium with additives (full media) and three different oxalate precursors. Those oxalate precursors were glyoxylate, glycolate or hydroxyproline and the incubation lasted 48 h. After

48 h, the supernatants were collected in 2 ml tubes on ice and frozen at -80 °C. The cells were rinsed with 1xPBS and their proteins were collected as described in section 2.2.7.1b.

2.2.13 Quantification of oxalate

2.2.13.1 Quantification of oxalate by Gas Chromatography Mass Spectrometry (GC-MS)

The applied method was described for the quantification of diethylene glycol, ethylene glycol, oxalic acid and further metabolites by Perala and colleagues (Perala et al. 2014) and conducted in cooperation with the Analytical Chemistry Unit at IfADo. Mouse urine samples were diluted appropriately in ultrapure water, if necessary, and 40 µl were filled in a 4 ml glass vial. Next, 40 µl internal standard ($^{13}C_2$ oxalic acid, 100 µg/ml), 1 ml 1 M HCl and 0.5 ml saturated NaCl-solution were added and mixed thoroughly with the urine. For extraction, 1 ml of 0.5% TOPO in MTBE was pipetted to the glass vials and followed by 1 min mixing using the vortex. Afterwards, the samples were centrifuged for 10 min at 4500xg and 600 µl of the supernatant were transferred to a 1.5 ml glass vial. During the repetition of this extraction process, the supernatant was vaporised with nitrogen. After the second centrifugation, 800 µl of the supernatant was added to the same vial as before and was vaporised again under nitrogen at room temperature. After the supernatant was evaporated completely, 150 µl toluene and 50 µl MTBSTFA were added to each sample and thoroughly mixed. The derivatisation was performed at 60 °C for 1 h in a shaker (4500 rpm). Next, 200 µL sample was transferred to inserts and placed in a 1.5 ml glass vial. Each vial was closed with a screw cap with a septum and placed into the autosampler of the GC-MS system. The injection port was heated to 275 °C and 0.2 µl of each sample was injected splitless. Helium was used as the carrier gas at a constant flow mode of 1.8 ml/min. The temperature programme started with 100 °C and linearly increased at 10 °C per minute until 280 °C. This temperature was held for 2 min. The MS detection was done in the electron impact ionization mode on an Agilent model 5973N quadrupole mass spectrometer operated in the single ion modus with these parameters: transfer line temperature = 250 °C, MS quadrupole temperature = 150 °C, and MS source temperature = 230 °C The following ions were used for the quantification of oxalic acid *m/z* 261 and $^{13}C_2$ oxalic acid *m/z* 263. Due to a device failure of the GC-MS, the urines of mice on the normal or the Western diet were analysed by LC-MS/MS.

2.2.13.2 Quantification of oxalate by Liquid Chromatography Tandem Mass Spectrometry (LC-MS/MS)

The sensitivity of the GC-MS method was limited and very small concentrations of oxalate were not measurable. For that reason, a cooperation with Prof. Heiko Hayen and Alexander Schriewer from the department of Analytical Chemistry, University of Münster, was started and a liquid chromatography with tandem mass spectrometry (LC-MS/MS), using a triple quadrupole, method was established. This method was used to quantify the secreted levels of oxalate in medium supernatant from cultivated cells. For HepG2 cells, the supernatants were treated with methanol (1:4) overnight at 4 °C to precipitate the proteins that arose mainly from the sera plus in the medium. Those supernatants were centrifuged at 2200xg for 5 min to remove the proteins. Subsequently, the protein-free supernatants were vaporised at 45 °C in a vacuum using the Eppendorf Concentrator plus. These dried extracts were stored at -80 °C and sent on dry ice to Münster. Supernatants of cultivated mouse hepatocytes did not contain sera plus and were directly sent on dry ice to Münster. In Münster, dried extracts were dissolved in water and supernatants of cultivated primary mouse hepatocytes as well as urine samples were diluted or directly used. $^{13}C_2$ oxalic acid was added as the internal standard. The eluent was a mixture of water and acetonitrile (70:30) with 0.1% Trifluoracetic acid (v/v/v). The flow rate was 0.3 ml/min and the injection volume was 20 µl. For ionisation, electrospray ionisation in negative mode was used. Oxalic acid was fragmented by a collision gas and its product ion was analysed. The concentration of oxalate was calculated with the aid of the internal standard. The quantified oxalate concentration was normalised to the protein amount of the monolayer.

2.2.14 Colorimetric quantification of creatinine in urine

Creatinine is a product of muscle metabolism and excreted by the kidneys (Skorecki et al. 2016). The excreted creatinine amount is often used as a benchmark for the concentration of urine. In this thesis, the urinary creatinine concentration was used to normalise the excreted oxalate amount since the daily excreted urine volumes were variable. The creatinine quantification is colorimetric and based on the so-called Jaffé reaction (Jaffe 1886). Creatinine reacts with picric acid under alkaline conditions and forms an orange complex with a maximum of absorbance at 492 nm.

Murine urine is diluted 1:20 with ultrapure water in a 1.5 ml tube, mixed and centrifuged at 6000 rpm for 5 minutes to remove potential fine particles. The supernatants were transferred to new tubes. Creatinine standards were prepared in water at a concentration range from 0 mg/ml to 70 mg/ml. 50 µl of each standard and sample were pipetted to a well of a transparent 96 microtiter plate with flat bottom. Furthermore, 50 µl of two differently concentrated control urines (1:50 diluted) were used as a quality control. 10 ml of 0.25 M NaOH-solution were mixed with 4.365 mM picric acid. 200 µl of this alkaline picric acid solution were added to each well and incubated in the dark for 45 min. Thereafter, the absorption at 492 nm was measured with a plate reader (Infinite M200 Pro, Tecan). The creatinine standard concentrations were plotted against the absorption at 492 nm and the creatinine concentrations of the samples were calculated with the help of the linear equation of the standard curve.

2.2.15 HR- MAS ^{1}H-NMR quantification of glycine and glycolate in liver tissue

The quantification of hepatic glycine and glycolate of *ob/+* and *ob/ob* livers was performed *via* high-resolution (HR) magic angle spinning (MAS) ^{1}H-nuclear magnetic resonance (NMR) spectroscopy in cooperation with Mikheil Gogiashvili and Dr. Roland Hergenröder at the Leibniz Institute for Analytical Sciences (ISAS), Dortmund. Snap frozen liver tissue was cut to fit into 50 µl volume MAS rotor at -10 °C under nitrogen atmosphere. To each sample, sodium 2,2,3,3-tetradeuterio-3-trimethylsilylpropanoate (TSP-d4, 0.1%) in deuterium oxide was added as an internal standard. Afterwards, the tissue was analysed on a NMR-spectrometer (Bruker) equipped with a ^{1}H/^{13}C MAS probe head. The measurement frequency was 600.35 MHz and the spinning frequency was set to 5 kHz. To identify metabolites, the Chenomx 7.6 database as well as literature were used. The concentration of the metabolites was determined according to the concentration of TPS applying Chenomx 7.6.

2.2.16 Oil Red O staining

Lipid droplets can be visualised with the lipophilic dye Oil Red O. This technique was applied to observe lipid droplet accumulation upon OA/BSA treatment in cell lines. Oil Red O powder was dissolved in 2-propanol to prepare a 0.5% stock solution. Right before usage, the stock solution was diluted with water (3:2). After 30 min, this working solution was filtered twice to remove precipitates. Medium from cells, which were seeded on round glass slides, was removed and the cells were carefully rinsed with 1xPBS. An appropriate volume of Oil Red O

working solution was added to the wells and left for 20 min. Then the Oil Red O solution was removed and the cells were washed three times with 1xPBS to eliminate excessive Oil Red O solution. The stained cells on the round slides were transferred to an object slide and immediately analysed with an optical microscope (Olympus BX41).

2.2.17 Immunofluorescence

Immunofluorescence is a widely-used technique to visualise specific proteins in tissue or cells using fluorophore-labelled antibodies. The antibody for a specific protein can either be conjugated with a fluorophore directly (direct immunofluorescence) or a second antibody against the protein specific antibody is labelled with a fluorophore (indirect immunofluorescence). Indirect immunofluorescence is advantageous because is results in a more specific signal with less background, and is more flexible since the secondary antibody can be used for different antibodies from the same species. In this thesis, only the indirect immunofluorescence was applied.

Primary mouse hepatocytes were seeded on glass slides (see Chapter 2.2.3.2) and incubated with different OA/BSA and BSA concentrations of full media for various time points. Then, the media was aspirated and cells were rinsed with 1xPBS. 4% paraformaldehyde was added to the wells and cells were fixed for 20 min at 37 °C. After fixation, the cells were washed with 1xPBS and permeabilised with 0.5% TritonX-100 for 15 min to enable the detection of intracellular compartments. The TritonX-100 solution was removed and cells were rinsed three times for 5 min with 1xPBS. To avoid unspecific antibody binding, cells were incubated with 10% BSA and 0.1% Tween20 in 1xPBS for 2 h at room temperature. The antibodies of interest (Table 2.24) were diluted in 3% BSA/0.1% Tween20 in 1xPBS and incubated with the cells overnight in a humidity chamber at 4 °C. The day after, the antibody solution was removed and the cells were washed three times with 1xPBS. Fluorescence labelled secondary antibody was diluted appropriately in 0.3% BSA/0.1% Tween20 in 1xPBS together with phalloidin-rhodamine (1:500) to visualise the F-actin and added to the cells for 1 h. After washing three times with 1xPBS, the slides were incubated for 45 min with 50 µg/ml Bodipy in 1xPBS to stain lipid droplets. Afterwards, the cells were washed 3x5 min with 1xPBS and treated with 4′,6-Diamidin-2-phenylindol (DAPI, 1:20 000 in water) for 15 min. Again, the DAPI solution was removed, the cells were rinsed three times with 1xPBS and once with ultrapure water to eliminate salts. Subsequently, the slides were mounted onto SuperFrost Plus

microscopic slides using FluorPreserve™ Reagent (Calbiochem). The slides were dried overnight at room temperature and kept at 4°C in the dark until imaging. For imaging, the light scattered microscope (FluoView TM FV1000; Olympus) was used.

Table 2.24: Parameters for antibody incubation (immunofluorescence)

Primary antibody	Secondary antibody	Dilution	Incubation
anti α-tubulin	anti mouse	1:1000/1:300	O/N 4 °C/ 2 h RT
anti DPPIV	anti goat	1:300/1:250	O/N 4 °C/ 2 h RT

To visualise only lipid droplets, cell nuclei and F-actin, the above-mentioned protocol was applied without the BSA blocking and the antibody incubation steps.

2.2.18 Histologic staining of paraffin embedded tissue

2.2.18.1 Fixation and paraffin embedding of tissue

After collection in cassettes, liver lobes and kidneys were fixed in 4% PFA at 4 °C for two days. Next, the cassettes were washed in sterile 1xPBS for additional two days at 4 °C before the tissue was embedded in paraffin. The paraffin infiltration was performed with the STP120 processor (Thermo Fisher Scientific) where the tissue was first dehydrated through an ethanol gradient, incubated in xylene and finally infiltrated with paraffin. Detailed procedure information is listed in the Table 2.25 below.

Table 2.25: Programme for paraffin infiltration of tissue

Step	Solution	Time [min]
1	70% Ethanol	30
2	70% Ethanol	60
3	90% Ethanol	30
4	90% Ethanol	30
5	99% Ethanol	30
6	99% Ethanol	35
7	99% Ethanol	60
8	Xylol	30
9	Xylol	35
10	Xylol	60
11	Paraffin Histowax	80
12	Paraffin Histowax	105

After this process, the liver lobes and kidneys were embedded in paraffin with the Microm HM450 automated embedding device.

Sections of paraffin-embedded liver or kidney tissue with a thickness of 4 µm were obtained with a feather blade type N35HR in a HM 450 Sliding Microtome (Thermo Fisher Scientific). The tissue sections were mounted on glass slides during a 20 min incubation at 60 °C. Before usage, the tissue slides were stored at 4 °C.

2.2.18.2 Haematoxylin and eosin staining

First, tissue sections were rehydrated as follows: the tissue was deparaffinised in Roti®-Histol three times à 10 min before rehydrated through a decreasing ethanol gradient (5 min in 100%, 95%, 90%, and 70% each) which ends in ultrapure water. After rehydration, the slides were immersed in freshly filtered haematoxylin for 5 min. The tissue was blued under running tap water for 10 min. Afterwards, the slides were stained with freshly filtered 1% Eosin Y for 3 min. Next, the slides were shortly rinsed in ultrapure water and dehydrated through an increasing ethanol gradient (70%, 90%, 95%, 2x100%, 5 s each), ending in Roti®-Histol. At the end, the tissue was mounted on a glass slide with Entellan®. For imaging, the optical microscope (Olympus BX41) was used.

2.2.18.3 Immunohistochemistry using Avidin-Biotin-Complex (ABC) method

Specific antigens, mainly proteins, can be visualised directly on tissue using the antibody based immunohistochemistry (IHC). This technique was used to identify the central vein *via* a staining of glutamine-synthetase and to analyse the expression as well as the distribution of Agxt in liver sections.

Therefore, the paraffin slides were deparaffinised and rehydrated as mentioned above. After the fixation, proteins can be cross-linked to formaldehyde which can result in a weak or negative signal. To unmask the proteins, the slides were processed with a combination of citrate buffer and heating. The tissue samples were immerged in 10 mM citrate buffer, pH adjusted to 6, and heated in a microwave twice for 7 min. After the slides were cooled, they were washed in 1xPBS two times for 5 min each. Next, the samples were treated with 3% H_2O_2 in 1xPBS to block endogenous peroxidase and to avoid unspecific background signals. Next, the tissue samples were rinsed three times for 5 min with 1xPBS and subsequently blocked with 3% BSA/3% Tween80 in 1xPBS in a humidified chamber for 60 min at room temperature to mask unspecific binding sites. After this blocking, a specific antibody was diluted in 0.3% BSA/3% Tween80 in 1xPBS appropriately (see Table 2.26) and the tissue samples were incubated over night at 4 °C in a humidified chamber. The next day, the slides were washed

three times à 5 min in 1xPBS to completely remove the primary antibody. The secondary antibody against rabbit was used from an ABC kit. 15 µl of the secondary antibody were mixed together with 30 µl of blocking reagent in 2 ml 1xPBS and added onto the slide for 30 min at room temperature. After this incubation, the samples were washed again in 1xPBS (three times, 5 min each). The next step comprised the treatment with avidin (reagent A) and biotinylated horseradish peroxidase (reagent B), i.e. 40 µl reagent A and 40 µl reagent B were mixed with 2 ml 1xPBS and pipetted onto the samples. After 30 min at room temperature, the solutions were discarded and the slides were washed three times with 1xPBS for 5 min each. Five drops of 3,3'-diaminobenzidine DAB were mixed with two drops H_2O_2 and two drops of buffer solution in 5 ml water; this solution was added onto the slides. After 2 - 10 min, brown colour development indicated the protein of interest. Next, the samples were washed for 5 min under running tap water before they were stained with haematoxylin for 2 min. The haematoxylin solution was removed and the slides were washed in running tap water for 10 min. Afterwards, the samples were dehydrated by an increasing ethanol gradient (70%, 90%, 95%, 2x100%, 5 s each), followed by Roti®-Histol before mounted with Entellan®. For imaging, the optical microscope (Olympus BX41) was used.

Table 2.26: Dilutions of primary antibodies used for IHC

Antibody	Host	Dilution
anti Agxt	Rabbit	1:1000
anti Glutamine synthetase	Rabbit	1:2000

2.2.18.4 Pizzolato staining

To visualise renal calcium oxalate deposits, the method of Pizzolato was performed (Pizzolato 1964). After rehydration of the kidney tissue (see 2.2.18.2), the tissue sections were covered with a freshly prepared silver nitrate-hydrogen peroxide solution (2.5% silver nitrate, 15% hydrogen peroxide). A 60-watt bulb was placed approximately 15 cm from the kidney tissue for 30 min. Next, the tissue was stained with nuclear fast red solution for 5 min and subsequently rinsed with ultrapure water. Then, the stained tissue sections were dehydrated with an increasing ethanol gradient and mounted as described above. Calcium oxalate deposits would be stained in black and the remaining tissue would appear in red. For imaging, the optical microscope (Olympus BX41) was used .This staining was conducted in cooperation and discussed with Prof. Anders from the Medizinische Klinik und Poliklinik IV, Klinikum der Universität München.

2.2.19 Methylation analysis of *Agxt* promotor

The methylation analysis of the *Agxt* promotor was conducted by Dr. Nina Gasparoni of the genetic/epigenetic research group of Prof. Jörn Walter at Saarland University.

2.2.19.1 Preparation

Freshly isolated human or mouse hepatocytes were counted and 5 million cells were transferred to a 2 ml tube. The samples were centrifuged at 4 °C and 400xg for 1 min. The supernatant was removed and the cell pellet was carefully washed with 1xPBS. After a second centrifugation step at the above-mentioned conditions, the supernatant was removed completely and the cell pellet was snap frozen in liquid nitrogen. The procedure was similarly performed for cultivated hepatocytes and cell lines. The medium of the plated cells was removed and the cells were washed with 1xPBS. Next, fresh 1xPBS was added and the cells were carefully detached using a cell scraper. This cell suspension was transferred into a 2 ml tube and centrifuged for 1 min at 400xg and 4 °C. The supernatant was discarded and the cell pellet was snap frozen in liquid nitrogen. Sections of liver tissue were snap frozen directly during the *in vivo* collection in liquid nitrogen. The samples were stored at -80 °C before they were sent on dry ice for analysis to Saarbrücken.

2.2.19.2 Amplicon-sequencing of bisulphite-treated DNA

Briefly, DNA was extracted and treated with bisulphite using the Zymo gold kit. The bisulphite treatment converted unmethylated cytosine to uracil, but methylated cytosine remained unconverted. In parallel, specific primers for the amplification of the *Agxt* promotor on bisulphite treated DNA were designed. The primers were fusion primers that had a sequence-specific part and a general Illumina adapter sequence. Next, a traditional PCR amplification of the bisulphite-treated DNA with the fusion-primers was performed. The PCR products were purified by Ampuro-beads and quantified using a Qubit fluorometer. PCR products of different samples went into different pools and a PCR amplification with primers binding to the general Illumina adaptors and addition of the rest of Illumina adaptors with indices, was performed. Each pool had its own index. After purification and quantification of the pool-PCR-products, the sequencing of these was conducted on MiSeq (Illumina, Inc.) using the sequencing by synthesis approach. Afterwards, the sequencing reads were extracted and pre-processed. The separation of the reads was performed by amplicon sequence and index. The analysis was conducted with BiQHT and the self-created scripts of the research group at Saarland

University. Finally, the amount of cytosines, representing methylated cytosines in the *Agxt* promotor, and thymine, representing unmethylated cytosines in the Agxt promotor, at CpG positions were quantified. This quantification indicated the methylation status of the Agxt promotor.

2.2.20 Statistical data analysis

All experiments were performed with three or more biological replicates if not mentioned otherwise. The numeric numbers were represented as mean values with standard deviation. To evaluate whether a difference between the control and the steatotic condition was significant, the unpaired T-test with Welsh correction was applied for mouse and *in vitro* samples. For human samples, the Mann Whitney test was performed, if not mentioned otherwise. P-values below 0.05 were accepted as significant. *GraphPad PRISM* 6.07 was used for these analyses.

3. Results

3.1 Leptin deficient *ob/ob* mice represent an appropriate rodent model for steatosis

Animal models of NAFLD provide valuable information for elucidating the pathogenesis of the disease. There are several rodent models available for NAFLD that can be classified into genetic and dietary models, as summarized in Chapter 1.4. The induced NAFLD ranges from simple steatosis to severe NASH and fibrosis. The choice of an appropriate animal model to work with depends on the aim of the study. In the current work, the leptin deficient *ob/ob* mouse model was chosen because it exhibits a simple steatosis phenotype, which does not progress to more severe liver diseases without further intervention. Therefore, it is an appropriate model to investigate the impact of lipid accumulation on the liver.

3.1.1 *Ob/ob* mice display a phenotype of obesity with hepatic steatosis

To verify hepatic lipid accumulation in *ob/ob* mice, *in vivo* collections of the liver were performed, and the body and liver weights of *ob/ob* and *ob/+* mice were measured (n = 8, age: 10 weeks). *Ob/ob* mice were nearly twice as heavy as their lean counterparts and their livers weighed more than twice that of *ob/+* mice as illustrated in Figure 3.1. This resulted in a shifted liver to body weight ratio in *ob/ob* mice, indicative of an enlarged liver in relation to the body weight (Figure 3.1 C). The enzymatic quantification of triglycerides extracted from liver tissue revealed an approximately 16 fold higher amount of triglycerides in livers of *ob/ob* mice. The accumulation of lipid droplets in *ob/ob* mice was confirmed by H&E stainings of paraffin sections of *ob/ob* and *ob/+* mouse livers, where lipid droplets were represented as white spots within the tissue. Figure 3.1 E shows representative pictures of H&E stainings of an *ob/+* and an *ob/ob* liver. A closer look at the lipid-loaded hepatocytes in the H&E staining indicated that nuclei were pushed towards the periphery of the cell due to the lipid accumulation (exemplified by yellow arrows in Figure 3.1 E). The shift of the nuclei could imply a disturbed cytoskeleton and altered cell organisation within lipid-loaded hepatocytes. Furthermore, the staining of the pericentrally-located glutamine synthetase enzyme revealed a zonation of lipid droplets within the pericentral and midzonal fields of the liver lobule. There were very little to no lipid droplets visible close to the portal vein in steatotic livers of *ob/ob* mice. Altogether, the expected steatotic phenotype in the leptin deficient *ob/ob* mouse could be confirmed.
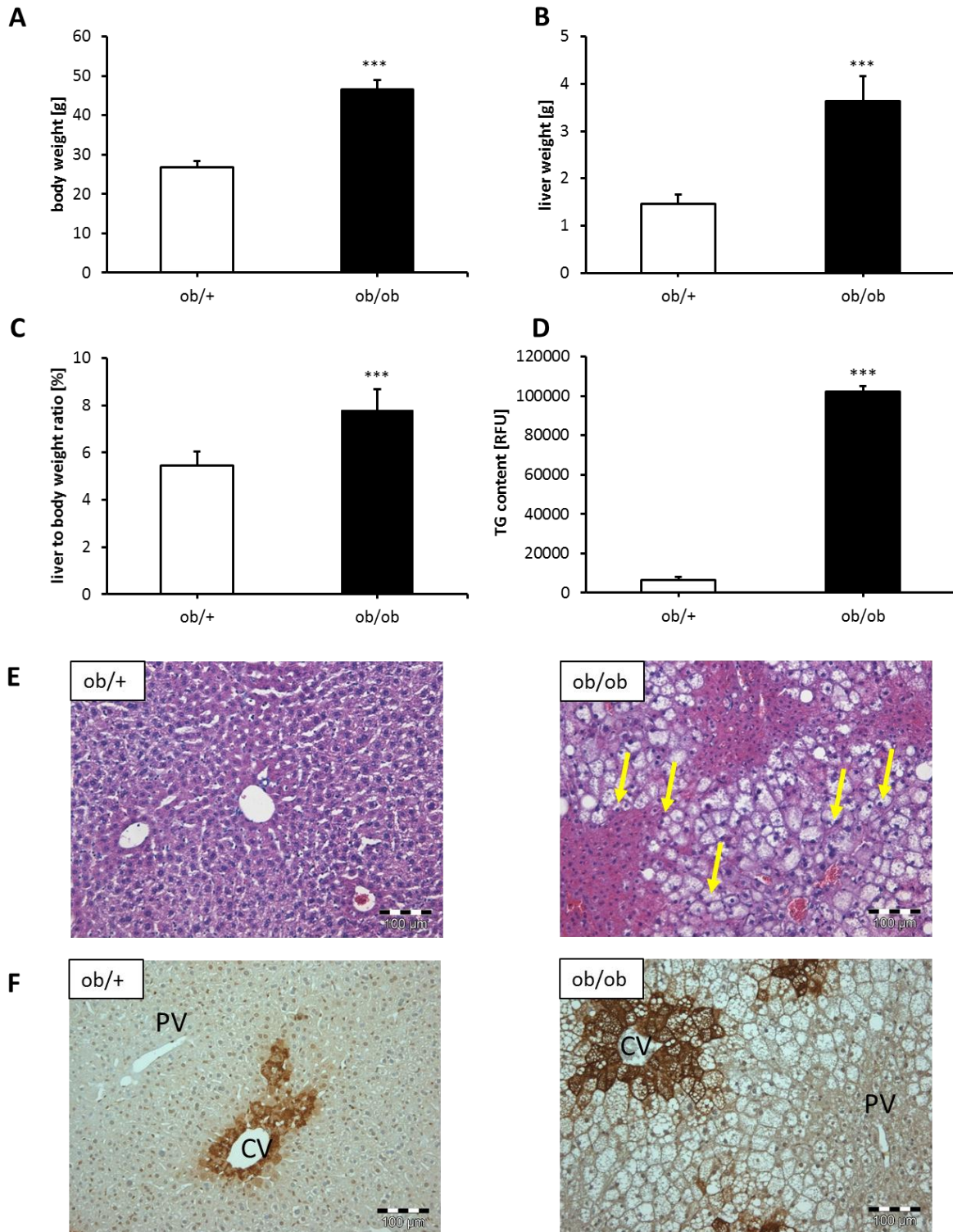
Figure 3.1: Steatotic *ob/ob* mice have an altered liver to body weight ratio and their livers show the shift of nuclei towards the periphery as well as lipid accumulation in the pericentral field. A) Body weight of *ob/ob* and *ob/+* mice (n = 8); B) Liver weight of *ob/ob* and *ob/+* mice (n = 8); C) Liver to body weight ratio (n = 8); D) Enzymatic triglyceride quantification of *ob/ob* and *ob/+* liver extracts (n = 4); E) Representative H&E staining of paraffin embedded liver slices; F) Representative glutamine synthetase staining of paraffin embedded liver slices; CV: central vein; PV: portal vein. Scale bars represent 100 µm. *** indicates $p < 0.001$.

3.1.2 The autophagic flux in *ob/ob* mouse livers is compromised

One cellular process often discussed to play a role in the development of a fatty liver and in the progression to more severe liver disease is autophagy. In the context of hepatic steatosis this clearance pathway is reported to be impaired by excessive lipid accumulation (Gonzalez-Rodriguez et al. 2014; Singh et al. 2009). As elucidated in Chapter 1.3, impaired autophagy has been linked to ER stress and insulin resistance in steatotic livers. Thus, an important question was whether autophagy is compromised in the steatotic liver of *ob/ob* mice.

The autophagic flux is a dynamic process that is challenging to monitor. Studying the protein levels of autophagy markers - the microtubule-associated protein 1A/1B-light chain 3 (LC3) and p62 - is a general approach to obtain an estimation of autophagic activity (Mizushima and Yoshimori 2007). LC3 is a soluble protein whose cytosolic form (LC3 I) is conjugated to phosphatidylethanolamine to form LC3 II during autophagy; LC3 II is recruited to the membrane of the autophagosomes, and hence reflects the number of autophagosomes present (Kabeya et al. 2000; Kabeya et al. 2004). After fusion with the lysosome, autophagosomal components, including LC3 II, are degraded (Tanida et al. 2008). An increase of LC3 II indicates an elevated amount of autophagosomes. This in turn can indicate an induced (more generation of autophagosomes) as well as a reduced autophagic flux (less degradation of autophagosomes). To distinguish between these two situations, the level of the protein p62 is usually investigated. P62 is an adaptor protein for polyubiquitinated protein cargo that binds to LC3 *via* an evolutionary conserved 22-residue motif (Komatsu et al. 2007; Pankiv et al. 2007). For this reason, p62 serves as a marker of autophagy. Increased levels of p62 indicate the presence of unremoved cargo, and therefore inhibited autophagy (Bjorkoy et al. 2005).

There are two studies reporting a defective hepatic autophagy in *ob/ob* mice. However, they contradict each other with respect to the step within the autophagic flux where the blockage occurs. Yang and colleagues described decreased levels of both LC3 I and LC3 II protein accompanied by an accumulation of p62 in livers of *ob/*ob mice indicating impaired autophagosomes formation (Yang et al. 2010). In contrast, Inami and co-workers (2011) demonstrated an accumulation of p62 and increased levels LC3 II in *ob/ob* compared to *ob/+* livers (Inami et al. 2011). These results indicate either an impaired fusion capacity of autophagosomes and lysosomes or the loss of degradation capability. To confirm the defective

hepatic autophagic flux in *ob/ob* mice and to elucidate at which point the dynamic process was impaired, Western blot analysis of liver lysates of *ob/+* and *ob/ob* mice was performed.
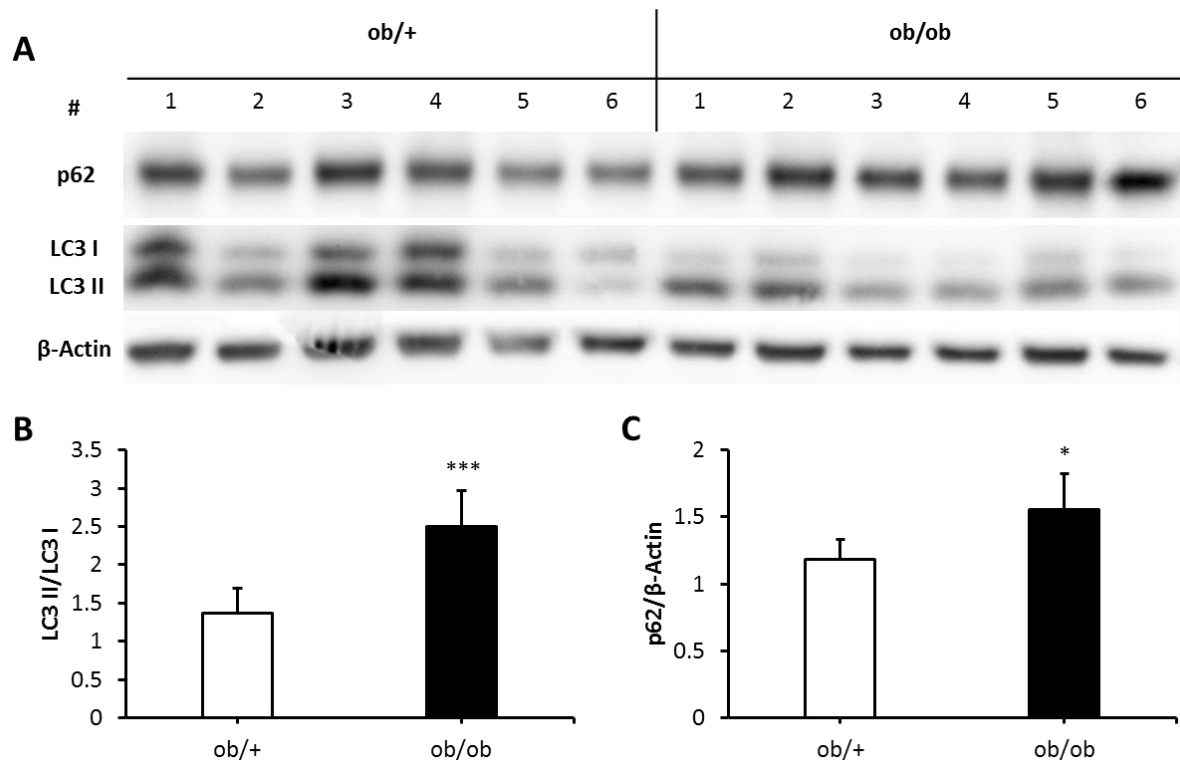

Figure 3.2: Markers of autophagy show heterogeneity within *ob/+* and *ob/ob* mouse liver lysates, but the density quantification indicates an impaired autophagic flux. A) Western blot of the protein expression of p62 and LC3I/II in protein lysates of liver tissue of *ob/ob* and *ob/+* mice (n = 6). β-Actin expression was used as loading control; B) Densitometric quantification of the expression of LC3 II and LC3 I illustrated as ratio of the density; C) Densitometric quantification of the expression of p62 and β-Actin illustrated as ratio of the density. * indicates p < 0.05; *** indicates p < 0.001.

As illustrated in Figure 3.2, the expression of the autophagic markers p62 and LC3 I/II differed between all mice within each genotype. Despite this heterogeneity, quantification of the LC3 I and LC3 II levels revealed a significantly elevated level of LC3 II and relative to the level of LC3 I in *ob/ob* mouse livers compared to lean mouse livers. This result was accompanied by a slightly, but significantly increased protein level of p62 in *ob/ob* mice. Altogether, these findings imply an inhibited autophagic flux after the formation of autophagosomes in *ob/ob* mouse livers in agreement with those of Inami et al. (2011). Thus, lipid accumulation in the steatotic livers of *ob/ob* mice was high enough to disturb the autophagic capacity of the cells.

3.1.3 Affymetrix gene array analysis of steatotic livers from *ob/ob* mice

The phenotypical morphological as well as histological alterations in *ob/ob* mice and their livers were very pronounced, as shown in the previous Chapter 3.1.1. However, how they impact liver physiology is not well understood. In order to identify gene expression changes relevant in steatosis, an Affymetrix gene array analysis of *ob/ob* and *ob/+* mouse livers was performed. The analysis of differentially expressed genes could help to identify genes, which play a role in steatosis or may be important for the progression of steatosis to a more severe liver diseases. Therefore, RNA from both *ob/ob* and control livers (n = 8) was isolated and transcriptomically analysed.

3.1.3.1 A significant number of genes are differentially expressed in steatotic livers from *ob/ob* mice compared to livers from control *ob/+* mice

To obtain an overview of the similarities and differences in gene expression between livers from *ob/+* and *ob/ob* mice, the statistical tool of a principle component analysis (PCA) was applied. This procedure helped to visualise the complex data in two dimensions while retaining most of the variation (Jolliffe 2002). The PCA blot in Figure 3.3 illustrates the large difference between the gene expression of *ob/ob* mouse livers and *ob/+* mouse livers, as well as the similarity between the individuals of each genotype. Remarkably, *ob/ob* mice clustered closer than the control *ob/+* mice.
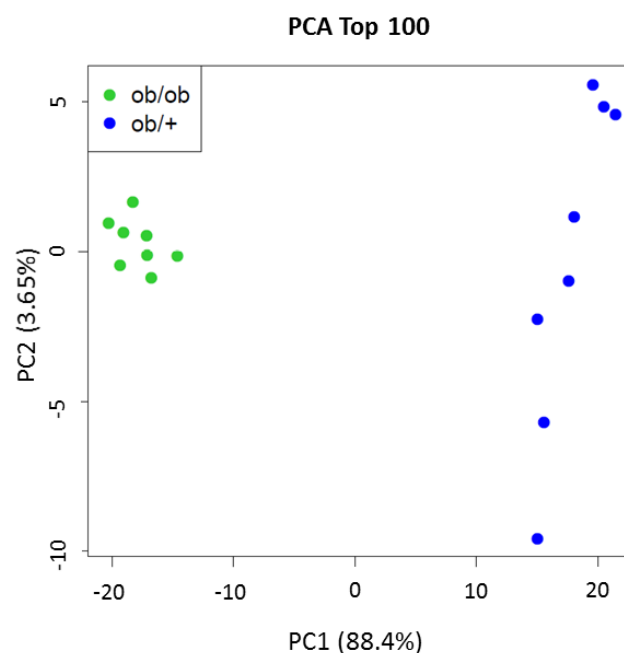
Figure 3.3 Gene array analysis reveals strong alterations of gene expression in steatotic livers of *ob/ob* mice. Gene array analysis of liver tissue from *ob/ob* and *ob/+* mice (n = 8) was performed and illustrated in a principle component analysis (PCA).

61

Results

The differential gene expression analysis of *ob/ob* mouse liver tissue revealed a total of 7399 genes, which were significantly deregulated in steatotic *ob/ob* mouse livers compared to livers of *ob/+* mice (adjusted p-value ≤ 0.05). As shown in Table 3.1, the number of deregulated genes was lower when a fold change of at least 1.5-fold compared to *ob/+* mice was considered.

Table 3.1: Numbers of significantly deregulated genes in the steatotic livers from *ob/ob* mice compared to control livers (adjusted p-value ≤ 0.05)

	Number of genes	Fold change ≥ 1.5
Upregulated	3775	887
Downregulated	3624	455

The top 20 up and downregulated genes in *ob/ob* mouse livers are listed in Figure 3.4. Among the top 20 of upregulated genes are several known to be associated with lipid metabolism.
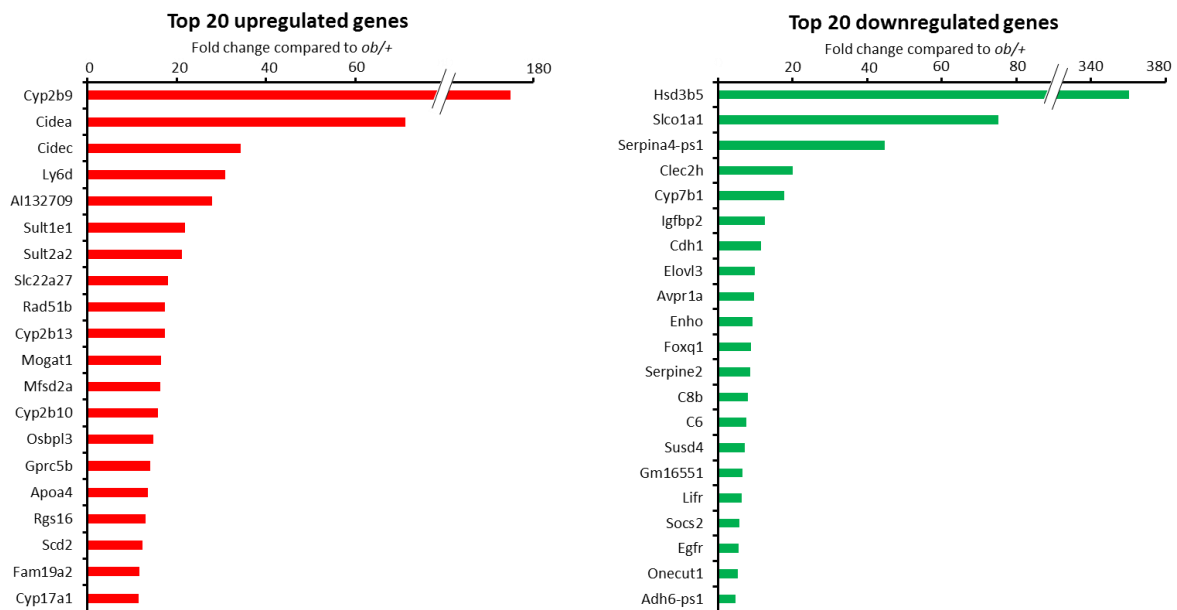
Figure 3.4: Top 20 deregulated genes in *ob/ob* mouse livers compared to *ob/+* mouse livers, adjusted p-value ≤ 0.05.

Cidea and *Cidec* are known to play a role in the regulation and enlargement of lipid droplets in adipocytes (Puri et al. 2007; Puri et al. 2008b). Moreover, *Mogat1* codes for a protein that catalyses the formation of diacylglycerol from 2-monoacylglycerol (Yen et al. 2002). *Apoa4* forms lipoproteins in conjunction with other apolipoproteins in order to maintain lipid homeostasis and is inducible by a lipid rich diet (Williams et al. 1986). Last, *Scd2* codes for a stearoyl-coenzyme A desaturase that catalyses the desaturation of C16:0 and C18:0 to

monounsaturated fatty acids (Miyazaki et al. 2006). In general, these examples indicated an overall increase in lipid metabolism in *ob/ob* mouse livers as expected due to the high triglyceride content in the these livers (compare Figure 3.1 D).

In contrast, the 20 most downregulated genes did not show a single strong biological motif as seen for the top 20 upregulated genes. The strongest downregulated gene was *Hsd3b5*, whose gene product, 3 beta-hydroxysteroid dehydrogenase V, converts dihydrotestosterone into an inactive androgen, 5 alpha-androstane-3 beta,17 beta-diol (Abbaszade et al. 1995). In addition, some genes could be assigned to the same biological pathways, such as bile acid transport and bile acid synthesis in the case of Slco1a1 (van de Steeg et al. 2010) and Cyp7b1 (Schwarz et al. 1997).

Altogether, the top 20 deregulated genes in *ob/ob* mice provided evidence of altered lipid metabolism. In order to identify additional biological motifs which were affected in the livers of leptin deficient mice, a gene ontology (GO) enrichment analysis was performed.

3.1.3.2 Lipid associated pathways are strongly upregulated in steatotic livers from *ob/ob* mice

To obtain an overall picture regarding the deregulated genes in *ob/ob* mouse livers, a GO enrichment analysis was performed using the Database for Annotation, Visualization and Integrated Discovery (DAVID) v *6.8* (Dennis et al. 2003; Huang et al. 2009; Huang et al. 2007). GO enrichment analysis is a bioinformatic tool to explore large gene lists that enables functional interpretation of gene lists. To represent gene product properties, gene ontology defines three domains, namely biological process (BP), molecular function (MF) and cellular component (CC). Each of these domains consists of subcategories that classify the group of genes more specifically. With the help of the GO enrichment, overrepresented groups of genes as well as biological themes in the *ob/ob* mouse liver could be identified. The following analysis was based on up- and downregulated genes which were at least 1.5-fold deregulated compared to the *ob/+* mouse liver. The analysis was narrowed down to overrepresented GO terms of the domain "biological process". This domain gives the most information on altered processes in steatotic livers from *ob/ob* mice. In Tables 3.2 and 3.3, the top ten overrepresented GO terms of up- and downregulated genes in *ob/ob* mouse liver are listed.

With respect to the upregulated genes in *ob/ob* mice, the GO enrichment analysis clearly identified the upregulation of processes involved in lipid metabolism, such as *lipid metabolic*

Results

process (GO:0006629) and *fatty acid metabolic process* (GO:0006631). This was not surprising considering the dramatic accumulation of lipids within the livers of *ob/ob* mice (Figure 3.1 D), as well as the high number of genes under the top 20 upregulated genes that were involved in lipid metabolism (Figure 3.4). The enrichment of the GO term *oxidation-reduction process* (GO: 0055114) was observed for up- as well as for downregulated genes in *ob/ob* mice. This provides evidence of potential alterations in redox status in livers of *ob/ob* mice.

Table 3.2: GO enrichment analysis of upregulated genes in *ob/ob* mouse livers in the domain "biological process"; Benjamini adjustment of p-value

Term	Genes	adj p-value
GO:0006629 lipid metabolic process	Ppara, Ldlr, Hmgcr, Ehhadh, Sgms1, Slc16a1, Elovl5, Agpat9, Mgll, Elovl6, Hadh, Thrsp, Agpat3, Hmgcl, Dhcr24, Lpat1, Sult2a2, Acnat2, Decr1, Lpin2, Lpin1, Chpt1, Pnpla3, Pnpla5, Lipo1, Pla2g7, Kdsr, Gpam, Slc27a4, Ech1, Cers6, Abhd3, Apoc2, Abhd2, Ptpmt1, Plin5, Ddhd2, Fasn, Hsd17b4, Acsl3, Pltp, Gal3st1, Scd1, Eci1, Soat1, Mogat1, Scd2, Nceh1, Pla2g15, Cyp46a1, Psap, Acer2, Il1rn, Acaca, Cidea, Fads2, Acly, Crat, Cpt1a, Brca1, Mttp, Pcx, Hmgcs2, Lipg, Aacs, Smpd3, Plcxd1, Vldlr	3.24E-16
GO:0008152 metabolic process	Arsg, Hexa, Ehhadh, Hexb, Hlcs, Acss2, Gstm2, Gstn3, Agpat9, Treh, Acad9, Agpat3, Idua, Aco2, Lpgat1, Suclg2, Pnpla3, Pnpla5, Umps, Aldh1b1, Pklr, Tnfaip3, Gpam, Ugp2, Slc27a4, Coasy, Ech1, Hk2, Acat1, Aldh3a2, Dct, L3hypdh, Galk1, Chil3, Fasn, Gys2, Uck1, Acsl3, Bdh1, Eci1, Lyz2, Mthfd2l, Lyz1, Nceh1, GUSB, Acaca, Acly, Nadk, Tkt, Uap1l1, Dlat, Eci3, Pcx, Hmgcs2, Sulf2, Aldh2, Aacs	8.46E-10
GO:0006631 fatty acid metabolic process	Ppara, Ech1, Ehhadh, Snca, Elovl5, Acot11, Per2, Fasn, Mgll, Elovl6, Hsd17b4, Hadh, Acsl3, Scd1, Eci1, Pla2g15, Scd2, Acnat2, Acaca, Fads2, Decr1, Crat, Lpin2, Brca1, Cpt1a, Cd36, Fabp4, Fabp2, Aacs, Gpam, Slc27a4	1.61E-09
GO:0006637 acyl-CoA metabolic process	Acot9, Acot8, Ehhadh, Acnat2, Acot11, Acot2, Acot1, Acot6, Gpam, Hmgcl, Acot4, Acot3	1.75E-05
GO:0007049 cell cycle	Dbf4, Aurka, Cdt1, Kif13a, Ccne2, Cdca8, Cgref1, Mis18a, Rala, Ccna2, Cdca3, Cdk1, Dab2ip, Rbl1, Nusap1, Cdk6, Mcm2, Mcm3, Ube2c, Mcm4, Ect2, Mcm5, Wee1, Mcm6, Ccnd1, Dclre1a, Uhrf1, Mad2l1, Zwint, Usp22, Haus8, Gadd45a, Anapc16, Usp2, Nek2, Chek1, Anln, Ensa, Ccng1, Spc24, Spc25, Ncapg2, Zwilch, Hells, Txnip, Mki67, Birc5, Cdc20, Cdkn3, Smc2, Brca1, Cdkn1a, Ccnb2, Rgs2, Ptp4a1, Cenpw, Smpd3	1.62E-05
GO:0055114 oxidation-reduction process	Htatip2, Vkorc1l1, Hmgcr, Ehhadh, Pgd, Snca, Mthfd1l, Gpx4, Loxl2, Hadh, Nqo1, Acad9, Dhcr24, Aifm2, Cbr3, Decr1, Cyp2b10, Dhrs7b, Vat1, Dhrs7, Aldh1b1, Rrm2, Hao2, Kdsr, Srxn1, Me1, Hsd17b10, Txn2, Cyp2b9, Rsad1, Aldh3a2, Fmo4, Fmo5, Cbr1, Fmo2, Fmo3, Fasn,	6.36E-05

	Hsd17b4, Bdh1, Scd1, Gpd2, Gpd1, Mthfd2l, Scd2, Ptgr2, Cyp46a1, Pyroxd2, Maoa, Fads2, Cryz, Cyba, Cyp17Aa1, Cybb, Hsdl2, Aldh2, Cyp2c38, Cyp4a14, Cyp2c39, Retsat	
GO:0050873 brown fat cell differentiation	Pex11a, Scd1, Adrb2, Lamb3, Rgs2, Itga6, Mrap, Pparg, Fabp4, Arl4a	0.00311531
GO:0007584 response to nutrient	Txn2, Hmgcr, Tgfbr2, Vcam1, Cybb, Tnfrsf11b, Bche, Pklr, Lipg, Aacs, Nqo1, Acsl3, Hmgcl, Slc27a4	0.00318681
GO:0006635 fatty acid beta-oxidation	Eci1, Ech1, Ehhadh, Abcd1, Abcd2, Decr1, Hsd17b4, Hadh, Acat1, Eci3, Cpt1a	0.0033165
GO:0051301 cell division	Anapc16, Nek2, Aurka, Anln, Ensa, Ccng1, Spc24, Ccne2, Kif13a, Spc25, Cdca8, Ncapg2, Mis18a, Rala, Zwilch, Ccna2, Hells, Cdca3, Cdk1, Nusap1, Cdk6, Cdc20, Birc5, Ube2c, Sms2, Ect2, Mcm5, Wee1, Ccnd1, Dclre1a, Ccnb2, Mad2l1, Zwint, Cenpw, Haus8	0.00488294

Among the GO groups of the downregulated genes, *circadian rhythm* (GO:0007623) was enriched. The reduced expression of genes important for circadian rhythm like Clock, indicates a disturbed light-dark rhythm in *ob/ob* mice. Also, *response to estradiol* (GO:0032355) and *hormonal stimuli* (GO:0032870) were reduced in *ob/ob* mice.

Table 3.3: GO enrichment analysis of downregulated genes in *ob/ob* mouse livers in the domain "biological process"; Benjamini adjustment of p-value

Term	Genes	adj p-value
GO:0007623 circadian rhythm	Egfr, Ddc, Klf9, Igf1, Arntl, F7, Cyp7b1, Npas2, Atf4, Ncoa2, Id2, Id3, Cry1, Clock	9.57E-04
GO:0032355 response to estradiol	Ifi27, Socs2, Dusp1, Foxa1, Prdm2, Ptch1, F7, Cyp1a2, Igfbp2, Dnmt3b, Gstp1, Ihh	0.009972805
GO:0045944 positive regulation of transcription from RNA polymerase II promoter	Fgfr2, Foxa2, Onecut1, Foxa3, Helz2, Nfix, Sox9, Cited2, Fos, Npas2, S1pr1, Hamp, Xbp1, Armcx3, Etv5, Wwox, Cyr61, Ihh, Egfr, Bmp4, Fzd8, Klf9, Klf12, Foxa1, Ptbp1, Mlxipl, Nr4a1, Igf1, Gper1, Arntl, Fzd5, Cela1, Foxp1, Prpf6, Atxn1, Hhex, Inhba, Atf4, Ncoa2, Irf5, Serpinf2, Clock	0.02084427
GO:0045892 negative regulation of transcription, DNA-templated	Sox9, Pdcd4, Cited2, Atp8b1, Meg3, Zfp217, Cry1, Kdm5b, Dnmt3b, Bmp4, Ptprk, Mup4, Crebzf, Mup3, Mlxipl, Tle1, Arntl, Foxn3, Foxp1, Atxn1, Hhex, Ncoa2, Id2, Nab2, Whsc1l1, Ptch1, Id3, Clock	0.05272735

Results

GO:0000122 negative regulation of transcription from RNA polymerase II promoter	Fgfr2, Ppard, Efna1, Nfix, Sox9, Cited2, Hamp, Xbp1, Zfp217, Cry1, Dnmt3b, Bmp4, Zfp36, Fzd8, Klf12, Arid5b, Foxa1, Mlxipl, Tle1, Hes6, Cela1, Foxp1, Atxn1, Hhex, Acvr2b, Ifi27, Dact1, Ncoa2, IdD2, Hopx, Ptch1, Id3	0.06973641
GO:0001889 liver development	Hhex, Onecut1, Xbp1, Otc, Meg3, Srd5a1, Cad, Asns, Lsr, Cited2	0.063543659
GO:0010466 negative regulation of peptidase activity	Reck, Serpina3k, Serpina9, Mug1, Serpina11, Serpine2, Serpinf2, Serpina12, Fetub, Itih5, Itih3	0.056690393
GO:0055114 oxidation-reduction process	Hsd3b2, Cyp2u1, Cyp2d9, Hsd3b3, Hsd17b2, Ethe1, Hsd3b5, Prdx4, Ero1lb, Cyp4A12a, Cyp39a1, Ivd, Adh4, Hsd17b6, Loxl4, Srd5a1, Kdm5b, Scr9c7, Wwox, Cyp2c70, Nox4, Cyp2c37, Cyp2c54, Cyp4f14, Cyp1a2, Cyp7b1, Cyp27a1, Aox3, Gulo, Steap2	0.060928127
GO:0006357 regulation of transcription from RNA polymerase II promoter	Zfp36, Tshz2, Onecut1, Foxa2, Foxa3, Arid5b, Foxa1, Mlxipl, Tle1, Hes6, Sox9, Med12l, Cited2, Fos, Inhba, Hhex, Atf4, Irf5, Xbp1, Rhoa, Etv5	0.070163046
GO:0032870 cellular response to hormone stimulus	Fos, Ncoa2, Socs2, Dusp1, Aypr1a, Asns, Igfbp2	0.093673777

All in all, the GO enrichment analysis confirmed the increased lipid metabolism as expected for *ob/ob* mice and gave evidence of a reduced hormonal capacity/responses in *ob/ob* mouse livers. Moreover, decreased gene expression of genes involved in circadian rhythm was an interesting finding, and agrees with an earlier report of disturbed circadian rhythm upon steatosis (Kohsaka et al. 2007).

3.2 Establishment of *in vitro* steatosis models

In addition to the leptin deficient *ob/ob* mouse model as an animal model to study NALFD, an *in vitro* steatosis model was established in the course of this PhD thesis. The establishment of this model helps reducing the number of animal experiments and can be easy manipulated for functional analyses. There are several possibilities to induce lipid droplet formation *in vitro*, e.g. treatment with fatty acids (Gomez-Lechon et al. 2007; Listenberger et al. 2003) or cultivation in methionine-choline deficient (MCD) media (Sahai et al. 2006). The most widely used approach is cultivation of cells in fatty acid-enriched medium to provoke the formation of lipid droplets (Malhi et al. 2006). The conversion of fatty acids to triglycerides is discussed as a protective mechanism to avoid lipotoxic effects of fatty acids, where monounsaturated fatty acids are more efficiently converted into triglycerides than saturated fatty acids, and are consequently less lipotoxic than saturated fatty acids (Listenberger et al. 2003; Mei et al. 2011). In both diet and serum, palmitic acid (C16:0) and oleic acid (C18:1) are the most abundant fatty acids (Baylin et al. 2002). Moreover, oleic acid is more steatogenic than palmitic acid in hepatocytes (Ricchi et al. 2009). For these reasons, oleic acid was used to establish *in vitro* models for steatosis in hepatocellular carcinoma cell lines as well as in primary mouse hepatocytes.

3.2.1 Lipid accumulation in HepG2 cells

The first step of this approach was to induce lipid droplet formation in HepG2 cells. The human hepatocellular carcinoma cell line HepG2 was chosen because HepG2 cells are readily available, easy to cultivate, and do not alter their gene expression during cultivation in contrast to primary hepatocytes (Godoy et al. 2013). HepG2 cells were incubated with various concentrations of oleic acid, complexed to BSA in a molecular ratio of 6:1 (OA/BSA), as well as with the corresponding BSA-only concentrations for several days. This was necessary to determine, which concentrations and time points of OA/BSA exposure could mimic an *in vivo* situation, leading to lipid droplet accumulation without affecting the viability of HepG2 cells. The pictures of an Oil Red O staining in Figure 3.5 illustrate the formation of lipid droplets upon OA/BSA treatment. After only 24 h, OA/BSA incubation stimulated the production of more and larger lipid droplets in HepG2 cells compared to the control situation without OA/BSA, and the accumulation of lipid droplets also increased with the incubation time. However, it must be noted that HepG2 cells which were incubated with 4.5 mM OA/BSA

seemed to decrease in cell number, especially after 72 h and 5 d of exposure. They also appeared stressed. For this reason, the highest OA/BSA concentration was not used in further experiments, but instead replaced with an OA/BSA concentration below 0.5 mM, namely 0.167 mM.
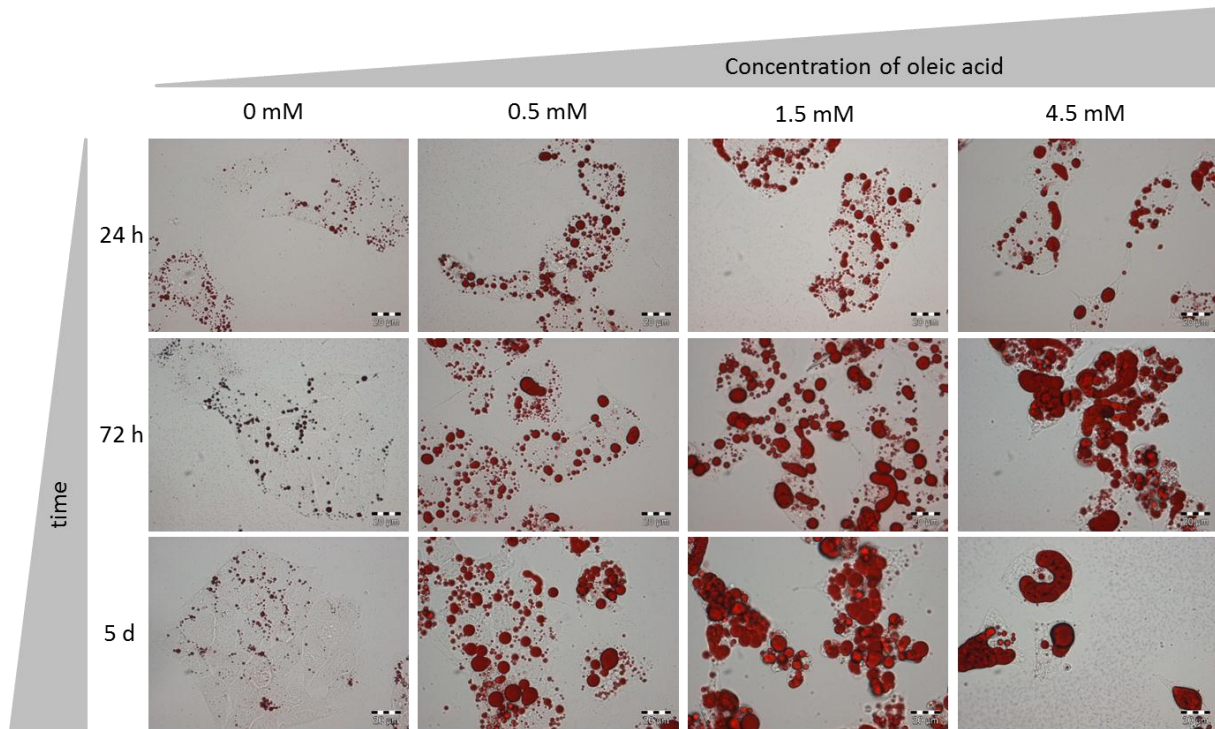
Figure 3.5: OA/BSA incubation induces lipid accumulation in HepG2 cells. Oil Red O staining revealed a time and concentration dependent formation of lipid droplets in HepG2 cells upon OA/BSA exposure; representative pictures. Scale bars represent 20 μm.

The Oil Red O staining of lipid-loaded HepG2 cells upon OA/BSA treatment revealed an obvious time and concentration-dependent lipid accumulation (see Figure 3.5). To obtain a more objective and measurable result, a triglyceride quantification, based on an enzymatic assay, was performed. The quantification results are listed in form of a diagram in Figure 3.6. As expected, increased OA/BSA concentrations led to increased amounts of cellular triglycerides. Interestingly, there was not such a well-defined time-dependent accumulation of lipids as seen in the Oil Red O staining. The same OA/BSA concentration either had no effect or only slightly elevated the triglyceride levels after prolonged incubation time.
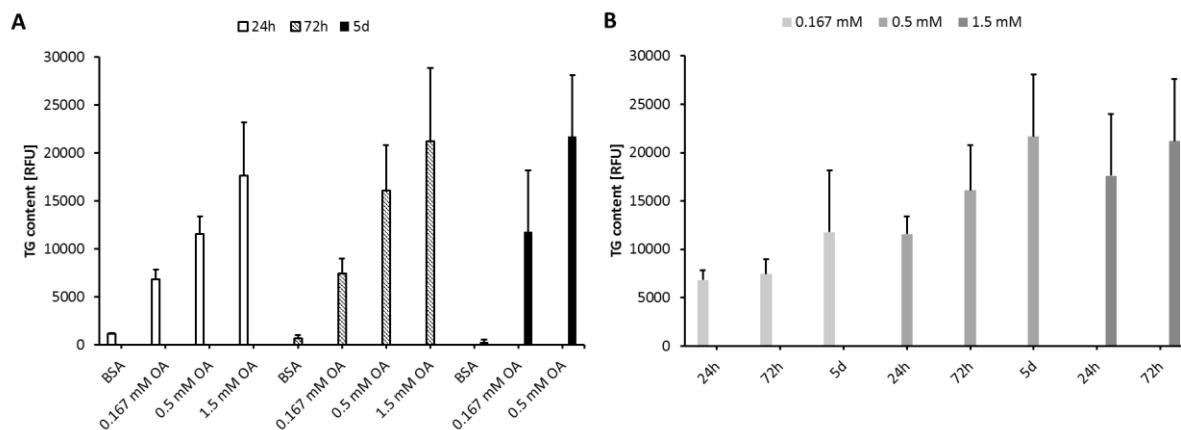
Figure 3.6: Triglyceride accumulation in HepG2 cells upon OA/BSA incubation. The triglyceride amount of HepG2 after OA/BSA treatment was quantified enzymatically. The relative contents of triglycerides were sorted by A) time points and B) OA/BSA concentrations (n = 3).

3.2.1.1 Effect of OA/BSA exposure on the viability of HepG2 cells

To assess the viability of OA/BSA-incubated HepG2 cells, CellTiter-Blue® assays (Promega) were performed. After 24 h and 72 h OA/BSA incubation with various concentrations, the viability was not markedly reduced at any of the applied OA/BSA concentration. However, after 5 days of incubation, the CellTiter-Blue® assay revealed a clearly reduced viability of HepG2 cells incubated with 0.5 mM OA/BSA, and even less viability in cells exposed to 1.5 mM OA/BSA. The low viability of HepG2 cells incubated with 1.5 mM OA/BSA for five days was in line with their appearance, as illustrated in Figure 3.7 C, where only detached and therefore most probably dead cells were obvious. However, the low viability observed in HepG2 cells exposed five days to 0.5 mM OA/BSA was not in agreement with their otherwise healthy appearance. In this case, the viability of HepG2 cells was confirmed by counting the viable and dead cells using the Casy counter. The counting of the cells revealed no loss in viability of HepG2 cells after 5 d incubation with 0.5 mM OA/BSA (Figure 3.7 B).

One explanation for the discrepancy between the results of the CellTiter-Blue® assay and the CASY counting could be a disturbed redox status in the lipid-loaded HepG2 cells leading to increased oxidative stress as previously reported (Anavi et al. 2015). The CellTiter-Blue® assay is based on the reduction of resazurin to resorufin depending on the redox system of the cell (O'Brien et al. 2000). Therefore, it is possible that HepG2 cells incubated with 0.5 mM OA/BSA for 5 days were still viable but with a reduced redox capacity.
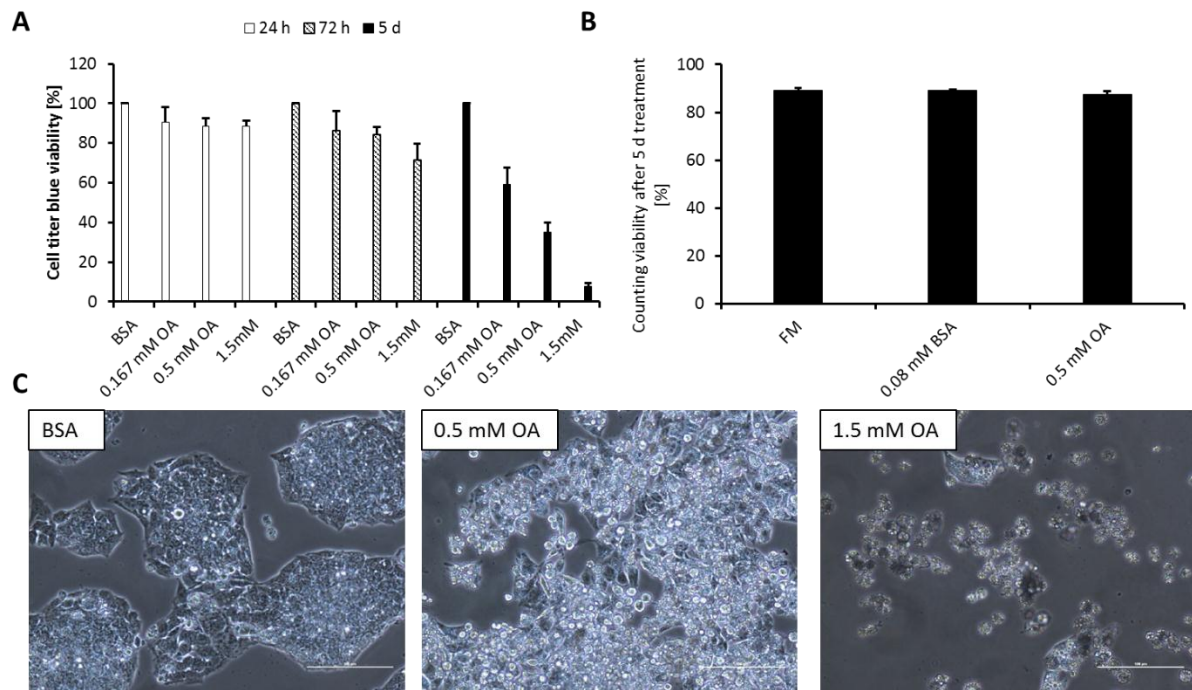
Figure 3.7: OA/BSA exposure has impact on the viability of HepG2 cells. A) CellTiter-Blue ® assay of HepG2 after OA/BSA incubation indicates reduced viability upon long OA/BSA exposure (n = 3); B) Casy counting results of HepG2 cell incubated 5 d with FM, 0.08 mM BSA and 0.5 mM OA/BSA (n = 3); C) Representative pictures of HepG2 cells after 5 d stimulation with 0.08 mM BSA or 0.5 mM OA/BSA or 1.5 mM OA/BSA: Scale bars represent 100 µm.

3.2.1.2 Compromised autophagy in lipid-loaded HepG2 cells

As demonstrated in the sections above, the induction of lipid accumulation in HepG2 cells due to OA/BSA incubation was successful and the optimal, non-toxic OA/BSA concentrations as well as length of exposure could be defined: HepG2 cells can be incubated with 1.5 mM OA/BSA for a maximum of three days, and with 0.5 mM OA/BSA for a maximum of five days. The next experiments were performed to elucidate if the *in vitro* steatosis model of HepG2 was able to recapitulate an impaired autophagic flux as a feature of steatosis as observed *in vivo* (Fukuo et al. 2014; Gonzalez-Rodriguez et al. 2014). It is controversially discussed if oleic acid incubation induces the autophagic flux in HepG2 cells (Mei et al. 2011) or not (Tan et al. 2012). Moreover, Miyagawa and co-workers suggested a blockage of autophagy due to impaired autophagosome-lysosomes fusion upon treatment with palmitic acid but not with oleic acid (Miyagawa et al. 2016). These studies used shorter exposure duration with oleic acid (maximal 24 h). Here, the aim was to investigate, which effect long term (72 h and 5 days) incubation with various concentrations of OA/BSA and the resulting lipid accumulation had on the autophagic flux in HepG2 cells.

As described in Chapter 3.1.2, the autophagy markers LC3 I/LC3 II and p62 were monitored by Western blot. After 24 h OA/BSA incubation, a slight accumulation of p62 as well as LC3 II was observed in cells incubated with the highest OA/BSA concentration (1.5 mM). The increased levels of p62 and LC3 II were more prominent after 72 h of OA/BSA treatment with all concentrations compared to the cells that were incubated with the corresponding BSA controls, with the highest levels seen after stimulation with 1.5 mM OA/BSA (Figure 3.8, yellow arrows). These observations were repeated for the 5 d time point: only with OA/BSA incubation there was a co-accumulation of p62 and LC3 II. These results suggest a time and concentration-dependent reduction or blockage of autophagy upon OA/BSA exposure *via* an impaired degradation of autophagosomes.
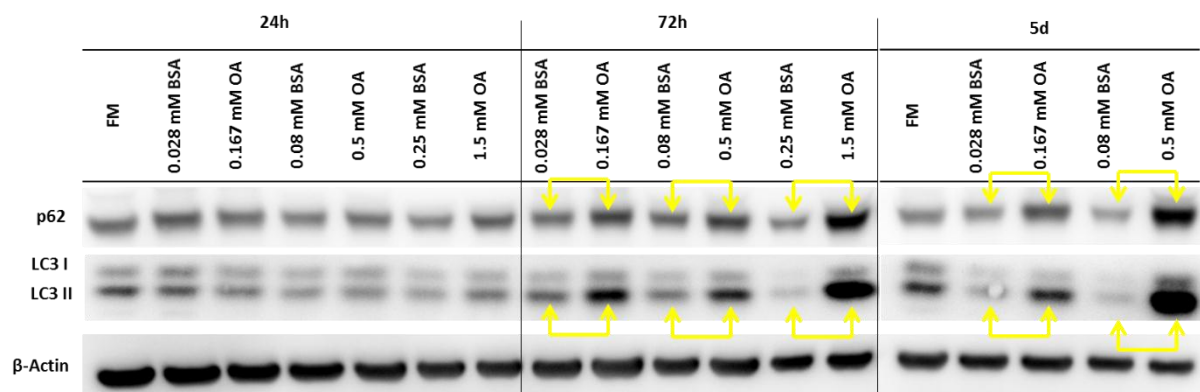
Figure 3.8: Increased levels of autophagy markers in lipid-loaded HepG2 cells indicate a disturbed autophagic flux. Representative Western blot of OA/BSA exposed HepG2 cells showing a time and concentration-dependent increase of p62 and LC3 II levels. β-Actin was used as loading.

To confirm these results, a LC3 II-turnover assay was performed according to the guidelines for monitoring autophagy (Klionsky et al. 2012). This assay uses inhibitors of autophagy turnover and analyses the consequences by monitoring the levels of LC3 II. Briefly, if the amount of LC3 II increases upon inhibitor treatment, this strongly indicates that the autophagic flux was previously intact and not compromised. In the following experiments, vinblastine or bafilomycin A were used as autophagy inhibitors. Vinblastine depolymerizes the normal and acetylated microtubule network and therefore inhibits the fusion of autophagosomes and lysosomes. Bafilomycin A is a V-ATPase inhibitor that elevates the lysosomal pH and inhibits degradation (Klionsky et al. 2012).

In the present study, HepG2 cells were incubated with three concentrations: 0.167 mM, 0.5 mM or 1.5 mM OA/BSA or with the corresponding BSA controls for three different time

periods: 24 h, 72 h or 5 d. Four hours before each harvest, the cells were pre-treated with 50 μM vinblastine or 100 nM bafilomycin A.

After 24 h OA/BSA incubation, the autophagy inhibitors caused an increase in LC3 II in each condition, which indicated an active autophagic flux (Figure 3.9 A). However, after 72 h incubation with 1.5 mM OA/BSA the inhibitor did not further increase the LC3 II levels (compare pink arrows in Figure 3.9 B), suggesting an impaired autophagy. The lower concentrations of OA/BSA as well as the full media (FM) and BSA controls showed an intact autophagic flux. A similar picture was seen after 5 d of OA/BSA incubation. There was an active autophagy in cells exposed to BSA or 0.167 mM OA, as evidenced by an additional increase in LC3 II upon inhibitor incubation. However, there was no further increment of LC3 II in HepG2 cells incubated with 0.5 mM OA/BSA, indicating a compromised/reduced autophagic flux.
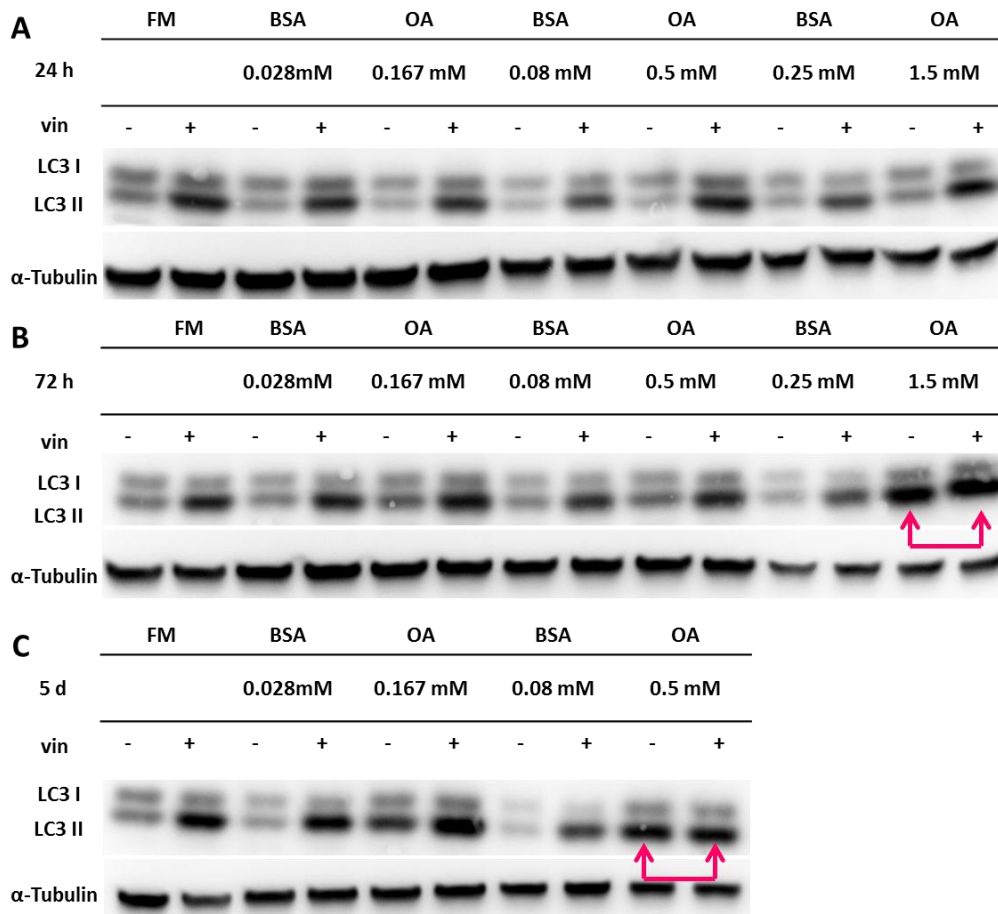
Figure 3.9: Confirmation of compromised autophagy in lipid-loaded HepG2 cells by the LC3 turnover assay. Representative Western blot of LC3 in the presence and absence of 50 μM vinblastine (vin) or 100 nM bafilomycin A (not shown) in control and lipid-loaded HepG2 cells. The time of OA/BSA stimulation varied from A) 24 h, B) 72 h to C) 5 days (n = 3). α-Tubulin served as loading control.

Altogether, the analysis of LC3 II and p62 levels in lipid-loaded HepG2 cells (Figure 3.8) as well as the LC3 II turnover assay (Figure 3.9) revealed a time and concentration-dependent effect on autophagy in HepG2 cells upon OA/BSA exposure. Whereas at lower concentrations of OA/BSA and/or shorter incubation times the autophagy flux was still active, the higher concentrations and/or longer incubation times resulted in a compromised autophagic flux.

3.2.2 Induction of steatosis in primary mouse hepatocytes

In addition to HepG2 cells, lipid accumulation was induced in primary mouse hepatocytes, cultivated in a collagen coated well and overlaid by a thick collagen layer. The advantage of cultivated primary mouse hepatocytes under these conditions is that they more resemble freshly isolated hepatocytes than HepG2 cells, even though primary mouse hepatocytes undergo massive gene expression changes during cultivation (Godoy et al. 2013). Moreover, primary mouse hepatocytes are more easily available than primary human hepatocytes since they can be isolated in house. A further advantage of this culture system is that primary cells are larger than HepG2 cells, and are still able to form bile canaliculi. Therefore, the impact of lipid accumulation on overall morphology and bile canaliculi morphology can be studied in this system.

OA/BSA incubation provoked lipid droplet accumulation in primary mouse hepatocytes as seen for HepG2 cells (Figure 3.10). The size of the lipid droplet was especially high in cells exposed to 1.5 mM OA/BSA. As illustrated in the left panel (0 mM OA/BSA) in Figure 3.10, the bile canaliculi were formed under control situations. In contrast, upon lipid accumulation (middle and right panels) the bile canaliculi could not be distinguished. Structural changes observed upon lipid excess are described in the next Chapter.
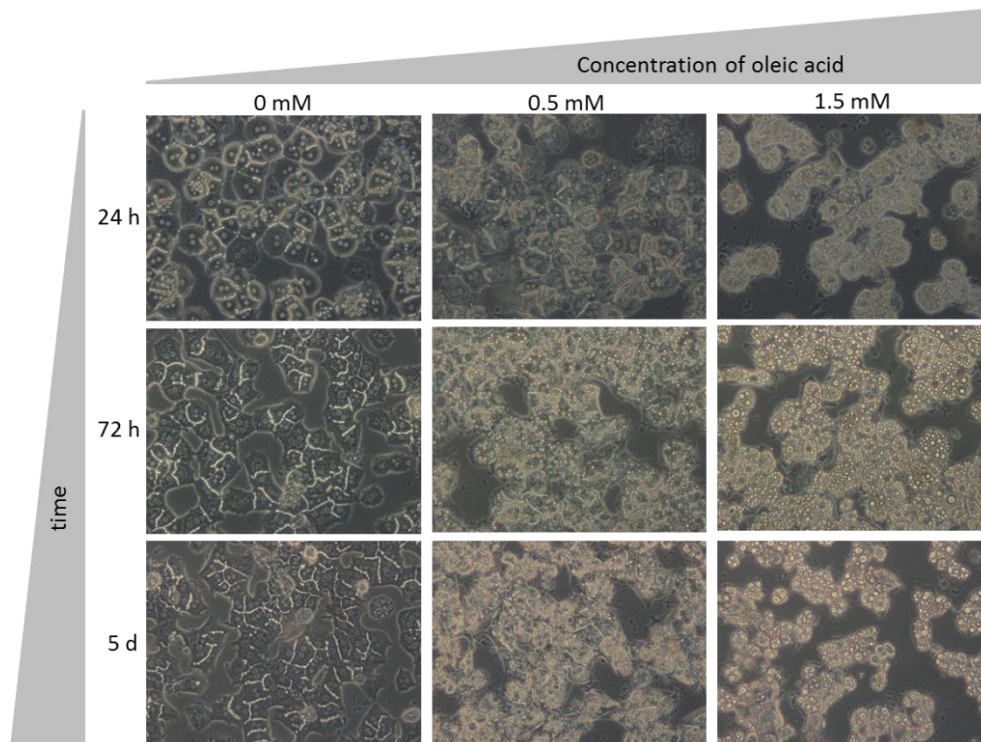
Figure 3.10: OA/BSA incubation induces lipid accumulation in primary mouse hepatocytes. Brightfield microscopy images show lipid droplets as bright spots in OA/BSA incubated cells (Magnification 200x).

3.2.2.1 Lipid accumulation affects the morphology and the bile canalicular structure of primary mouse hepatocytes

In the livers of steatotic *ob/ob* mice, a strong accumulation of lipid droplets was associated with a displacement of the nucleus towards the periphery of the cell (see Figure 3.1 E). To evaluate whether this feature was present in the *in vitro* steatosis model of primary mouse hepatocytes, OA/BSA exposed cells as well as control cells were stained for lipid droplets, the nucleus and the cell membranes. The white arrows in Figure 3.11 show some examples of shifted nuclei in lipid-loaded hepatocytes, indicating that displacement of nuclei by the increased quantity of cytoplasmic lipid droplets, as seen *in vivo*, is an event that can be recapitulated *in vitro*.
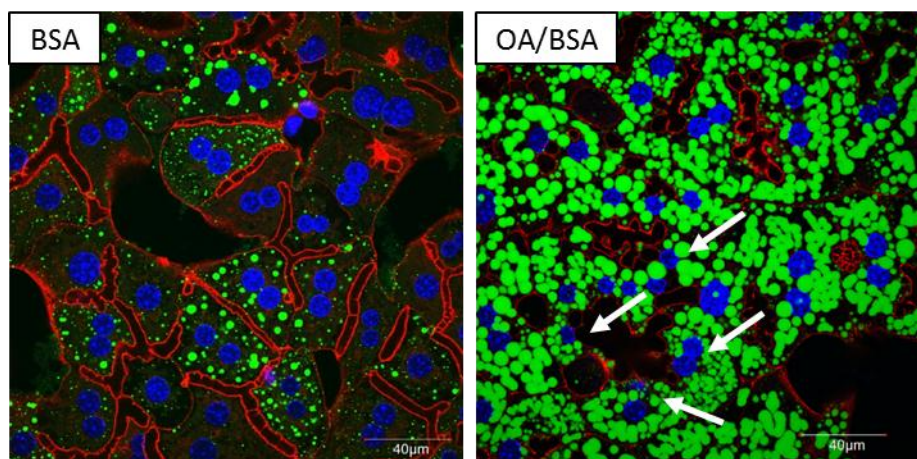
Figure 3.11: Intracellular lipid overload results in nuclear displacement. Primary mouse hepatocytes were cultivated 24 h before incubated with 0.8 mM OA/0.133 mM BSA or 0.133 mM BSA for 48 h. The nuclei were stained with DAPI (illustrated in blue), lipid droplets were visualised by Bodipy (green), and the membranes - more precisely F-actin filaments - were visualised with rhodamine-phalloidin (red); representative pictures. Scale bars represent 40 µm.

To explore whether this excessive amount of lipid droplets also influenced the cytoskeleton, an immunofluorescence staining of α-tubulin as a marker for microtubular network was applied. Figure 3.12 revealed a totally different arrangement of the microtubules in lipid-loaded primary mouse hepatocytes compared to control cells. Whereas under lean circumstances the microtubule fibres were spread throughout the cell, in the lipid-loaded situation these fibres were forced to squeeze around/through the lipid droplets and were no longer distributed throughout the entire cytoplasm.
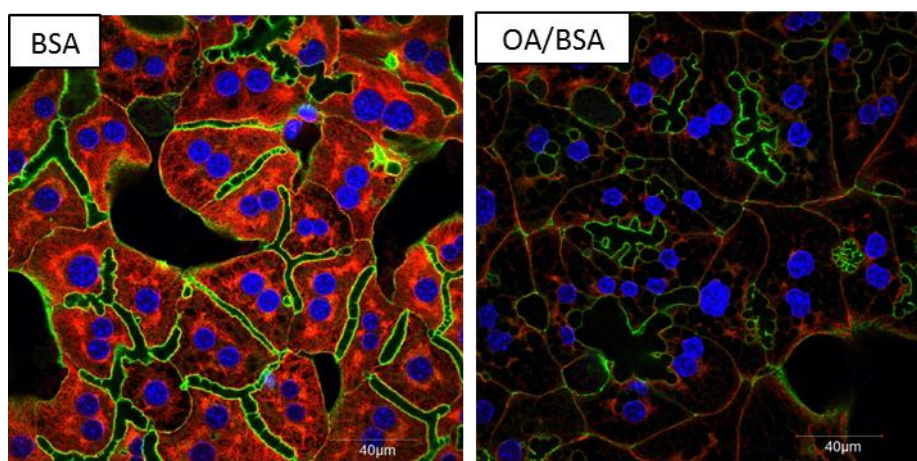
Figure 3.12: Tubulin network in steatotic hepatocytes is altered. Primary mouse hepatocytes were cultivated for 24 h before incubated with 0.8 mM OA/0.133 mM BSA or 0.133 mM BSA for 48 h. The nuclei were stained with DAPI (illustrated in blue), the microtubule network was detected with a tubulin-specific antibody by indirect immunofluorescence (red) and the membranes - more precisely F-actin filaments - were visualised with rhodamine-phalloidin (green); representative pictures. Scale bars represent 40 µm.

Results

This de-arranged tubulin network suggested a modified and restricted cytoskeleton in lipid-loaded primary mouse hepatocytes. Importantly, alterations of the cytoskeleton may affect or restrict microtubule-dependent vesicle trafficking of the cell.

The membrane staining in Figure 3.12 demonstrated an altered bile canaliculi morphology in steatotic primary mouse hepatocytes.

To visualise the bile canaliculi more clearly, DPPIV, a marker for bile canaliculi, was labelled using a specific anti-DPPIV antibody. After 24 h exposure to OA/BSA, the bile canaliculi in lipid-loaded hepatocytes appeared broader than and not as uniform as those in the control cells (Figure 3.13, upper panel). This observation became even more obvious after longer cultivation times. At 72 h incubation, the control cells formed long, thin bile canalicular structures with even shape. In contrast, the bile canaliculi network of the OA/BSA stimulated cells had not that even shape and appeared broader between some cells.
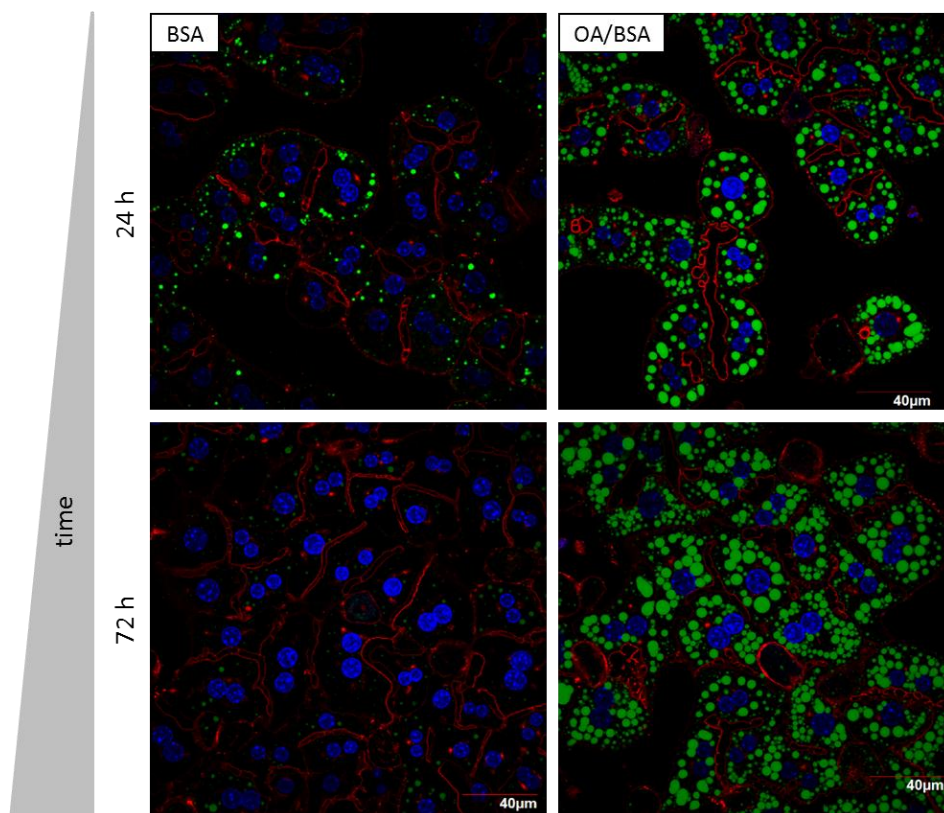
Figure 3.13: Lipid-loaded primary mouse hepatocytes show an altered morphology of bile canaliculi. Primary mouse hepatocytes were cultivated for 24 h before incubated with 0.5 mM OA/0.08 mM BSA or 0.08 mM BSA for 24 h or for 72 h. The nuclei were stained with DAPI (illustrated in blue), the bile canaliculi were detected with a DPPIV-specific antibody by indirect immunofluorescence (red) and lipid droplets were visualised by Bodipy (green); representative pictures. Scale bars represent 40 μm.

3.2.2.2 Lipid-loaded primary mouse hepatocytes display a reduced autophagy

In order to investigate whether the autophagy flux was compromised in lipid-loaded primary mouse hepatocytes in a similar manner as shown for lipid-loaded HepG2 cells, the LC3 II turnover assay was performed as described in Chapter 3.2.1.2. Since the microtubular network was completely modified in primary mouse hepatocytes due to intracellular lipid accumulation (Figure 3.12), and a disturbed microtubule network is known to impair fusion of autophagosomes with lysosomes (Kochl et al. 2006; Webb et al. 2004), this strongly indicated an impaired fusion capacity in lipid-loaded primary mouse hepatocytes. Figure 3.14 illustrates the protein levels of p62 and LC3 in primary mouse hepatocytes exposed for 72 h (left panel) or 5 d (right panel) to two different OA/BSA and BSA concentrations in the presence or absence of 100 nM bafilomycin A.
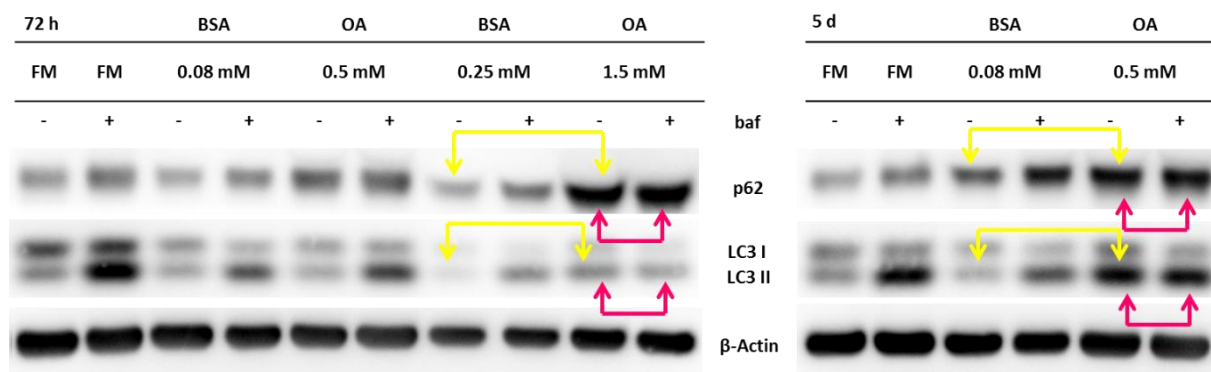
Figure 3.14: OA/BSA incubation compromises the autophagic flux in primary mouse hepatocytes in a time- and concentration-dependent manner. Representative Western blot of LC3 and p62 in the presence and absence of 100 nM bafilomycin A (baf) in control and lipid-loaded primary mouse hepatocytes. The time of OA/BSA stimulation varied from 72 h (left panel) to 5 days (right panel). β-Actin was used as a loading control (n = 3).

After 72 h incubation with 1.5 mM OA/BSA, the level of p62 accumulated compared to the corresponding 0.25 mM BSA control, this was accompanied by increased levels of LC3 II (yellow arrows). Co-treatment with 100 nM bafilomycin A did not seem to further elevate the levels of p62 or LC3 II (pink arrows), suggesting an impaired autophagy process. Under control conditions (FM, BSA) and lower fatty acid concentrations (0.5 mM OA/BSA), incubation with bafilomycin A resulted in p62 and LC3 II accumulation and revealed a functional autophagic flux in those cells. Thus, impaired autophagy flux at 72 h occurred only at high OA/BSA concentrations.

After 5 days, a similar picture was seen in primary mouse hepatocytes exposed to OA/BSA; however, the compromised autophagy occurred at lower OA/BSA concentrations (Figure 3.14, right panel). Cells incubated for 5 days with 0.5 mM OA/BSA showed elevated levels of p62 as

well as LC3 II in contrast to full media or BSA exposed cells (yellow arrows). Moreover, co-treatment with bafilomycin A did not further increase the levels of p62 and LC3 II, indicating a compromised autophagic flux. In contrast, control cells (FM or BSA) showed increased expression of p62 and LC3 II upon bafilomycin A co-treatment and suggested an intact autophagic flux in these cells.

All in all, the LC3 II turnover assay gave evidence of a compromised autophagic flux in primary mouse hepatocytes exposed to OA/BSA for three and five days depending on the OA/BSA concentration. Notable, the concentrations of OA/BSA as well as the duration of incubation leading to a disturbed autophagy were the same in primary mouse hepatocytes and HepG2 cells (see Figure 3.9).

3.2.3 Affymetrix gene array analysis of the *in vitro* steatosis model of HepG2 cells

To characterise genome-wide expression alterations in the *in vitro* steatosis model, Affymetrix gene array analysis was performed. The decision to analyse global gene expression alterations in OA/BSA exposed HepG2 cells was based on the fact that they are of human and not murine origin since gene array analysis was already performed for the murine steatosis situation in the *ob/ob* mouse model (see Chapter 3.1.3). To understand gene expression changes caused by lipid accumulation in a time-dependent manner, a single concentration of OA/BSA was used to stimulate the cells for several days. Thus, HepG2 cells were incubated for 24 h, 72 h or 5 days with 0.5 mM OA complexed to BSA, before RNA was isolated. Of note, these were the same time points where the cells were already characterized in terms of lipid accumulation, viability, and autophagic capacity. RNA from control cells in full media (FM) was used as the reference (calibrator) for each time point. In the following Chapter, the differential gene expression analysis of oleic acid treated HepG2 cells compared to the HepG2 cells in FM was performed.

3.2.3.1 The number of deregulated genes increases upon prolonged lipid stimulation

Two observations could be made from the PCA plot in Figure 3.15: First, there were profound gene expression differences between OA/BSA-incubated and control cells. Second, a time dependent change of gene expression within both groups was visible. Additionally, after 5 days of OA/BSA incubation, the variability between the replicates increased.
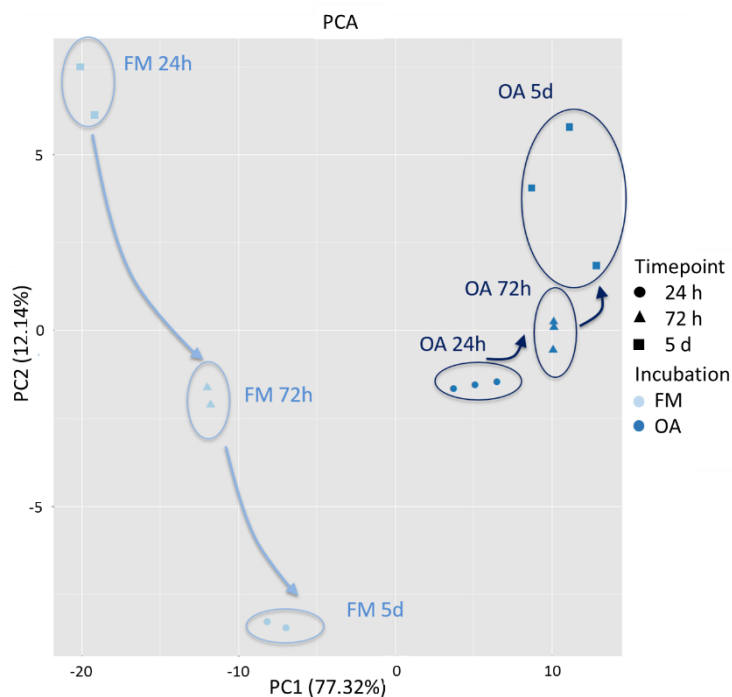
Figure 3.15: Gene array analysis reveals alterations of gene expression in lipid-loaded HepG2 cells. Gene array analysis was performed in HepG2 cells, which were incubated with 0.5 mM OA/BSA or full media (FM) for various time points. Gene expression differences were illustrated in a principle component analysis.

In Table 3.4, the numbers of significantly deregulated genes are listed. These increased upon prolonged OA/BSA incubation time. The duration of OA/BSA exposure, and consequently the amount of lipid accumulation seemed to be a crucial factor in determining gene expression alterations.

Table 3.4: Number of significantly deregulated genes in OA/BSA-exposed HepG2 cells compared to control HepG2 cells (n = 2-3; adjusted p-value < 0.05)

Comparison	Upregulated genes	Downregulated genes
24 h 0.5 mM OA vs FM	1859	1089
72 h 0.5 mM OA vs FM	2624	2509
5 d 0.5 mM OA vs FM	4336	3522

3.2.3.2 GO enrichment analysis of deregulated genes in lipid-loaded HepG2 cells

To interpret the set of deregulated genes obtained by the gene array analysis, a GO enrichment analysis was performed as described in Chapter 3.1.3.2. This analysis was done for each incubation time point of OA/BSA, including all significantly deregulated genes with a defined cut off of 1.5-fold change compared to FM. Again, the focus was on the domain "biological process". Detailed Tables of the enriched GO groups of up and downregulated genes in lipid-loaded HepG2 cells are listed below (Tables 3.5 – 3.7). Unexpectedly, the

upregulated genes did not significantly overrepresent a lipid metabolism associated GO term, as seen for the GO enrichment of steatotic livers of *ob/ob* mice (Chapter 3.1.3.2). Only after 24 h and 72 h was the set of upregulated genes enriched in the GO terms *reverse cholesterol transport* (GO:0043691) as well as *cholesterol homeostasis* (GO:0042632), although the over-representation was not significant. Altogether, there was rarely a group of significantly over represented upregulated genes in lipid-loaded HepG2 cells. Interestingly, there were only two overrepresented GO terms for the downregulated genes at all time points, namely *canonical glycolysis* (GO:0061621) and *cellular response to cadmium ions* (GO:0071276). Moreover, there was no GO term consistently overrepresented in the set of upregulated genes for all time points.

Table 3.5: GO enrichment analysis of deregulated genes in HepG2 cells after 24 h OA/BSA exposure. Top 10 GO terms

Upregulated genes		Downregulated genes	
GO term	adj p-value	GO term	adj p-value
GO:0043691 reverse cholesterol transport	0.17385035	GO:0061621 canonical glycolysis	1.02E-05
GO:0042632 cholesterol homeostasis	0.27564986	GO:0051301 cell division	0.00127925
GO:0043547 positive regulation of GTPase activity	0.32774281	GO:0007067 mitotic nuclear division	0.00159505
GO:0086091 regulation of heart rate by cardiac conduction	0.38073581	GO:0045926 negative regulation of growth	0.00184302
GO:0030198 extracellular matrix organization	0.5813412	GO:0071294 cellular response to zinc ion	0.00184302
GO:0006814 sodium ion transport	0.58244121	GO:0007062 sister chromatid cohesion	0.06863568
GO:0051923 Sulfation	0.60032032	GO:0007080 mitotic metaphase plate congression	0.07045449
GO:0006497 protein lipidation	0.60032032	GO:0071276 cellular response to cadmium ion	0.13532592
GO:0045820 negative regulation of glycolytic process	0.60032032	GO:0043433 negative regulation of sequence-specific DNA binding transcription factor activity	0.14331527
GO:0016311 dephosphorylation	0.61210795	GO:0006096 glycolytic process	0.20848852

Table 3.6: GO enrichment analysis of deregulated genes in HepG2 cells after 72 h OA/BSA exposure. Top 10 GO terms

Upregulated genes		Downregulated genes	
GO term	**adj p-value**	**GO term**	**adj p-value**
GO:0071230 cellular response to amino acid stimulus	0.62371738	GO:0006953 acute-phase response	0.09410289
GO:0008203 cholesterol metabolic process	0.72357658	GO:0071294 cellular response to zinc ion	0.10038109
GO:0043691 reverse cholesterol transport	0.73727257	GO:0045926 negative regulation of growth	0.10038109
GO:0050821 protein stabilization	0.76651022	GO:0061621 canonical glycolysis	0.12228612
GO:0042632 cholesterol homeostasis	0.77032103	GO:0006357 regulation of transcription from RNA polymerase II promoter	0.2217959
GO:0034613 cellular protein localisation	0.79240717	GO:0007568 aging	0.23752302
GO:0007050 cell cycle arrest	0.79583579	GO:0071222 cellular response to lipopolysaccharide	0.24045939
GO:1904262 negative regulation of TORC1 signaling	0.83103311	GO:0070201 regulation of establishment of protein localization	0.24239769
GO:0000122 negative regulation of transcription from RNA polymerase II promoter	0.84265134	GO:0045944 positive regulation of transcription from RNA polymerase II promoter	0.24902068
GO:0042981 regulation of apoptotic process	0.84554807	GO:0071276 cellular response to cadmium ion	0.25510946

Results

Table 3.7: GO enrichment analysis of deregulated genes in HepG2 cells after 5 d OA/BSA exposure. Top 10 GO terms

Upregulated genes		Downregulated genes	
GO term	adj p-value	GO term	adj p-value
GO:0006351 transcription, DNA-templated	0.00601903	GO:0071456 cellular response to hypoxia	0.00133296
GO:0006355 regulation of transcription, DNA-templated	0.05966979	GO:0061621 canonical glycolysis	0.04043354
GO:0042981 regulation of apoptotic process	0.61394741	GO:0007179 transforming growth factor beta receptor signaling pathway	0.04105637
GO:0032436 positive regulation of proteasomal ubiquitin-dependent protein catabolic process	0.6253193	GO:0006953 acute-phase response	0.04323332
GO:0061041 regulation of wound healing	0.83350723	GO:0006879 cellular iron ion homeostasis	0.04689641
GO:2000134 negative regulation of G1/S transition of mitotic cell cycle	0.9143135	GO:0001666 response to hypoxia	0.05036888
GO:0043434 response to peptide hormone	0.94249894	GO:0030855 epithelial cell differentiation	0.07109188
GO:0006977 DNA damage response, signal transduction by p53 class mediator resulting in cell cycle arrest	0.94416011	GO:0071276 cellular response to cadmium ion	0.08586923
GO:0097193 intrinsic apoptotic signaling pathway	0.94417028	GO:0001657 ureteric bud development	0.08690167
GO:0060348 bone development	0.94617806	GO:0045893 positive regulation of transcription, DNA-templated	0.08944533

As already seen by the increasing numbers of deregulated genes upon prolonged incubation with OA/BSA (Table 3.4), the time of the OA/BSA exposure *per se* or the continuous lipid accumulation had profound impact on the gene expression in HepG2 cells.

3.3 Published gene expression data sets of human NAFLD

In addition to the steatosis-related gene expression alterations in *ob/ob* mice and in the *in vitro* steatosis model of HepG2, two publically available data sets of human NAFLD were used to identify steatosis-relevant genes in human NAFLD.

One dataset on hepatic gene expression that was employed, was the study conducted by Moylan and colleagues, published in 2014. In this study, two groups of patients were defined: one group with patients at low risk for liver-related morbidity and mortality ("mild NAFLD"); the other group containing patients who were at high risk for the mentioned complications ("severe NAFLD") (Moylan et al. 2014). The classification of patients was based on the fibrosis stage of the liver. Patients with a fibrosis stage of 0 - 1 were in the group "mild NAFLD" (n = 40) and those with a fibrosis stage of 3 - 4 were grouped as "severe NAFLD" (n = 32). The aim of the study was to find gene expression alterations which could be used as biomarker for progression or as possible treatment targets. This data set is found under GSE49541 in the Gene Expression Omnibus (GEO) repository.

The second human data set on hepatic gene expression alterations aimed to describe global gene expression changes with regard to the progression of human NAFLD (Lake et al. 2011). From this study, we used the published microarray dataset called E-MEXP-3291 (http://www.webcitation.org/5zyojNu7T), and compared the hepatic gene expression of patients diagnosed as healthy (n =19) with patients suffering from NASH with or without steatosis (n = 16).

3.4 Approach for selecting steatosis-relevant genes

The gene expression alterations upon steatosis of the *ob/ob* mouse model, of lipid-loaded HepG2 cells as well as of the above mentioned publically available human data sets of NAFLD were compared to identify commonly deregulated genes in steatosis and NAFLD. For that reason, a pipeline was designed aimed at identifying steatosis-relevant genes across species and models.

Genes were considered to be relevant and of potential interest when they were found to be deregulated in both the *ob/ob* mouse model and in the publically available data sets of human NAFLD, as opposed to genes which were only altered in the fatty liver in one of both species. This approach ensured the identification of genes that were possibly relevant in human NAFLD, and offered the possibility of being studied in an animal model. In a next step, the overlapping genes were compared to deregulated genes in the *in vitro* HepG2 steatosis model. Thus, this would potentially allow the identification of genes altered in human and mouse NAFLD that could be studied in an *in vitro* system. This step has the risk of losing interesting *in vivo* relevant genes but on the other hand it offers the advantage of understanding the mechanism of deregulation by fatty acids/lipid accumulation *in vitro.*

3.4.1 Commonly differentially expressed genes in *ob/ob* mice and human NAFLD

In the first step of the pipeline, significantly (adjusted p-value < 0.05) deregulated genes from the two human data sets were compared to significantly (adjusted p-value < 0.05) deregulated genes in *ob/ob* mouse livers. They were then differentiated between the upregulated genes and the downregulated genes. In Figure 3.16, the overlaps between the three datasets are illustrated. For the three datasets, there are 102 commonly upregulated genes and 17 commonly downregulated genes. For further analysis, only those genes which were deregulated in all three data sets were considered.
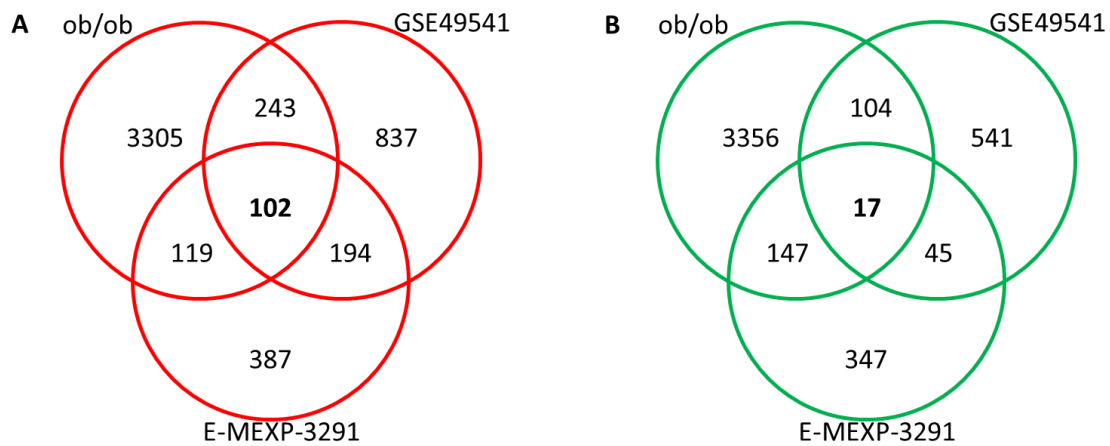
Figure 3.16: Overlap of deregulated genes in the *ob/ob* mouse model and in two human NAFLD data sets.
A) Venn diagram of upregulated genes in *ob/ob* mice and in the human data sets GSE49541 and E-MEXP-3291;
B) Venn diagram of significantly downregulated genes in *ob/ob* mice and in the human data sets GSE49541 and
E-MEXP-3291.

3.4.2 Overlap of deregulated genes in *ob/ob* mouse model, human NAFLD and OA/BSA incubated HepG2 cells

The second step of the pipeline involved the comparison of the newly identified deregulated genes in *ob/ob* mice and human datasets with significantly (adjusted p-value < 0.05) deregulated genes in the *in vitro* steatosis model of HepG2 cells. This overlap should encompass genes that are altered in human and mouse NAFLD caused by exposure to fatty acids *in vitro*. Using this approach, the number of genes considerably decreased.

As demonstrated in Figure 3.17, 18 genes were upregulated in the *in vitro* steatosis model of HepG2 as well as in the *ob/ob* mouse models and human data sets of NAFLD. Moreover, there were only four commonly downregulated genes. Lists of these deregulated genes are depicted in Tables 3.8 and 3.9.
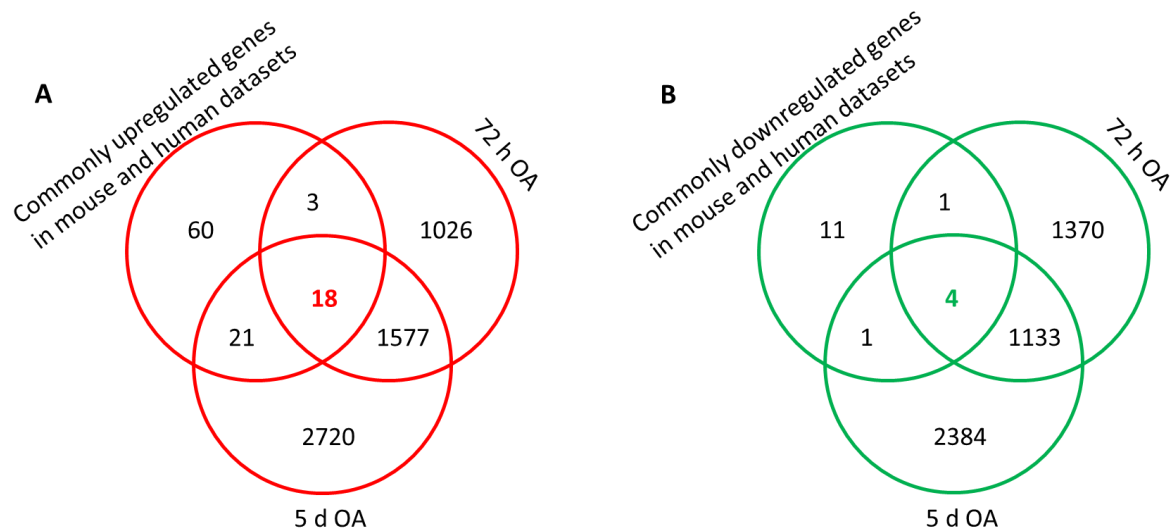
Figure 3.17: Overlap of deregulated genes of the HepG2 *in vitro* steatosis model and the extracted deregulated genes of the *ob/ob* mouse model and human datasets of NAFLD. A) Upregulated and B) downregulated genes of HepG2 cells incubated with 0.5 mM OA for 72 h or 5 d were compared to up- or downregulated genes in *ob/ob* livers and human NAFLD datasets.

Table 3.8: Commonly upregulated genes in *ob/ob* mouse livers, in human NAFLD and in OA/BSA exposed HepG2 cells (72 h and 5 d time points)

Gene	Encoding
DNAJB4	DnaJ homolog subfamily B member4
HSPA2	Heat shock related 70 kDa protein 2
SULF2	Extracellular sulfatase
NPNT	Nephronectin
THBS1	Thrombospondin
TIMP3	Metalloproteinase inhibitor 3
FAM102B	Protein FAM102B
ROBO1	Roundabout homolog
S100A10	Protein S100-A10
GLIPR1	Glioma pathogenesis-related protein 1
SPARC	Secreted protein acidic and cysteine rich
BIRC3	Baculoviral IAP repeat-containing protein 3
TCF4	Transcription factor 4
SPP1	Osteopontin
TPM1	Tropomyosin alpha-1 chain
FBN1	Fibrillin-1
TAGLN	Transgelin
MARCKS	Myristoylated alanine-rich C-kinase substrate

Table 3.9: Commonly downregulated genes in *ob/ob* mouse livers, in human NAFLD and in OA/BSA exposed HepG2 cells (72 h and 5 d time points)

Gene	Encoding
RXRA	Retinoic acid receptor RXR-alpha
AGXT	Alanine-glyoxylate aminotransferase
DNAJC12	DnaJ homolog subfamily C member 12
SLC13A5	Solute carrier family 13 member 5

3.4.3 Identification of *AGXT* as a steatosis-relevant gene

For all the deregulated genes mentioned above, a literature search was performed, and one gene was selected by the pipeline- *AGXT,* which encodes the alanine-glyoxylate aminotransferase. AGXT was of special interest because: i) it has never been described in the context of steatosis, and ii) its loss of function mutations are responsible for an impaired glyoxylate detoxification that results in increased production and excretion of oxalate. Elevated urinary oxalate concentration can result in the formation of insoluble calcium oxalate depositions in the kidney that injure the renal system. The resulting disease is an autosomal recessive disorder called primary hyperoxaluria type 1 (PH1; Online Mendelian Inheritance in Man 259900).

Interestingly, there is evidence linking the risk of kidney stones and the metabolic syndrome as well as elevated oxalate excretion in terms of obesity. In Table 3.10, a selection of publications that describe an association of urolithiasis with features of the metabolic syndrome is shown. However, the molecular mechanism which could explain the incidence of kidney stone disease in patients suffering from the metabolic syndrome, in particular NAFLD, was not elucidated. However, if AGXT is reduced to the extent that glyoxylate detoxification is compromised, the downregulation of AGXT in the fatty liver could provide an explanation.

Results

Table 3.10: Selection of publications regarding a link between the metabolic syndrome and the risk of kidney stones

Reference	Result/Conclusion
Akarken et al. 2015	Hypertension, hyperlipidemia and metabolic factors increase the risk of urolithiasis.
Einollahi et al. 2013	The prevalence of renal stone disease is higher in NAFLD than in healthy individuals.
Jeong et al. 2011	The metabolic syndrome is associated with an increased risk of kidney stone formation.
Kohjimoto et al. 2013	The severity of urolithiasis is associated with clustering of metabolic syndrome features.
Negri et al. 2008	Overweight and obesity increase the urinary excretion of the stone promotors oxalate and uric acid.
Polat et al. 2015	Patients with increased BMI and hypertension are at higher risk of calcium oxalate stone development.
Sakhaee et al. 2012	The more features of the metabolic syndrome the higher is the risk of forming calcium oxalate stone in patients without kidney stone history.
Semins et al. 2010	An obese BMI is associated with an increased risk of kidney stone disease.
Taylor et al. 2005	Obesity and weight gain increase the risk of kidney stone formation.
Taylor and Curhan 2006	Greater BMI is associated with elevated excretion of the stone promotors oxalate and uric acid.

In conclusion, applying the pipeline allowed the identification of *AGXT* as an interesting gene that is deregulated in mouse and human steatosis, and by fat accumulation *in vitro* that may contribute to kidney stone disease. Thus, the subsequent work in this thesis focused on the importance of AGXT in fatty liver - kidney interactions.

3.5 Validation of Agxt expression in steatosis models

The aim of the following experiments was to validate the downregulation of Agxt - observed in the genome-wide datasets - in liver samples of the *ob/ob* mouse model, in the *in vitro* steatosis systems of primary mouse hepatocytes and human hepatocellular carcinoma cell lines and in primary human hepatocytes. Confirmation of the downregulation of Agxt would justify the need for further experiments to investigate the consequences of the downregulation of Agxt.

3.5.1 Repressed Agxt expression in steatotic *ob/ob* mouse liver tissue

To confirm the downregulation of Agxt in steatosis as identified in the above delineated genome-wide studies, quantitative real-time PCR was performed using a specific Agxt Taqman assay. The quantitative real-time PCR revealed a 1.86 ± 0.34 fold downregulation of Agxt at the RNA level in livers of *ob/ob* mice (Figure 3.18 A) and thus, confirmed the gene array results used for the pipeline (showing a fold change of - 1.91). Furthermore, protein analysis using both the Western blot technique and immunohistochemistry showed reduced expression of the protein Agxt. In addition, for the first time a pericentral zonation of Agxt in mouse liver was discovered (Figure 3.18).
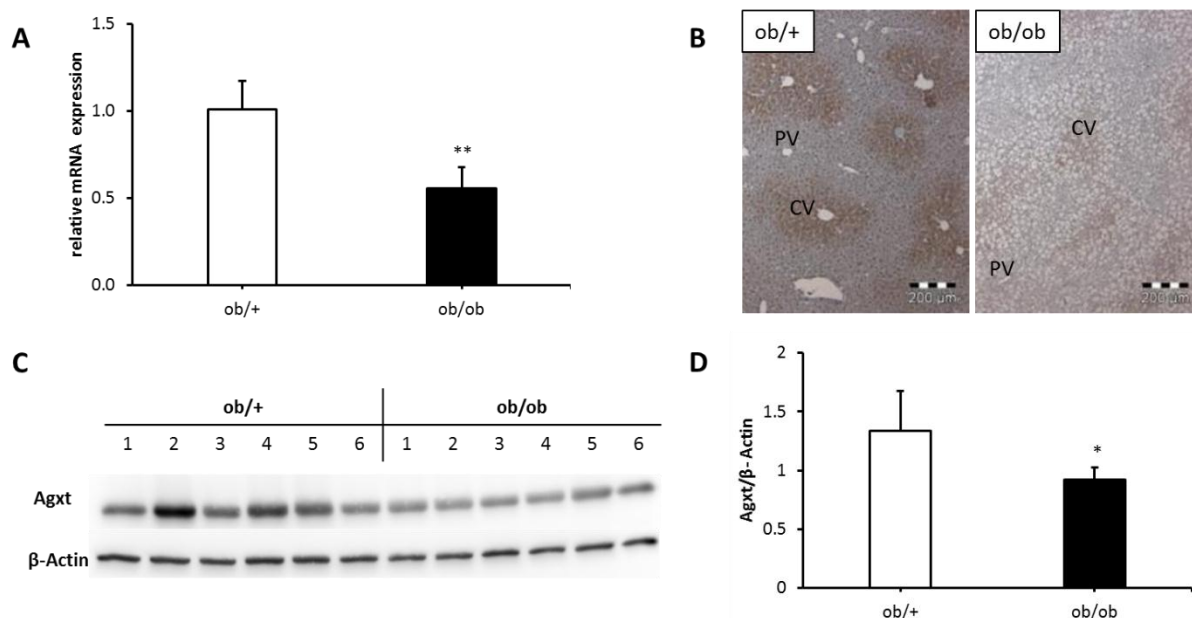
Figure 3.18: Livers of *ob/ob* mice display a reduced expression of Agxt. A) The RNA level of Agxt of *ob/ob* mouse livers was analysed by quantitative real-time PCR relative to *ob/+* mouse livers. Eif2a was used as the endogenous control (n = 5); B) The protein expression and zonation of Agxt were assessed by immunohistochemistry in paraffin embedded liver slides. The scale bars represent 200 µm, CV: central vein, PV: portal vein; C) Western blot and D) its densitometric quantification of Agxt expression in liver lysates of *ob/+* and *ob/ob* mice (n = 6). β-Actin was used as a loading control. * indicates $p < 0.05$; ** indicates $p < 0.01$.

3.5.2 Reduced Agxt expression in *in vitro* models of steatosis

After having demonstrated the downregulation of Agxt in *ob/ob* mouse livers, the next step was the validation of Agxt expression in *in vitro* steatosis models of primary mouse hepatocytes and an additional liver cancer cell line. These results would provide evidence of a direct association between lipid accumulation in hepatocytes and the downregulation of Agxt. The Affymetrix gene array of lipid-loaded HepG2 cells and corresponding control cells revealed a significant repression of AGXT, starting after 72 h of oleic acid exposure that remained until 5 days of treatment.

First, the expression of Agxt was investigated in the *in vitro* steatosis system of primary mouse hepatocytes. Figure 3.19 shows the analysis of Agxt expression at the RNA level (A) and protein level (B). After 72 h incubation with OA/BSA, the expression of Agxt was reduced upon both applied concentrations of OA/BSA compared to BSA controls. 5 d stimulation with OA/BSA caused strong variations in the RNA levels of Agxt between the biological replicates, and the difference between BSA and OA/BSA incubation was no longer obvious. One potential explanation could be a cultivation sensitivity of Agxt after plating the primary mouse hepatocytes.

Protein levels of Agxt were not reduced after 72 h but after 5 d incubation with 1.5 mM OA/BSA. This result indicated a relative long cellular half-time of the Agxt protein, which appears stable for several days despite a reduction of its transcript.
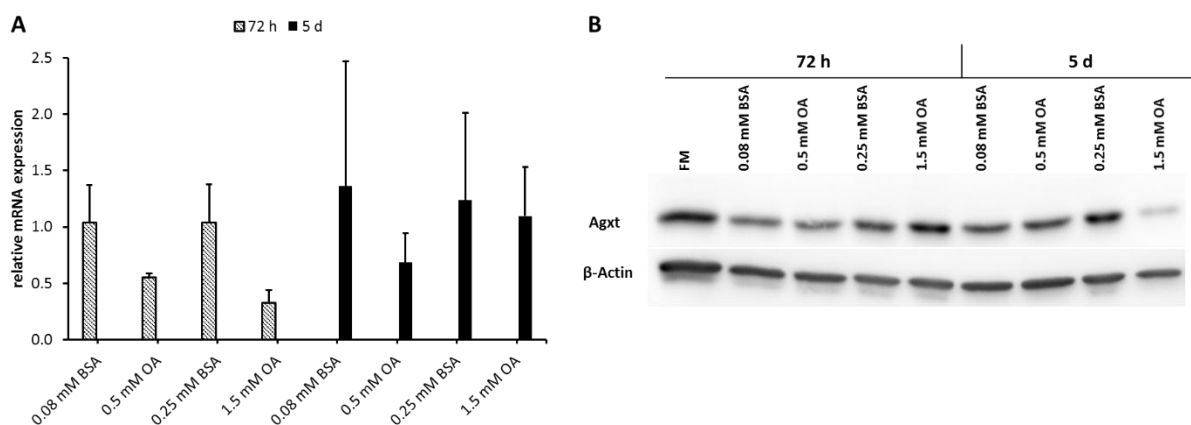
Figure 3.19: Downregulation of Agxt in primary mouse hepatocytes upon OA/BSA incubation. A) RNA level of Agxt of OA/BSA exposed primary mouse hepatocytes was analysed by quantitative real-time PCR relative to the BSA controls and time points; Gapdh was used as the endogenous control (n = 4); B) Representative Western blot of Agxt expression of FM and BSA or OA/BSA treated primary mouse hepatocytes. β-Actin was used as a loading control (n = 3).

All in all, the *in vitro* steatosis model of primary mouse hepatocytes indicated a lipid-dependent downregulation of Agxt. To confirm this observation, OA/BSA-induced lipid accumulation was applied in the additional human hepatocellular carcinoma cell line Huh7. In these cells, we could also demonstrate lipid droplet accumulation upon OA/BSA exposure, using the Oil Red O staining (Figure 3.20). In the subsequent experiments, AGXT expression in lean and lipid-loaded Huh7 cells was analysed at the RNA as well as at the protein level.
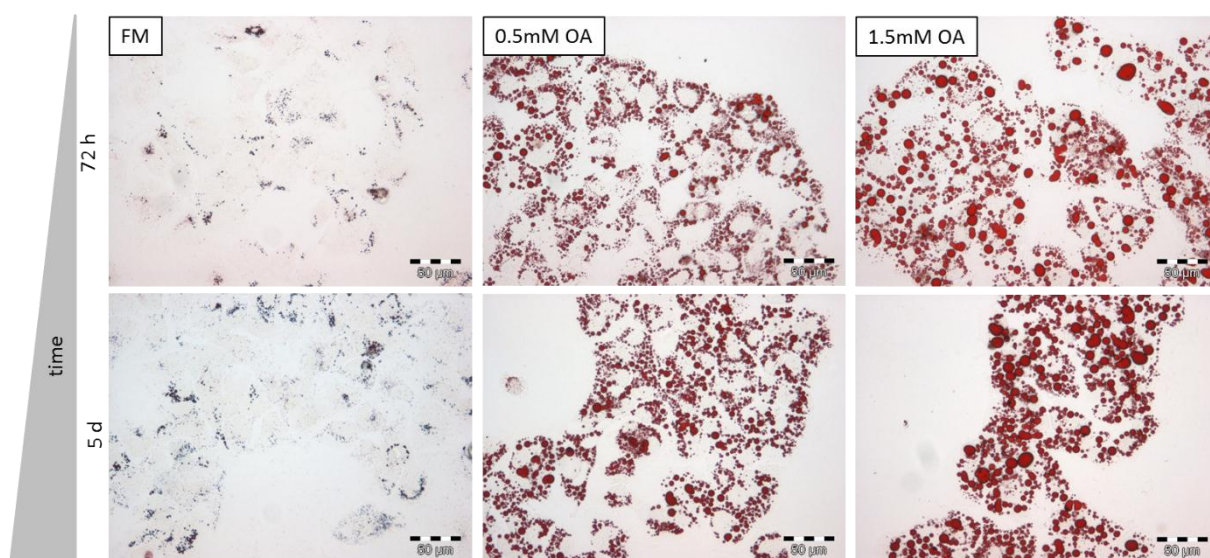
Figure 3.20: Induced lipid accumulation in Huh7 cells upon OA/BSA incubation. Oil Red O staining visualised lipid droplets after 72 h and 5 d incubation with 0.5 mM or 1.5 mM OA/BSA. Scale bars represent 50 µm.

As demonstrated in Figure 3.21, there was a reduction of the AGXT expression at the RNA level after 72 h incubation with 0.5 mM or 1.5 mM OA/BSA. In contrast, there was no decrease in AGXT protein expression after 72 h incubation with OA/BSA. Instead, the protein level of AGXT was clearly reduced after 5 d exposure to 1.5 mM OA/BSA.
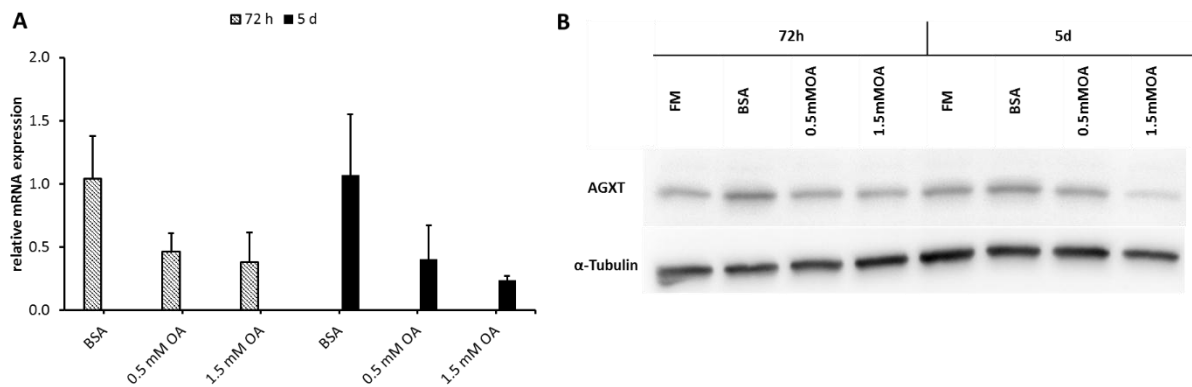
Figure 3.21: Downregulation of AGXT in Huh7 cells upon OA/BSA incubation. A) RNA level of AGXT of OA/BSA incubated Huh7 cells was analysed by quantitative real-time PCR relative to the BSA control (0.25 mM) and time point, UBC was used as the endogenous control (n = 4); B) Representative Western blot of AGXT expression of FM and BSA (0.25 mM) or OA/BSA exposed Huh7 cells (n = 3). α-Tubulin was used as a loading control.

These experiments in primary mouse hepatocytes as well as in human Huh7 cells confirmed a time-dependent downregulation of Agxt expression upon OA/BSA stimulation. The protein level Agxt did not decrease concurrently with the RNA levels but exhibited a delay. In addition, only the highest concentration of OA/BSA was able to decrease Agxt at the protein level.

Altogether, these experiments demonstrated successful a time- and concentration-dependent downregulation of Agxt upon OA/BSA incubation in both murine and human *in vitro* steatosis systems, suggesting a similar mechanism of downregulation.

3.6 Inverse correlation between the lipid content and AGXT expression in primary human hepatocytes

The experiments so far showed a strong association between lipid accumulation in hepatocytes and the downregulation of Agxt. This result was true for liver tissue from *ob/ob* mice and for the *in vitro* steatosis model with primary mouse hepatocytes as well as with Huh7 cells. To validate the downregulation of AGXT in human steatosis, primary human hepatocytes were used. Freshly isolated primary human hepatocytes from thirteen male donors were obtained from clinics or purchased from Hepacult. RNA was isolated for gene expression studies and cellular triglycerides were extracted and analysed for the determination of steatosis.

As illustrated in Figure 3.22, the RNA level of AGXT was reduced in several individuals. Moreover, there were pronounced differences regarding the cellular triglyceride content among the donors.
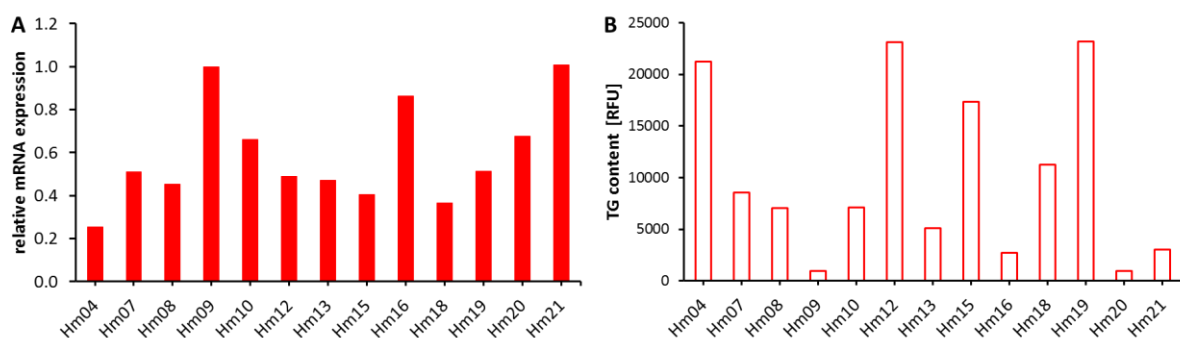
Figure 3.22: RNA expression of AGXT as well as the content of triglycerides are highly variable among the human hepatocytes donors. A) AGXT RNA expression in human male hepatocytes was quantified by real-time PCR relative to Hm09. GAPDH was used as the endogenous control; B) Enzymatic quantification of triglycerides in primary human hepatocytes (Hm: short for human male hepatocytes; number: individual donor).

The comparison of the AGXT expression in relation to the triglyceride amount for each individual showed an inverse correlation between the lipid content and the downregulation of AGXT, meaning less AGXT expression in hepatocyte samples containing higher triglycerides. This negative linear dependence was significant according to Spearman correlation (Figure 3.23 A). For the subsequent analysis, the available samples of primary human hepatocytes were separated into two groups according to their levels of triglycerides. All samples which had RFU values below 4000 were defined as the control, non steatotic, and those with RFU

values higher than 4000 were declared as steatotic. Using this approach, a significant

downregulation of AGXT in steatotic primary human hepatocytes was discovered as illustrated

in Figure 3.23 B.
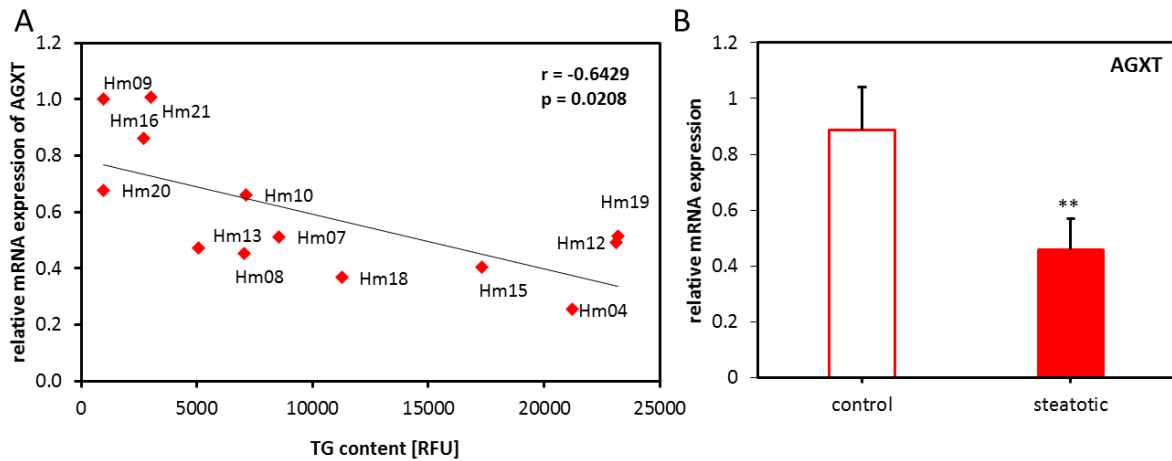
Figure 3.23: AGXT is downregulated in steatotic primary human hepatocytes. A) The negative Spearman correlation coefficient (r = -0.6429) indicated a negative linear dependence of the AGXT expression and the amount of triglycerides of male primary human hepatocytes that was significant (p = 0.0208); B) Steatotic human hepatocytes, defined by a TG content with RFU values higher than 4000, displayed a significant downregulation of AGXT RNA relative to non-steatotic hepatocytes (control n = 4, steatotic n = 9); GAPDH was used as the endogenous control. ** indicates p < 0.01.

This result supported and confirmed the hypothesis of a connection between the AGXT RNA

expression and the content of lipids within hepatocytes. Moreover, this experiment prove that

the previously observed downregulation of Agxt in livers of *ob/ob* mice and in the *in vitro*

steatosis systems also occurred in the human situation.

3.7 Deregulation of glyoxylate-associated genes in steatosis

As illustrated in Figure 3.24, AGXT is one of several enzymes involved in the glyoxylate pathway. To obtain an overall picture of the glyoxylate metabolism in steatotic liver, the RNA expression of some enzymes contributing to the glyoxylate metabolism was investigated in the *ob/ob* mouse model, in steatotic and non-steatotic primary human hepatocytes and in the *in vitro* steatosis model.
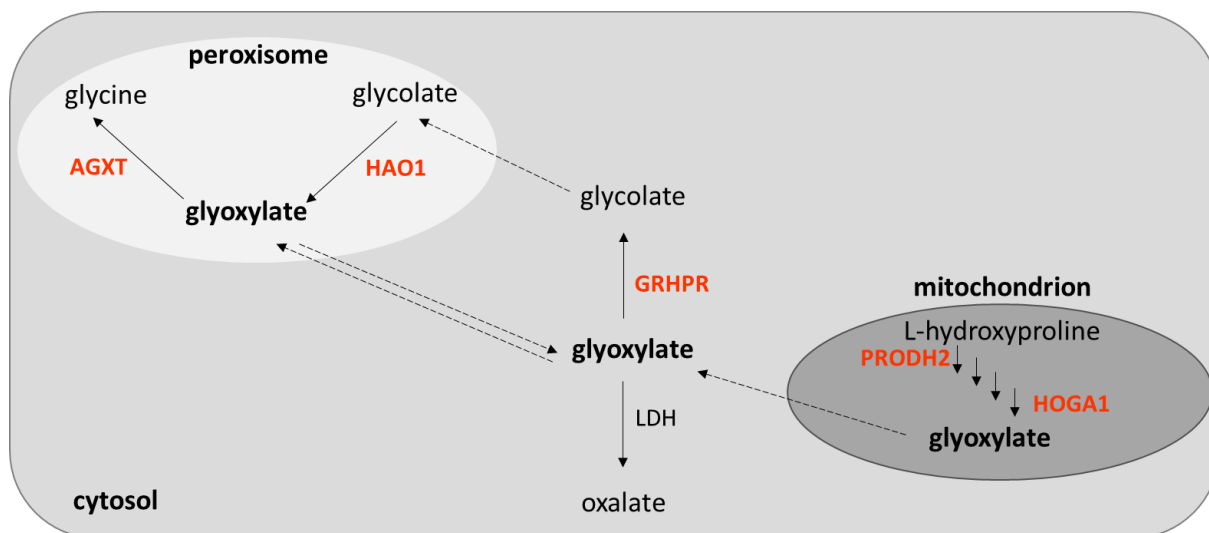
Figure 3.24: Simplified schematic illustration of glyoxylate metabolism and glyoxylate precursors in human hepatocytes. Figure does not cover the entire glyoxylate metabolism.

3.7.1 Hao1 is downregulated in the steatotic livers from *ob/ob* mice

According to the Affymetrix gene array analysis (Chapter 3.1.3), the RNA expression level of Hao1 but not Grhpr was significantly decreased in *ob/ob* mouse liver (fold change: -1.42). Downregulation of Hao1 was confirmed by real-time PCR showing approximately a 1.5-fold (1.50 ± 0.4) decreased level of *Hao1* mRNA in livers of *ob/*ob mice relative to *ob/+* mice, as illustrated in Figure 3.25. Its product, the peroxisomal enzyme hydroxyacid oxidase 1, preferably oxidises glycolate to glyoxylate. Its reduced RNA expression suggested a decreased oxidation capacity of *ob/ob* mice to form glyoxylate from glycolate.

Grhpr encodes the enzyme glyoxylate reductase/hydroxypyruvate reductase and mutations in the *GRHPR* gene are responsible for elevated oxalate excretion and formation of kidney stones in humans suffering from primary hyperoxaluria type 2 (Cramer et al. 1999). Detoxification of

glyoxylate by this enzyme did not appear to be compromised in the steatotic liver of *ob/ob* mice, as suggested by a lack of alteration of its RNA level (Figure 3.25).
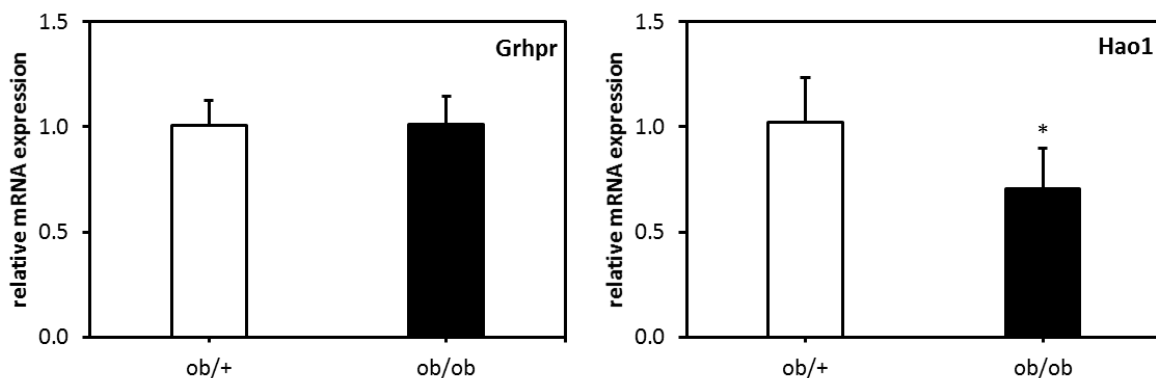
Figure 3.25: Hao1 is downregulated in *ob/ob* mouse livers. Quantitative real-time PCR confirmed the unaltered expression of Grhpr RNA and the downregulation of Hao1 RNA in *ob/ob* mouse livers relative to the expression in *ob/+* livers (n = 5). Eifa2 was used as the endogenous control. * indicates $p < 0.05$.

In contrast, two genes whose protein products are key enzymes involved in generating glyoxylate in the mitochondria *via* hydroxyproline breakdown, namely Prodh2 and Hoga1, were not downregulated in *ob/ob* mice, according to Affymetrix gene array. Prodh2 encodes the enzyme proline dehydrogenase 2 which catalyses the first step in the catabolism of hydroxyproline (Adams and Frank 1980; Summitt et al. 2015). In the catabolic pathway of hydroxyproline, two further enzymatic reactions take place before the enzyme 4-hydroxy-2-oxoglutarate aldolase (Hoga1) cleaves 4-hydroxy-2-oxoglutarate to pyruvate and glyoxylate (Adams and Frank 1980). Hoga1 is encoded by the gene *Hoga1* and mutations of this gene are responsible for primary hyperoxaluria type 3 (Belostotsky et al. 2010; Riedel et al. 2011).

Overall, these results indicate a selective alteration of the peroxisomal glyoxylate metabolism in steatotic livers of *ob/ob* mice. On the one hand, the downregulation of Agxt, whose mutations are responsible for primary hyperoxaluria type 1, indicate an increased risk for urolithiasis in *ob/ob* mice. On the other hand, we also observed a downregulation of Hao1, which is involved in peroxisomal generation of glyoxylate from glycolate. Thus, the consequences of these changes for the overall glyoxylate metabolism remain unclear.

3.7.2 Expressions of GRHPR and HAO1 are reduced in steatotic primary human hepatocytes

As shown in Figure 3.23, AGXT expression in primary human hepatocytes correlated inversely with the intracellular amount of triglycerides, and the classification of human hepatocytes into *non-steatotic* and *steatotic* confirmed its downregulation in steatosis. In the published human datasets of NAFLD, the expression of GRHPR, HAO1, HOGA1 and PRODH2 are either slightly but significantly reduced (Moylan et al. 2014) or not altered (Lake et al. 2011). For this reason, they were not discovered by the pipeline (Chapter 3.4). To analyse the expression of GRHPR and HAO1 in our collection of primary human hepatocytes, the hepatocytes were once more classified as control (non-steatotic) and steatotic according to their TG content as described in Chapter 3.6.

Quantitative real-time PCR analysis revealed a significant reduction in the GRHPR expression in steatotic primary human hepatocytes. In contrast, the RNA expression of HAO1 showed a non-significant trend of HAO1 downregulation in steatotic primary human hepatocytes (Figure 3.26).
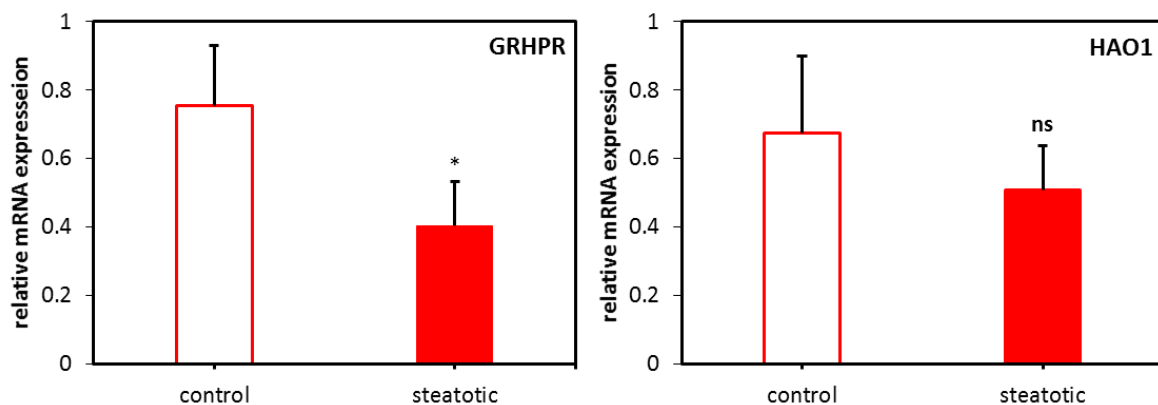
Figure 3.26: RNA expressions of GRHPR and HAO1 are reduced in steatotic primary human hepatocytes. Quantitative real-time PCR revealed a decrease in expression of GRHPR and HAO1 (not significant) in steatotic compared to non-steatotic human hepatocytes. GAPDH was used as the endogenous control (control: n = 4, steatotic: n = 9). * indicates $p < 0.05$, ns: not significant.

3.7.3 *In vitro* model of steatosis reveals a tendency of reduced RNA expression of Grhpr and Hao1

In addition to primary human hepatocytes, the *in vitro* steatosis model of primary mouse hepatocytes was analysed for it expression of Grhpr and Hao1. As illustrated in Figure 3.27, 72 h incubation with OA/BSA clearly reduced the RNA expression of Grhpr and Hao1. However, this effect was not clear after 5 d of OA/BSA stimulation. The reason could not be elucidated but one possibility may be a cultivation dependent effect. Nevertheless, induced lipid accumulation was able to alter – at least transiently - the expression of Grhpr and Hao1 in primary mouse hepatocytes.
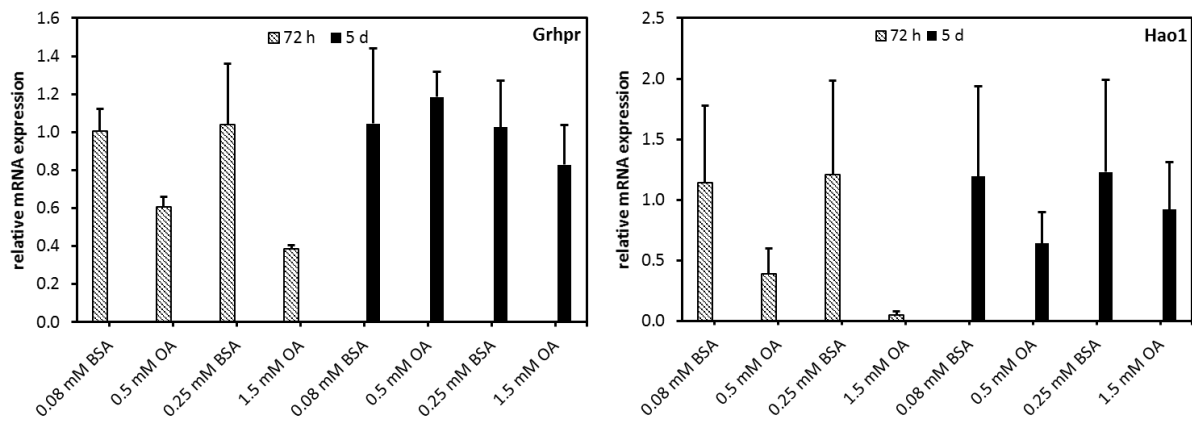
Figure 3.27: I*n vitro* steatosis model shows reduced levels of Grhpr and Hao1 RNA. OA/ BSA exposed primary mouse hepatocytes had decreased levels of Grhpr and Hao1 compared to BSA treated cells at 72 h time point. After 5 days of OA/BSA incubation, the expression levels of Grhpr and Hao1 were not as clear reduced as seen after 72 h incubation; Gadph was used as the endogenous control (n = 4).

3.8 Consequences of reduced Agxt expression in *ob/ob* mice

The downregulation of Agxt in the liver upon steatosis was confirmed in the leptin deficient *ob/ob* mouse model, in the fatty acid-induced steatosis *in vitro* and in primary human hepatocytes. The next step was to investigate the consequences of this downregulation for glyoxylate metabolism and hepatic oxalate generation in *ob/ob* mice. Figure 3.28 illustrates the different approaches and samples used for this purpose: i) glyoxylate-related metabolites in liver tissue were quantified by HR-MAS ^{1}H-NMR; ii) oxalate levels in the urine were quantified by GC-MS; and iii) the presence of calcium oxalate crystals in kidney tissue was investigated by Pizzolato staining.

As depicted in Figure 3.24, Agxt detoxifies glyoxylate to glycine. Therefore, even though, glycine is involved in and generated *via* various metabolic pathways, a decreased concentration of glycine within the liver of *ob/ob* mice could be expected and may indicate a disrupted glyoxylate detoxification. In addition, reduced Agxt activity upon decreased Agxt expression might lead to less effective glyoxylate removal, and consequently augmented oxidation to oxalate, which might be elevated in the urine of *ob/ob* mice. Finally, since increased urinary oxalate concentrations increase the risk of renal calcium oxalate depositions, the formation of kidney stones as a result of decreased Agxt expression in *ob/ob* mice was also analysed.
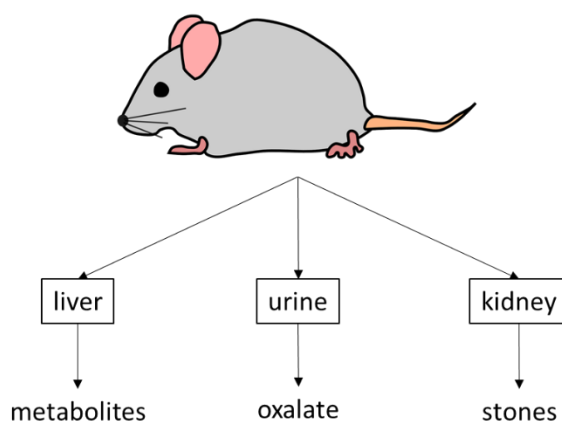
Figure 3.28 Illustration of the different approaches to analyse possible consequences of reduced Agxt expression in the *ob/ob* mouse model.

3.8.1 Steatotic *ob/ob* mouse livers have decreased concentrations of glycine and glycolate

For the metabolic profiling of steatotic *ob/ob* and *ob/+* mouse livers (n = 8), the high resolution magic angle ^{1}H-NMR (HR-MAS ^{1}H-NMR) technique was applied. This method allowed the identification of significant quantitative differences of several metabolites between *ob/+* and *ob/ob* mouse livers. Glycine and glycolate, but unfortunately not oxalate and glyoxylate, were among the glyoxylate-related metabolites that could be detected by this method. The results showed significantly lower concentrations of glycine as well as glycolate in steatotic livers of *ob/ob* mice compared to lean livers of *ob/+* mice (Figure 3.29). These data, generated with collaboration partners at ISAS Dortmund, were recently published (Gogiashvili et al. 2016).

The reduced concentration of glycine in steatotic mice may be a consequence of the steatosis-dependent repression of Agxt as described above. The lower glycolate concentration in livers from *ob/ob* mice may be a result of the decreased activity of Grhpr in *ob/ob* mice, although its expression level was not altered. These changes in metabolite levels may reflect physiological consequences of the altered glyoxylate metabolism in *ob/ob* mice.
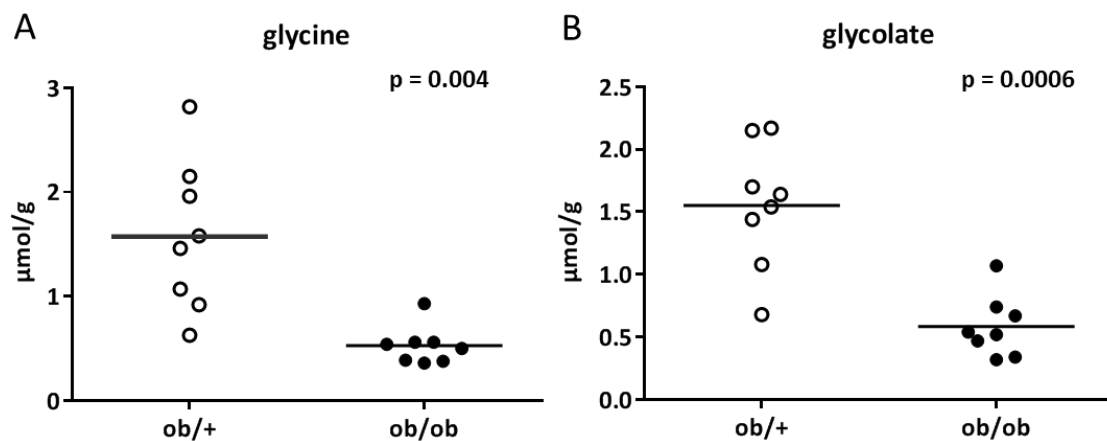
Figure 3.29: *Ob/ob* mice have reduced hepatic concentrations of glycine and glycolate. HR-MAS ^{1}HNMR results of glycine (A) and glycolate (B) concentrations in *ob/ob* and *ob/+* mouse livers (n = 8).

3.8.2 *Ob/ob* mice excrete more urinary oxalate than *ob/+* mice

The following experiments were designed to determine whether there was an increase in oxalate excretion of *ob/ob* mice. This was analysed in two situations: 1) under a normal diet and 2) under a diet that included an oxalate precursor. The goals of these two approaches were to determine whether oxalate levels are increased *per se* and/or if administration of an oxalate precursor exacerbated the amount of excreted oxalate, ultimately leading to the formation of kidney stones in *ob/ob* mice compared to *ob/+* mice.

In the literature, there are several challenges described that are shown to increase the formation of oxalate or induce the deposition of calcium oxalate stones under certain conditions in mice, e.g. administration of ethylene glycol (Salido et al. 2006), hydroxyproline (Knight et al. 2012), or glyoxylate (Khan and Glenton 2010) in water or in food. These oxalate precursors must be first metabolised in the body to glyoxylate; subsequently, the latter is either detoxified, or if generated in excess, converted to oxalate. Ethylene glycol is metabolised *via* an alcohol dehydrogenase to glycolaldehyde and then further oxidized to glycolate by an aldehyde dehydrogenase (Brent 2001). Glycolate is oxidized by Hao1 to glyoxylate. Since *ob/ob* mouse livers expressed less Hao1 than *ob/+* mouse livers, it was assumed that *ob/ob* mice could not oxidise glycolate as efficiently as the *ob/+* mice. Hydroxyproline is metabolised *via* several enzymatic steps as described in Chapter 3.7.1 and Figure 3.24. Enzymes involved in this pathway were not reduced in steatotic livers of *ob/ob* mice compared to livers of *ob/+* mice, suggesting a normal hydroxyproline breakdown in *ob/ob* mice.

A recent study reported that *ob/ob* but not *ob/+* mice develop kidney calcium oxalate stones upon daily intraabdominal injection of 50 mg/kg glyoxylate for six days (Fujii et al. 2013). This finding was a strong indication that *ob/ob* mice may have lost the capacity to detoxify an excess of glyoxylate. Thus, glyoxylate itself was selected in the first experiment to stimulate the oxalate production in *ob/+* and *ob/ob* mice.

3.8.2.1 Challenge with 0.5% glyoxylate in drinking water increases urinary oxalate excretion of *ob/+* and *ob/ob* mice

At the age of nine to thirteen weeks ten *ob/+* mice and ten *ob/ob* mice were divided in two groups. The first group of *ob/+* mice (n = 5) received drinking water that contained 0.5% sodium glyoxylate monohydrate for eight days. The second group of *ob/+* mice (n = 5) received

normal drinking water. The same conditions and animal numbers were used for *ob/ob* mice. Body weight and water consumption was carefully monitored during the experiment.

As Figure 3.30 illustrates neither the body weight nor the water consumption were affected by the glyoxylate challenge in *ob/+* and *ob/ob* mice. One mouse belonging to the control group of *ob/ob* mice drank more than 30 ml water per day and was excluded from the study. Interestingly, *ob/ob* mice ingested significantly less glyoxylate than the lean mice, as observed after adjustment to body weight.
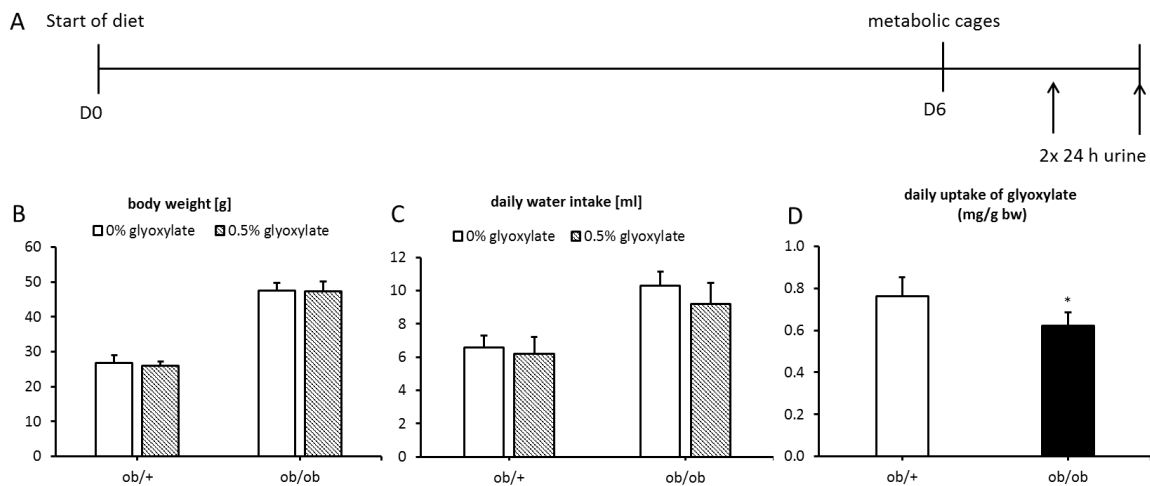
Figure 3.30: O*b/ob* **mice ingest less glyoxylate per body weight than** *ob/+* **mice on 0.5% glyoxylate diet**. A) Time line of diet; B) Average body weight; C) Daily intake of water and D) Ingestion of glyoxylate during 8 days of 0.5% glyoxylate challenge of *ob/+* and *ob/ob* mice; (n = 4-5). * indicates p > 0.05.

On day six of the glyoxylate diet, mice were transferred to a single mouse-metabolic cage and 24 h urine was collected on two consecutive days. The volume of daily excreted urine differed between the genotypes but did not differ between the glyoxylate diet and the corresponding control group, indicating that the glyoxylate challenge had no impact on the urine filtration and excretion (Figure 3.31 A). The higher urine volume in the *ob/ob* mouse groups was reflected by the decreased creatinine concentration in urine. Again, the glyoxylate supplementation did not impact the urinary creatinine concentration of each genotype. Quantification of oxalate by gas chromatographic analysis revealed several important aspects: 1) the urinary oxalate concentration did not differ significantly between the *ob/+* and *ob/ob* mice in the control situation. When the daily urinary excretion of oxalate was considered, this was significantly higher in the control *ob/ob* mice (300 ± 26 µg oxalate/mg creatinine) compared to control *ob/+* mice (202 ± 54 µg oxalate/mg creatinine), as demonstrated by the increased oxalate/creatinine ratio in Figure 3.31 D. 2) Upon 0.5% glyoxylate challenge, the

urinary concentration of oxalate increased in both genotypes, but was higher in *ob/+* mice (482 ± 73 vs 291 ± 61 µg/ml). 3) On 0.5% glyoxylate diet, the *ob/ob* mice excreted significantly more oxalate than *ob/+* mice on diet (1634 ± 283 vs 1162 ± 177 µg oxalate/mg creatinine). Several important conclusions can be drawn from this first experiment. First, *ob/ob* control mice excrete more oxalate on a daily basis than *ob/+* mice. Second, eight days of 0.5% glyoxylate diet increased the urinary oxalate excretion in both the *ob/ob* and in *ob/+* mice, but *ob/ob* mice excreted more oxalate than *ob/+* mice. The impact of the downregulation of Agxt is seen in the increased daily excretion of oxalate in urine of *ob/ob* mice.
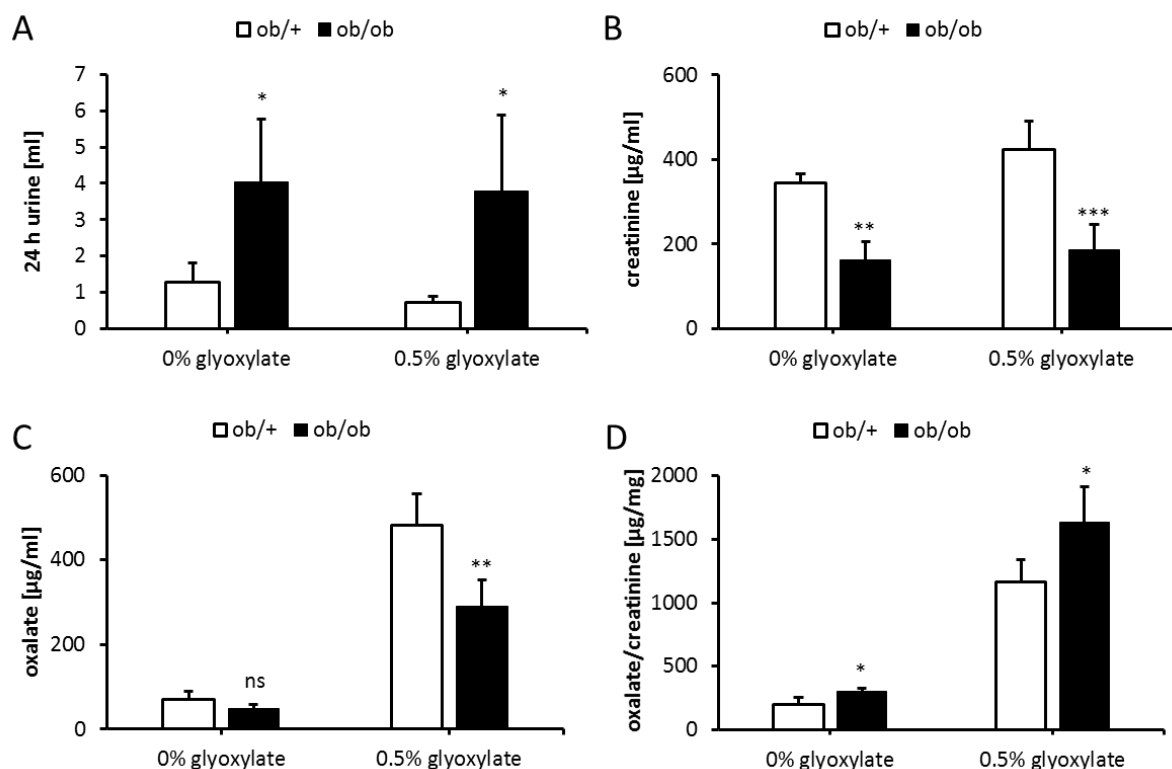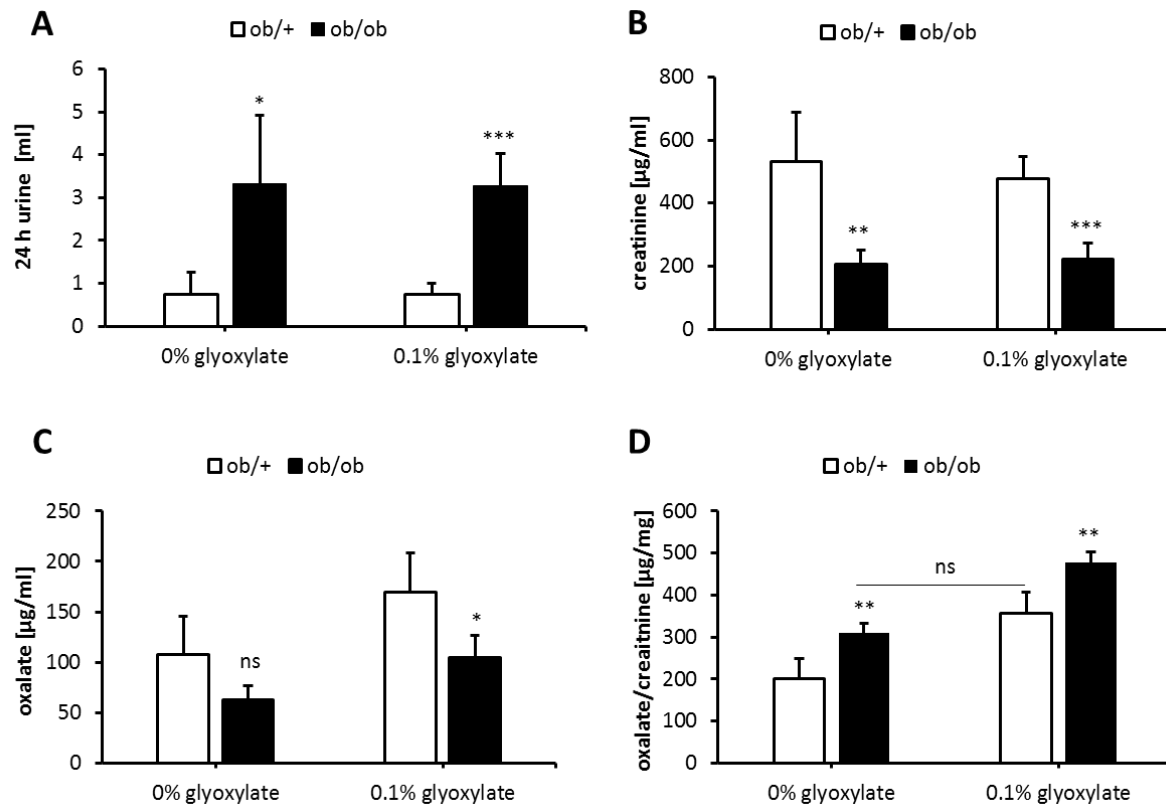

Figure 3.31: 0.5% glyoxylate in drinking water results in an increased excretion of oxalate of *ob/+* and *ob/ob* mice. A) Daily excreted urine volume of *ob/+* and *ob/ob* mice with or without 0.5% glyoxylate challenge; B) Urinary creatinine concentration of *ob/+* and *ob/ob* mice with or without 0.5% glyoxylate challenge; C) Urinary oxalate concentration of *ob/+* and *ob/ob* mice with or without 0.5% glyoxylate challenge (quantification by GC-MS); D) Daily urinary oxalate excretion normalised to creatinine level of *ob/+* and *ob/ob* mice with or without 0.5% glyoxylate challenge; (n = 4-5). ns: not significant * indicates p < 0.05; ** indicates p < 0.01; *** indicates p < 0.001.

The fact that 0.5% glyoxylate challenge elevated the excreted oxalate amounts in both *ob/+* and *ob/ob* mice indicated that the concentration of the glyoxylate diet might be too high to be detoxified under normal Agxt expression in *ob/+* mice. In a next step, a concentration of glyoxylate that should be well tolerated by *ob/+* mice was tested. For that reason, a challenge with decreased glyoxylate concentration was applied with the same mouse groups mentioned above after the urinary oxalate concentrations returned to normal (data not shown).

3.8.2.2 Challenge of *ob/+* mice with 0.1% glyoxylate increases the oxalate excretion to a level excreted by the *ob/ob* mice without diet

After three weeks of recovery, the glyoxylate diet was repeated with tap water containing 0.1% sodium glyoxylate monohydrate. The corresponding control groups drank tap water without any additives. The experimental set up was the same as drafted in Figure 3.30 A. The body weights were measured routinely and the daily consumption of water of each mouse was recorded. There were no differences between the glyoxylate and their control groups regarding their body weight and daily drinking volume as illustrated in Figure 3.32. But the daily ingestion of glyoxylate relative to their body weight was clearly reduced in *ob/ob* mice.
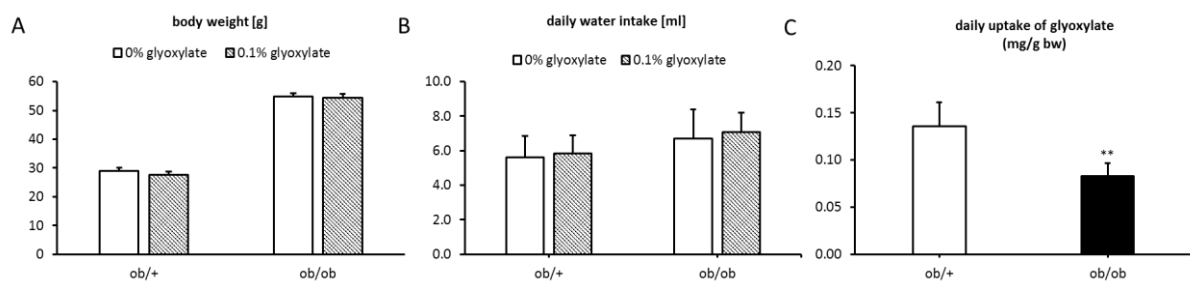
Figure 3.32: O*b/ob* mice ingest less glyoxylate per body weight than *ob/+* mice on 0.1% glyoxylate diet. A) Average body weight; B) Daily intake of water and C) Ingestion of glyoxylate during 8 days of 0.1% glyoxylate challenge of *ob/+* and *ob/ob* mice; (n = 4-5). ** indicates $p < 0.01$.

On day six of the diet, the mice were transferred to a single mouse metabolic cage and 24 h urine was collected on two consecutive days.

The daily excreted urine volumes (Figure 3.33 A) were comparable to those during the 0.5% glyoxylate diet. Again, *ob/ob* mice excreted more urine than *ob/+* mice. In addition, the creatinine concentrations in urine of *ob/ob* mice were significantly reduced. The urinary concentrations of oxalate were increased upon 0.1% glyoxylate challenge in both genotypes. However, the daily excreted amount of oxalate, indicated by the ratio of oxalate to creatinine, was significantly higher in *ob/ob* mice, both in the 0.1% glyoxylate group (477 ± 25 µg oxalate/mg creatinine) and in the untreated group (310 ± 22 µg oxalate/mg creatinine), compared to *ob/+* mice (356 ± 51 µg oxalate/mg creatinine and 202 ± 48 µg oxalate/mg creatinine, respectively). Remarkably, the oxalate/creatinine ratio in the urine of the *ob/ob* mice without glyoxylate challenge did not significantly differ compared to the glyoxylate-treated group of the *ob/+* genotype (Figure 3.33 D).

Figure 3.33: 0.1% glyoxylate in drinking water results in an increased excretion of oxalate of o*b/+* and *ob/ob* mice. A) Daily excreted urine volume of *ob/+* and *ob/ob* mice with or without 0.1% glyoxylate challenge; B) Urinary creatinine concentration of *ob/+* and *ob/ob* mice with or without 0.1% glyoxylate challenge; C) Urinary oxalate concentration of *ob/+* and *ob/ob* mice with or without 0.1% glyoxylate challenge (quantification by GC-MS); D) Daily urinary oxalate excretion normalised to creatinine level of *ob/+* and *ob/ob* mice with or without 0.1% glyoxylate challenge; (n = 4-5). * indicates $p < 0.05$; ** indicates $p < 0.01$; *** indicates $p < 0.001$; ns: not significant**.**

3.8.2.3 Glyoxylate-enriched drinking water does not induce formation of kidney stones in *ob/+* and in *ob/ob* mice

As described above, *ob/ob* mice were slightly hyperoxaluric compared to *ob/+* mice under normal condition, as indicated by an elevated daily oxalate excretion level. Glyoxylate-enriched drinking water increased the amount of excreted oxalate per day in both genotypes. To investigate whether the augmented daily production and renal excretion of oxalate results in calcium oxalate depositions, paraffin embedded kidney sections were stained for calcium oxalate stones according to the protocol of Pizzolato (Pizzolato 1964). In this staining, calcium oxalate stones appear as black/brownish deposits. As illustrated in Figure 3.34, a 0.1% glyoxylate-enriched diet did neither induce calcium oxalate deposits in kidneys of *ob/ob* mice nor of *ob/+* mice. This showed that the increased level of urinary oxalate observed was not severe enough to result in calcium oxalate stone formation.
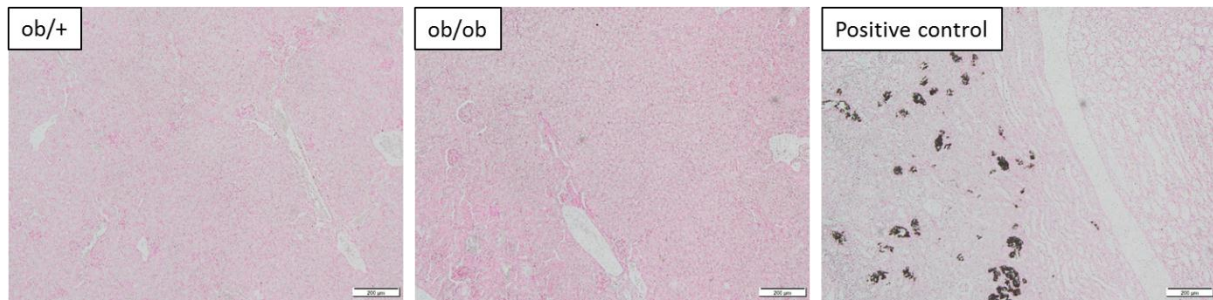
Figure 3.34: Glyoxylate enriched diet for 8 days does not induce calcium oxalate stones in kidneys of *ob/+* and *ob/ob* mice. Pizzolato staining of right and left kidneys were performed and neither kidney showed any indication of calcium oxalate deposits. Shown are representative pictures of the right kidneys; data for left kidney are not shown. The positive control was a courtesy of Prof. Hans-Joachim Anders from the Medizinische Klinik und Poliklinik IV, Klinikum der Universität München. Scale bars represent 200 μm.

3.9 Glyoxylate metabolism and urinary oxalate excretion in additional mouse models of NAFLD

The leptin deficient *ob/ob* mouse model of NAFLD showed a convincing downregulation of Agxt and suggested a steatosis-dependent deficient detoxification of glyoxylate. Moreover, the slight increase in urinary oxalate excretion of *ob/ob* mice may be the consequence of the reduced expression of Agxt. To exclude that these alterations occurred due to the specific deficiency of the mouse model itself (leptin deficiency), two additional mouse models of NAFLD were investigated with regard to their glyoxylate metabolism.

3.9.1 Glyoxylate metabolism in *db/db* mice

In addition to the leptin deficient *ob/ob* mouse model, the leptin receptor-deficient *db/db* mouse model was explored. The main difference between these two genetic mouse models for NAFLD is that *ob/ob* mice are not able to produce leptin due to a mutation in the *leptin* gene; whereas, *db/db* mice have a mutation in the *leptin receptor* gene. As a consequence, *db/db* mice produce leptin but cannot respond to it due to the defective receptor (Trak-Smayra et al. 2011). Therefore, the aim of this study was to investigate whether the findings in the *ob/ob* mice also apply to the *db/db* mice and to identify similarities and differences between the two models regarding the urinary oxalate excretion and expression of Agxt and the other glyoxylate metabolism-associated genes. First, *db/db* and *db/+* mice (n = 5) were placed in single mouse metabolic cages and 24 h urines were collected in order to quantify the oxalate concentrations. Afterwards, four mice of each genotype were sacrificed and their

liver tissues were examined. Additionally, hepatocytes isolated from livers of *db/db* and *db/+* mice (n = 2) were isolated and analysed.

3.9.1.1 *Db/db* mice do not excrete more oxalate than *db/+* mice

Oxalate and creatinine levels were quantified in the collected 24 h urines of each mouse. As illustrated in Figure 3.35 A, oxalate levels decreased in the urine of *db/db* mice. Furthermore, the creatinine concentrations were also significantly lower in the urine of *db/db* mice, reflecting the large urine volumes, and thus decreased metabolite concentrations in the urine of *db/db* mice. After adjustment of the urinary oxalate concentration to the creatinine concentration, there was no significant difference in the daily oxalate excretion between *db/db* mice and *db/+* mice (Figure 3.35 D). In conclusion, *db/db* mice were not hyperoxaluric, in contrast to *ob/ob* mice.
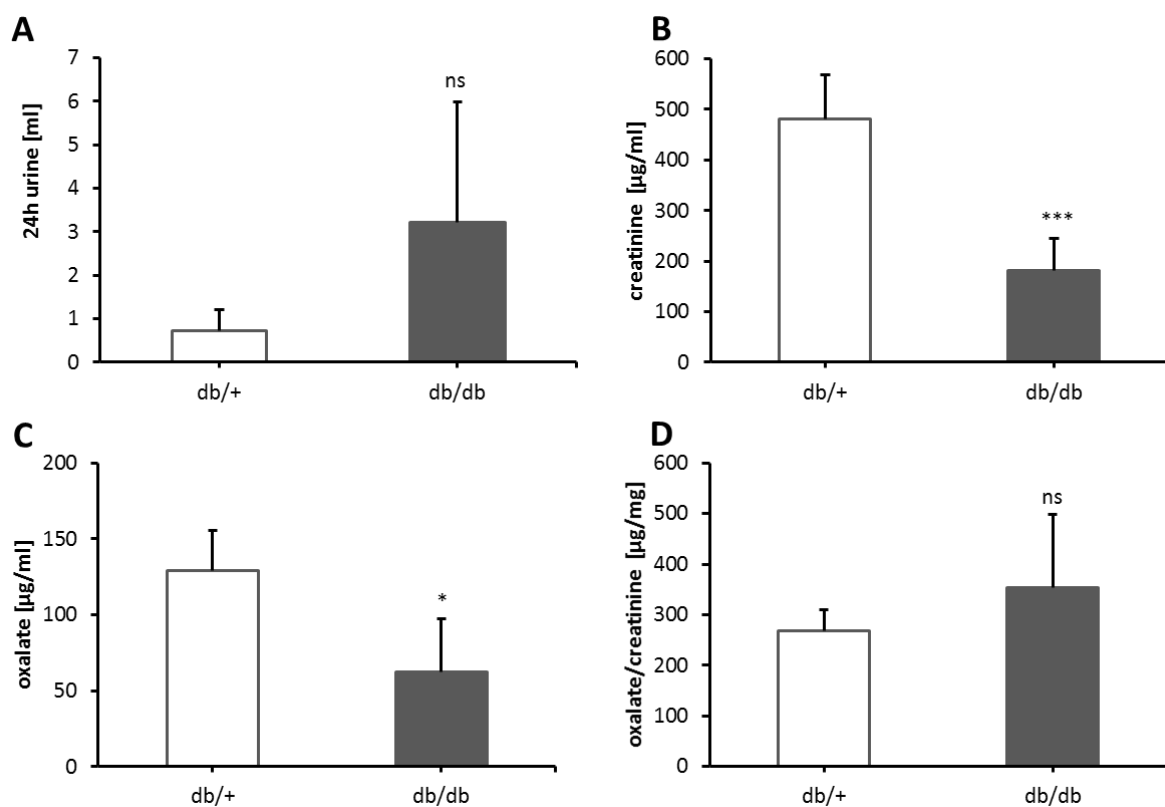
Figure 3.35: *Db/db* mice do not excrete more oxalate than *db/+* mice. A) Daily excreted urine volume of *db/+* and *db/db* mice (n = 5); B) Urinary creatinine concentration of *db/+* and *db/db* mice (n = 5); C) Urinary oxalate concentration of *db/+* and *db/db* mice (n = 5; quantification by GC-MS); D) Daily urinary oxalate excretion normalised to creatinine level of *db/+* and *db/db* mice (n = 5). ns: not significant; * indicates $p < 0.05$; *** indicates $p < 0.001$.

3.9.1.2 *Db/db* mice have the same liver to body ratio as *db/+* mice and hepatic lipid accumulation in the pericentral field

During the liver tissue collection, the body weight and the liver weight of each mouse was measured. D*b/db* mice had increased body and liver weights compared to the *db/+* mice as exemplified in Figure 3.36. In contrast to *ob/ob* mice, see Figure 3.1 C, the liver to body weight ratio was not altered in *db/db* mice. Enzymatic triglyceride quantification revealed an approximately 3.5-fold higher concentration of triglycerides in *db/db* livers compared to *db/+* livers. In contrast, the *ob/ob* mice had a 16-fold increased content of triglycerides compared to control mice (see Figure 3.1 D). H&E staining of paraffin sections of the liver was performed. A pericentral to midzonal accumulation of lipid droplets was observed in the livers of *db/db* mice; whereas no lipid droplets were observed in the periportal region. Furthermore, a large number of lipid-loaded hepatocytes displayed nuclei that were shifted towards the periphery of the cells (exemplified by yellow arrows in Figure 3.36 E). Altogether, these findings indicate that the steatotic phenotype in *db/db* mice is qualitatively similar but less severe than in *ob/ob* mice.
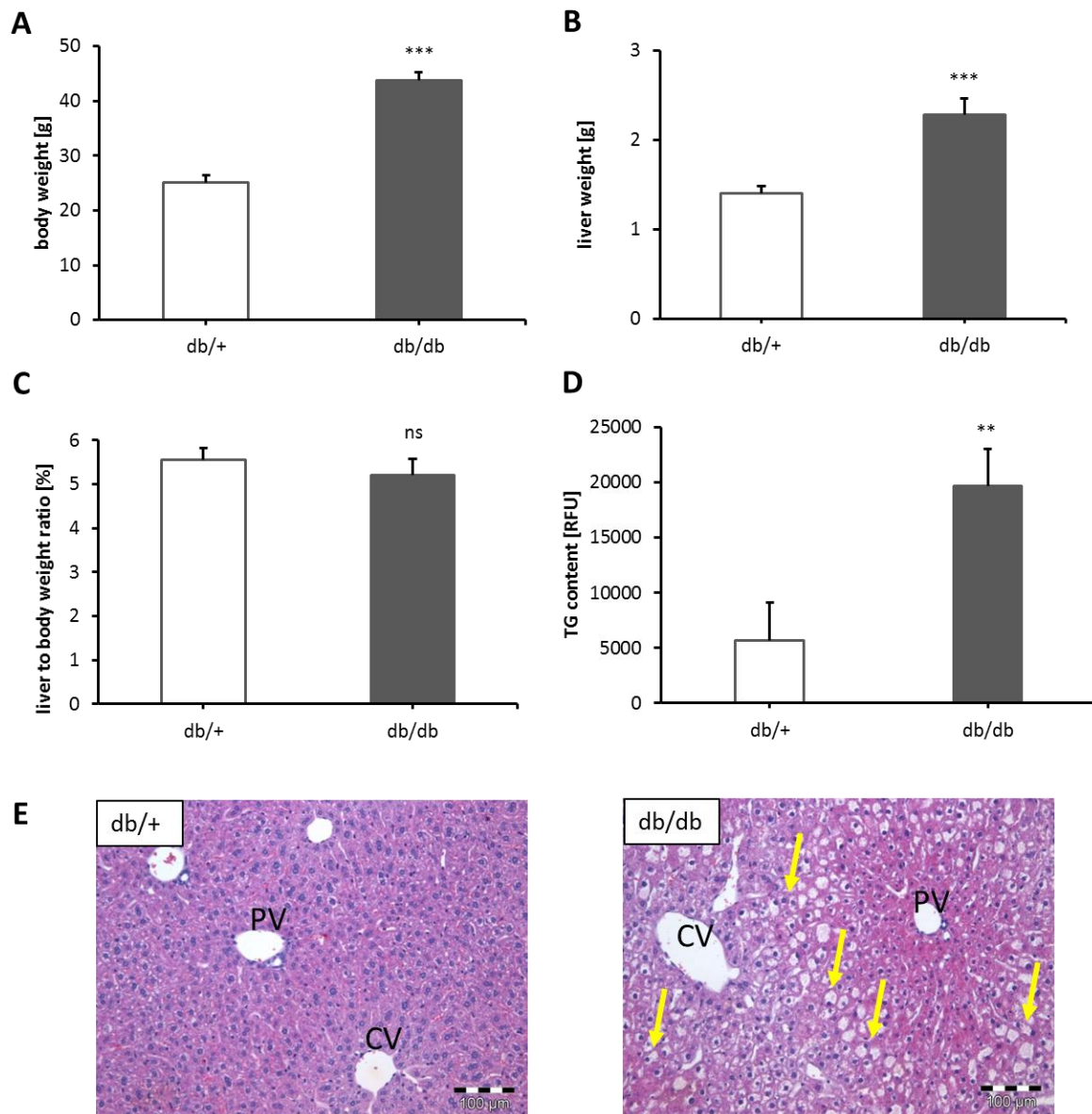
Figure 3.36: Steatotic *db/db* mice have the same liver to body weight ratio and show hepatic lipid accumulation in the pericentral field. A) Body weight of *db/db* and *db/+* mice (n = 4); B) Liver weight of *db/db* and *db/+* mice (n = 4); C) Liver to body weight ratio (n = 4); D) Enzymatic triglyceride quantification of *db/db* and *db/+* mouse livers extracts; E) Representative H&E staining of paraffin embedded liver sections of *db/+* and *db/db* mice. Scale bars represent 100 µm. CV: central vein, PV: portal vein. ns: not significant; ** indicates $p < 0.01$; *** indicates $p < 0.001$.

3.9.1.3 *Db/db* mice show no Agxt reduction

Since *db/db* mice did not secrete more oxalate than the *db/+* mice, Agxt levels were compared in the both genotypes in the next step. RNA was isolated from liver tissue as well as from hepatocytes and quantitative real-time PCR was performed. Interestingly, Agxt RNA expression was not reduced in liver tissue of *db/db* compared to *db/+* mice (Figure 3.37 A).

Results

The unaltered expression of Agxt in *db/db* hepatocytes was confirmed using isolated hepatocytes.

Moreover, protein expression of Agxt was analysed by Western blot using protein lysates from liver tissue of *db/+* and *db/db* mice. There was no decrease in the protein level of Agxt in *db/db* mice compared to their lean counterparts (Figure 3.37 C,D) explaining why *db/db* mice did not have elevated oxalate excretion compared to *db/+* mice.
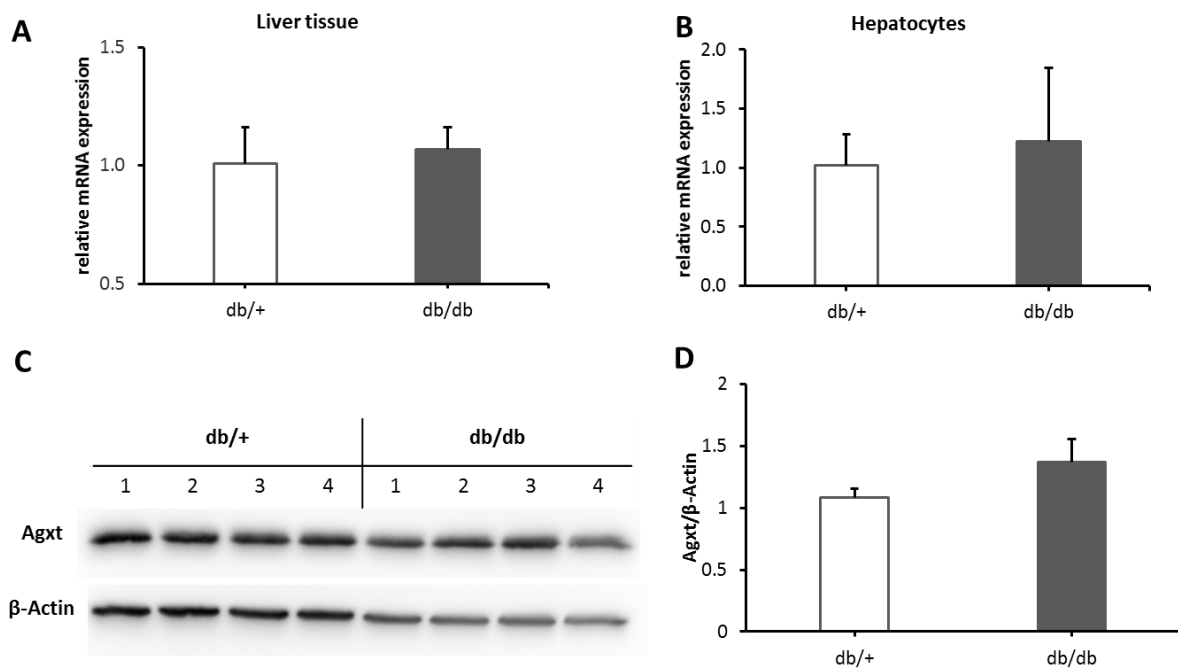
Figure 3.37: Livers from *db/db* mice have no repression of Agxt. The RNA level of Agxt in *db/db* mice A) in livers (n = 4) and B) in hepatocytes (n = 2) were analysed by quantitative real-time PCR relative to *db/+* mice. Eif2a was used as the endogenous control; C) Western blot and D) its densitometric quantification of Agxt expression in liver extracts of *db/+* and *db/db* mice (n = 4). β-Actin was used as a loading control.

3.9.1.4 Glyoxylate associated genes in *db/db* mice liver tissue

As described in the previous Chapter, the expression of Agxt was not reduced in *db/db* mice. The next step was to study whether the glyoxylate metabolism-associated genes Grhpr and Hao1 were affected in this mouse model of NAFLD. Quantitative real-time PCR demonstrated that Grhpr was approximately 1.6 fold upregulated in liver tissue of *db/db* mice relative to *db/+* liver tissue. The expression of Hao1 was not altered in *db/db* mouse livers (Figure 3.38), suggesting that the glyoxylate metabolism in *db/db* mice was not similarly affected as seen for the *ob/ob* mouse model.
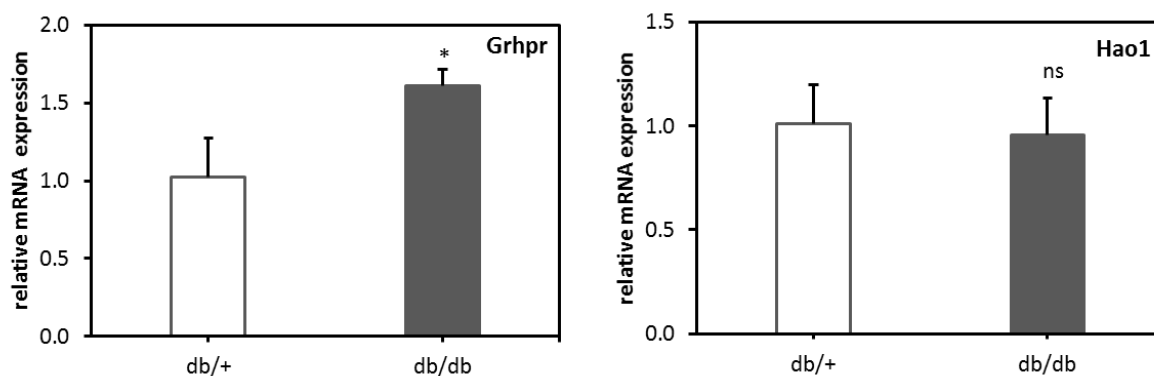
Figure 3.38: Grhpr expression is slightly increased in *db/db* mouse livers. Quantitative real-time PCR revealed a slight upregulation of Grhpr, Hao1 was not altered in *db/db* mouse livers relative to the expression in *db/+* mouse livers (n = 4). Eif2a was used as the endogenous control. ns: not significant; * indicates $p < 0.05$.

3.9.2 Glyoxylate metabolism in mice on the Western diet

In addition to the genetic mouse models mentioned above, liver tissues were collected and analysed from mice, which were fed with a Western diet, a type of high fat diet, for several weeks. After 6, 12, 18, 24, and 30 weeks on the Western diet, five mice per group were sacrificed and liver tissues were collected. On the 29th week of diet, four mice per group were placed in a single mouse metabolic cage to collect 24 h urines and to analyse the urinary oxalate concentrations in these mice. This diet study was conducted by Dr. Ahmed Ghallab who kindly allowed us to collect urine as well as liver tissue for RNA analysis, and liver sections for histopathological characterisation.

3.9.2.1 Western diet induces hepatic lipid accumulation and displacement of nuclei

As illustrated in Figure 3.39 A, mice on the Western diet exhibited a time dependent increase in body and liver weight. The liver to body weight ratio was elevated after eighteen weeks on the Western diet compared to those mice on the normal diet. In addition, H&E staining of paraffin embedded liver slides showed an accumulation of intracellular lipid droplets in hepatocytes of the pericentral and middle zone. Moreover, several hepatocytes had nuclei that were shifted towards the periphery of hepatocytes (exemplified by yellow arrows in Figure 3.39 B).
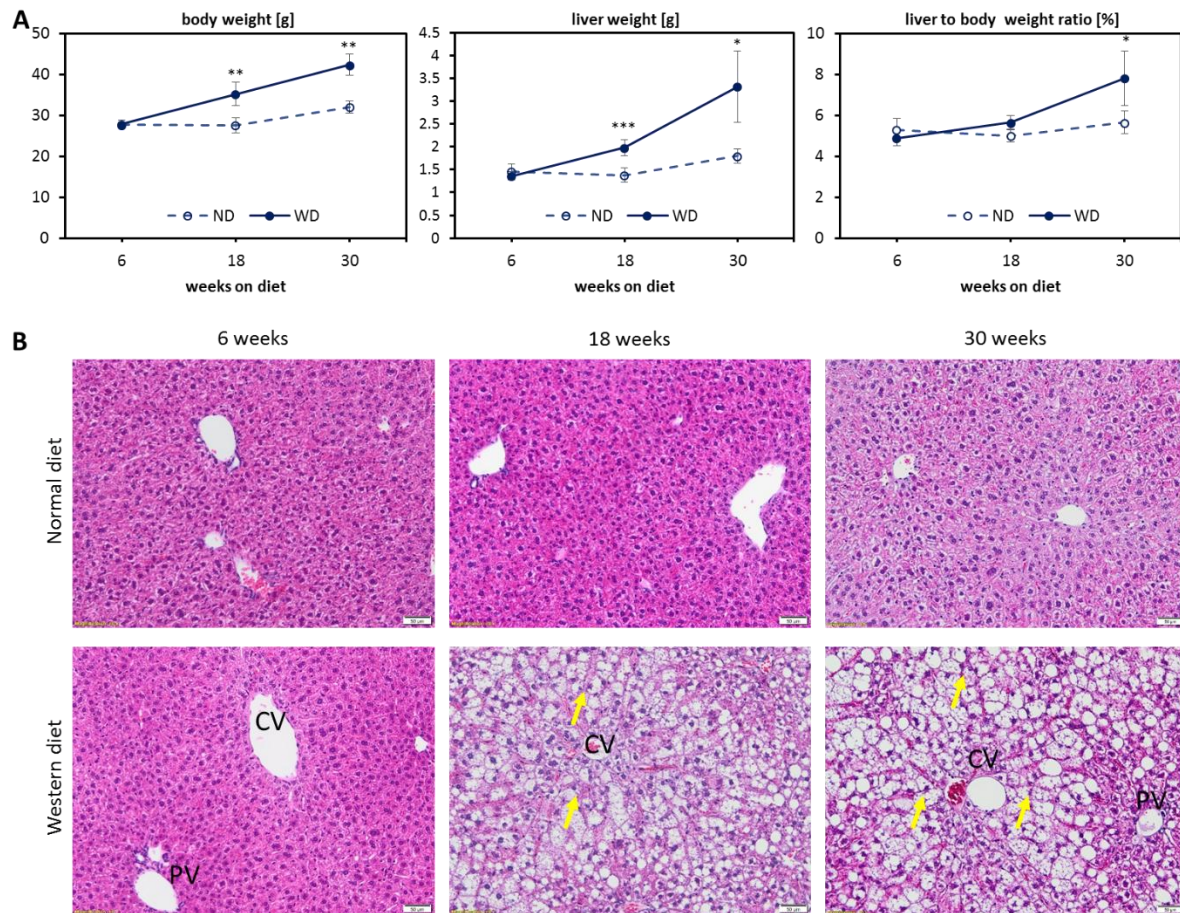
Figure 3.39: Western diet induces a time-dependent increase in body and liver weight as well as hepatic lipid accumulation. A) Body and liver weights of mice on the normal or the Western diet (n = 5); B) H&E stainings of paraffin embedded liver sections of mice on the normal or the Western diet for several weeks. The yellow arrows indicate examples of hepatocytes with a shifted nucleus. Scale bars represent 50 µm. ND: normal diet; WD Western diet; CV: central vein, PV: portal vein. * indicates $p < 0.05$; ** indicates $p < 0.01$; *** indicates $p < 0.001$.

3.9.2.2 Western diet causes a repression of Agxt

After liver tissue was collected at the assigned time points, RNA was isolated and transcribed into cDNA. Afterwards, quantitative real-time analysis was performed to investigate the expression of Agxt and further genes associated with the glyoxylate metabolism. Moreover, IHC of paraffin embedded liver sections was performed to investigate the expression and distribution of Agxt in the liver tissue of mice which were on the normal or the Western diet for 24 weeks and 30 weeks.

The RNA level of Agxt was significantly reduced in livers of mice on the sixth week (fold change: -1.97 ± 0.34) of the Western diet, and stayed reduced until the end of the diet (fold change: -2.97 ± 0.96; Figure 3.40 A). The staining of Agxt indicated reduced protein expression in livers of mice after 30 weeks on the Western diet (Figure 3.40 B).
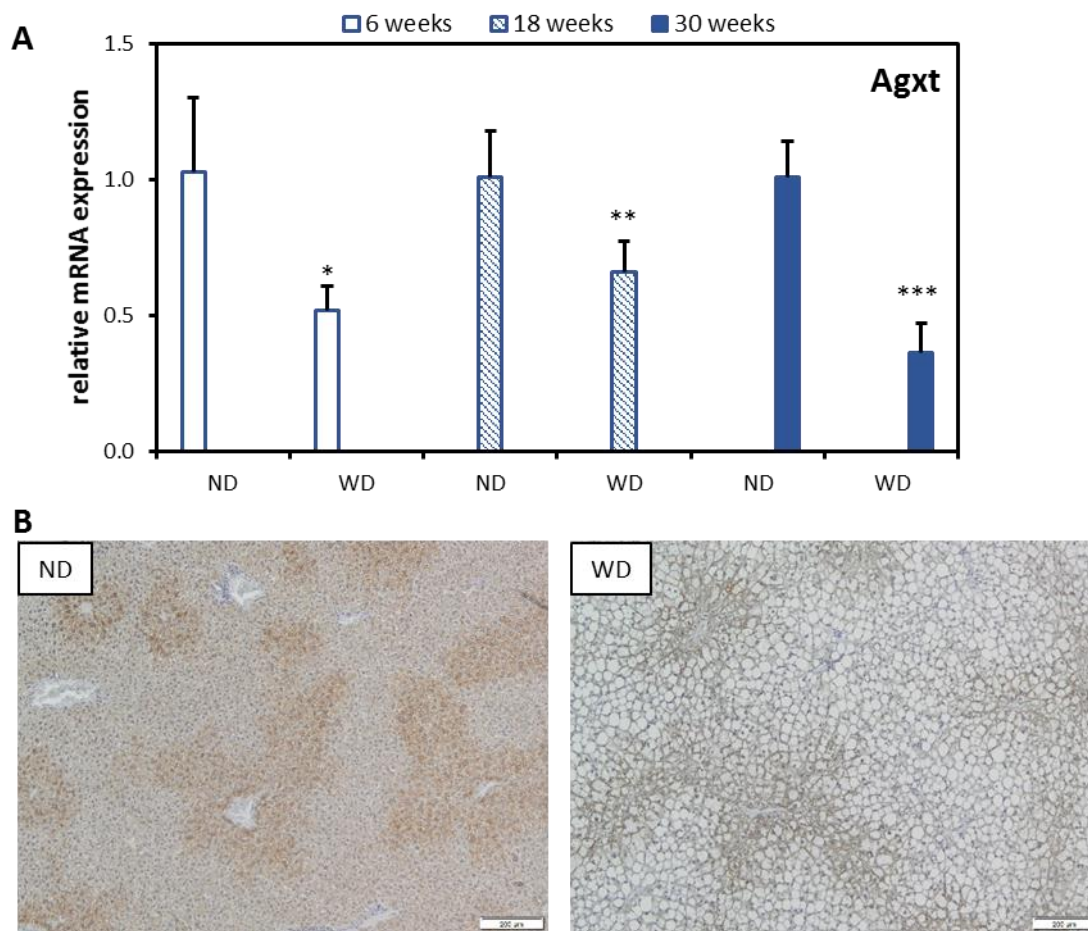
Figure 3.40: Western diet reduces the expression of Agxt. A) Quantitative real-time PCR revealed a down-regulation of Agxt in livers of mice after 6, 18 and 30 weeks on the Western diet relative to mice on the normal diet. Gapdh was used as the endogenous control (n = 5); B) Representative IHC indicated a reduction of Agxt protein level after 24 weeks (data not shown) and 30 weeks on the Western diet. Scale bars represent 200 μm. * indicates $p < 0.05$; ** indicates $p < 0.01$; *** indicates $p < 0.001$.

The expression of further glyoxylate metabolism-associated genes was not altered as strongly or as early on the diet as seen for Agxt. Grhpr and Hao1 RNA expressions were not significantly reduced with the Western diet; however, there was a trend towards lower expression of Hao1 in liver of mice that were on the Western diet for 30 weeks (Figure 3.41).

All in all, Agxt was similarly downregulated in the liver of mice on the Western diet model as well as the *ob/ob* mouse model. In addition, Hao1 RNA expression was slightly but significantly downregulated in *ob/ob* mouse livers; whereas, only a trend towards decreased expression was observed in the livers of mice after 30 weeks on the Western diet.
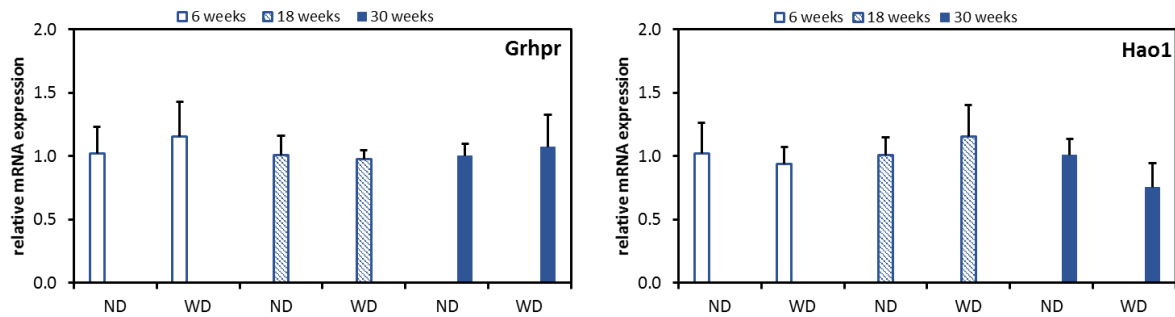
Figure 3.41: Mice on the Western diet tend to have a reduced Hao1 expression after 30 weeks of diet. Quantitative real-time PCR showed no significant deregulation of Grhpr or Hao1 at the RNA level in livers of mice on the Western diet relative to those of mice on the normal diet at each time point. The expression of Hao1 showed a reduced trend at the RNA level after 30 weeks on the Western diet ($p < 0.077$). Gapdh was used as the endogenous control (n = 5).

3.9.2.3 Mice on the Western diet are not hyperoxaluric

After 29 weeks on the Western diet, four mice as well as four control mice were placed in a single mouse metabolic cage and 24 h urine was collected on two consecutive days. As illustrated in Figure 3.42, mice on the Western diet excreted less urine, which was accompanied by increased creatinine and oxalate concentrations. After normalization of the urinary oxalate concentration to the creatinine concentration, daily oxalate excretion was quite similar between the control group and the Western diet group. One explanation may be the unchanged expression of Grhpr, which might compensate for the lack in glyoxylate detoxification due to decreased Agxt expression.
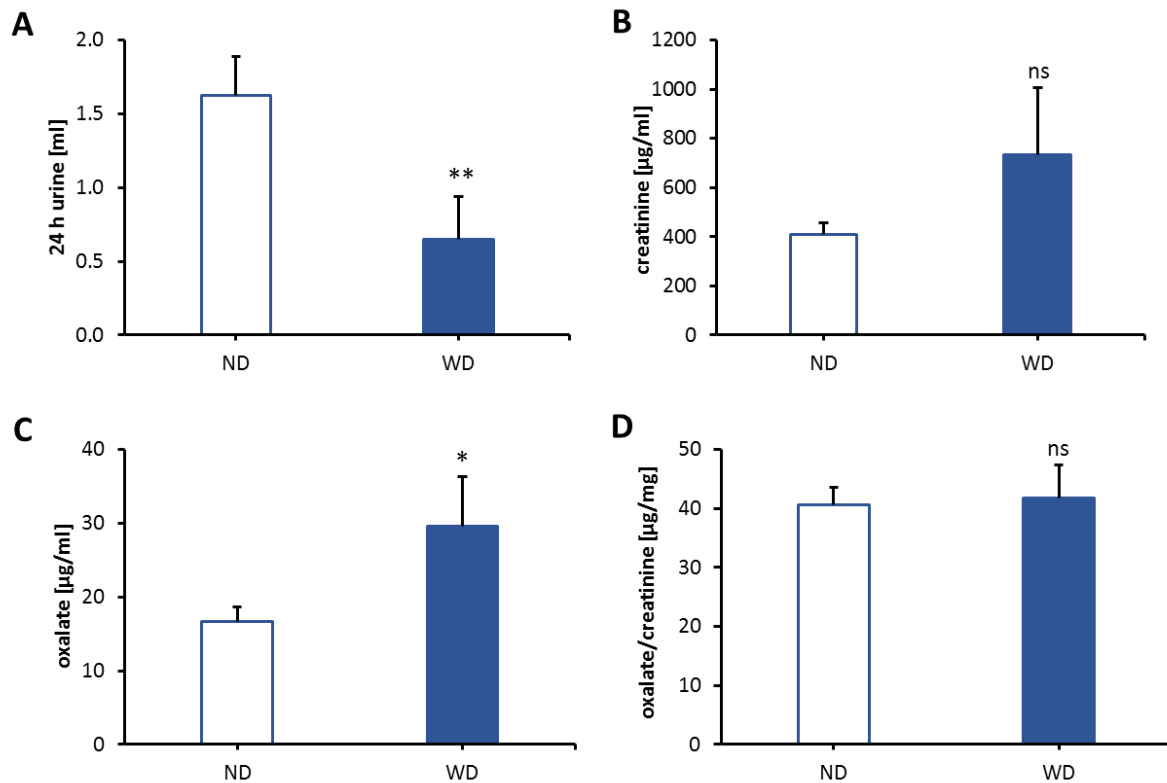
Figure 3.42: Mice on the Western diet are not hyperoxaluric. A) Daily excreted urine volume; B) Urinary creatinine concentration; C) Urinary oxalate concentration of mice on the normal or the Western diet (29 weeks on diet; n = 4; quantification by LC-MS/MS); D) Daily urinary oxalate excretion normalised to creatinine excretion (n = 4). ND: normal diet; WD: Western diet; ns: not significant; * indicates $p < 0.05$; ** indicates $p < 0.01$.

3.10 Oxalate production *in vitro*

In the Chapters above, the association between lipid accumulation and the downregulation of AGXT was thoroughly demonstrated. So far, only the *ob/ob* mouse model showed a reduced Agxt expression accompanied by a slightly increased excretion of oxalate. The purpose of the next experiments was to study the consequence of Agxt repression *in vitro*. In the *in vitro* steatosis models, the protein expression of Agxt did not immediately decrease in response to lipid accumulation, but remained stable for three to five days, before the decrease was observed (Figures 3.19 and 3.21). Therefore, an AGXT knockdown model was established initially in HepG2 cells and subsequent, cultivated hepatocytes isolated from the *ob/+* and *ob/ob* mice were investigated with regard to their oxalate excretion.

Results

3.10.1 AGXT knockdown in HepG2 cells does not elevate oxalate excretion

HepG2 cells are known to express AGXT and have been suggested to represent an appropriate model to study glyoxylate metabolism with regard to primary hyperoxaluria type 1 (Wanders et al. 1991). For that reason, an AGXT knockdown was established in HepG2 cells. After a long optimisation period where several transfection reagents and siRNA oligos against AGXT mRNA were used, AGXT was successfully knocked down at the RNA level after 72 h transfection using three siRNA oligos. The expression of AGXT was reduced more than 80% with oligos B and E and more than 70% with oligo D (Figure 3.43).
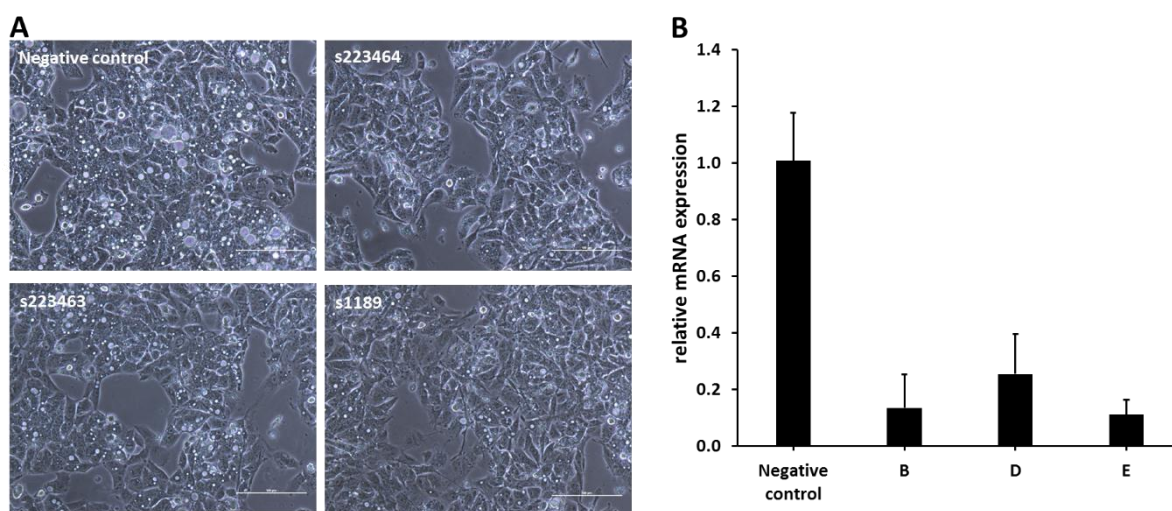
Figure 3.43: Reduced AGXT RNA expression in HepG2 cells after AGXT knockdown. After 72 h of transfection using lipofectamine RNAiMAX transfection reagent with 10 nM oligo B (s223464), 10 nM oligo D (s223463) and 10 nM oligo E (s1189; representative pictures in A, scale bars represent 100 µm), a reduced expression of AGXT relative to HepG2 cells incubated with 10 nM scrambled siRNA (negative control) was achieved (B). UBC was used as the endogenous control (n = 2).

To more thoroughly investigate the expression of AGXT at the protein level, several time points were investigated after transfection. Western blot analysis (Figure 3.44) revealed that the decrease of AGXT protein levels was already evident 48 h after transfection, and became stronger at later time points. On the fifth day after transfection, there appeared to be no AGXT protein left in the cells. This experiment indicated that the transient AGXT knockdown efficiently depleted AGXT protein levels for several days and could be applied to investigate the consequences of a loss of AGXT. Importantly, by measuring both RNA and protein, the results showed that a dramatic decrease in AGXT RNA expression did not result in an immediate loss of protein expression as it was seen in the *in vitro*-steatosis system (e.g. Figure 3.21).
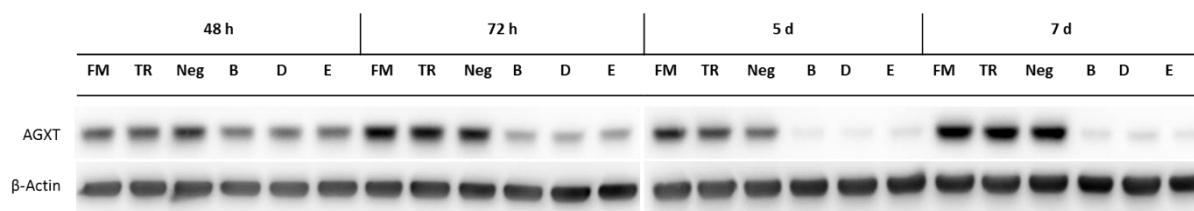
Figure 3.44: Time dependent downregulation of AGXT at the protein level. Representative Western blot of AGXT expression measured in protein lysates of transient transfected HepG2 cells. β-Actin was used as a loading control. FM: full media; TR: transfection reagent; Neg (negative control): scrambled siRNA, B: oligo s223464; C: oligo s223463, D: oligo s1189; concentration: each 10 nM.

To investigate whether the transient knockdown of AGXT had any physiological consequences, HepG2 cells with and without AGXT knockdown were challenged with glyoxylate. The ability of HepG2 cells to form oxalate upon glyoxylate treatment and to excrete it into the supernatant has been previously reported (Baker et al. 2004). Thus, here it was investigated whether, i) HepG2 cells with AGXT knockdown produce more oxalate than control HepG2 cells; ii) the knockdown of AGXT increased the susceptibility upon challenge with glyoxylate, resulting in even higher oxalate excretion.

For this purpose, HepG2 cells were transfected with AGXT siRNA for six days, followed by incubation with two different glyoxylate concentrations for 24 h. The supernatants as well as the cells were collected, and the efficiency of the AGXT knockdown was verified *via* Western blot analysis (data not shown).

The diagram in Figure 3.45 illustrates the oxalate concentrations of the HepG2 supernatants, quantified by LC-MS/MS and normalised to the protein amount in the cell monolayer. Unexpectedly, the results showed no significant increase in excreted oxalate in the siRNA transfected HepG2 cells without or with 0.2 mM glyoxylate challenge (white and shaded bars). In addition, only 1 mM glyoxylate was able to stimulate the oxalate formation in HepG2 cells. Upon challenge with 1 mM glyoxylate both siRNA transfected and non-transfected cells produced and excreted similar amounts of oxalate.
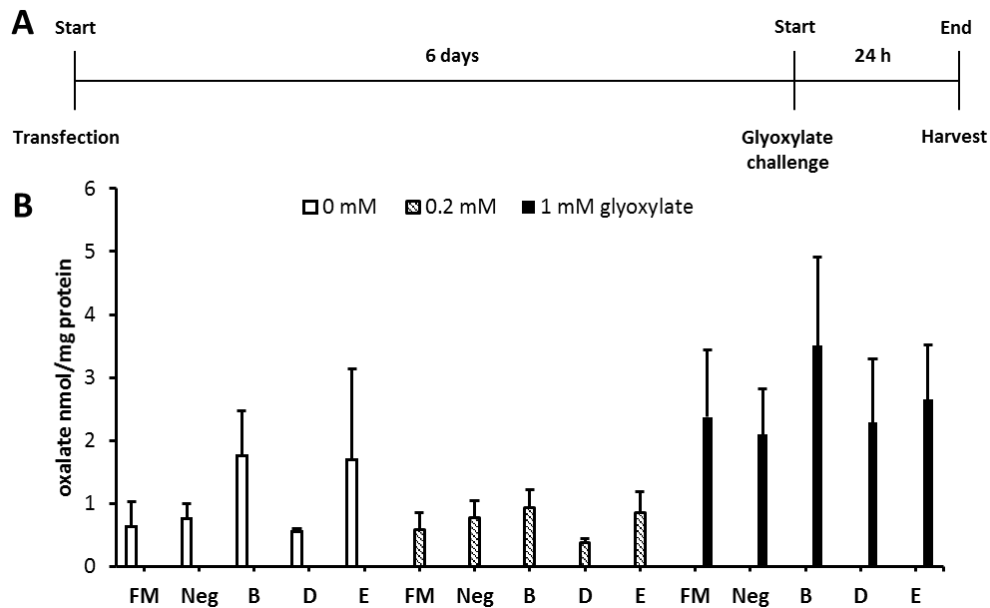
Figure 3.45: HepG2 cells with AGXT knockdown do not secrete more oxalate than control cells. A) Experimental set up: after 6 days of transfection and AGXT knockdown, HepG2 cells were treated with 0.2 mM or 1 mM glyoxylate for 24 h. The supernatants as well as the proteins of the cell monolayer were collected. B) Chromatographic quantification of the oxalate concentration in supernatants (LC MS/MS) normalised to the protein concentration of the monolayer (n = 3). FM: full media; Neg: scrambled siRNA, B: oligo s223464; C: oligo s223463, D: oligo s1189.

One possible explanation for this unexpected result is that HepG2 cells may not import exogenously added glyoxylate into the peroxisomes, resulting in immediate and direct oxidation to oxalate by the cytosolic lactate dehydrogenase.

To ensure peroxisomal generation of glyoxylate, HepG2 cells must be incubated with glycolate which is oxidized to glyoxylate by HAO1 within the peroxisomes. However, HepG2 cells are known to have a markedly decreased activity of HAO1, and it has been suggested that these cells have a peroxisomal-independent pathway to form oxalate from glycolate (Baker et al. 2004). Quantitative real-time PCR analysis revealed a very low gene expression of HAO1 in HepG2 cells, as demonstrated in Ct-values above 33. This gave evidence that the peroxisomal glyoxylate generation from glycolate in HepG2 was negligible. Thus, neither glyoxylate nor glycolate seem to be adequate challenges for studying the consequence of Agxt knockdown in HepG2 cells *in vitro*.

In conclusion, it was not possible to show the consequences of reduced AGXT expression in terms of oxalate production in HepG2 cells. The HepG2 cell line may not be the adequate model to study AGXT consequences due to the reduced expression of HAO1. The cell line Huh7 also revealed low RNA expression of HAO1 and therefore was also not an appropriate system.

3.10.2 Oxalate excretion of cultivated *ob/+* and *ob/ob* mouse hepatocytes

3.10.2.1 Agxt expression is cultivation sensitive in *ob/+* and *ob/ob* hepatocytes

Before oxalate precursor studies were performed with hepatocytes from *ob/+* and *ob/ob* mice, the stability of Agxt expression in cultivated hepatocytes was analysed, since it is known that not only hepatocytes isolation changes gene expression within 24 h (Zellmer et al. 2010) but also the cultivation has an enormous impact on gene expression (Godoy et al. 2013). The RNA expression of Agxt was clearly reduced after 24 h cultivation with a collagen overlay compared to freshly isolated hepatocytes, independently of the genotype (Figure 3.46 A). The comparison of the cultivation effect in *ob/ob* hepatocytes to that in *ob/+* hepatocytes still revealed a decreased Agxt expression in *ob/ob* hepatocytes as demonstrated at the RNA (Figure 3.46 B) as well as at the protein level (Figure 3.46 C). After 7 days of cultivation, the expression of Agxt was reduced to very low levels regardless of the genotype; thus, there was hardly any difference between its expression in *ob/+* and *ob/ob* hepatocytes.

After 72 h of cultivation, Agxt protein was still expressed in both genotypes. At 5 d of cultivation, there was hardly any protein left in *ob/ob* mice. This observation was an important fact to consider during *in vitro* experiments of primary hepatocytes of *ob/+* and *ob/ob* mice, because it revealed that studies are only possible for a time period of 72h.
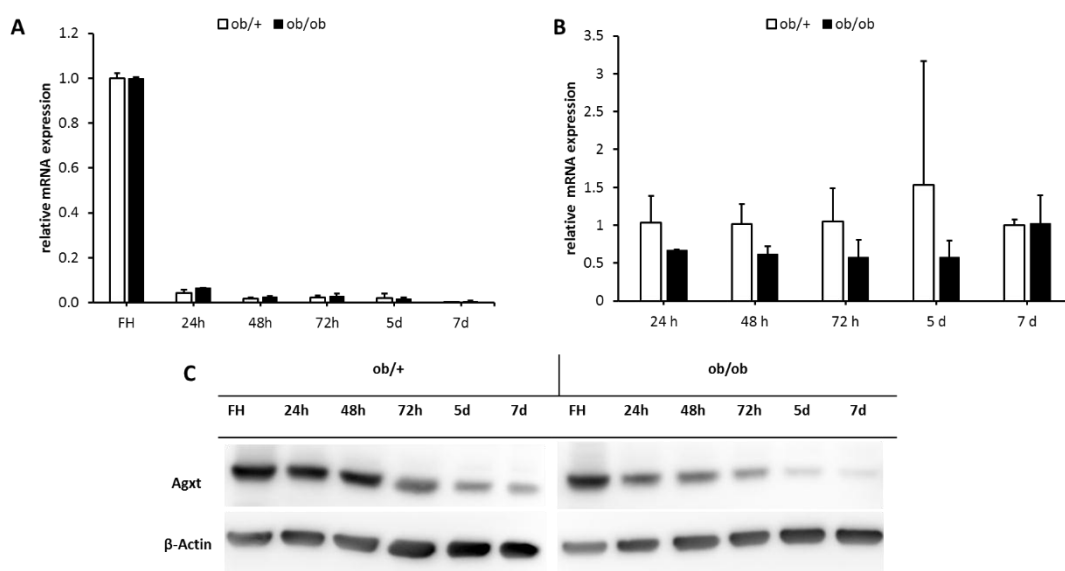
Figure 3.46: Agxt expression is cultivation-sensitive in hepatocytes from *ob/+* and *ob/ob* mice. The Agxt RNA expression was analysed by quantitative real-time PCR and calculated A) for *ob/+* and *ob/ob* hepatocytes relative to their corresponding freshly isolated hepatocytes (n =2) or B) for *ob/ob* hepatocytes relative to *ob/+* hepatocytes at each time point of cultivation (n =2); Gapdh was used as the endogenous control; C) Representative Western blot of Agxt expression of freshly isolated and cultivated hepatocytes from *ob/+* and *ob/ob* mice. β-Actin was used as a loading control (n = 2).

3.10.2.2 O*b/ob* hepatocytes are more susceptible towards hydroxyproline than *ob/+* hepatocytes

The purpose of the following experiment was to investigate how the gene expression changes observed in *ob/ob* mouse livers, as described in Chapter 3.7.1, influence their capacity to metabolise glyoxylate precursors and to detoxify glyoxylate. With this goal, cultivated primary hepatocytes from *ob/+* and *ob/ob* mice were exposed to glyoxylate precursors and oxalate excretion into the medium was quantified by LC-MS/MS. Glyoxylate was selected as a positive control for oxalate production in general. Glycolate was used to explore the consequence of Hao1 downregulation (observed in *ob/ob* mouse livers) as a compensatory mechanism to Agxt downregulation in *ob/ob* mouse hepatocytes. Accordingly, oxalate production in hepatocytes of *ob/ob* mice was expected to be lower since RNA levels of Hao1 were decreased, and thus less oxidation of glycolate to glyoxylate should occur. Finally, hydroxyproline was employed for two reasons. First, hydroxyproline is not only found in the human diet but is also endogenously released by collagen turnover and thus reflects the *in vivo* situation. Second, the RNA level of the two key enzymes Prodh2 and Hoga1 involved in the catabolic breakdown of hydroxyproline was not altered in *ob/ob* mouse liver according to the Affymetrix gene array analysis. Therefore, hydroxyproline incubation could be an adequate challenge for enhancing glyoxylate production and studying the consequences of Agxt downregulation (and thus possible compromised glyoxylate detoxification) in *ob/ob* hepatocytes.

For the experimental design the cultivation sensitivity of Agxt, as addressed in the previous section was considered. Therefore, the maximal time of exposure to challenge was set to 48 h after 24 h in culture (Figure 3.47 A).
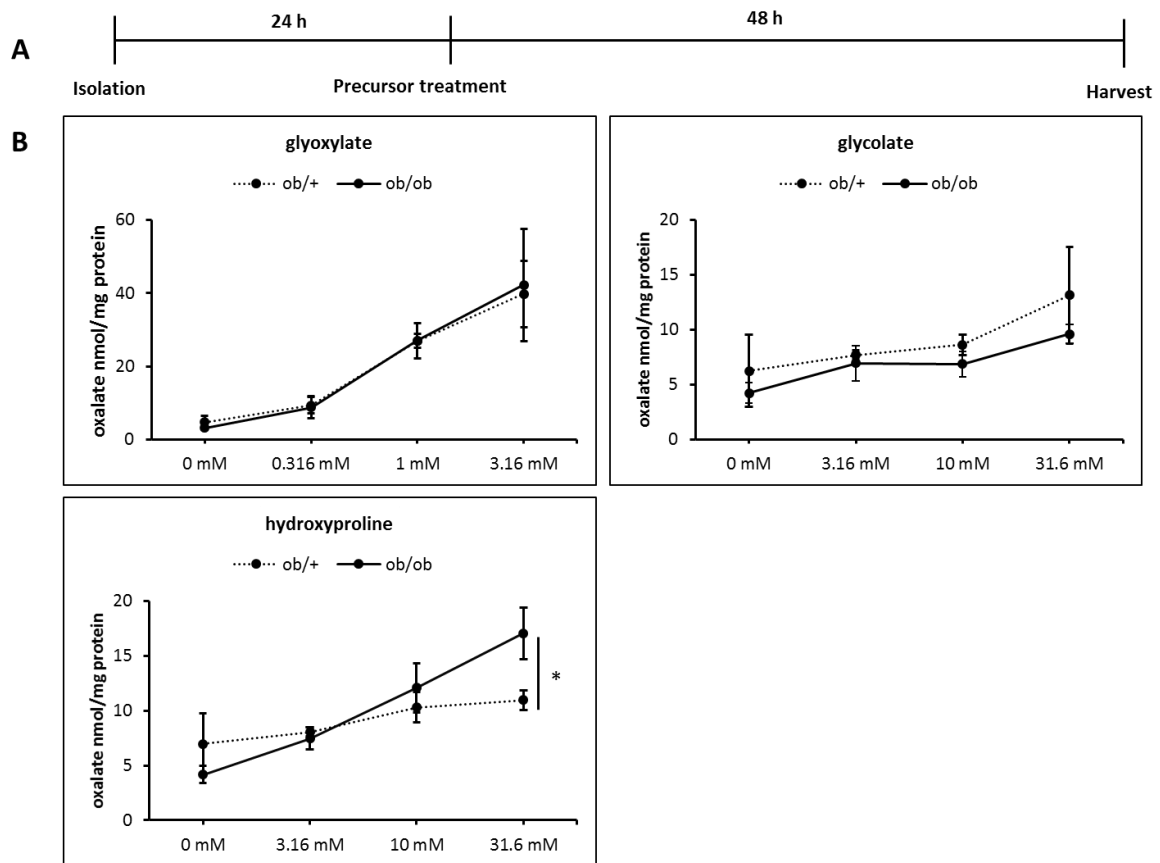
Figure 3.47: The type of oxalate precursor has a strong impact on the oxalate production of *ob/+* and *ob/ob* hepatocytes. A) Experimental set up for this experiment: hepatocytes of *ob/+* and *ob/ob* mice were isolated and cultivated for 24 h before stimulated for 48 h using several oxalate producers. The supernatants and proteins were collected; B) Chromatographic quantification of the oxalate concentrations in supernatants (LC-MS/MS) normalised to the protein concentration of the monolayer. * indicates $p < 0.05$.

Cultivated *ob/ob* mouse hepatocytes excreted less oxalate than cultivated *ob/+* hepatocytes in the absence of any oxalate precursor. Depending on the applied challenge, the amount of excreted oxalate was similar or different between cultivated *ob/ob* and *ob/+* hepatocytes. As expected, glyoxylate incubation increased the oxalate formation in both cultivated *ob/+* and *ob/ob* hepatocytes without any difference between these two hepatocyte populations. Moreover, glyoxylate was the most potent stimulator of oxalate production. Most likely, the applied glyoxylate is immediately converted to oxalate by the cytosolic lactate dehydrogenase and this step is not influenced by decreased Agxt levels.

The glycolate exposure led to a higher oxalate production in *ob/+* than in *ob/ob* hepatocytes even though the differences were not strong. This was attributed to the reduced expression of Hao1 in *ob/ob* hepatocytes. Thus, *ob/ob* hepatocytes generated less glyoxylate from glycolate, which consequently resulted in decreased production of oxalate despite decreased Agxt expression.

Remarkably, hydroxyproline challenge led to the opposite result. This oxalate precursor stimulated the formation of oxalate in a concentration-dependent manner, especially in hepatocytes from *ob/ob* mice. There was a clear tendency of more excreted oxalate by *ob/ob* hepatocytes than by *ob/+* hepatocytes that was significant at the highest hydroxyproline concentration. Because the expression of enzymes involved in the catabolism of hydroxyproline to glyoxylate were not altered, the elevated excretion of oxalate by steatotic hepatocytes upon hydroxyproline incubation can be attributed to their reduced detoxification capacity due to Agxt downregulation.

These experiments were a pivotal contribution towards understanding the interplay between the glyoxylate-associated enzymes and the different oxalate precursors in steatotic hepatocytes and identified the hydroxyproline catabolism as the critical pathway leading to enhanced oxalate generation in steatosis.

3.11 Reduced AGXT expression in steatosis is associated with hypermethylation of the *AGXT* promotor *in vivo*

Altogether, the results obtained from *ob/ob* mice, steatotic primary human hepatocytes and the *in vitro* steatosis models clearly showed a steatosis-dependent downregulation of AGXT. However, the mechanism behind this downregulation was unknown. DNA methylation is one mechanism that cells use to modulate gene expression. Thus, it was explored whether downregulation of AGXT in steatosis was associated with *AGXT* promoter methylation.

During this PhD project, the IfADo groups Systems Toxicology and Cellular Toxicology participated in the German Epigenetic Programme (DEEP) with the aim to identify epigenetic alterations in NAFLD. For this purpose, samples from *ob/ob* mice (liver tissue and hepatocytes) as well as primary human hepatocytes were prepared and delivered to partners within the consortium for epigenetic analysis. Within the consortium, RNA sequencing was performed, which confirmed the significant downregulation of Agxt and Hao1 in livers and hepatocytes from *ob/ob* mice compared to *ob/+* mice. One of the applied methods to map genome-wide DNA methylation was reduced representation bisulphite sequencing (RRBS). Application of this method in hepatocytes from *ob/+* and *ob/ob* mice resulted in the identification of a hypermethylated DNA region in the putative promoter of the *Agxt* gene in *ob/ob* hepatocytes. Methylation within a promoter is usually associated with the repression of gene expression. Thus, this finding suggested that the hypermethylation of the Agxt promoter is a possible cause for its downregulation. In order to confirm the observed hypermethylation, amplicon sequencing using specific primers for the promotor of *Agxt* was performed.

3.11.1 *Agxt* promotor of *ob/ob* mouse hepatocytes is hypermethylated

The steatotic *ob/ob* mice have reduced Agxt expression in their livers as well as in their hepatocytes. Amplicon sequencing revealed a comparable methylation state of the *Agxt* promotor in liver tissue from *ob/ob* mice and *ob/+* mice (Figure 3.48). In contrast, the mean methylation of the *Agxt* promotor in *ob/ob* hepatocytes was significantly higher than in *ob/+* hepatocytes. Overall, the degree of methylation in liver tissue was higher in both the steatotic and the control livers compared to the isolated hepatocytes. Surprisingly, the analysis of liver tissue was not able to discriminate the methylation differences observed in the hepatocytes. This showed the importance of the methylation analysis at the cell level without the tissue matrix.

As seen in the IHC staining of Agxt in *ob/+* and *ob/ob* mouse liver (Figure 3.18 B), only a subpopulation of hepatocytes in zone 3, surrounding the central vein, expressed Agxt. This may explain the striking pattern observed in the patternmaps of methylation status, which shows only a small percentage of hepatocytes with methylated CpG sites in the *Agxt* promoter. How the methylation status of the *Agxt* promoter correlates with its spatiotemporal expression is at this time point not well understood. However, the present findings do support an increase in the number of steatotic hepatocytes showing hypermethylation of the *Agxt* promotor, which accompanies the transcriptional repression observed in steatotic *ob/ob* hepatocytes.
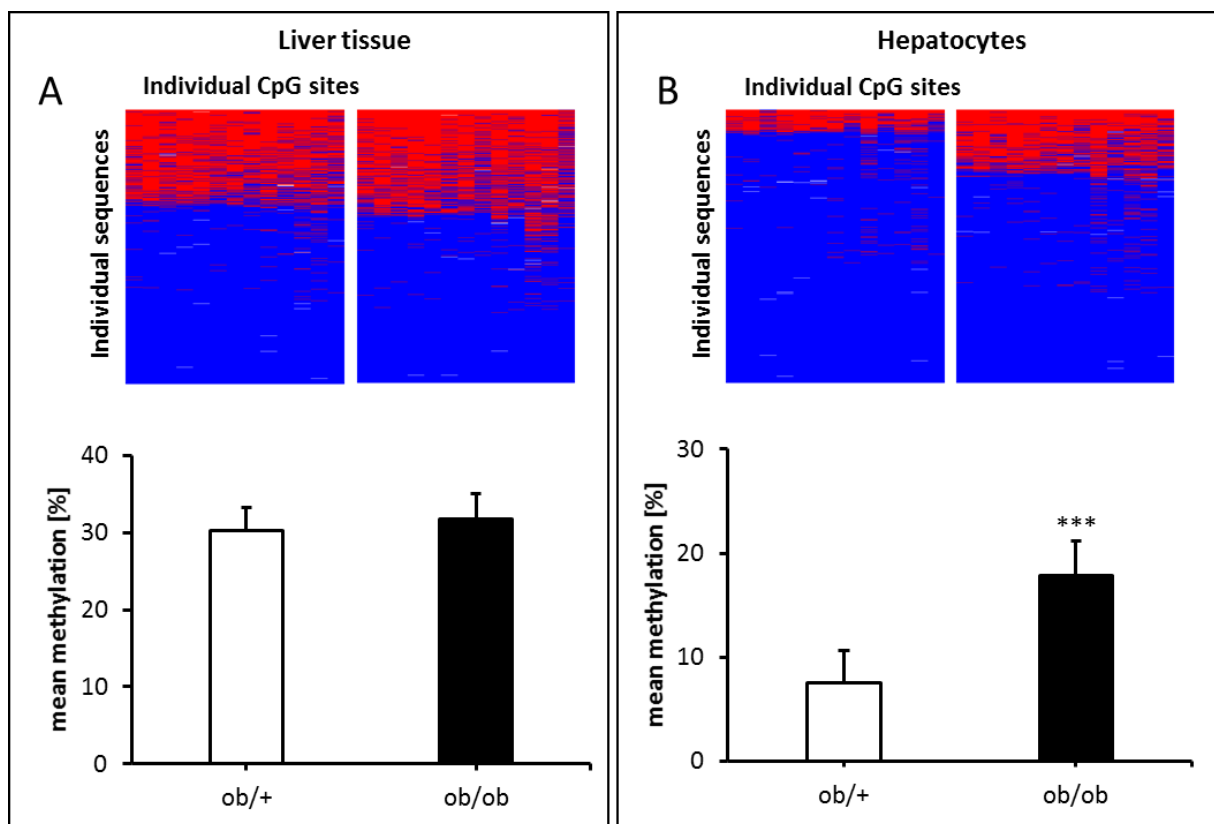
Figure 3.48: *Agxt* **promotor is hypermethylated in steatotic hepatocytes of** *ob/ob* **mice.** A) Representative patternmaps of methylated CpG sites (red) in the promotor region of murine *Agxt* in liver tissue from *ob/+* and *ob/ob* mice and the mean methylation values (n = 5); B) Representative patternmap of methylated CpG sites (red) in the promotor region of murine *Agxt* in hepatocytes from *ob/+* and *ob/ob* mice and the mean methylation values (n = 6); *** indicating p < 0.001.

3.11.2 *Db/db* mice do not show a hypermethylation in the *Agxt* promotor

As illustrated in Figure 3.37, *db/db* mouse livers and hepatocytes did not show a repression of Agxt. The amplicon sequencing of the *Agxt* promotor in the liver tissue from these mice showed a similar degree of methylation as seen for the liver tissue from *ob/+* and *ob/ob* mice and no differences between both genotypes. The hepatocytes of steatotic *db/db* mice revealed a small tendency towards more methylation of *Agxt* compared to *db/+* hepatocytes, but this was not significant (Figure 3.49). This observation strengthens the suggestion that the hypermethylation of the *Agxt* promotor might be responsible for its downregulation seen in the *ob/ob* mice; whereas, the missing hypermethylation in the *db/db* mouse model may explain why Agxt was not repressed in that mouse model.
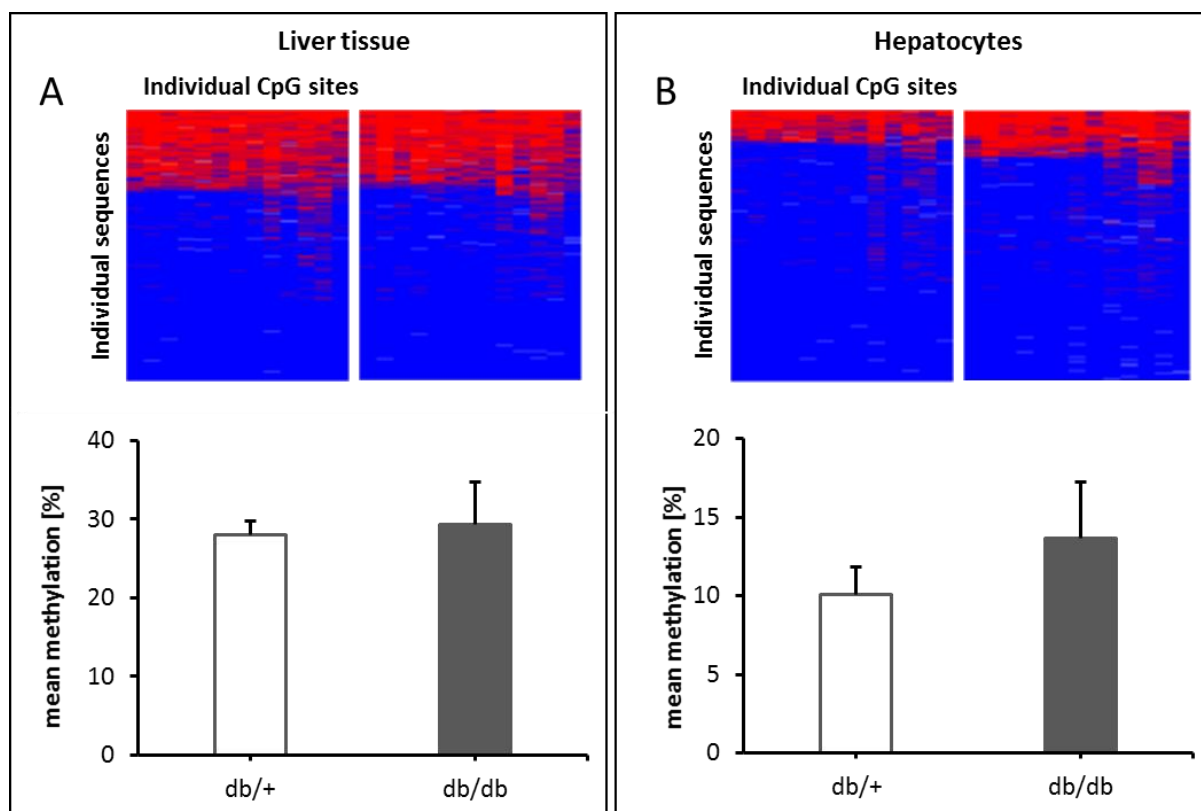
Figure 3.49: *Agxt* promotor is not hypermethylated in steatotic hepatocytes of *db/db* mice. A) Representative patternmaps of methylated CpG sites (red) in the promotor region of the murine *Agxt* in liver tissue from *db/+* and *db/db* mice and the mean methylation values (n = 4); B) Representative patternmaps of methylated CpG sites (red) in the promotor region of the murine *Agxt* in hepatocytes from *db/+* and *db/db* mice and the mean methylation values; p = 0.3759 (n = 2).

3.11.3 *AGXT* promotor is hypermethylated in steatotic primary human hepatocytes

As described in Chapter 3.6, there was a significant negative correlation between the lipid content of primary human hepatocytes and their AGXT RNA expression level. In the next step, a selection of those hepatocytes were sent for methylation analysis by amplicon sequencing. Again, the primary hepatocytes were separated into the control, non-steatotic, group and the steatotic group according to their amount of triglycerides as defined in Chapter 3.6. Figure 3.50 illustrates a significant increase of the mean methylation in the *AGXT* promotor of the steatotic group compared to the control group, indicating a steatosis-dependent increase in human hepatocytes showing methylation in the promotor region of the human *AGXT* gene, as observed in mouse hepatocytes.
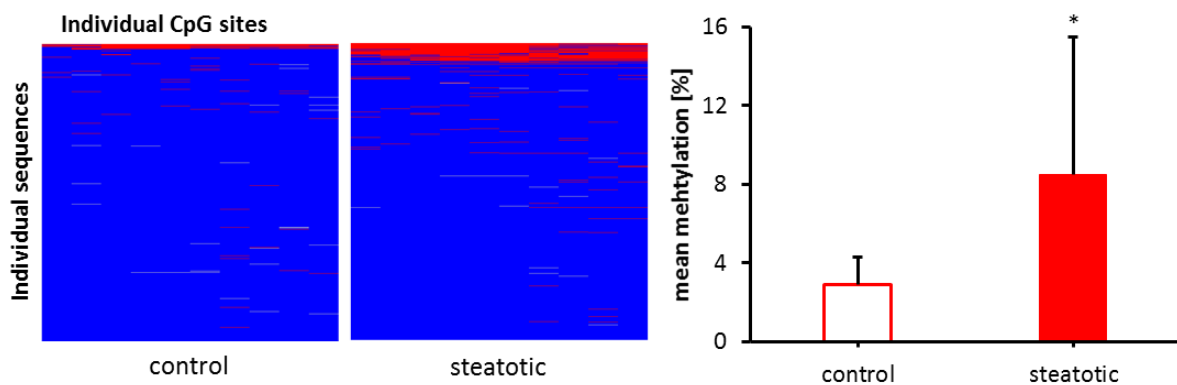
Figure 3.50: *AGXT* promotor is hypermethylated in steatotic primary human hepatocytes. Representative patternmaps of methylated CpG sites (red) in the promotor region of the human *AGXT* gene and the mean methylation values (control: n = 3, steatotic: n = 6). *indicating $p < 0.05$.

However, there was no significant correlation between the AGXT RNA expression and the promotor methylation of *AGXT* (Figure 3.51). This result weakened a link between the downregulation of AGXT and the hypermethylation of its promotor in human steatotic hepatocytes. Hence, hypermethylation of the *AGXT* promotor in primary human hepatocytes might not be the only cause for the downregulation of AGXT in each of the investigated samples. Different individual mechanisms may explain the downregulation of AGXT in human steatotic hepatocytes, with *AGXT* promotor hypermethylation being one potential explanation. Additionally, it was possible that a higher number of samples is required to achieve statistical significance.
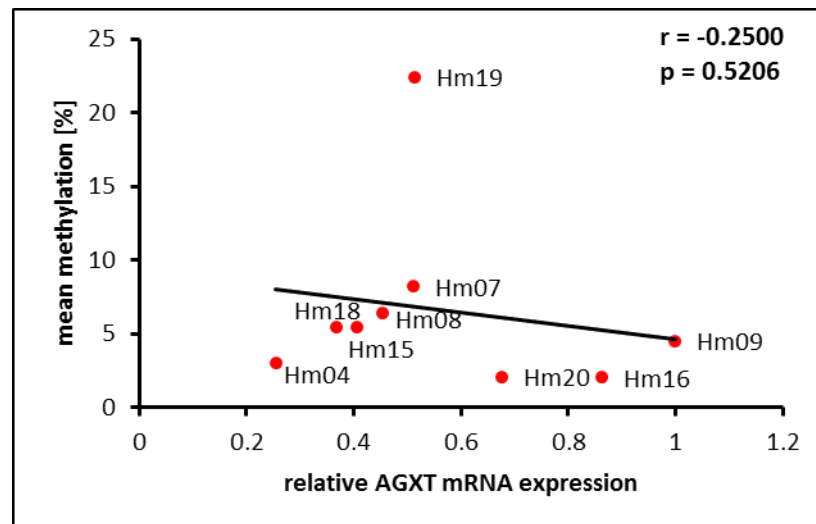
Figure 3.51: RNA expression of AGXT in male primary human hepatocytes does not correlate with the degree of methylation in the *AGXT* promotor (n = 9). The Spearman coefficient was r = -0.2500 and the p-value was p = 0.5206.

3.11.4 Downregulation of AGXT in *in vitro* steatosis model is not associated with hypermethylation of the *AGXT* promotor

Upon prolonged OA/BSA stimulation, the expression of Agxt was reduced in primary mouse hepatocytes as well as in human hepatocellular cell lines (Figures 3.19 and 3.21). Next, samples were analysed for methylation in the promotor of *AGXT*, using Amplicon sequencing, to investigate whether lipid-accumulation in hepatocellular carcinoma cell lines and primary mouse hepatocytes effected the methylation status of the *AGXT* promotor. Cancer cell lines and primary mouse hepatocytes were cultured for 5 d with 0.5 mM OA/BSA or the corresponding controls. These particular concentration and incubation time point were chosen since the downregulation of AGXT at the RNA level lasted for at least two days.

In Figure 3.52, representative patternmaps are illustrated and show that OA/BSA treatment did not alter the level of methylation of the *AGXT* promotor in any of the used cell systems.
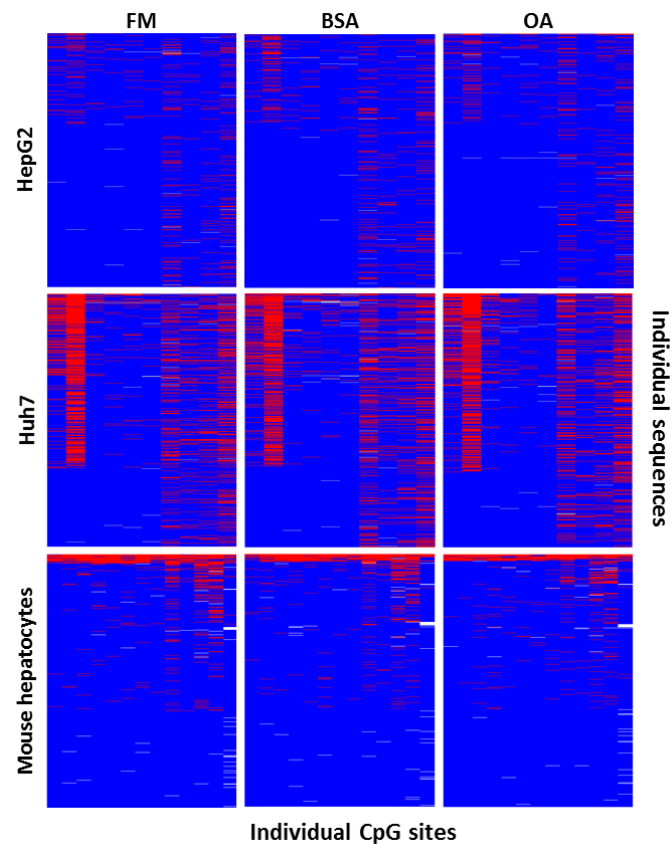
Figure 3.52: Accumulation of lipids upon OA/BSA incubation does not lead to hypermethylation of the *AGXT* promotor. HepG2 cells/ Huh7 cells and primary mouse hepatocytes were incubated with FM or 0.08 mM BSA or 0.5 mM OA/0.08 mM BSA for 5 d. Afterwards, the cells were harvested and their DNA was analysed for methylation in the human/murine promotor region of *AGXT*. Representative patternmaps of methylated CpG sites (red) in the human/murine promotor region of the *AGXT* gene in lipid loaded and control cells.

This result could lead to several conclusions. First, the mechanism underlying the downregulation of AGXT expression by oleic acid in the *in vitro* steatosis model was different from the *in vivo* situation. Secondly, the mechanism behind the downregulation of AGXT in steatosis was not promotor methylation, rather promotor methylation was a consequence of the repression of AGXT. Third, the methylation of the *AGXT* promotor might not be seen in the *in vitro* model due to insufficient OA/BSA stimulation time.

4. Discussion

Non-alcoholic fatty liver disease (NAFLD) is tightly associated with the metabolic syndrome (Marchesini et al. 2001). It is also of high clinical relevance because it may progress to severe liver diseases and increase the risk of cardiovascular (Targher et al. 2010) and renal diseases, such as chronic kidney disease (Musso et al. 2014) and urolithiasis (Nam et al. 2016). Thus, understanding the factors that contribute to disease progression and to systemic complications is of great importance. Hepatic fat accumulation has been shown to compromise hepatocellular processes, as seen in the impaired autophagy in human (Gonzalez-Rodriguez et al. 2014) and in murine NAFLD (Inami et al. 2011). Moreover, gene expression profiles of human NAFLD revealed alterations in lipid metabolism, insulin signalling and inflammation, all of which are significantly associated with the hepatic lipid content (Greco et al. 2008). Furthermore, patients with NAFLD have altered drug metabolism (reviewed by Merrell and Cherrington 2011) and an increased risk of drug induced liver injury (Tarantino et al. 2007). These alterations may act as "second hits" promoting adverse outcome.

In the course of this PhD thesis, the impact of lipids on the metabolic function of hepatocytes was investigated. For this purpose, the leptin deficient *ob/ob* mouse model of NAFLD was examined, and an *in vitro* steatosis model was established. After studying and evaluating these models, a genomic approach was applied to explore gene expression differences upon steatosis. This approach let to the finding of a lipid-dependent downregulation of the glyoxylate detoxifying enzyme alanine-glyoxylate aminotransferase (AGXT).

Mutations in the *AGXT* gene are responsible for the initiation and progression of primary hyperoxaluria type 1. Patients have elevated levels of oxalate in their urine that forms renal oxalate deposits and ultimately kidney damage (Danpure and Jennings 1986). So far, no molecular link has been identified that explains the association of NAFLD or the metabolic syndrome with urolithiasis. In this study, it was hypothesised that the downregulation of AGXT upon hepatic lipid accumulation may represent the molecular basis for the association between NAFLD and the occurrence of oxalate kidney stones. Thus, one major goal of the work was to investigate the consequences of reduced expression of AGXT on oxalate excretion *in vivo* as well as *in vitro.* In addition to the expression of AGXT, further glyoxylate metabolism-associated genes were analysed at the RNA level to estimate the impact of lipid accumulation on the overall glyoxylate metabolism. Finally, a steatosis-associated hypermethylation of the

AGXT promoter was identified in both mouse and human hepatocytes, supporting an epigenetic induced downregulation of AGXT in steatotic livers due to hypermethylation of its promotor*.*

The most important results are discussed in detail in the following sub-chapters.

4.1 Leptin deficient mouse model and *in vitro* steatosis models recapitulate several features of human NAFLD

The leptin deficient *ob/ob* mouse model of NAFLD is widely-used to study NAFLD (Anstee and Goldin 2006). *Ob/ob* mice are obese and hyperphagic; they have a fatty liver and display features of the metabolic syndrome (Schattenberg and Galle 2010). This model was applied in the current study to investigate the influence of lipid accumulation on hepatic function and hepatic gene expression. An initial step in the current project was therefore to verify the steatotic phenotype. The livers of *ob/ob* mice showed a marked pericentral (and midzonal) accumulation of lipids (Figure 3.1 E/F), which is also the predominant zonation of human steatosis (Chalasani et al. 2008). Autophagy was also compromised in the steatotic livers, confirming the findings of previous studies (Inami et al. 2011; Yang et al. 2010). To analyse genome-wide gene expression changes in steatotic livers, an Affymetrix gene array analysis of liver tissue of *ob/ob* mice and *ob/+* mice was performed. The subsequent GO enrichment analysis revealed an overrepresentation of GO terms associated with lipid metabolism among the upregulated genes, which was expected due to the high triglyceride content of the livers (Figure 3.1 D). Therefore, overall, the demonstrated gene expression changes matched this metabolic abnormality.

In addition to this mouse model, *in vitro* steatosis models were established in HepG2 cells as well as in primary mouse hepatocytes. The major aim of this approach was to induce lipid accumulation in order to identify genes that respond to such lipid excess, and to investigate the consequences of this accumulation on hepatocyte functionality and morphology.

The impact of lipid accumulation on cellular morphology was dramatic. Lipid-loaded primary mouse hepatocytes showed a clear displacement of nuclei towards the periphery of the cell, which was also seen in the steatotic livers of mice (Figure 3.11), and is a histological feature of macrovesicular steatosis (Takahashi and Fukusato 2014). Additionally, the bile canaliculi network was morphologically altered in lipid-loaded primary mouse hepatocytes (Figure 3.13),

suggesting compromised hepatocyte polarity. Furthermore, there was an impairment of the autophagic flux in both *in vitro* steatosis models as observed in human NAFLD (Fukuo et al. 2014; Gonzalez-Rodriguez et al. 2014; Kashima et al. 2014). One potential reason for the perturbation is the impaired fusion of the autophagosomes with the lysosomes due to a disturbed microtubule-dependent vesicular trafficking. An intact microtubule network is required for the fusion of autophagosomes and lysosomes (Kochl et al. 2006; Webb et al. 2004). This network appeared disturbed by lipid droplet accumulation as shown by tubulin staining of lipid-loaded primary mouse hepatocytes (Figure 3.12). Whether the autophagic flux in human NAFLD is similarly inhibited remains to be elucidated. Altogether, the alterations triggered in hepatocytes by lipid exposure *in vitro* resembled those in steatotic liver tissue.

To assess the lipid induced genome wide expression changes in the *in vitro* steatosis model, a time-resolved Affymetrix gene array analysis was performed using HepG2 cells, which were cultivated in presence of oleic acid. As seen in the progressively increasing number of deregulated genes and in the categories of overrepresented GO groups upon prolonged stimulation, the time and amount of lipid accumulation had a strong impact on the gene expression changes. This offered the opportunity to study lipid-induced deregulations in a time-dependent manner.

4.2 Applied approach for selecting steatosis relevant genes is a useful tool to identify genes across species

A pipeline (Chapter 3.4) was generated with the aim to explore global gene expression changes caused by NAFLD across species. This interspecies approach was selected in order to exclude mouse specific gene alterations, which would be irrelevant for human NAFLD.

At the time point of the present PhD project, two human datasets were available investigating genome wide gene expression changes in NAFLD (Lake et al. 2011; Moylan et al. 2014). These were both used to compare deregulated genes in human NAFLD with those found deregulated in steatotic livers of *ob/ob* mice that were identified in the Affymetrix gene array analysis as described above. This comparison revealed 119 significantly deregulated genes that were common to both species with NAFLD. To our knowledge, there is only one publication addressing the topic of global gene alterations in NAFLD in human and in mouse (Teufel et al. 2016). Teufel and colleagues compared gene expression alterations between nine mouse models of NAFLD and human NAFLD samples, identifying only 1-18 genes, which were

Discussion

significantly deregulated in both species (Teufel et al. 2016). In contrast to our interspecies NALFD analysis, Teufel and co-workers defined a threshold of significant fold change of gene expression, and considered only diet-induced murine models of NAFLD. Additionally, although they analysed both genders, most were predominantly female mice; whereas, our mouse model comprised only males. Thus, gender disparity, as well as heterogeneity among the investigated mouse models could explain the lack of a common mouse-human gene expression signature in steatosis in the study of Teufel et al. (2016).

In addition to the commonly deregulated genes of mouse and human NAFLD, the gene expression analysis of the *in vitro* model of steatosis in HepG2 cells was applied as a third parameter to search for genes that are directly affected by lipid accumulation. Here, the *in vitro* steatosis model was evaluated to determine the extent to which it was able to reproduce *in vivo* relevant differential gene expression upon NAFLD. Altogether, 22 genes were found that were commonly and robustly deregulated in the *in vitro* model, in the *ob/ob* mouse model and in both human NAFLD datasets. To our knowledge, this was the first genomic approach combining two species and an *in vitro* model of steatosis to explore steatosis-dependent gene expression alterations, and represented a reliable selection of genes for further analysis. Among the deregulated genes, the downregulation of *AGXT* prove to be a very interesting finding. *AGXT* encodes the hepatic enzyme, alanine-glyoxylate aminotransferase that detoxifies glyoxylate, thus preventing its accumulation and subsequent conversion to oxalate. Mutations in *AGXT*, an underlying cause of primary hyperoxaluria type 1, cause high urinary oxalate levels and kidney stones due to defective detoxification capacity (Danpure and Jennings 1986; Hoppe et al. 2009). An association between NAFLD (Einollahi et al. 2013; Nam et al. 2016), the metabolic syndrome (Jeong et al. 2011; Sakhaee et al. 2012) and obesity (Taylor et al. 2005) with an increased risk of urolithiasis has been reported, but no explanation for the underlying mechanism has been proposed to date. Therefore in the current work, it was hypothesised that the steatosis-dependent downregulation of AGXT and the possible reduced detoxification capacity of glyoxylate could represent the missing link between NAFLD and urolithiasis.

4.3 Reduced expression of Agxt in mouse models of NAFLD is not necessarily accompanied by increased oxalate excretion

Three different mouse models of NAFLD were investigated with respect to their Agxt expression and their daily urinary oxalate excretion. The Table below summarizes some important results and differences among those models.

Table 4.1: Summarized information of three different mouse models of NAFLD compared to corresponding control mice. Numbers indicate the fold change compared to control mice. Data are shown in the appropriate figures.

Fold change	*ob/ob*	*db/db*	Western diet
Body weight	1.9	1.7	1.3
Liver to body ratio	1.7	ns	1.4
Agxt expression	- 2.4	ns	- 3.0
Hao1 expression	- 1.6	ns	ns
Urine volume	4.4	4.4	- 2.5
Hyperoxaluric	Yes	No	No

ns: not significant

The comparison of these mouse models of NAFLD revealed important differences. Of the three models, the leptin deficient *ob/ob* mice (age: 15 – 18 weeks) was the only one showing a reduction in hepatic Agxt expression (fold change -2.4 ± 0.7, data not shown) accompanied by an increased daily excretion of urinary oxalate. Of note, the oxalate concentration in the *ob/ob* mouse urine was lower than that of *ob/+* mice, but when the urinary volume, estimated by the creatinine level, was considered, oxalate excretion per day was significantly higher (Figures 3.31 D and 3.33 D). Surprisingly, Agxt expression was not downregulated in the liver of the *db/db* mice (age: 10 weeks). In contrast, mice fed a Western-type diet for 30 weeks (age: ca 40 weeks) showed a strong and significant downregulation of Agxt, but no increased daily excretion of oxalate.

The reason for the lack of downregulation of Agxt in the liver of *db/db* mice at the examined age of 10 weeks can only be speculated: The liver tissue of *db/db* mice showed only 3.5 fold more hepatic triglycerides than the corresponding controls; whereas, the *ob/ob* mice had 16 fold more triglycerides than their corresponding controls at the age of 10 weeks (Figure 3.1). This could indicate that Agxt downregulation is only triggered after a certain amount of lipid storage is reached. Likewise, *db/db* mice displayed no increased liver to body weight ratio, and thus no liver hypertrophy, in contrast to *ob/ob* mice, suggesting that the *db/db* mice exhibit a

milder phenotype than the *ob/ob* mice. It cannot be excluded that as they age, *db/db* mice display reduced Agxt expression. For example, in a proteomics study, 48 weeks old *db/db* mice were reported to have less hepatic mitochondrial Agxt compared to control mice (Nesteruk et al. 2014).

The mice on the Western diet already had reduced liver Agxt levels after 6 weeks on the diet, and this level stayed reduced until week 30 on the diet (Figure 3.40). Analysis of publically available data (GSE38141) from an earlier study also showed the downregulation of Agxt mRNA in mice after 20 weeks on the Western diet (Kobori et al. 2011).

Interestingly, despite a strong downregulation of Agxt in the liver after 30 weeks on the Western diet, these mice did not excrete higher levels of oxalate compared to their controls. Even though they had higher urinary oxalate concentrations – most likely due to lower urine volume - the daily excretion of oxalate was similar to mice on the control diet (Figure 3.42 D). Thus, in contrast to the *ob/ob* mouse model, downregulation of Agxt upon Western diet does not correlate with increased oxalate excretion. The reason for this discrepancy is not understood. Here, both RNA and protein levels of Agxt were measured, but not the (remaining) enzymatic activity. Despite the reduced Agxt expression, residual Agxt activity working together with the glyoxylate-detoxifier enzyme Grhpr may be enough to remove endogenous glyoxylate and, as a result mice on the Western diet with reduced Agxt expression do not excrete more oxalate. To investigate this further, urinary glycolate should be measured, which might be elevated in urine of mice on the Western diet due to increased glyoxylate detoxification by Grhpr.

In addition to Agxt, the expression of the glycolate oxidising enzyme Hao1 was only reduced at the RNA level (fold change -1.6 ± 0.2, data not shown) in *ob/ob* mouse livers, which is indicative of reduced endogenous peroxisomal glyoxylate production from glycolate in *ob/ob* mice. Hao1 plays an important role in endogenous glyoxylate production in mice, as shown in several publications (Dutta et al. 2016; Li et al. 2016; Martin-Higueras et al. 2016). Agxt knockout mice with impaired transcription of Hao1 excrete less oxalate than Agxt knockout mice with normal transcription of Hao1 (Dutta et al. 2016; Li et al. 2016). This observation supported an earlier report where *ob/ob* mice excreted less oxalate upon ethylene glycol challenge than *ob/+* mice (Taguchi et al. 2015). The fact that inactivation of Hao1 rescues the

phenotype of the Agxt knockout mice highlights the importance of hepatic peroxisomal production of glyoxylate from glycolate in the pathogenesis of kidney stones.

In addition to oxalate excretion, the hepatic glycine content of *ob/ob* and *ob/+* mouse livers was also analysed. As glyoxylate is transaminated by Agxt to glycine, the hepatic glycine concentration can partly indicate the functionality of Agxt. As shown by HR MAS ^{1}HNMR, livers of *ob/ob* mice had less glycine than those of the lean control mice (Figure 3.29). These findings support those of a previous study where a metabolite profiling of plasma from 20 weeks old *ob/ob* and *db/db* mice indicating reduced concentration of glycine compared to corresponding control mice (Giesbertz et al. 2015). Glycine is involved in multiple processes, such as collagen formation, the generation of purines, and glutathione production (Wang et al. 2013). The synthesis of glycine from glyoxylate is, at least in humans, a minor but relevant pathway, contributing to the endogenous production of glycine (Melendez-Hevia et al. 2009). The reduced hepatic glycine concentration in the livers of *ob/ob* mice, accompanied by the slightly increased oxalate excretion strengthens the assumption that the reduced expression of Agxt has physiological consequences in the *ob/ob* mouse model.

4.4 HepG2 cells are not a suitable tool to investigate the peroxisomal glyoxylate metabolism

Knockdown of AGXT followed by quantification of oxalate excretion into the medium was performed as a *"proof of concept"* experiment. This was to confirm increased oxalate levels as an immediate consequence of decreased AGXT expression in hepatocytes. Moreover, it would elucidate the degree to which AGXT has to be decreased until a raise of oxalate in the supernatant occurs. Here, HepG2 cells, transfected with siRNA against AGXT, showed a robust and convincing knockdown of AGXT at the RNA as well as at the protein level (Figure 3.43 and 3.44). However, in contrast to what was expected, there was no elevated formation and excretion of oxalate into the cell supernatant. An explanation for this unexpected result could be found in two studies reporting the presence of very low activity of HAO1 in HepG2 cells and proposing a peroxisomal independent metabolism of oxalate from glycolate by lactate dehydrogenase. (Baker et al. 2004; Holmes et al. 1999). The low activity of HAO1 may be due to the very low expression of HAO1 at RNA level observed in HepG2 cells. This supported the hypothesis that the endogenously-produced oxalate in HepG2 cells was not generated from peroxisomal precursors. Moreover, the glyoxylate challenge applied to HepG2 cells was not

able to selectively induce oxalate formation in the AGXT knockdown-HepG2 cells, even though several glyoxylate concentration were used. One possible explanation may be a missing uptake of glyoxylate into the HepG2 peroxisome, which was reported for glycolate (Baker et al. 2004). This is however controversial, since treating HepG2 cells with C13-labeled hydroxyproline resulted in C13-labeled glycine indicating that mitochondrial-produced glyoxylate can enter peroxisomes for the AGXT-dependent conversion to glycine (Jiang et al. 2012). Thus, it is still not fully known why exogenous glyoxylate treatment did not selectively increase oxalate production in HepG2 cells after AGXT knockdown. Most probably, glyoxylate was directly oxidised to oxalate in the cytosol by LDH before it could enter the peroxisomes. Therefore, to optimise HepG2 cells for the analysis of reduced AGXT expression, it would be necessary to simultaneously overexpress HAO1 and knockdown AGXT in these cells.

4.5 Hepatocytes from *ob/ob* mice are more susceptible to the formation of oxalate upon hydroxyproline incubation

To investigate the consequences of reduced Agxt expression in primary hepatocytes from *ob/ob* mice, oxalate excretion into the supernatants was measured in presence or absence of glyoxylate and its known precursors, glycolate and hydroxyproline (Figure 3.47). Glycolate-exposed *ob/ob* hepatocytes excreted less oxalate into the supernatant than *ob/+* hepatocytes, indicating reduced glyoxylate generation from glycolate upon decreased Hao1 expression. This may counteract the diminished glyoxylate detoxification capacity of the steatotic hepatocytes. This assumption was supported by the following studies: It was reported that glycolate is only toxic to those cells which express Hao1 but not Agxt and Grhpr (Behnam et al. 2006). Moreover, if cultivated primary hepatocytes of Agxt knockout mice were incubated with glycolate the oxalate formation was stimulated but abrogated upon co-treatment with the Hao1 inhibitor 4-carboxy-5-[(4-chlorophenyl) sulfanyl]-1,2,3-thiadiazole (CCPST) (Martin-Higueras et al. 2016).

In contrast to glycolate, high concentrations of hydroxyproline increased the oxalate formation, particularly in *ob/ob* hepatocytes. This stimulation with hydroxyproline represented an increased susceptibility of *ob/ob* hepatocytes towards oxalate production, most probably due to decreased expression of Agxt and thus decreased glyoxylate detoxification capability. This result was of particular importance because it identified hydroxyproline catabolism as a critical pathway leading to enhanced oxalate generation in

steatosis. On the basis of this result, an *in vivo* experiment was planned to supply mice with a hydroxyproline-rich diet.

4.6 Downregulation of AGXT is associated with promotor methylation *in vivo*

The steatosis-dependent repression of AGXT was consistent at the RNA level. A possible mechanism responsible for the downregulation of AGXT could be the significant increase in methylation of the *AGXT* promotor in hepatocytes of *ob/ob* mice as well as in primary human hepatocytes, which were defined as steatotic based on their lipid content. Hypermethylation of the promotor of a gene is usually associated with repression of gene expression (Cedar 1988). This could indicate that hypermethylation of the *AGXT* promotor is the mechanism behind its downregulation in lipid-loaded hepatocytes.

In whole liver tissue of *ob/ob* mice, the aforementioned steatosis-dependent hypermethylation of the *Agxt* promotor was not obvious, thus indicating the importance of isolating different cell types of the liver for epigenetic analysis. Minor, yet significant alterations in the methylation status of genes may not be detected in whole liver tissue, especially when these alterations occur only in one cell type, or even in a subpopulation of a single cell type as it is the case for Agxt. As seen in the IHC staining of Agxt in liver tissue of mice (e.g. Figure 3.18 B), a positive signal was only obtained in the hepatocytes in the pericentral field of the liver. This suggests that only a subpopulation of murine hepatocytes transcribe *Agxt*, which supports the observation that only a percentage of hepatocytes showed hypermethylation of its promotor (Figure 3.48 B).

The overall most important finding was that primary human hepatocytes exhibited a significant negative correlation between their triglyceride content and their RNA expression level of AGXT, meaning the higher the lipid content of the cell the less the expression of AGXT (Figure 3.23). This provided further convincing evidence of a steatosis-dependent downregulation of AGXT at the RNA level. Secondly, the degree of methylation of the AGXT promotor was higher in the steatotic human hepatocytes, suggesting that the steatosis-dependent hypermethylation of the *AGXT* promotor is true across species. Despite the significant associations between lipid content and AGXT expression as well as between lipid content and AGXT methylation, there was no significant correlation between the methylation status and the extent of the reduction of AGXT expression in primary human hepatocytes. Additional samples may be required to achieve statistical significance.

In the *in vitro* models of steatosis, there was no lipid-dependent hypermethylation of the *AGXT* promotor in any of the applied cell models. Several explanations are possible: it is conceivable that the mechanism behind the downregulation of AGXT by lipid accumulation *in vitro* is different from that *in vivo*. Perhaps, the *in vitro* steatosis model was incapable of recapitulating the *in vivo* mechanisms leading to the downregulation of AGXT. On the other hand, the failure of the *in vitro* model to show an association between the repression of AGXT and its increased promotor methylation could indicate that hypermethylation of the *AGXT* promoter is the consequence rather than the cause for the downregulation of AGXT. That means that methylation may occur after the gene silencing, a mechanism that has been observed and reported in cancer cells (Clark and Melki 2002; Stirzaker et al. 2004). In this context, it is possible that the duration of lipid exposure and the downregulation of AGXT was too short to result in hypermethylation of the *AGXT* promotor.

In conclusion, steatosis-dependent methylation of both mouse and human *AGXT* promoter was found to be associated with the reduction of AGXT expression. This provided evidence of an epigenetic contribution to the alteration of the AGXT expression upon steatosis. A subsequent experiment will be to perform a transfection assay to study the effect of methylated *AGXT* promotor on the transcription of *AGXT* using a CpG-free luciferase reporter vector as described by Klug and Rehli (Klug and Rehli 2006). This assay should unequivocally elucidate whether the hypermethylation of the *AGXT* promotor results in the silencing or repression of the *AGXT* gene. Nevertheless, it remains to be determined how lipid accumulation or it consequences trigger the methylation of the *AGXT* promotor and the downregulation of AGXT.

4.7 Steatosis-dependent repression of AGXT increases the susceptibility for kidney stones

Patients suffering from PHI do not always have a complete loss of AGXT functionality and activity. There is an enormous heterogeneity between the severity and outcome of this disease for patients, which is largely dependent on the residual activity of peroxisomal AGXT, among other factors (Danpure et al. 1994; Danpure et al. 1987). In the current study, a steatosis-induced downregulation of AGXT in mouse as well as in human samples was clear. However, the main question was whether this downregulation was strong enough to cause insufficient detoxification of glyoxylate. All in all, we concluded that the impact of the

repression of AGXT on the urinary oxalate excretion depended on several factors, among which two are crucial: 1) the residual activity of AGXT, and 2) the endogenous glyoxylate production. The reduced expression of AGXT does not necessarily lead to increased urinary oxalate excretion and urolithiasis if the endogenous production of glyoxylate is dampened. As three studies from 2016 showed, the peroxisomal production of glyoxylate from glycolate *via* Hao1 enormously influences the urinary oxalate excretion in Agxt knockout mice, and inhibition of Hao1 might be a therapeutic approach for PH1 (Dutta et al. 2016; Li et al. 2016; Martin-Higueras et al. 2016). Additionally, pharmaceutical inhibition of Prodh2 expression successfully reduced oxalate excretion in Agxt knockout mice and is also discussed as a potential therapeutic approach to reduce endogenous oxalate production from hydroxyproline in primary hyperoxaluria (Li et al. 2016). For this reason, it was essential to study AGXT as well as the expression of genes involved in glyoxylate metabolism. Accordingly, the collection of human hepatocytes not only revealed a lipid-dependent downregulation of AGXT, but also showed a trend towards a downregulation of HAO1 and GRHPR. That was in line with the published data (GSE49541), which also showed a downregulation of HAO1 and GRHPR in severe NAFLD (Moylan et al. 2014), suggesting not only a reduced capacity for the removal of glyoxylate but also decreased endogenous production of glyoxylate from glycolate. This could actually lead to a situation in which the fatty liver is more protected towards glycolate-toxicity. However, stimulation of glyoxylate production by other glyoxylate-precursors present in the diet could overwhelm the capacity of the remaining AGXT and GRHPR, which would cause increased oxidation of glyoxylate to oxalate, as seen for the hydroxyproline stimulation of *ob/ob* hepatocytes. Thus, identifying additional sources and routes of glyoxylate generation are of crucial importance.

In conclusion, the steatosis-dependent downregulation of AGXT in humans might increase the susceptibility for elevated urinary oxalate excretion, which would be dependent on various parameters, e.g. the residual activity of AGXT, the endogenous production of glyoxylate, the expression as well as the activity of GRHPR, and most importantly the consumed diet. The endogenous oxalate production may be lower in some individuals due to reduced expression of HAO1. Depending on the amount of the glyoxylate precursors - glycolate and hydroxyproline - in the consumed diet, the diet and nutrients may be the cause for an extraordinary high concentration of glyoxylate that may not be efficiently detoxified in the

case of steatosis-triggered AGXT downregulation. Consequently, increased formation of oxalate may result, which could increase the risk of renal calcium oxalate deposits (Figure 4.1).
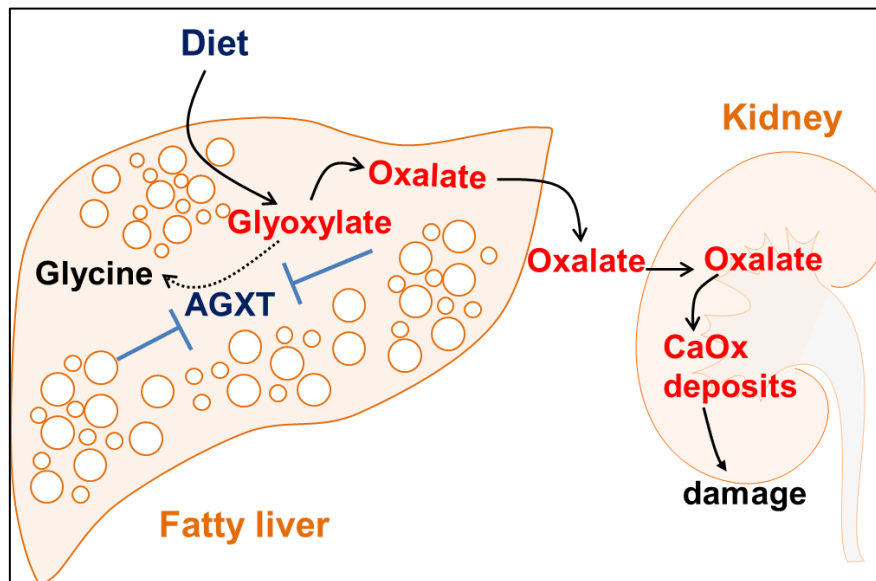
Figure 4.1: Steatosis-induced repression of AGXT increases the susceptibility for high urinary oxalate concentrations and thus elevates the risk for renal calcium oxalate stones. Diet induced stimulation of glyoxylate production could overwhelm the remaining detoxification activity of AGXT (as well as GRHPR) that consequently increased the pool of glyoxylate, which would be oxidised to oxalate.

4.8 Future perspectives

During this thesis, a strategy was developed to identify deregulated genes upon hepatic lipid accumulation. With this approach, the steatosis-dependent downregulation of AGXT, encoding a glyoxylate detoxifying enzyme, was recognized across species in both human steatotic hepatocytes and mouse models of NAFLD.

In agreement with its downregulation, leptin deficient *ob/ob* mice were found to be slightly hyperoxaluric. Since the hepatocytes of *ob/ob* mice showed an increase in the formation of oxalate compared to *ob/+* hepatocytes upon hydroxyproline incubation, a subsequent experiment would be to determine whether a hydroxyproline enriched diet induces the endogenous production of glyoxylate particularly in *ob/ob* mice. Similar experiments will be performed in mice fed the Western diet, which will show whether mice with steatotic livers are particularly susceptible or more prone to hyperoxaluria after consumption of the glyoxylate precursor, hydroxyproline.

In this study, the consequences of AGXT downregulation in steatotic human hepatocytes could not be investigated due to lack of urine samples from surgery patients. However, in obese children, an increased urinary oxalate excretion was reported to be positively associated with body fatness (Shi et al. 2010). To investigate whether obese children who excrete higher levels of urinary oxalate show a steatosis-dependent repression of AGXT, a new cooperation with the Charité Berlin has been established, which will provide liver biopsies and 24 h urine samples from obese children suffering from NAFLD. RNA will be isolated from the liver biopsies to measure the expression levels of AGXT, which will then be correlated to the oxalate levels of the corresponding urine samples.

All in all, these experiments will strengthen the link between the steatosis-dependent downregulation of AGXT and the development of hyperoxaluria. However, whether insufficient AGXT levels alone are responsible for an elevated oxalate excretion in steatosis can only be proven in an animal model *via* recovery of Agxt expression. Thus, a future experiment should be done to investigate whether overexpression of Agxt in the steatotic liver of *ob/ob* mice, e.g. *via* virus mediated gene transfer, can rescue the hyperoxaluric phenotype.

There is little information available on the regulatory machinery of AGXT. Cloning experiments revealed that human *AGXT* gene has transcription factor binding sites for NF-κB, NF-Y and others, as well as five IFNγ response elements (Sato et al. 2002). Moreover, cAMP responsive elements as well as other transcription factors and binding sites seem to be involved in the regulation of Agxt in mice (Li et al. 1999) and in rats (Oda et al. 1993). Furthermore, it is reported that glutamine (Ferrara et al. 2008) as well as glucagon (Li et al. 1999) increase the expression of Agxt in mice. Moreover, multiple polymorphisms and mutations within the human *AGXT* gene are known that result in mistargeted or/and non-functional AGXT protein (Williams et al. 2009). Conversely, several gene alterations are closely associated with the nativity of the individual (Santana et al. 2003). In the present study, AGXT expression upon steatosis across species was proposed to be epigenetically regulated since hypermethylation of the *AGXT* promotor was found in steatotic *ob/ob* mouse hepatocytes (Figures 3.48) as well as in steatotic human hepatocytes (Figures 3.50). The mechanism behind the hypermethylation has not yet been elucidated. Kim and colleagues reported an obesity-induced expression and activity of DNA methyltransferase 1 (DNMT1) (Kim et al. 2015). Therefore, characterizing DNMT1 and further DNMTs could be a first step to clarify the

mechanisms of Agxt promoter hypermethylation. In addition, the aforementioned luciferase assay will clarify the promotor methylation dependent repression of AGXT.

Finally, only male mice and male donors of hepatocytes - the gender with the higher prevalence for kidney stones (Scales et al. 2012), have been investigated so far. Thus, it is reasonable to investigate glyoxylate metabolism in females in order to elucidate whether there are gender specific differences with regard to glyoxylate producing and glyoxylate detoxifying enzymes, which might explain the increased prevalence of kidney stones in men.

5. References

Abbaszade IG, Clarke TR, Park CH, Payne AH (1995) The mouse 3 beta-hydroxysteroid dehydrogenase multigene family includes two functionally distinct groups of proteins. Molecular endocrinology (Baltimore, Md) 9(9):1214-22

Abdel-Misih SR, Bloomston M (2010) Liver anatomy. The Surgical clinics of North America 90(4):643-53

Adams E, Frank L (1980) Metabolism of proline and the hydroxyprolines. Annual review of biochemistry 49:1005-61

Adams LA, Lymp JF, St Sauver J, et al. (2005) The natural history of nonalcoholic fatty liver disease: a population-based cohort study. Gastroenterology 129(1):113-21

Ahrens M, Ammerpohl O, von Schonfels W, et al. (2013) DNA methylation analysis in nonalcoholic fatty liver disease suggests distinct disease-specific and remodeling signatures after bariatric surgery. Cell metabolism 18(2):296-302

Akarken I, Tarhan H, Ekin RG, et al. (2015) Visceral obesity: A new risk factor for stone disease. Canadian Urological Association journal = Journal de l'Association des urologues du Canada 9(11-12):E795-9

Ambros V (2004) The functions of animal microRNAs. Nature 431(7006):350-355

Amir M, Czaja MJ (2011) Autophagy in nonalcoholic steatohepatitis. Expert review of gastroenterology & hepatology 5(2):159-66

Anavi S, Ni Z, Tirosh O, Fedorova M (2015) Steatosis-induced proteins adducts with lipid peroxidation products and nuclear electrophilic stress in hepatocytes. Redox Biology 4:158-68

Anstee QM, Goldin RD (2006) Mouse models in non-alcoholic fatty liver disease and steatohepatitis research. International journal of experimental pathology 87(1):1-16

Arita Y, Kihara S, Ouchi N, et al. (1999) Paradoxical decrease of an adipose-specific protein, adiponectin, in obesity. Biochem Biophys Res Commun 257(1):79-83

Baker PR, Cramer SD, Kennedy M, Assimos DG, Holmes RP (2004) Glycolate and glyoxylate metabolism in HepG2 cells. American journal of physiology Cell physiology 287(5):C1359-65

Baylin A, Kabagambe EK, Siles X, Campos H (2002) Adipose tissue biomarkers of fatty acid intake. The American journal of clinical nutrition 76(4):750-7

Bedogni G, Miglioli L, Masutti F, Tiribelli C, Marchesini G, Bellentani S (2005) Prevalence of and risk factors for nonalcoholic fatty liver disease: the Dionysos nutrition and liver study. Hepatology 42(1):44-52

Behnam JT, Williams EL, Brink S, Rumsby G, Danpure CJ (2006) Reconstruction of human hepatocyte glyoxylate metabolic pathways in stably transformed Chinese-hamster ovary cells. The Biochemical Journal 394(Pt 2):409-16

Belfort R, Harrison SA, Brown K, et al. (2006) A placebo-controlled trial of pioglitazone in subjects with nonalcoholic steatohepatitis. The New England journal of medicine 355(22):2297-307

Belostotsky R, Seboun E, Idelson GH, et al. (2010) Mutations in DHDPSL Are Responsible For Primary Hyperoxaluria Type III. The American Journal of Human Genetics 87(3):392-399

Benjamini Y, Hochberg Y (1995) Controlling the False Discovery Rate: A Practical and Powerful Approach to Multiple Testing. Journal of the Royal Statistical Society Series B (Methodological) 57(1):289-300

References

Birdsey GM, Lewin J, Cunningham AA, Bruford MW, Danpure CJ (2004) Differential enzyme targeting as an evolutionary adaptation to herbivory in carnivora. Molecular biology and evolution 21(4):632-46

Bjorkoy G, Lamark T, Brech A, et al. (2005) p62/SQSTM1 forms protein aggregates degraded by autophagy and has a protective effect on huntingtin-induced cell death. J Cell Biol 171(4):603-14

Boza C, Riquelme A, Ibanez L, et al. (2005) Predictors of nonalcoholic steatohepatitis (NASH) in obese patients undergoing gastric bypass. Obesity surgery 15(8):1148-53

Brent J (2001) Current Management of Ethylene Glycol Poisoning. Drugs 61(7):979-988

Browning JD, Szczepaniak LS, Dobbins R, et al. (2004) Prevalence of hepatic steatosis in an urban population in the United States: impact of ethnicity. Hepatology 40(6):1387-95

Bruun JM, Lihn AS, Verdich C, et al. (2003) Regulation of adiponectin by adipose tissue-derived cytokines: in vivo and in vitro investigations in humans. American journal of physiology Endocrinology and metabolism 285(3):E527-33

Bugianesi E, Leone N, Vanni E, et al. (2002) Expanding the natural history of nonalcoholic steatohepatitis: from cryptogenic cirrhosis to hepatocellular carcinoma. Gastroenterology 123(1):134-40

Bugianesi E, Pagotto U, Manini R, et al. (2005) Plasma adiponectin in nonalcoholic fatty liver is related to hepatic insulin resistance and hepatic fat content, not to liver disease severity. The Journal of clinical endocrinology and metabolism 90(6):3498-504

Buzzetti E, Pinzani M, Tsochatzis EA (2016) The multiple-hit pathogenesis of non-alcoholic fatty liver disease (NAFLD). Metabolism 65(8):1038-48

Caldwell SH, Swerdlow RH, Khan EM, et al. (1999) Mitochondrial abnormalities in non-alcoholic steatohepatitis. J Hepatol 31(3):430-4

Cani PD, Bibiloni R, Knauf C, et al. (2008) Changes in Gut Microbiota Control Metabolic Endotoxemia-Induced Inflammation in High-Fat Diet–Induced Obesity and Diabetes in Mice. Diabetes 57(6):1470-1481

Cedar H (1988) DNA methylation and gene activity. Cell 53(1):3-4

Cellini B, Bertoldi M, Montioli R, Paiardini A, Borri Voltattorni C (2007) Human wild-type alanine:glyoxylate aminotransferase and its naturally occurring G82E variant: functional properties and physiological implications. The Biochemical Journal 408(Pt 1):39-50

Chalasani N, Wilson L, Kleiner DE, Cummings OW, Brunt EM, Unalp A (2008) Relationship of steatosis grade and zonal location to histological features of steatohepatitis in adult patients with non-alcoholic fatty liver disease. J Hepatol 48(5):829-34

Chalasani N, Younossi Z, Lavine JE, et al. (2012) The diagnosis and management of non-alcoholic fatty liver disease: practice Guideline by the American Association for the Study of Liver Diseases, American College of Gastroenterology, and the American Gastroenterological Association. Hepatology 55(6):2005-23

Chen H, Charlat O, Tartaglia LA, et al. (1996) Evidence that the diabetes gene encodes the leptin receptor: identification of a mutation in the leptin receptor gene in db/db mice. Cell 84(3):491-5

Chomczynski P, Sacchi N (1987) Single-step method of RNA isolation by acid guanidinium thiocyanate-phenol-chloroform extraction. Analytical Biochemistry 162(1):156-159

Clark SJ, Melki J (2002) DNA methylation and gene silencing in cancer: which is the guilty party? Oncogene 21(35):5380-7

Cochat P, Deloraine A, Rotily M, Olive F, Liponski I, Deries N (1995) Epidemiology of primary hyperoxaluria type 1. Societe de Nephrologie and the Societe de Nephrologie

Pediatrique. Nephrology, dialysis, transplantation : official publication of the European Dialysis and Transplant Association - European Renal Association 10 Suppl 8:3-7

Coe FL, Evan A, Worcester E (2005) Kidney stone disease. The Journal of clinical investigation 115(10):2598-608

Coleman DL (1978) Obese and diabetes: two mutant genes causing diabetes-obesity syndromes in mice. Diabetologia 14(3):141-8

Cousin SP, Hugl SR, Wrede CE, Kajio H, Myers MG, Jr., Rhodes CJ (2001) Free fatty acid-induced inhibition of glucose and insulin-like growth factor I-induced deoxyribonucleic acid synthesis in the pancreatic beta-cell line INS-1. Endocrinology 142(1):229-40 doi:10.1210/endo.142.1.7863

Cramer SD, Ferree PM, Lin K, Milliner DS, Holmes RP (1999) The gene encoding hydroxypyruvate reductase (GRHPR) is mutated in patients with primary hyperoxaluria type II. Human molecular genetics 8(11):2063-9

Crespo J, Cayon A, Fernandez-Gil P, et al. (2001) Gene expression of tumor necrosis factor alpha and TNF-receptors, p55 and p75, in nonalcoholic steatohepatitis patients. Hepatology 34(6):1158-63

Curhan GC, Willett WC, Speizer FE, Stampfer MJ (2001) Twenty-four-hour urine chemistries and the risk of kidney stones among women and men. Kidney international 59(6):2290-8

da Silva Correia J, Soldau K, Christen U, Tobias PS, Ulevitch RJ (2001) Lipopolysaccharide is in close proximity to each of the proteins in its membrane receptor complex. transfer from CD14 to TLR4 and MD-2. The Journal of biological chemistry 276(24):21129-35

da Silva RP, Kelly KB, Al Rajabi A, Jacobs RL (2014) Novel insights on interactions between folate and lipid metabolism. BioFactors (Oxford, England) 40(3):277-83

Danpure CJ (1997) Variable peroxisomal and mitochondrial targeting of alanine: glyoxylate aminotransferase in mammalian evolution and disease. BioEssays : news and reviews in molecular, cellular and developmental biology 19(4):317-26

Danpure CJ, Jennings PR (1986) Peroxisomal alanine:glyoxylate aminotransferase deficiency in primary hyperoxaluria type I. FEBS letters 201(1):20-4

Danpure CJ, Jennings PR, Fryer P, Purdue PE, Allsop J (1994) Primary hyperoxaluria type 1: Genotypic and phenotypic heterogeneity. Journal of Inherited Metabolic Disease 17(4):487-499

Danpure CJ, Jennings PR, Watts RW (1987) Enzymological diagnosis of primary hyperoxaluria type 1 by measurement of hepatic alanine: glyoxylate aminotransferase activity. Lancet (London, England) 1(8528):289-91

Day CP (2002) Pathogenesis of steatohepatitis. Best practice & research Clinical gastroenterology 16(5):663-78

Day CP, James OF (1998) Steatohepatitis: a tale of two "hits"? Gastroenterology 114(4):842-5

Dennis G, Jr., Sherman BT, Hosack DA, et al. (2003) DAVID: Database for Annotation, Visualization, and Integrated Discovery. Genome biology 4(5):P3

Donnelly KL, Smith CI, Schwarzenberg SJ, Jessurun J, Boldt MD, Parks EJ (2005) Sources of fatty acids stored in liver and secreted via lipoproteins in patients with nonalcoholic fatty liver disease. The Journal of clinical investigation 115(5):1343-51

Dowman JK, Tomlinson JW, Newsome PN (2010) Pathogenesis of non-alcoholic fatty liver disease. QJM : monthly journal of the Association of Physicians 103(2):71-83

Dutta C, Avitahl-Curtis N, Pursell N, et al. (2016) Inhibition of Glycolate Oxidase With Dicer-substrate siRNA Reduces Calcium Oxalate Deposition in a Mouse Model of Primary

References

Hyperoxaluria Type 1. Molecular therapy : the journal of the American Society of Gene Therapy 24(4):770-8

Eccleston HB, Andringa KK, Betancourt AM, et al. (2011) Chronic exposure to a high-fat diet induces hepatic steatosis, impairs nitric oxide bioavailability, and modifies the mitochondrial proteome in mice. Antioxidants & redox signaling 15(2):447-59

Einollahi B, Naghii MR, Sepandi M (2013) Association of nonalcoholic fatty liver disease (NAFLD) with urolithiasis. Endocrine regulations 47(1):27-32

Ekstedt M, Franzen LE, Mathiesen UL, et al. (2006) Long-term follow-up of patients with NAFLD and elevated liver enzymes. Hepatology 44(4):865-73

European Association for the Study of the Liver EAftSoD, European Association for the Study of, Obesity (2016) EASL–EASD–EASO Clinical Practice Guidelines for the management of non-alcoholic fatty liver disease. Journal of Hepatology 64(6):1388-1402

Evan AP (2010) Physiopathology and etiology of stone formation in the kidney and the urinary tract. Pediatric nephrology (Berlin, Germany) 25(5):831-41

Expert Panel on Detection Evaluation and Treatment of High Blood Cholesterol iA (2001) Executive summary of the third report of the national cholesterol education program (ncep) expert panel on detection, evaluation, and treatment of high blood cholesterol in adults (adult treatment panel iii). Jama 285(19):2486-2497

Faggioni R, Fantuzzi G, Gabay C, et al. (1999) Leptin deficiency enhances sensitivity to endotoxin-induced lethality. The American journal of physiology 276(1 Pt 2):R136-42

Farhadi A, Gundlapalli S, Shaikh M, et al. (2008) Susceptibility to gut leakiness: a possible mechanism for endotoxaemia in non-alcoholic steatohepatitis. Liver international : official journal of the International Association for the Study of the Liver 28(7):1026-33

Feldstein AE, Werneburg NW, Canbay A, et al. (2004) Free fatty acids promote hepatic lipotoxicity by stimulating TNF-alpha expression via a lysosomal pathway. Hepatology 40(1):185-94

Ferrara CT, Wang P, Neto EC, et al. (2008) Genetic networks of liver metabolism revealed by integration of metabolic and transcriptional profiling. PLoS genetics 4(3):e1000034

Ferreira DM, Simao AL, Rodrigues CM, Castro RE (2014) Revisiting the metabolic syndrome and paving the way for microRNAs in non-alcoholic fatty liver disease. The FEBS journal 281(11):2503-24

Fire A, Xu S, Montgomery MK, Kostas SA, Driver SE, Mello CC (1998) Potent and specific genetic interference by double-stranded RNA in Caenorhabditis elegans. Nature 391(6669):806-811

Fotbolcu H, Zorlu E (2016) Nonalcoholic fatty liver disease as a multi-systemic disease. World Journal of Gastroenterology 22(16):4079-90

Friedman JM, Leibel RL, Siegel DS, Walsh J, Bahary N (1991) Molecular mapping of the mouse ob mutation. Genomics 11(4):1054-62

Fujii Y, Okada A, Yasui T, et al. (2013) Effect of adiponectin on kidney crystal formation in metabolic syndrome model mice via inhibition of inflammation and apoptosis. PLoS One 8(4):e61343

Fukuo Y, Yamashina S, Sonoue H, et al. (2014) Abnormality of autophagic function and cathepsin expression in the liver from patients with non-alcoholic fatty liver disease. Hepatology research : the official journal of the Japan Society of Hepatology 44(9):1026-36

Giesbertz P, Padberg I, Rein D, et al. (2015) Metabolite profiling in plasma and tissues of ob/ob and db/db mice identifies novel markers of obesity and type 2 diabetes. Diabetologia 58(9):2133-43

Godoy P, Hewitt NJ, Albrecht U, et al. (2013) Recent advances in 2D and 3D in vitro systems using primary hepatocytes, alternative hepatocyte sources and non-parenchymal liver cells and their use in investigating mechanisms of hepatotoxicity, cell signaling and ADME. Archives of toxicology 87(8):1315-530 doi:5

Gogiashvili M, Edlund K, Gianmoena K, et al. (2016) Metabolic profiling of ob/ob mouse fatty liver using HR-MAS 1H-NMR combined with gene expression analysis reveals alterations in betaine metabolism and the transsulfuration pathway. Analytical and Bioanalytical Chemistry:1-16

Gomez-Lechon MJ, Donato MT, Martinez-Romero A, Jimenez N, Castell JV, O'Connor JE (2007) A human hepatocellular in vitro model to investigate steatosis. Chemico-biological interactions 165(2):106-16

Gonzalez-Rodriguez A, Mayoral R, Agra N, et al. (2014) Impaired autophagic flux is associated with increased endoplasmic reticulum stress during the development of NAFLD. Cell death & disease 5:e1179

Gordon RS, Cherkes A (1956) Unesterified fatty acid in human blood plasma. Journal of Clinical Investigation 35(2):206-212

Greco D, Kotronen A, Westerbacka J, et al. (2008) Gene expression in human NAFLD. American journal of physiology Gastrointestinal and liver physiology 294(5):G1281-7

Halaas JL, Gajiwala KS, Maffei M, et al. (1995) Weight-reducing effects of the plasma protein encoded by the obese gene. Science 269(5223):543-6

Harte AL, da Silva NF, Creely SJ, et al. (2010) Elevated endotoxin levels in non-alcoholic fatty liver disease. Journal of inflammation (London, England) 7:15

Herceg Z, Murr R (2011) Chapter 3 - Mechanisms of Histone Modifications A2 - Tollefsbol, Trygve Handbook of Epigenetics. Academic Press, San Diego, p 25-45

Higuchi R, C. Fockler, G. Dollinger, and R. Watson (1993) Kinetic PCR analysis: real- time monitoring of DNA amplification reactions. . Biotechnology (NY) 11:1026-1030

Holland PM, Abramson RD, Watson R, Gelfand DH (1991) Detection of specific polymerase chain reaction product by utilizing the 5'----3' exonuclease activity of Thermus aquaticus DNA polymerase. Proceedings of the National Academy of Sciences of the United States of America 88(16):7276-7280

Holmes RP, Assimos DG (1998) Glyoxylate synthesis, and its modulation and influence on oxalate synthesis. The Journal of urology 160(5):1617-24

Holmes RP, Sexton WJ, Applewhite JC, Kennedy M, Assimos DG (1999) Glycolate metabolism by Hep G2 cells. Journal of the American Society of Nephrology : JASN 10 Suppl 14:S345-7

Hoppe B, Beck BB, Milliner DS (2009) The primary hyperoxalurias. Kidney international 75(12):1264-71

Hoppe B, Leumann E, von Unruh G, Laube N, Hesse A (2003) Diagnostic and therapeutic approaches in patients with secondary hyperoxaluria. Frontiers in bioscience : a journal and virtual library 8:e437-43

Horton JD, Goldstein JL, Brown MS (2002) SREBPs: activators of the complete program of cholesterol and fatty acid synthesis in the liver. The Journal of clinical investigation 109(9):1125-31

References

Hotta K, Funahashi T, Arita Y, et al. (2000) Plasma concentrations of a novel, adipose-specific protein, adiponectin, in type 2 diabetic patients. Arteriosclerosis, thrombosis, and vascular biology 20(6):1595-9

Huang DW, Sherman BT, Lempicki RA (2009) Systematic and integrative analysis of large gene lists using DAVID bioinformatics resources. Nature protocols 4(1):44-57

Huang DW, Sherman BT, Tan Q, et al. (2007) DAVID Bioinformatics Resources: expanded annotation database and novel algorithms to better extract biology from large gene lists. Nucleic acids research 35(Web Server issue):W169-75

Hummel KP, Dickie MM, Coleman DL (1966) Diabetes, a new mutation in the mouse. Science 153(3740):1127-8

Inami Y, Yamashina S, Izumi K, et al. (2011) Hepatic steatosis inhibits autophagic proteolysis via impairment of autophagosomal acidification and cathepsin expression. Biochem Biophys Res Commun 412(4):618-25

Ingalls AM, Dickie MM, Snell GD (1950) Obese, a new mutation in the house mouse. The Journal of heredity 41(12):317-8

Irizarry RA, Hobbs B, Collin F, et al. (2003) Exploration, normalization, and summaries of high density oligonucleotide array probe level data. Biostatistics 4(2):249-264

Ito M, Suzuki J, Tsujioka S, et al. (2007) Longitudinal analysis of murine steatohepatitis model induced by chronic exposure to high-fat diet. Hepatology research : the official journal of the Japan Society of Hepatology 37(1):50-7

Jaffe M (1886) Ueber den Niederschlag, welchen Pikrinsäure in normalem Harn erzeugt und über eine neue Reaction des Kreatinins Zeitschrift für physiologische Chemie. vol 10, p 391

Jeong IG, Kang T, Bang JK, et al. (2011) Association between metabolic syndrome and the presence of kidney stones in a screened population. American journal of kidney diseases : the official journal of the National Kidney Foundation 58(3):383-8

Jiang J, Johnson LC, Knight J, et al. (2012) Metabolism of [13C5]hydroxyproline in vitro and in vivo: implications for primary hyperoxaluria. American journal of physiology Gastrointestinal and liver physiology 302(6):G637-43

Jolliffe IT (2002) Principal Component Analysis. Springer, New York 2nd edition

Kabeya Y, Mizushima N, Ueno T, et al. (2000) LC3, a mammalian homologue of yeast Apg8p, is localized in autophagosome membranes after processing. The EMBO journal 19(21):5720-8

Kabeya Y, Mizushima N, Yamamoto A, Oshitani-Okamoto S, Ohsumi Y, Yoshimori T (2004) LC3, GABARAP and GATE16 localize to autophagosomal membrane depending on form-II formation. Journal of cell science 117(Pt 13):2805-12

Kadlec AO, Greco K, Fridirici ZC, Hart ST, Vellos T, Turk TM (2012) Metabolic syndrome and urinary stone composition: what factors matter most? Urology 80(4):805-10

Kaser S, Moschen A, Cayon A, et al. (2005) Adiponectin and its receptors in non-alcoholic steatohepatitis. Gut 54(1):117-21

Kashima J, Shintani-Ishida K, Nakajima M, et al. (2014) Immunohistochemical study of the autophagy marker microtubule-associated protein 1 light chain 3 in normal and steatotic human livers. Hepatology research : the official journal of the Japan Society of Hepatology 44(7):779-87

Kaufman RJ (2002) Orchestrating the unfolded protein response in health and disease. The Journal of clinical investigation 110(10):1389-98

Khan SR, Glenton PA (2010) Experimental induction of calcium oxalate nephrolithiasis in mice. The Journal of urology 184(3):1189-96

Kim AY, Park YJ, Pan X, et al. (2015) Obesity-induced DNA hypermethylation of the adiponectin gene mediates insulin resistance. Nature communications 6:7585

Klionsky DJ, Abdalla FC, Abeliovich H, et al. (2012) Guidelines for the use and interpretation of assays for monitoring autophagy. Autophagy 8(4):445-544

Klug M, Rehli M (2006) Functional analysis of promoter CpG methylation using a CpG-free luciferase reporter vector. Epigenetics 1(3):127-30

Knight J, Holmes RP, Cramer SD, Takayama T, Salido E (2012) Hydroxyproline metabolism in mouse models of primary hyperoxaluria. American journal of physiology Renal physiology 302(6):F688-93

Knight J, Jiang J, Assimos DG, Holmes RP (2006) Hydroxyproline ingestion and urinary oxalate and glycolate excretion. Kidney international 70(11):1929-34

Knight J, Wood KD, Lange JN, Assimos DG, Holmes RP (2016) Oxalate formation from glyoxal in erythrocytes Urology 88:226.e11-5

Kobori M, Masumoto S, Akimoto Y, Oike H (2011) Chronic dietary intake of quercetin alleviates hepatic fat accumulation associated with consumption of a Western-style diet in C57/BL6J mice. Molecular nutrition & food research 55(4):530-40

Kochl R, Hu XW, Chan EY, Tooze SA (2006) Microtubules facilitate autophagosome formation and fusion of autophagosomes with endosomes. Traffic (Copenhagen, Denmark) 7(2):129-45

Koga H, Kaushik S, Cuervo AM (2010) Altered lipid content inhibits autophagic vesicular fusion. FASEB journal : official publication of the Federation of American Societies for Experimental Biology 24(8):3052-65

Kohjimoto Y, Sasaki Y, Iguchi M, Matsumura N, Inagaki T, Hara I (2013) Association of metabolic syndrome traits and severity of kidney stones: results from a nationwide survey on urolithiasis in Japan. American journal of kidney diseases : the official journal of the National Kidney Foundation 61(6):923-9

Kohsaka A, Laposky AD, Ramsey KM, et al. (2007) High-fat diet disrupts behavioral and molecular circadian rhythms in mice. Cell metabolism 6(5):414-21

Koliwad SK, Streeper RS, Monetti M, et al. (2010) DGAT1-dependent triacylglycerol storage by macrophages protects mice from diet-induced insulin resistance and inflammation. The Journal of clinical investigation 120(3):756-67

Komatsu M, Waguri S, Koike M, et al. (2007) Homeostatic levels of p62 control cytoplasmic inclusion body formation in autophagy-deficient mice. Cell 131(6):1149-63

Kopp N, Leumann E (1995) Changing pattern of primary hyperoxaluria in Switzerland. Nephrology, dialysis, transplantation : official publication of the European Dialysis and Transplant Association - European Renal Association 10(12):2224-7

Korenblat KM, Fabbrini E, Mohammed BS, Klein S (2008) Liver, Muscle and Adipose Tissue Insulin Action is Directly Related to Intrahepatic Triglyceride Content in Obese Subjects. Gastroenterology 134(5):1369-75

Kozlitina J, Smagris E, Stender S, et al. (2014) Exome-wide association study identifies a TM6SF2 variant that confers susceptibility to nonalcoholic fatty liver disease. Nature genetics 46(4):352-6

Kriz W, Bankir L (1988) A standard nomenclature for structures of the kidney. The Renal Commission of the International Union of Physiological Sciences (IUPS). Kidney international 33(1):1-7

Kwanten WJ, Martinet W, Michielsen PP, Francque SM (2014) Role of autophagy in the pathophysiology of nonalcoholic fatty liver disease: a controversial issue. World Journal of Gastroenterology 20(23):7325-38

References

Lake AD, Novak P, Fisher CD, et al. (2011) Analysis of global and absorption, distribution, metabolism, and elimination gene expression in the progressive stages of human nonalcoholic fatty liver disease. Drug metabolism and disposition: the biological fate of chemicals 39(10):1954-60

Lau JK, Zhang X, Yu J (2017) Animal models of non-alcoholic fatty liver disease: current perspectives and recent advances. The Journal of pathology 241(1):36-44

Leclercq IA, Farrell GC, Schriemer R, Robertson GR (2002) Leptin is essential for the hepatic fibrogenic response to chronic liver injury. J Hepatol 37(2):206-13

Lee J, Kim Y, Friso S, Choi SW (2017) Epigenetics in non-alcoholic fatty liver disease. Molecular aspects of medicine 54:78-88

Lee JH, Friso S, Choi SW (2014) Epigenetic mechanisms underlying the link between non-alcoholic fatty liver diseases and nutrition. Nutrients 6(8):3303-25

Lee JY, Kim KM, Lee SG, et al. (2007) Prevalence and risk factors of non-alcoholic fatty liver disease in potential living liver donors in Korea: a review of 589 consecutive liver biopsies in a single center. J Hepatol 47(2):239-44

Leite NC, Salles GF, Araujo AL, Villela-Nogueira CA, Cardoso CR (2009) Prevalence and associated factors of non-alcoholic fatty liver disease in patients with type-2 diabetes mellitus. Liver international : official journal of the International Association for the Study of the Liver 29(1):113-9

Lewis GF, Carpentier A, Adeli K, Giacca A (2002) Disordered fat storage and mobilization in the pathogenesis of insulin resistance and type 2 diabetes. Endocrine reviews 23(2):201-29

Li X, Knight J, Fargue S, et al. (2016) Metabolism of (13)C5-hydroxyproline in mouse models of Primary Hyperoxaluria and its inhibition by RNAi therapeutics targeting liver glycolate oxidase and hydroxyproline dehydrogenase. Biochimica et biophysica acta 1862(2):233-9

Li XM, Salido EC, Shapiro LJ (1999) The mouse alanine:glyoxylate aminotransferase gene (Agxt1): cloning, expression, and mapping to chromosome 1. Somatic cell and molecular genetics 25(2):67-77

Lindl T, Gstraunthaler G (2008) Zell- und Gewbekultur, 6 edn. Spektrum Akademischer Verlag

Ling C, Groop L (2009) Epigenetics: a molecular link between environmental factors and type 2 diabetes. Diabetes 58(12):2718-25

Listenberger LL, Han X, Lewis SE, et al. (2003) Triglyceride accumulation protects against fatty acid-induced lipotoxicity. Proc Natl Acad Sci U S A 100(6):3077-82

Liu HY, Han J, Cao SY, et al. (2009) Hepatic autophagy is suppressed in the presence of insulin resistance and hyperinsulinemia: inhibition of FoxO1-dependent expression of key autophagy genes by insulin. The Journal of biological chemistry 284(45):31484-92

Liu YL, Reeves HL, Burt AD, et al. (2014) TM6SF2 rs58542926 influences hepatic fibrosis progression in patients with non-alcoholic fatty liver disease. Nature communications 5:4309

Livak KJ, Schmittgen TD (2001) Analysis of Relative Gene Expression Data Using Real-Time Quantitative PCR and the 2−ΔΔCT Method. Methods 25(4):402-408

Lorenzo V, Torres A, Salido E (2014) Primary hyperoxaluria. Nefrologia : publicacion oficial de la Sociedad Espanola Nefrologia 34(3):398-412

Luster MI, Germolec DR, Yoshida T, Kayama F, Thompson M (1994) Endotoxin-induced cytokine gene expression and excretion in the liver. Hepatology 19(2):480-8

Machado M, Marques-Vidal P, Cortez-Pinto H (2006) Hepatic histology in obese patients undergoing bariatric surgery. J Hepatol 45(4):600-6

Malhi H, Bronk SF, Werneburg NW, Gores GJ (2006) Free fatty acids induce JNK-dependent hepatocyte lipoapoptosis. The Journal of biological chemistry 281(17):12093-101

Marchesini G, Brizi M, Bianchi G, et al. (2001) Nonalcoholic fatty liver disease: a feature of the metabolic syndrome. Diabetes 50(8):1844-50

Marchesini G, Brizi M, Morselli-Labate AM, et al. (1999) Association of nonalcoholic fatty liver disease with insulin resistance. The American journal of medicine 107(5):450-5

Marcos A, Fisher RA, Ham JM, et al. (2000) Selection and outcome of living donors for adult to adult right lobe transplantation. Transplantation 69(11):2410-5

Mari M, Caballero F, Colell A, et al. (2006) Mitochondrial free cholesterol loading sensitizes to TNF- and Fas-mediated steatohepatitis. Cell metabolism 4(3):185-98

Martin-Higueras C, Luis-Lima S, Salido E (2016) Glycolate Oxidase Is a Safe and Efficient Target for Substrate Reduction Therapy in a Mouse Model of Primary Hyperoxaluria Type I. Molecular therapy : the journal of the American Society of Gene Therapy 24(4):719-25

Matteoni CA, Younossi ZM, Gramlich T, Boparai N, Liu YC, McCullough AJ (1999) Nonalcoholic fatty liver disease: a spectrum of clinical and pathological severity. Gastroenterology 116(6):1413-9

Mayer J, Russell RE, Bates MW, Dickie MM (1953) Metabolic, nutritional and endocrine studies of the hereditary obesity-diabetes syndrome of mice and mechanism of its development. Metabolism 2(1):9-21

Medzhitov R (2001) Toll-like receptors and innate immunity. Nature reviews Immunology 1(2):135-45

Medzhitov R, Preston-Hurlburt P, Janeway CA (1997) A human homologue of the Drosophila Toll protein signals activation of adaptive immunity. Nature 388(6640):394-397

Mei S, Ni HM, Manley S, et al. (2011) Differential roles of unsaturated and saturated fatty acids on autophagy and apoptosis in hepatocytes. The Journal of pharmacology and experimental therapeutics 339(2):487-98

Melendez-Hevia E, De Paz-Lugo P, Cornish-Bowden A, Cardenas ML (2009) A weak link in metabolism: the metabolic capacity for glycine biosynthesis does not satisfy the need for collagen synthesis. Journal of biosciences 34(6):853-72

Merrell MD, Cherrington NJ (2011) Drug metabolism alterations in nonalcoholic fatty liver disease. Drug metabolism reviews 43(3):317-34

Miele L, Valenza V, La Torre G, et al. (2009) Increased intestinal permeability and tight junction alterations in nonalcoholic fatty liver disease. Hepatology 49(6):1877-87

Milliner DS, Wilson DM, Smith LH (2001) Phenotypic expression of primary hyperoxaluria: comparative features of types I and II. Kidney international 59(1):31-6

Miyagawa K, Oe S, Honma Y, Izumi H, Baba R, Harada M (2016) Lipid-Induced Endoplasmic Reticulum Stress Impairs Selective Autophagy at the Step of Autophagosome-Lysosome Fusion in Hepatocytes. The American journal of pathology 186(7):1861-73 doi:10.1016/j.ajpath.2016.03.003

Miyazaki M, Bruggink SM, Ntambi JM (2006) Identification of mouse palmitoyl-coenzyme A Delta9-desaturase. Journal of lipid research 47(4):700-4

Mizushima N, Yoshimori T (2007) How to interpret LC3 immunoblotting. Autophagy 3(6):542-5

Monico CG, Rossetti S, Belostotsky R, et al. (2011) Primary hyperoxaluria type III gene HOGA1 (formerly DHDPSL) as a possible risk factor for idiopathic calcium oxalate urolithiasis. Clinical journal of the American Society of Nephrology : CJASN 6(9):2289-95

Motley A, Lumb MJ, Oatey PB, et al. (1995) Mammalian alanine/glyoxylate aminotransferase 1 is imported into peroxisomes via the PTS1 translocation pathway. Increased

References

degeneracy and context specificity of the mammalian PTS1 motif and implications for the peroxisome-to-mitochondrion mistargeting of AGT in primary hyperoxaluria type 1. J Cell Biol 131(1):95-109

Moylan CA, Pang H, Dellinger A, et al. (2014) Hepatic gene expression profiles differentiate presymptomatic patients with mild versus severe nonalcoholic fatty liver disease. Hepatology 59(2):471-82

Murphy SK, Yang H, Moylan CA, et al. (2013) Relationship between methylome and transcriptome in patients with nonalcoholic fatty liver disease. Gastroenterology 145(5):1076-87

Musso G, Gambino R, Durazzo M, et al. (2005) Adipokines in NASH: postprandial lipid metabolism as a link between adiponectin and liver disease. Hepatology 42(5):1175-83

Musso G, Gambino R, Tabibian JH, et al. (2014) Association of non-alcoholic fatty liver disease with chronic kidney disease: a systematic review and meta-analysis. PLoS medicine 11(7):e1001680

Nakabayashi H, Taketa K, Miyano K, Yamane T, Sato J (1982) Growth of Human Hepatoma Cell Lines with Differentiated Functions in Chemically Defined Medium. Cancer Research 42(9):3858-3863

Nam IC, Yoon JH, Park SH, J. R, Kim SH, Lee Y (2016) Association of non-alcoholic fatty liver disease with renal stone disease detected on computed tomography. European Journal of Radiology Open 3:195-9

National Center for Health Statistic (1994) Plan and operation of the Third National Health and Nutrition Examination Survey, 1988-94. Series 1: programs and collection procedures. Vital and health statistics Ser 1, Programs and collection procedures(32):1-407

Negri AL, Spivacow FR, Del Valle EE, Forrester M, Rosende G, Pinduli I (2008) Role of overweight and obesity on the urinary excretion of promoters and inhibitors of stone formation in stone formers. Urol Res 36(6):303-7

Nesteruk M, Hennig EE, Mikula M, et al. (2014) Mitochondrial-related proteomic changes during obesity and fasting in mice are greater in the liver than skeletal muscles. Functional & integrative genomics 14(1):245-59

Nikiforova VJ, Giesbertz P, Wiemer J, et al. (2014) Glyoxylate, a new marker metabolite of type 2 diabetes. Journal of diabetes research 2014:685204

Nishikawa S, Yasoshima A, Doi K, Nakayama H, Uetsuka K (2007) Involvement of sex, strain and age factors in high fat diet-induced obesity in C57BL/6J and BALB/cA mice. Experimental animals 56(4):263-72

Noguchi T, Minatogawa Y, Takada Y, Okuno E, Kido R (1978) Subcellular distribution of pyruvate (glyoxylate) aminotransferases in rat liver. The Biochemical Journal 170(1):173-5

O'Brien J, Wilson I, Orton T, Pognan F (2000) Investigation of the Alamar Blue (resazurin) fluorescent dye for the assessment of mammalian cell cytotoxicity. European journal of biochemistry 267(17):5421-6

Oda T, Nishiyama K, Ichiyama A (1993) Characterization and sequence analysis of rat serine:pyruvate/alanine:glyoxylate aminotransferase gene. Genomics 17(1):59-65

Ogata M, Hino S, Saito A, et al. (2006) Autophagy is activated for cell survival after endoplasmic reticulum stress. Molecular and cellular biology 26(24):9220-31

Ong JP, Elariny H, Collantes R, et al. (2005) Predictors of nonalcoholic steatohepatitis and advanced fibrosis in morbidly obese patients. Obesity surgery 15(3):310-5

Ong JP, Pitts A, Younossi ZM (2008) Increased overall mortality and liver-related mortality in non-alcoholic fatty liver disease. J Hepatol 49(4):608-12

Ozcan U, Yilmaz E, Ozcan L, et al. (2006) Chemical chaperones reduce ER stress and restore glucose homeostasis in a mouse model of type 2 diabetes. Science 313(5790):1137-40

Pais R, Pascale A, Fedchuck L, Charlotte F, Poynard T, Ratziu V (2011) Progression from isolated steatosis to steatohepatitis and fibrosis in nonalcoholic fatty liver disease. Clinics and research in hepatology and gastroenterology 35(1):23-8

Pankiv S, Clausen TH, Lamark T, et al. (2007) p62/SQSTM1 binds directly to Atg8/LC3 to facilitate degradation of ubiquitinated protein aggregates by autophagy. The Journal of biological chemistry 282(33):24131-45

Papackova Z, Dankova H, Palenickova E, Kazdova L, Cahova M (2012) Effect of short- and long-term high-fat feeding on autophagy flux and lysosomal activity in rat liver. Physiological research 61 Suppl 2:S67-76

Pelleymounter MA, Cullen MJ, Baker MB, et al. (1995) Effects of the obese gene product on body weight regulation in ob/ob mice. Science 269(5223):540-3

Perala AW, Filary MJ, Bartels MJ, McMartin KE (2014) Quantitation of diethylene glycol and its metabolites by gas chromatography mass spectrometry or ion chromatography mass spectrometry in rat and human biological samples. Journal of analytical toxicology 38(4):184-93

Pérez-Carreras M, Del Hoyo P, Martín MA, et al. (2003) Defective hepatic mitochondrial respiratory chain in patients with nonalcoholic steatohepatitis. Hepatology 38(4):999-1007

Pessayre D, Berson A, Fromenty B, Mansouri A (2001) Mitochondria in steatohepatitis. Seminars in liver disease 21(1):57-69

Pessayre D, Fromenty B (2005) NASH: a mitochondrial disease. J Hepatol 42(6):928-40

Phang J, Valle D, Hu C (2001) Disorders of Proline and Hydroxyproline Metabolism. In: The Metabolic and Molecular Bases of Inherited Disease. New York: McGraw-Hill, edited by Scriver CR, Beaudet AL, Sly WS, Vallee D, Childs B, Kinzler KW, and Vogelstein B, p 1821–1838

Pizzolato P (1964) Histochemical recognition of calcium oxalate. The journal of histochemistry and cytochemistry : official journal of the Histochemistry Society 12:333-6

Polat EC, Ozcan L, Cakir SS, Dursun M, Temur AO, Ozbek E (2015) Relationship between Calcium Stone Disease and Metabolic Syndrome. Urol J 12(6):2391-5

Postic C, Girard J (2008) Contribution of de novo fatty acid synthesis to hepatic steatosis and insulin resistance: lessons from genetically engineered mice. The Journal of clinical investigation 118(3):829-38

Powell EE, Cooksley WG, Hanson R, Searle J, Halliday JW, Powell LW (1990) The natural history of nonalcoholic steatohepatitis: a follow-up study of forty-two patients for up to 21 years. Hepatology 11(1):74-80

Purdue PE, Lumb MJ, Fox M, et al. (1991) Characterization and chromosomal mapping of a genomic clone encoding human alanine:glyoxylate aminotransferase. Genomics 10(1):34-42

Puri P, Mirshahi F, Cheung O, et al. (2008a) Activation and dysregulation of the unfolded protein response in nonalcoholic fatty liver disease. Gastroenterology 134(2):568-76

Puri V, Konda S, Ranjit S, et al. (2007) Fat-specific protein 27, a novel lipid droplet protein that enhances triglyceride storage. The Journal of biological chemistry 282(47):34213-8

Puri V, Ranjit S, Konda S, et al. (2008b) Cidea is associated with lipid droplets and insulin sensitivity in humans. Proc Natl Acad Sci U S A 105(22):7833-8

References

Ratziu V, Bellentani S, Cortez-Pinto H, Day C, Marchesini G (2010) A position statement on NAFLD/NASH based on the EASL 2009 special conference. J Hepatol 53(2):372-84

Ricchi M, Odoardi MR, Carulli L, et al. (2009) Differential effect of oleic and palmitic acid on lipid accumulation and apoptosis in cultured hepatocytes. Journal of gastroenterology and hepatology 24(5):830-40

Riedel TJ, Johnson LC, Knight J, Hantgan RR, Holmes RP, Lowther WT (2011) Structural and biochemical studies of human 4-hydroxy-2-oxoglutarate aldolase: implications for hydroxyproline metabolism in primary hyperoxaluria. PLoS One 6(10):e26021

Rinella ME, Siddiqui MS, Gardikiotes K, Gottstein J, Elias M, Green RM (2011) Dysregulation of the unfolded protein response in db/db mice with diet-induced steatohepatitis. Hepatology 54(5):1600-9

Rivera CA, Adegboyega P, van Rooijen N, Tagalicud A, Allman M, Wallace M (2007) Toll-like receptor-4 signaling and Kupffer cells play pivotal roles in the pathogenesis of non-alcoholic steatohepatitis. J Hepatol 47(4):571-9

Robertson WG (2004) Kidney models of calcium oxalate stone formation. Nephron Physiology 98(2):p21-30

Rodionov RN, Jarzebska N, Weiss N, Lentz SR (2014) AGXT2: a promiscuous aminotransferase. Trends in pharmacological sciences 35(11):575-82

Rokka A, Antonenkov VD, Soininen R, et al. (2009) Pxmp2 is a channel-forming protein in Mammalian peroxisomal membrane. PLoS One 4(4):e5090

Romeo S, Kozlitina J, Xing C, et al. (2008) Genetic variation in PNPLA3 confers susceptibility to nonalcoholic fatty liver disease. Nature genetics 40(12):1461-5

Sahai A, Malladi P, Pan X, et al. (2004) Obese and diabetic db/db mice develop marked liver fibrosis in a model of nonalcoholic steatohepatitis: role of short-form leptin receptors and osteopontin. American journal of physiology Gastrointestinal and liver physiology 287(5):G1035-43

Sahai A, Pan X, Paul R, Malladi P, Kohli R, Whitington PF (2006) Roles of phosphatidylinositol 3-kinase and osteopontin in steatosis and aminotransferase release by hepatocytes treated with methionine-choline-deficient medium. American journal of physiology Gastrointestinal and liver physiology 291(1):G55-62

Sakhaee K, Capolongo G, Maalouf NM, et al. (2012) Metabolic syndrome and the risk of calcium stones. Nephrology, dialysis, transplantation : official publication of the European Dialysis and Transplant Association - European Renal Association 27(8):3201-9

Salido E, Pey AL, Rodriguez R, Lorenzo V (2012) Primary hyperoxalurias: disorders of glyoxylate detoxification. Biochimica et biophysica acta 1822(9):1453-64

Salido EC, Li XM, Lu Y, et al. (2006) Alanine-glyoxylate aminotransferase-deficient mice, a model for primary hyperoxaluria that responds to adenoviral gene transfer. Proc Natl Acad Sci U S A 103(48):18249-54

Santana A, Salido E, Torres A, Shapiro LJ (2003) Primary hyperoxaluria type 1 in the Canary Islands: A conformational disease due to I244T mutation in the P11L-containing alanine:glyoxylate aminotransferase. Proc Natl Acad Sci U S A 100(12):7277-82

Sanyal AJ, Campbell-Sargent C, Mirshahi F, et al. (2001) Nonalcoholic steatohepatitis: association of insulin resistance and mitochondrial abnormalities. Gastroenterology 120(5):1183-92

Sato M, Tone S, Ishikawa T, Purdue PE, Danpure CJ, Minatogawa Y (2002) Functional analysis of the 5'-flanking region of the human alanine:glyoxylate aminotransferase gene AGXT. Biochimica et biophysica acta 1574(2):205-9

Scales CD, Jr., Smith AC, Hanley JM, Saigal CS (2012) Prevalence of kidney stones in the United States. European urology 62(1):160-5

Schaffner F, Thaler H (1986) Nonalcoholic fatty liver disease. Progress in liver diseases 8:283-98

Schattenberg JM, Galle PR (2010) Animal models of non-alcoholic steatohepatitis: of mice and man. Digestive diseases (Basel, Switzerland) 28(1):247-54

Schwarz M, Lund EG, Lathe R, Bjorkhem I, Russell DW (1997) Identification and characterization of a mouse oxysterol 7alpha-hydroxylase cDNA. The Journal of biological chemistry 272(38):23995-4001

Seglen PO (1976) Preparation of isolated rat liver cells. Methods in cell biology 13:29-83

Semins MJ, Shore AD, Makary MA, Magnuson T, Johns R, Matlaga BR (2010) The association of increasing body mass index and kidney stone disease. The Journal of urology 183(2):571-5

Shapiro AL, Viñuela E, V. Maizel J (1967) Molecular weight estimation of polypeptide chains by electrophoresis in SDS-polyacrylamide gels. Biochemical and Biophysical Research Communications 28(5):815-820

Shavit L, Ferraro PM, Johri N, et al. (2015) Effect of being overweight on urinary metabolic risk factors for kidney stone formation. Nephrology, dialysis, transplantation : official publication of the European Dialysis and Transplant Association - European Renal Association 30(4):607-13

Shi H, Kokoeva MV, Inouye K, Tzameli I, Yin H, Flier JS (2006) TLR4 links innate immunity and fatty acid-induced insulin resistance. The Journal of clinical investigation 116(11):3015-25

Shi L, Berkemeyer S, Buyken AE, Maser-Gluth C, Remer T (2010) Glucocorticoids and body fat associated with renal uric acid and oxalate, but not calcium excretion, in healthy children. Metabolism 59(1):134-9

Shimano H, Yahagi N, Amemiya-Kudo M, et al. (1999) Sterol regulatory element-binding protein-1 as a key transcription factor for nutritional induction of lipogenic enzyme genes. The Journal of biological chemistry 274(50):35832-9

Siener R, Glatz S, Nicolay C, Hesse A (2004) The role of overweight and obesity in calcium oxalate stone formation. Obesity research 12(1):106-13

Singh R, Kaushik S, Wang Y, et al. (2009) Autophagy regulates lipid metabolism. Nature 458(7242):1131-5

Singh S, Allen AM, Wang Z, Prokop LJ, Murad MH, Loomba R (2015) Fibrosis progression in nonalcoholic fatty liver vs nonalcoholic steatohepatitis: a systematic review and meta-analysis of paired-biopsy studies. Clinical gastroenterology and hepatology : the official clinical practice journal of the American Gastroenterological Association 13(4):643-54.e1-9; quiz e39-40

Skorecki K, Chertow G, Marsden P, Taal M, Yu A (2016) Brenner and Rector's The Kidney, 10 edn. Elsevier

Smith PK, Krohn RI, Hermanson GT, et al. (1985) Measurement of protein using bicinchoninic acid. Analytical Biochemistry 150(1):76-85

Smits MM, Ioannou GN, Boyko EJ, Utzschneider KM (2013) Non-alcoholic fatty liver disease as an independent manifestation of the metabolic syndrome: results of a US national survey in three ethnic groups. Journal of gastroenterology and hepatology 28(4):664-70

Smyth GK, Michaud J, Scott HS (2005) Use of within-array replicate spots for assessing differential expression in microarray experiments. Bioinformatics 21(9):2067-2075

References

St-Pierre J, Buckingham JA, Roebuck SJ, Brand MD (2002) Topology of superoxide production from different sites in the mitochondrial electron transport chain. The Journal of biological chemistry 277(47):44784-90

Stamatelou KK, Francis ME, Jones CA, Nyberg LM, Curhan GC (2003) Time trends in reported prevalence of kidney stones in the United States: 1976-1994. Kidney international 63(5):1817-23

Stepanova M, Rafiq N, Makhlouf H, et al. (2013) Predictors of all-cause mortality and liver-related mortality in patients with non-alcoholic fatty liver disease (NAFLD). Digestive diseases and sciences 58(10):3017-23

Stirzaker C, Song JZ, Davidson B, Clark SJ (2004) Transcriptional gene silencing promotes DNA hypermethylation through a sequential change in chromatin modifications in cancer cells. Cancer Res 64(11):3871-7

Summitt Candice B, Johnson Lynnette C, Jönsson Thomas J, Parsonage D, Holmes Ross P, Lowther WT (2015) Proline dehydrogenase 2 (PRODH2) is a hydroxyproline dehydrogenase (HYPDH) and molecular target for treating primary hyperoxaluria. Biochemical Journal 466(2):273-281 doi:10.1042/bj20141159

Taguchi K, Okada A, Hamamoto S, et al. (2015) Proinflammatory and Metabolic Changes Facilitate Renal Crystal Deposition in an Obese Mouse Model of Metabolic Syndrome. The Journal of urology 194(6):1787-96

Takada Y, Noguchi T (1982) Subcellular distribution, and physical and immunological properties of hepatic alanine: glyoxylate aminotransferase isoenzymes in different mammalian species. Comparative biochemistry and physiology B, Comparative biochemistry 72(4):597-604

Takahashi Y, Fukusato T (2014) Histopathology of nonalcoholic fatty liver disease/nonalcoholic steatohepatitis. World Journal of Gastroenterology 20(42):15539-48

Tan SH, Shui G, Zhou J, et al. (2012) Induction of autophagy by palmitic acid via protein kinase C-mediated signaling pathway independent of mTOR (mammalian target of rapamycin). The Journal of biological chemistry 287(18):14364-76 doi:10.1074/jbc.M111.294157

Tanida I, Ueno T, Kominami E (2008) LC3 and Autophagy. Methods in molecular biology (Clifton, NJ) 445:77-88

Tarantino G, Conca P, Basile V, et al. (2007) A prospective study of acute drug-induced liver injury in patients suffering from non-alcoholic fatty liver disease. Hepatology research : the official journal of the Japan Society of Hepatology 37(6):410-5

Targher G, Day CP, Bonora E (2010) Risk of cardiovascular disease in patients with nonalcoholic fatty liver disease. The New England journal of medicine 363(14):1341-50

Taylor EN, Curhan GC (2006) Body size and 24-hour urine composition. American journal of kidney diseases : the official journal of the National Kidney Foundation 48(6):905-15

Taylor EN, Stampfer MJ, Curhan GC (2005) Obesity, weight gain, and the risk of kidney stones. Jama 293(4):455-62

Teli MR, James OF, Burt AD, Bennett MK, Day CP (1995) The natural history of nonalcoholic fatty liver: a follow-up study. Hepatology 22(6):1714-9

Teufel A, Itzel T, Erhart W, et al. (2016) Comparison of Gene Expression Patterns Between Mouse Models of Nonalcoholic Fatty Liver Disease and Liver Tissues From Patients. Gastroenterology 151(3):513-525.e0

Tian Y, Wong VW, Chan HL, Cheng AS (2013) Epigenetic regulation of hepatocellular carcinoma in non-alcoholic fatty liver disease. Seminars in cancer biology 23(6 Pt B):471-82

Tilg H, Moschen AR (2006) Adipocytokines: mediators linking adipose tissue, inflammation and immunity. Nature reviews Immunology 6(10):772-783

Tilg H, Moschen AR (2010) Evolution of inflammation in nonalcoholic fatty liver disease: the multiple parallel hits hypothesis. Hepatology 52(5):1836-46

Tollefsbol TO (2011) Epigenetics: The New Science of Genetics Handbook of Epigenetics. Academic Press, San Diego, p 1-6

Torricelli FC, De SK, Gebreselassie S, Li I, Sarkissian C, Monga M (2014) Dyslipidemia and kidney stone risk. The Journal of urology 191(3):667-72

Trak-Smayra V, Paradis V, Massart J, Nasser S, Jebara V, Fromenty B (2011) Pathology of the liver in obese and diabetic ob/ob and db/db mice fed a standard or high-calorie diet. International journal of experimental pathology 92(6):413-21

Valenti L, Al-Serri A, Daly AK, et al. (2010) Homozygosity for the patatin-like phospholipase-3/adiponutrin I148M polymorphism influences liver fibrosis in patients with nonalcoholic fatty liver disease. Hepatology 51(4):1209-17

Valenti L, Rametta R, Dongiovanni P, et al. (2008) Increased expression and activity of the transcription factor FOXO1 in nonalcoholic steatohepatitis. Diabetes 57(5):1355-62

van de Steeg E, Wagenaar E, van der Kruijssen CM, et al. (2010) Organic anion transporting polypeptide 1a/1b-knockout mice provide insights into hepatic handling of bilirubin, bile acids, and drugs. The Journal of clinical investigation 120(8):2942-52

Vernon G, Baranova A, Younossi ZM (2011) Systematic review: the epidemiology and natural history of non-alcoholic fatty liver disease and non-alcoholic steatohepatitis in adults. Alimentary pharmacology & therapeutics 34(3):274-85

Wanders RJ, van Roermund CW, Griffioen M, Cohen L (1991) Peroxisomal enzyme activities in the human hepatoblastoma cell line HepG2 as compared to human liver. Biochimica et biophysica acta 1115(1):54-9

Wang W, Wu Z, Dai Z, Yang Y, Wang J, Wu G (2013) Glycine metabolism in animals and humans: implications for nutrition and health. Amino acids 45(3):463-77

Webb JL, Ravikumar B, Rubinsztein DC (2004) Microtubule disruption inhibits autophagosome-lysosome fusion: implications for studying the roles of aggresomes in polyglutamine diseases. The international journal of biochemistry & cell biology 36(12):2541-50

Weinberg AE, Patel CJ, Chertow GM, Leppert JT (2014) Diabetic severity and risk of kidney stone disease. European urology 65(1):242-7

West B, Luke A, Durazo-Arvizu RA, Cao G, Shoham D, Kramer H (2008) Metabolic syndrome and self-reported history of kidney stones: the National Health and Nutrition Examination Survey (NHANES III) 1988-1994. American journal of kidney diseases : the official journal of the National Kidney Foundation 51(5):741-7

West DB, Boozer CN, Moody DL, Atkinson RL (1992) Dietary obesity in nine inbred mouse strains. The American journal of physiology 262(6 Pt 2):R1025-32

Wieckowska A, Papouchado BG, Li Z, Lopez R, Zein NN, Feldstein AE (2008) Increased hepatic and circulating interleukin-6 levels in human nonalcoholic steatohepatitis. The American journal of gastroenterology 103(6):1372-9

Wigg AJ, Roberts-Thomson IC, Dymock RB, McCarthy PJ, Grose RH, Cummins AG (2001) The role of small intestinal bacterial overgrowth, intestinal permeability, endotoxaemia, and tumour necrosis factor alpha in the pathogenesis of non-alcoholic steatohepatitis. Gut 48(2):206-11

Williams EL, Acquaviva C, Amoroso A, et al. (2009) Primary hyperoxaluria type 1: update and additional mutation analysis of the AGXT gene. Human mutation 30(6):910-7

References

Williams SC, Bruckheimer SM, Lusis AJ, LeBoeuf RC, Kinniburgh AJ (1986) Mouse apolipoprotein A-IV gene: nucleotide sequence and induction by a high-lipid diet. Molecular and cellular biology 6(11):3807-14

Woerden van CS, Groothoff JW, Wanders RJ, Davin JC, Wijburg FA (2003) Primary hyperoxaluria type 1 in The Netherlands: prevalence and outcome. Nephrology, dialysis, transplantation : official publication of the European Dialysis and Transplant Association - European Renal Association 18(2):273-9

Wolf AM, Wolf D, Rumpold H, Enrich B, Tilg H (2004) Adiponectin induces the anti-inflammatory cytokines IL-10 and IL-1RA in human leukocytes. Biochem Biophys Res Commun 323(2):630-5 doi:10.1016/j.bbrc.2004.08.145

Wong VW, Wong GL, Chan HY, et al. (2015) Bacterial endotoxin and non-alcoholic fatty liver disease in the general population: a prospective cohort study. Alimentary pharmacology & therapeutics 42(6):731-40

Wong VW, Wong GL, Choi PC, et al. (2010) Disease progression of non-alcoholic fatty liver disease: a prospective study with paired liver biopsies at 3 years. Gut 59(7):969-74

Wu GD, Chen J, Hoffmann C, et al. (2011) Linking long-term dietary patterns with gut microbial enterotypes. Science 334(6052):105-8

Xie Z, Klionsky DJ (2007) Autophagosome formation: core machinery and adaptations. Nature cell biology 9(10):1102-9

Yamaguchi K, Yang L, McCall S, et al. (2007) Inhibiting triglyceride synthesis improves hepatic steatosis but exacerbates liver damage and fibrosis in obese mice with nonalcoholic steatohepatitis. Hepatology 45(6):1366-74

Yang L, Li P, Fu S, Calay ES, Hotamisligil GS (2010) Defective hepatic autophagy in obesity promotes ER stress and causes insulin resistance. Cell metabolism 11(6):467-78

Yang SQ, Lin HZ, Lane MD, Clemens M, Diehl AM (1997) Obesity increases sensitivity to endotoxin liver injury: implications for the pathogenesis of steatohepatitis. Proc Natl Acad Sci U S A 94(6):2557-62

Yen CL, Stone SJ, Cases S, Zhou P, Farese RV, Jr. (2002) Identification of a gene encoding MGAT1, a monoacylglycerol acyltransferase. Proc Natl Acad Sci U S A 99(13):8512-7

Yokota T, Oritani K, Takahashi I, et al. (2000) Adiponectin, a new member of the family of soluble defense collagens, negatively regulates the growth of myelomonocytic progenitors and the functions of macrophages. Blood 96(5):1723-32

Younossi ZM, Koenig AB, Abdelatif D, Fazel Y, Henry L, Wymer M (2016) Global epidemiology of nonalcoholic fatty liver disease-Meta-analytic assessment of prevalence, incidence, and outcomes. Hepatology 64(1):73-84

Zellmer S, Schmidt-Heck W, Godoy P, et al. (2010) Transcription factors ETF, E2F, and SP-1 are involved in cytokine-independent proliferation of murine hepatocytes. Hepatology 52(6):2127-36 doi:10.1002/hep.23930

Zhang X, Roe SM, Hou Y, et al. (2003) Crystal structure of alanine:glyoxylate aminotransferase and the relationship between genotype and enzymatic phenotype in primary hyperoxaluria type 1. Journal of molecular biology 331(3):643-52

Zhang Y, Proenca R, Maffei M, Barone M, Leopold L, Friedman JM (1994) Positional cloning of the mouse obese gene and its human homologue. Nature 372(6505):425-32

[1]   https://www.uclh.nhs.uk/OURSERVICES/SERVICEA-Z/PATH/PATHBIOMED/CBIO/Pages/Phmdatabase.aspx (06.04.2017)

6. Appendix

6.1 Abbreviations

%	Percent
Adj	Adjusted
AGXT	Alanine-glyoxylate aminotransferase
APS	Ammonium persulphate
Baf A/vin	Bafilomycin A/Vinblastine sulphate
BCA	Bicinchoninic acid
BisTris	Bis-(2-hydroxy-ethyl)-amino-tris(hydroxymethyl)-methane
BMI	Body mass index
BSA	Bovine serum albumin
° C	Degree Celsius
$CaCl_2$	Calcium chloride
cAMP	Cyclic adenosine monophosphate
cDNA	Complementary DNA
CpG	5'—cytosine—phosphate—guanine—3'
d	Days
DAPI	4',6-diamidino-2-phenylindole
DEPC	Diethyl pyrocarbonate
DMEM	Dulbecco's modified Eagle's medium
DMSO	Dimethyl sulfoxide
DNA/RNA	Deoxyribonucleic acid/Ribonucleic acid
DNMT	DNA methyltransferase
DPPIV	Dipeptidyl peptidase-4
DTT	Dithiothreitol
EDTA	Ethylenediaminetetraacetic acid
EGTA	Ethylene glycol-bis(β-aminoethyl ether)-N,N,N',N'-tetraacetic acid
Eif2a	Eukaryotic translation initiation factor 2A
e.g.	For example
et al.	And others
ESKD	End stage kidney disease
FM	Full media
FOXO1	Forkhead box protein O1
g/mg/μg	gram/milligram/microgram
GAPDH	Glyceraldehyde 3-phosphate dehydrogenase

Appendix

GC-MS	Gas chromatography–mass spectrometry
GO	Gene ontology
GRHPR	Glyoxylate reductase/hydroxypyruvate reductase
h	hours
HAO1	Hydroxyacid oxidase1
Hepes	4-(2-hydroxyethyl)-1-piperazineethanesulfonic acid
Hm	Male human primary hepatocytes
Hoga1	4-hydroxy-2-oxoglutarate aldolase 1
HRP	Horseradish peroxidase
HR MAS ^{1}HNMR	High resolution magic angle spinning ^{1}H nuclear magnetic resonance spectroscopy
H&E	Haematoxylin and Eosin Y
i.e.	that is
IfADo	Leibniz-Institut für Arbeitsforschung an der TU Dortmund
IFNγ	Interferon gamma
IHC	Immunohistochemistry
Il-6/Il-10	Interleukin-6/-10
IR	Insulin resistance
JNK	c-Jun N-terminal kinase
KH_2PO_4	Potassium dihydrogenphosphate
l/ml/µl	litre/millilitre/microlitre
LC-MS/MS	Liquid chromatography-mass spectrometry/ mass spectrometry
LC3	Microtubule-associated protein 1A/1B-light chain 3
LDH	Lactate dehydrogenase
LPS	Lipopolysaccharide
M/mM/µM/nM	Molar/millimolar/micromolar/nanomolar
$MgSO_4$	Magnesium sulphate
Mm	Male murine primary hepatocytes
MTBE	Methyl tert-butyl ether
MTBSTFA	N-(tert-butyldimethylsilyl)-N-methyltrifluoroacetamide
n	Number of biological replicates
Na_2HPO_4	Sodium hydrogen phosphate
NaCl	Sodium chloride
NAFL	Non-alcoholic fatty liver
NAFLD	Non-alcoholic fatty liver disease
NASH	Non-alcoholic steatohepatitis
ND/WD/HFD	Normal diet/Western diet/High fat diet

NF-κB	nuclear factor kappa-light-chain-enhancer of activated B cells
NF-Y	Nuclear transcription factor Y
nm	Nanometre
NP-40	Nonidet P-40 substitute
OA; OA/BSA	Oleic acid; Oleic acid complexed to BSA (6:1)
O/N	Over night
PAGE	Polyacrylamide gel electrophoresis
PBS	Phosphate-buffered saline
PFA	Paraformaldehyde
PH (1, 2, 3)	Primary hyperoxaluria (type 1, 2 or 3)
Prodh2	Proline dehydrogenase 2
PTS1	Peroxisomal targeting sequence type 1
PVDF	Polyvinylidene fluoride
qPCR	Quantitative real-time polymerase chain reaction
RFU	Relative fluorescence units
Rpm	Rounds per minute
ROS	Reactive oxygen species
RRBS	Reduced representation bisulphite sequencing
RT	Room temperature
SDS	Sodium dodecyl sulphate
siRNA	Small interfering RNA
SREBP-1c	sterol regulatory element-binding protein-1c
TBS-T	Tris-buffered saline
TEMED	Tetramethylethylenediamine
TG	Triglycerides
TLR	Toll-like receptor
TNF	Tumor necrosis factor
TOPO	Trioctylphosphine oxide
Tris	Tris(hydroxymethyl)aminomethane
UBC	Ubiquitin C
UPR	Unfolded protein response
vs	Versus
v/v, w/v	Volume per volume, weight per volume
xg	Standard gravity

Appendix

6.2 List of Figures

Appendix

6.3 List of Tables

6.4 Publications

6.4.1 Articles

Combining transcription factor binding affinities with open-chromatin data for accurate gene expression prediction. Schmidt F, Gasparoni N, Gasparoni G, **Gianmoena K**, Cadenas C, Polansky JK, Ebert P, Nordström K, Barann M, Sinha A, Fröhler S, Xiong J, Dehghani Amirabad A, Behjati Ardakani F, Hutter B, Zipprich G, Felder B, Eils J, Brors B, Chen W, Hengstler JG, Hamann A, Lengauer T, Rosenstiel P, Walter J, Schulz MH. Nucleic Acids Res. 2017 Jan 9;45(1):54-66.

Metabolic profiling of ob/ob mouse fatty liver using HR-MAS 1H-NMR combined with gene expression analysis reveals alterations in betaine metabolism and the transsulfuration pathway. Gogiashvili M, Edlund K, **Gianmoena K**, Marchan R, Brik A, Andersson JT, Lambert J, Madjar K, Hellwig B, Rahnenführer J, Hengstler JG, Hergenröder R, Cadenas C. Anal Bioanal Chem. 2017 Feb;409(6):1591-1606.

Imprinting of Skin/Inflammation Homing in CD4+ T Cells Is Controlled by DNA Methylation within the Fucosyltransferase 7 Gene. Pink M, Ratsch BA, Mardahl M, Durek P, Polansky JK, Karl M, Baumgrass R, Wallner S, Cadenas C, **Gianmoena K**, Floess S, Chen W, Nordstroem K, Tierling S, Olek S, Walter J, Hamann A, Syrbe U. J Immunol. 2016 Oct 15;197(8):3406-3414.

Gene network activity in cultivated primary hepatocytes is highly similar to diseased mammalian liver tissue. Godoy P, Widera A, Schmidt-Heck W, Campos G, Meyer C, Cadenas C, Reif R, Stöber R, Hammad S, Pütter L, **Gianmoena K**, Marchan R, Ghallab A, Edlund K, Nüssler A, Thasler WE, Damm G, Seehofer D, Weiss TS, Dirsch O, Dahmen U, Gebhardt R, Chaudhari U, Meganathan K, Sachinidis A, Kelm J, Hofmann U, Zahedi RP, Guthke R, Blüthgen N, Dooley S, Hengstler JG. Arch Toxicol. 2016 Oct;90(10):2513-29

Fatty acid elongation in non-alcoholic steatohepatitis and hepatocellular carcinoma. Kessler SM, Simon Y, Gemperlein K, **Gianmoena K**, Cadenas C, Zimmer V, Pokorny J, Barghash A, Helms V, van Rooijen N, Bohle RM, Lammert F, Hengstler JG, Mueller R, Haybaeck J, Kiemer AK. Int J Mol Sci. 2014 Apr 4;15(4):5762-73

6.4.2 Contribution on congresses

Talk: **Altered glyoxylate metabolism in non-alcoholic fatty liver disease (NAFLD).** **Gianmoena K**, Cadenas C, Hengstler JG. Tag der Chemie, 24 February 2017 in Dortmund, Germany (Award for best talk)

Poster: **AGXT downregulation in the fatty liver results in increased urinary oxalate – a molecular link between NAFLD and kidney stone disease? Gianmoena K**, Cadenas C, Hengstler JG. Tag der Chemie 24 February 2017 in Dortmund, Germany

Poster: **Hepatic fat accumulation leads to cellular dysfunction in hepatocytes**. **Gianmoena K**, Cadenas C, Hengstler JG. European Fatty Liver Conference 05-06 March 2015 in Maastricht, Netherlands

Poster: **In vitro method to investigate susceptibility of hepatocytes to drug-induced toxicity in patients with metabolic disease. Gianmoena K**, Cadenas C, Hengstler JG. 4th Marketplace bio.dortmund 28 October 2014 in Dortmund, Germany

Appendix

6.5 Eidesstattliche Versicherung (Affidavit)

_____
Name, Vorname
(Surname, first name)

_____
Matrikel-Nr.
(Enrolment number)

Belehrung:	Official notification:
Wer vorsätzlich gegen eine die Täuschung über Prüfungsleistungen betreffende Regelung einer Hochschulprüfungsordnung verstößt, handelt ordnungswidrig. Die Ordnungswidrigkeit kann mit einer Geldbuße von bis zu 50.000,00 € geahndet werden. Zuständige Verwaltungsbehörde für die Verfolgung und Ahndung von Ordnungswidrigkeiten ist der Kanzler/die Kanzlerin der Technischen Universität Dortmund. Im Falle eines mehrfachen oder sonstigen schwerwiegenden Täuschungsversuches kann der Prüfling zudem exmatrikuliert werden, § 63 Abs. 5 Hochschulgesetz NRW.	Any person who intentionally breaches any regulation of university examination regulations relating to deception in examination performance is acting improperly. This offence can be punished with a fine of up to EUR 50,000.00. The competent administrative authority for the pursuit and prosecution of offences of this type is the chancellor of the TU Dortmund University. In the case of multiple or other serious attempts at deception, the candidate can also be unenrolled, Section 63, paragraph 5 of the Universities Act of North Rhine-Westphalia.
Die Abgabe einer falschen Versicherung an Eides statt ist strafbar.	The submission of a false affidavit is punishable.
Wer vorsätzlich eine falsche Versicherung an Eides statt abgibt, kann mit einer Freiheitsstrafe bis zu drei Jahren oder mit Geldstrafe bestraft werden, § 156 StGB. Die fahrlässige Abgabe einer falschen Versicherung an Eides statt kann mit einer Freiheitsstrafe bis zu einem Jahr oder Geldstrafe bestraft werden, § 161 StGB.	Any person who intentionally submits a false affidavit can be punished with a prison sentence of up to three years or a fine, Section 156 of the Criminal Code. The negligent submission of a false affidavit can be punished with a prison sentence of up to one year or a fine, Section 161 of the Criminal Code.
Die oben stehende Belehrung habe ich zur Kenntnis genommen.	I have taken note of the above official notification.

_____
Ort, Datum
(Place, date)

_____
Unterschrift
(Signature)

Titel der Dissertation:
(Title of the thesis):

_____

_____

_____

| Ich versichere hiermit an Eides statt, dass ich die vorliegende Dissertation mit dem Titel selbstständig und ohne unzulässige fremde Hilfe angefertigt habe. Ich habe keine anderen als die angegebenen Quellen und Hilfsmittel benutzt sowie wörtliche und sinngemäße Zitate kenntlich gemacht. Die Arbeit hat in gegenwärtiger oder in einer anderen Fassung weder der TU Dortmund noch einer anderen Hochschule im Zusammenhang mit einer staatlichen oder akademischen Prüfung vorgelegen. | I hereby swear that I have completed the present dissertation independently and without inadmissible external support. I have not used any sources or tools other than those indicated and have identified literal and analogous quotations. The thesis in its current version or another version has not been presented to the TU Dortmund University or another university in connection with a state or academic examination.* |

*Please be aware that solely the German version of the affidavit ("Eidesstattliche Versicherung") for the PhD thesis is the official and legally binding version.

_____
Ort, Datum
(Place, date)

_____
Unterschrift
(Signature)

Appendix

6.6 Acknowledgement

To complete this PhD thesis was challenging and I am deeply thankful for a numerous of people who supported and encouraged me during the whole time, only some of whom it is possible to give particular mention here.

Foremost, I would like to thank Prof. Hengstler for giving me the opportunity to work in his laboratory and for his committed supervision. His door was always open for questions and discussions.

I am deepest grateful to Dr. Cristina Cadenas for her excellent guidance and for her joy in science. You were always supporting and full of ideas! Thank you so much for being the supervisor you were!

My gratitude goes to our collaboration partners who contributed to this project, in particular: Beate Aust and Dr. Meinolf Blaszkewicz from the Analytical Chemistry Unit at Ifado, Dr. Nina Gasparoni from the Epigenetic unit, University of Saarbrücken, as well as Alexander Schriewer and Prof. Hayen from the Department of Analytical Chemistry, WWU Münster.

My thanks go to all members of the CellTox group, the Systox group and the LivTox group. You all supported me in some way or other. In particular, I thank Katharina Rochlitz and Dr. Sonja Vosbeck for technical advises and help but especially for a lot of laughter in lab and in office. You gave me a great time here. In addition, I am grateful to Dr. Rosemarie Marchan who helped me with the English corrections and to Dr. Karolina Edlund who introduced DAVID to me. You two had always a friendly ear and good suggestions, thank you!

Moreover, I would like to express my gratitude to Beate Graf and Silke Hankinson. You were not only organizing talents but also good motivators.

I thank Dr. Regina Stöber und Larissa Pütter for the fun we had despite/due to a lot of learning during tox courses!

Mein größter Dank gebührt meiner Familie. Mama und Lena: ihr seid die Besten und ich bin sehr dankbar, dass ihr mich immer unterstützt und ermutigt habt. Außerdem danke ich Markus von Herzen dafür, dass er immer an meiner Seite war. Zu guter Letzt bedanke ich mich bei meinen Freunden, die immer mit Rat und Tat für mich da waren und einfach großartig sind.